CZECH TECHNICAL UNIVERSITY IN PRAGUE
FACULTY OF ELECTRICAL ENGINEERING
DEPARTMENT OF ELECTROMAGNETIC FIELD

Doctoral Thesis

Modal Analysis and Optimization of Radiating Planar Structures

Miloslav Čapek

Ph.D. Programme: Electrical Engineering and Information Technology
Branch of Study: Radioelectronics

Supervisor: Doc. Ing. Pavel Hazdra, Ph.D.
Co-supervisor: Prof. Ing. Miloš Mazánek, CSc.

Prague, Spring 2014

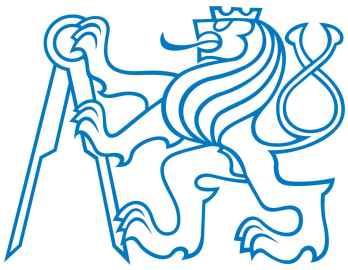

Author's Declaration

I declare that, except where explicit reference is made to the contribution of others, this dissertation is the result of my own work. I certify that, to the best of my knowledge, my thesis does not infringe upon anyone's copyright nor violate any proprietary rights and that any ideas, techniques, quotations, or any other material from the work of other people included in my thesis, published or otherwise, are fully acknowledged in accordance with the standard referencing practices.

Author

In Prague, 24. 4. 2014

Acknowledgement

It is my pleasant privilege to offer my sincere thanks to my supervisors and my friends, Pavel Hazdra and Miloš Mazánek from the Czech Technical University in Prague, for their unremitting support. I would also like to express my thanks to Jan Eichler. It was my pleasure to collaborate with him on antenna topics. Likewise, brisk cooperation with Lukáš Jelínek is highly appreciated, particularly on some difficult problems that have been solved over the last year. In particular, some critical remarks by Prof. Macháč in early stages of my Ph.D. studies were welcomed and led to new, hopefully better, scientific results. I am grateful to have had the opportunity to engage in fruitful discussions with Prof. Kulhánek, Doc. Sobotíková and Dr. Sokol, and to have had the opportunity to spend one inspiring month at KU Leuven with Prof. Vandenbosch.

I am also indebted to many colleagues from Department of Electromagnetic Field at CTU, namely to Pavel Hamouz, Zdeněk Hradecký, Ota Jícha, Tomáš Kořínek, Milan Polívka, Filip Kozák, Vašek Kabourek, Martin Mudroch, Vítězslav Pankrác, Zbyněk Škvor, Milan Příhoda, Petr Černý, Stanislav Zvánovec and many others, to a lot of (often quite "tasty") discussions.

Last, but certainly not least, I would like to express my thanks to my family and to Eva for their unceasing encouraging. Without them, this work would never have been possible.

Dedicated to Eva.

Abstract

This thesis aims to an analysis and a synthesis of electrically small antennas, a focal point in antenna design in recent years due to their massive use in present-day wireless devices. The practical design of electrically small antennas is however encumbered by the intricate and as yet not fully understood trade-off between basic parameters such as a bandwidth, efficiency, directivity, and antenna size. The evaluation of these parameters and the relationships between them is studied in this thesis, including their fundamental limits.

In order to understand the underlying physical mechanism of radiation, an advanced modal decomposition, the so-called theory of characteristic modes is used. Its key property is that just a few modes are usually sufficient to make a good characterization of the behaviour of an electrically small antenna. This thesis resolves some important issues of characteristic decomposition, i.e. direct superposition of the antenna parameters in their modal form, and also an eigennumber sorting, for which a new robust and reliable algorithm has been proposed.

The modal radiation Q factors are derived in this thesis, using a novel superposition formula, orthogonal relations for radiated power and a definition of stored electromagnetic energy in the time-harmonic domain. The modal radiation efficiencies are derived for cases of a strong skin effect in an antenna conductor. This progress facilitates synthesis of the feeding networks.

Nowadays widely exploited Q factor, based on differentiation of the input impedance, is reformulated in this thesis as a function of currents only. Thanks to this new formulation, practical fundamental lower bounds for spherical modes are established. The interrelations between existing definitions of Q are discussed. A new scheme for evaluating the stored electromagnetic energy in the time domain is introduced, and is tested on some canonical circuits.

This thesis also presents a study of fractal antennas. Their specific features are described, including reduction of the resonant frequency and its dependence on fractal iteration, higher radiation losses, multi- but narrow-band behaviour, and ground plane effects.

An original full-wave simulator is implemented, so that all design steps from specification of the geometry to extensive post-processing are presented, including robust heuristic optimization and acceleration of the computation.

The methods proposed in this thesis are finally verified on selected antenna candidates, which are simulated both in an in-house tool and in commercial softwares, and are then fabricated and measured to verify the proposed methods.

Key Words

Electrically small antennas, theory of characteristic modes, Q factor, stored electromagnetic energy, fractal antennas, heuristic optimization.

Abstrakt

Cílem disertační práce je systematická analýza a syntéza elektricky malých antén, jež jsou nedílnou součástí všech moderních bezdrátových zařízení. Praktický návrh je zatížen zejména doposud ne zcela známou vzájemnou závislostí všech klíčových parametrů těchto velice specifických zářičů, jimiž jsou zejména pracovní šířka pásma, vyzařovací účinnost, směrovost a jejich elektrická velikost. Právě vzájemné vztahy mezi těmito parametry a hledání jejich principiálních limitů je úkolem této práce.

Za účelem lepšího pochopení samotných fyzikálních principů vyzařování elektromagnetických vln je využita teorie charakteristických modů. Její velkou výhodou je skutečnost, že pro popis elektricky malé antény stačí zpravidla pouze několik málo modů. V této práci jsou vyřešeny některé dlouho přetrvávající problémy základního výzkumu související s modální dekompozicí, například přímý součet vybraných anténních parametrů na základě modálních veličin. Je vyřešen problém tzv. rozdílového modu a navržena nová a robustní metoda třídění vlastních čísel a modů.

Modální činitel jakosti Q je nově odvozen s využitím součtových a ortogonálních relací pro vyzářený výkon a uloženou energii. Ztráty vyzařováním jsou formulovány na základě tepelných ztrát v kovu konečné vodivosti generovaných jednotlivými charakteristickými mody. Tyto formulace umožňují jednoduchou syntézu napájení.

Široce užívaný činitel jakosti Q, charakterizovaný frekvenční změnou vstupní impedance, je odvozen jako funkce zdrojových proudů. Tato formulace umožňuje nalézt důležité limity Q a nalezne využití v rámci numerických metod jako je konvexní optimalizace. Dále je detailně prozkoumán vztah mezi jednotlivými definicemi Q. Je popsán a prakticky ověřen nový způsob výpočtu energie uložené v blízkém okolí antény.

Práce se rovněž věnuje problematice fraktálních antén. Jsou diskutována jejich specifika, jako je snížení resonanční frekvence vlivem nepravidelností geometrie, menší účinnost nebo vícepásmové a potenciálně širokopásmové chování fraktálních antén.

V rámci práce byl vytvořen nový výpočetní nástroj, který představuje ucelený systém pro návrh antén. Program zahrnuje tvorbu geometrie, tvorbu diskretizační sítě, dekompozici do charakteristických modů, následné zpracování dat a řadu optimalizačních nástrojů.

Metody a teoretické závěry prezentované v této práci jsou ověřeny výpočty v komerčních simulátorech a výrobou vybraných typů antén.

Klíčová slova

Elektricky malé antény, theorie charakteristických modů, činitel jakosti Q, energie uložená v elektromagnetickém poli, fraktální antény, heuristická optimalizace.

Contents

Chapter 1

Introduction

"... that which we are, we are;
One equal temper of heroic hearts,
Made weak by time and fate, but strong in will
To strive, to seek, to find, and not to yield."

— Alfred Lord Tennyson, Ulysses, 1833

The design of an electrically small antenna (ESA) consists of an analysis and an optimization, or a synthesis. Antenna analysis first specifies the geometry including the material distribution and the boundary conditions, and then evaluates the sources of the field (currents and charges). Finally, it evaluates selected antenna parameters. For this kind of approach, the designer must have previous experience with similar antennas, and it usually takes many attempts to find a structure that is good enough to satisfy all the requirements from the impedance and radiation point of view. While antenna analysis has been satisfactorily resolved, thanks to modern analytical and numerical methods, antenna synthesis involves two challenging tasks. The first task is to find what radiator geometry is the most suitable for a given purpose, and the second is to reveal the best excitation for this shape. These two steps are closely interconnected through the fundamental laws of classical electrodynamics, the Maxwell equations [1, 2]. However, the steps can advantageously be separated, e.g. via modal methods, or – more specifically – via characteristic mode decomposition. Both of these tasks are extremely difficult in all cases when one needs a radiator with parameters reaching out to the fundamental physical limitations. This is often the case for ESA, in which we seek small (subwavelength) dimensions of the radiating device in comparison with its operating frequency. Antenna synthesis presents an as yet unsolved problem, which has been addressed to some extent in antenna arrays. One of the major issues is the principally infinite number of degrees of freedom in possible shapes of the antenna body satisfying particular criteria. Absolutely, any geometry can form the shape of a potential antenna. Thus the antenna synthesis is a seriously difficult problem. The primordial idea of the synthesis lies in determining the best shape from among an infinite number of options.

An ESA is an essential part of present-day wireless communication systems, which are used in everyday life by billions of users around the globe (in mobile cell phones, tablets, GPS receivers, cars, etc.). However, the demand for higher transfer and smaller

physical dimensions has made the antenna a serious bottleneck that is hindering further progress. Typically, the antenna fractional bandwidth, the radiation efficiency, and the gain are considered as the key parameters of electrically small antennas, since they are significantly affected by reducing the electrical size. Keeping in mind that these parameters are contradictory, it is not an easy task to designate the optional trade-off. Even worse, all limits and restrictions are analytically known only for a few basic shapes (e.g. the lower bounds of the quality factor of a sphere, the radiation losses of a half-wave dipole) and the explicit relationship between these parameters is a subject of current research.

Many crucial steps towards ESA synthesis have already been taken. The most important breakthrough was the introduction of the source concept, which attempts to represent all antenna characteristics solely by means of the currents flowing on the antenna body. This source concept is one of the core topics of the thesis. It will be demonstrated that this concept can be used for defining the stored energy, various definitions of the Q, radiation efficiencies and radiation patterns, both in modal form and in overall form. The source concept is nowadays a leading approach to antenna analysis. By resolving some principal problems, it also promises to handle ESA synthesis. Some of these crucial problems have been studied and solved in this work.

It is important have in mind, that the history of antenna analysis and synthesis covers more than one century, and we are still not at the end. In this work, we focus on theoretical difficulties of small antenna synthesis, the relating perspective techniques. We also point out that the present developments have been tending toward a concept referred to called in this thesis as the source concept.

1.1 Organisation of the Thesis

The thesis is intended as a brief abstract that attempts to recapitulate the author's work on ESA analysis and synthesis, and to relate this work to the current state of knowledge. In order to distinguish the author's publications from the work of others, all original works by the author are denoted by a bullet (e.g. as [0•]), and all diploma thesis that were supervised by the author and relate to the topic are denoted by an asterisk (e.g. as [0∗]).

It is important to stress that only published results are explicitly discussed here. Note however, that the author tackled other issues during Ph.D. studies (namely the problem of negative energies, invariance of the energetic functional, a closed form formula for the characteristic mode on a dipole, limits of the quality factor for elliptical obstacles, etc.). These topics are mentioned here for completeness, and will be addressed in future publications.

In order to make the whole text as readable as possible, the author tries to avoid any mathematics in the body of the thesis – the whole mathematical apparatus and the formalism that has been used can be found in the attached papers and in the references. The short text submitted here serves as an accompanying document that summarizes all his publication efforts.

The rest of Chapter 1 draws attention to international cooperation that has been initiated. Then, projects worked on and grants received in relation to the author's Ph.D. studies are enumerated. Chapter 2 presents the state-of-the-art in the field of electrically small antennas and associated topics, and relates historical developments with the latest

findings. The author's own contribution is discussed in Chapter 3. The thesis is concluded in Chapter 4 in which all the objectives of the thesis are recapitulated, the author's scientific plans for the near future are discussed in some details, and finally, the long term goal for antenna synthesis based on the source concept is set. Selected author's papers are attached in Appendix A.1.

1.2 International Cooperation

During the author's Ph.D. studies, some international cooperation was initiated. Colleagues Dipl.-Ing. Eugen Safin and Dipl.-Ing. Robert Martens from Kiel University visited CTU in Prague in 2013 on one-week short-term scientific mission (STSM) to study the modal Q factors of their Multiple-input multiple-output system (MIMO). Two STSMs by the author at KU Leuven with Prof. Vandenbosch led to a deeper understanding of issues in electromagnetic energy. A further one month stay in Leuven is planned in summer 2014. The STSMs have led to a joint paper [3•], which was recently submitted to AP Transactions, and also to another joint paper [4•] with Prof. Cyril Luxey from University of Nice. Some of the work done by the author, for example the CM analyzer, was also utilized during the European School of Antennas.

1.3 Projects Solved Within the Frame of the Dissertation

The thesis as well as a lot of published results have arisen thanks to the following projects:

- European cooperation in Science and Technology:
  COST IC0603 ASSIST, COST IC1102 VISTA,
- Ministry of Education Youth and Sports of the Czech Republic:
  MSM6840770014, OC08018, LD12055, FRVS 2470/2012, FRVS 1141/2009,
- Czech Science Foundation:
  GAP102/12/2223, GD102/08/H018,
- Czech Technical University in Prague:
  SGS10/170/OHK3/2T/13, SGS11/065/OHK3/1T/13, SGS12/142/OHK3/2T/13,
- others:
  NBU SOD 201110.

It is the author's pleasure to thank all grant holders and co-workers both for their material support and for scholarship funding. All projects have led to a deeper understanding of EM theory.

Chapter 2

State-of-the-Art

Any antenna with $ka \leq 0.5$, where k is the wavenumber and a is the radius of the smallest sphere completely circumscribing the antenna, can be considered[1] as an ESA [6]. ESAs were in fact the first practical antennas, due to the inaccessibility of high frequencies [7]. During their long evolution, the original simple monopole antennas [8] have been transformed into modern composite antenna systems, see e.g. [7, 9] and references therein.

This definition sometimes suffers from a noteworthy criticism: the spherical region is seldom fully occupied by an antenna body. Instead, the radiator occupies a cylindrical space (thin-wire antennas like dipoles, meandered dipoles, etc.) or more likely a rectangular box (e.g. patch antennas), and thus it would be better to compare its volume with the wavelength [10].

The history of ESA development is linked with attempts to make the electrical size of the antenna as small as possible, while retaining directivity, radiation efficiency, the quality factor and input impedance on a bearable level. However, these parameters are mutually bound, see the schematic sketch in Fig. 2.1, and the history of ESAs development is thus full of failures. A survey of these effects is presented in [5, 6], covering all topics including miniaturization techniques, fundamental limits, analysis methods, simulation, manufacturing and measuring.

The following subsections cover those parts of ESA history which are closely connected with the goals of the thesis: modal decomposition (Section 2.1) and the related problem of modal superposition (Section 2.2), the radiation Q factor (Section 2.3), the problem of the definition of stored electromagnetic energy (Section 2.4), antenna directivity and gain (Section 2.5), fractal antennas (Section 2.6) and optimization (Section 2.7) are discussed in this Chapter.

2.1 Theory of Characteristic Modes

Modal decomposition of integro-differential operators [11, 12] into modes and the corresponding eigenvalues [13, 14] offers a unique opportunity to understand the underlying physical mechanism of antenna operation. Characteristic modes (CM) were found to be a natural basis for radiating structures. This decomposition for Perfectly Conducting (PEC) scatterers was first published by Garbacz and Turpin [15] and was later significantly refor-

[1] For other classifications, see e.g. [5].

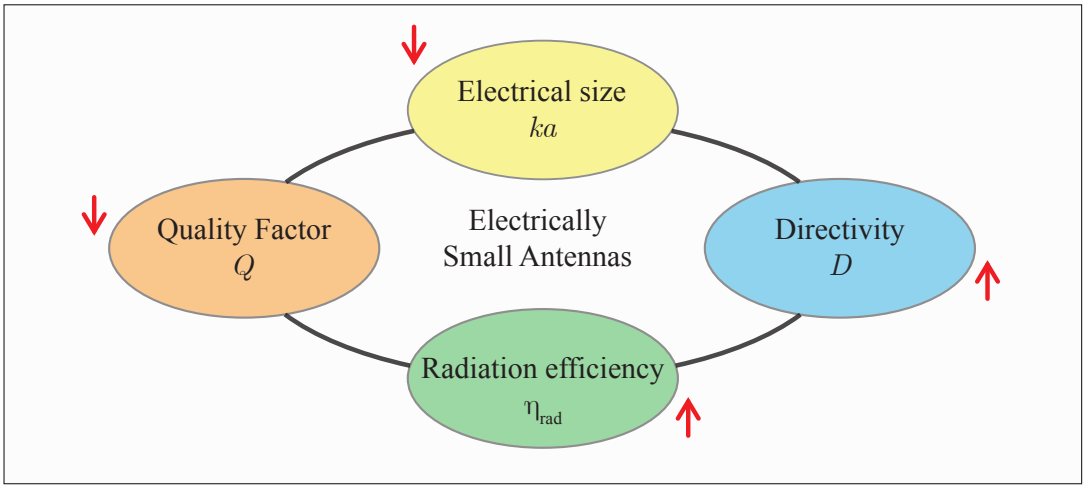

Figure 2.1: Fundamental limitations of electrically small antennas (ESAs). The design of ESA is encumbered by the principal limits and by contradictory parameters – the size, efficiency, directivity and bandwidth of the antenna. The aim is to reach out to the fundamental limits, keeping the antenna as small as possible, while fulfilling other requirements like the prescribed radiation pattern of impedance matching. Red arrows indicate common ESA requirements.

mulated by Harrington and Mautz [16, 17]. The general development of CM starts from the Helmholtz wave equation and the Electric Field Integral Equation (EFIE) [18], which is tested by an unknown current. The integro-differential kernel is discretized into the impedance matrix [19], and the variational energetic functional is established as the ratio between reactive power and real power. This variational prescription [20] can be reformulated as a generalized eigenvalue problem (GEP) [21], and its solution minimizes the energetic functional which leads to the characteristic numbers and characteristic vectors (modal currents).

CMs are equiphasal, i.e. all modes and numbers can be chosen to be real. The value of eigennumber indicates the behaviour of the corresponding mode. The nth mode is considered as inductive if the value is positive (i.e. $W_{\mathrm{m}}^n > W_{\mathrm{e}}^n$, in which W_{m}^n is the magnetic energy and W_{e}^n is the electric energy of the nth mode), and capacitive if the value is negative ($W_{\mathrm{m}}^n < W_{\mathrm{e}}^n$). For zero value the mode is in resonance ($W_{\mathrm{m}}^n = W_{\mathrm{e}}^n$). The eigenvalue is commonly recalculated to the eigenangle [22], which has a bounded range (from 180° to 270°).

At specific frequencies, the decomposition problem may be numerically ill-posed and also non-uniquely defined [17]. The mode order may be switched, or an unphysical solution arises. Moreover, some modes can show up (or disappear) at any frequency point. The challenge here is to design a heuristic tracking method that can overcome all these deficiencies. The original procedure, which utilized a simple correlation [23] was improved in [24, 25], and a new correlation formula, called Pearson's correlation, was recently proposed in [26]. However, these methods are still not as robust as they should be, and tracking problems often occur (e.g. fractal structures of high iteration, high-order or degenerate modes). Since the tracking problem is more or less the same for any class of

GEP, it has also been attacked in other branches, see e.g. [27].

CMs are orthogonal with respect to their radiation patterns [16]. This condition generates orthogonal relations and the superposition formula for the eigenmodes (characteristic currents). More recently, the theory has been generalized to dielectric, magnetic and lossy bodies [28], apertures [29], and low frequency coupling [30]. Note that the variational functional can be written both for Hilbert spaces $\mathcal{L}^2$ and $\mathbb{C}^n$, but the solution for a general antenna body is known only for the discretized (matrix) form [31].

A big advantage of CM decomposition is that typically only the first few modes are important for decomposing the source quantities on ESA [32]. This is one of the most important property that is usually required of any modal decomposition. The CMs are analytically known only in some special cases – an important case is the spherical PEC shell [33]. In order to decide what modes are important (and for what purpose), the modal significance coefficients were derived from the current amplitude [34, 35], or from the current amplitude with respect to the feeding [36]. The magnitude of the eigenvalue itself corresponds to the ratio between the reactive power and the radiated power (smaller value means better radiating properties). The overall parameters of the antenna, e.g. input impedance, Q factor, directivity or efficiency, can also be decomposed into their modal form, see Section 2.2.

Although CM theory provides very powerful tool for decomposition of scatterers, it was forgotten for almost 30 years, mainly because there was a lack of powerful computers able to solve realistic designs. CMs have been revisited in the last decade [35] and are widely used at the present time. However, little is known about the theory of CMs – as yet, only two book chapters have marginally dealt with CMs [37, 38]. Some recent papers have contributed to the CM theory, [39–41], but most of them use CMs simply as a tool, e.g. for defining entire-domain basis functions [42], for general antenna design [23], for studies of the influence of the ground plane on the antenna performance [23, 33, 43, 44], for the design of multiband antennas and reflectarrays [45–49], for analysis and design of MIMO antennas [50–56], antennas positioned on Unmanned Aerial Vehicles (UAV) [57, 58], for bandwidth enhancement or for reducing Q [59, 60], and for other applications [61–66].

The resurgence of interest in CMs is documented by a number of dissertation theses in the last 5 years that have dealt with CMs, namely the work by Sonkki on wideband multielement antennas [67], by Obeidat on reconfigurable antennas [68], by Adams on multimode small antennas [69], by Raines on reduction of mutual coupling [70], by Strojny on antennas for UAV [71], and by Ethier on feedless optimization techniques [72]. Despite this remarkable progress, many problems and challenges remain, especially in connection with modal superposition of antenna parameters and antenna synthesis. These issues will be introduced and discussed in the following Section and in Chapter 3.

CM decomposition can be further generalized towards Generalized Characteristic Modes [52] or towards Inagaki modes [73]. Inagaki modes may be orthogonal not only to the far-field but also to any specified region of space. These modes have been used for antenna pattern synthesis. In addition to spherical harmonics [74] and the possibility of CM reconstruction of them [40], there are also other modal decompositions, e.g. the Singularity Expansion Method [75], SEM, in which the transient response of a scatterer is represented by several damped sinusoids. Unfortunately, by definition, SEM produces complex eigennumbers, and this is not so convenient as CMs. Another interesting work [76, 77]

dealt with decomposition into non-radiating (near-field) and radiating (far-field) modes. Dealing with CMs, a different weighting can be used, or the definition of the energetic functional can be slightly changed (one can e.g. obtain modes that embody the minimal modal radiation Q factor).

The first commercial software that contains CM analysis is FEKO, [78], from version 6.0, which appeared in 2013. All features are constantly being improved, but as will be pointed out in Chapter 3, some features have not yet been implemented.

2.2 Superposition of Modal Quantities

Modal quantities leave aside the effect of feeding (i.e. the modes are eigensolutions that exist without excitation). However, the completeness of the modes also allows structures with feeding to be considered using superposition. Several feeding models have been considered, including coaxial and proximity feeding [23], excitation by an L-probe, [79] and the incident plane wave. Interestingly, superposition can be derived not only for modal currents and charges (i.e. source quantities) but directly for the Q factor (from modal stored energies and lost powers), for radiation efficiency (from the modal efficiencies) and also for the directivity (from the modal directivities).

Modes that change slowly with frequency have the lowest Q factor. Taking this fact into account, the modal Q factor was approximately found [80] from differentiation of the Rayleigh quotient formula [81]. This approach is equivalent to differentiation of the reactive power, introduced in Section 2.3. In [80], modification of the CM decomposition is proposed in such a way that the lowest Q current modes (other than the CM) can be found. The estimation of the modal Q factors was rectified in [82] using the input impedance definition [83]. See also Section 2.3 for a detailed explanation.

The superposition of modal radiation patterns [84] is simplified by the orthogonal relations [16] and was, in fact, widely used to synthesise the required radiation pattern, see e.g. pattern synthesis by the N-port scatterer [85]. The directivity of the antenna [84] can then be simply evaluated.

Radiation efficiency [84] is probably the least examined ESA parameter, as it requires knowledge of the currents flowing inside the penetrable body. CM decomposition for lossy (penetrable) structures is briefly introduced in [28]. Following the same approach, modal radiation efficiency was approximately treated in [72]. It was indicated in [86] that the radiation losses (Joule heating) can be established directly from the CM of the PEC body. However, in [86] the structure was still infinitely thin (no skin-effect [87] was considered) and no superposition formula was derived. The efficiency is often influenced by the (lossy) matching network, which was investigated in [88], and a new set of CM was found by including the network elements into the impedance matrix. This is similar to the original approach, using the reactive loading method [80].

It is important to stress that for correct superposition, the CM decomposition has to be complete and all modes have to be found properly. This means that, for example, the modal radiation efficiencies have to be superposed in such a way that the resultant efficiency is equal to the efficiency obtained from calculation with the Impedance Boundary Condition (IBC) [89]. These necessary conditions are sometimes questioned, for details see e.g. [42].

In order to eliminate coupling between selected parts of a structure, the radiation and coupling modes are used in [72,90], see also [70]. This opens new ways to suppress the coupling by using optimization. This approach enables modal and structural decomposition to be combined, but these techniques are extremely time-consuming.

2.3 Radiation Q Factor

The fractional bandwidth (FBW) is a parameter of primary importance, especially in the case of ESA. By definition, it represents the relative bandwidth in which the power received by the antenna from the feed port can be effectively radiated [84]. It is believed that FBW is inversely proportional to the quality factor Q. Originally [91], Q was used as a circuit parameter and its generalization to antennas was performed *ex post*, see e.g. [5,6] and references therein.

Probably the first rigorous study of the Q of ESAs was performed by Wheeler [92]. He investigated a small loop (TM mode) and a small capacitor (TE mode) operating as small antennas. Since it is known that ESAs have low radiation resistance and high reactance [8], a parallel capacitor or a serial inductor brings these antennas to resonance. Thus, the problem could have been simplified to solving the serial or parallel RLC circuit [93]. These two important, though particular, circuits lead to the same results, if Q factor is calculated as the ratio of the angular frequency times the stored energy over the lost power [94], or from differentiation of the input reactance [6].

Hence, and because it has the same meaning in general physics [95], Q based on the stored energy is referred to as classical. More specifically, "The ratio of 2π times the energy stored in the fields excited by the antenna to the energy radiated and dissipated per cycle." is used, and in fact this is the standard definition of Q for an antenna (IEEE Std. 145-1993, 2.304). However, this definition will be shown to be a little problematic, since the correct formula for the stored electromagnetic energy of radiating structures is not yet fully known. Therefore, several other definitions of Q factor exist concurrently [6] all of them attempting to approximate the proportionality to FBW, see Fig. 2.2.

From the point of view of practical antenna design, it is important to know what is the minimum Q that can be achieved with an arbitrary structure in a given space. This value bounds the best available bandwidth. The fundamental lower bound of Q is definitely the most investigated parameter in ESA theory. In a classical work, Chu considered a sphere that encloses an ESA [96]. The normalized radial wave impedance for the dominant spherical TM mode was expressed as a continued fraction equivalent to a ladder network with particular R,L,C elements. The fundamental limits of Q for spherical TM and TE modes can be found in this way. However, Chu's method is restricted to spherical modes only, and does not include the internal energy of the sphere, making the limit overly optimistic. Harrington [97] investigated the principal limits of the gain and the Q of spherical TM and TE modes using electromagnetic fields. A field-based technique was also utilized by Collin and Rothschild [98], using Poynting's theorem [99] and a novel subtraction technique. The fundamental bounds of Q for several canonical shapes can be found in this way. While this method is very easy to explain, it is, however, not clear whether the subtraction is physically correct. Fante studied the Q of an ideal antenna with both TM and TE spherical modes simultaneously excited [100]. Inspirational work

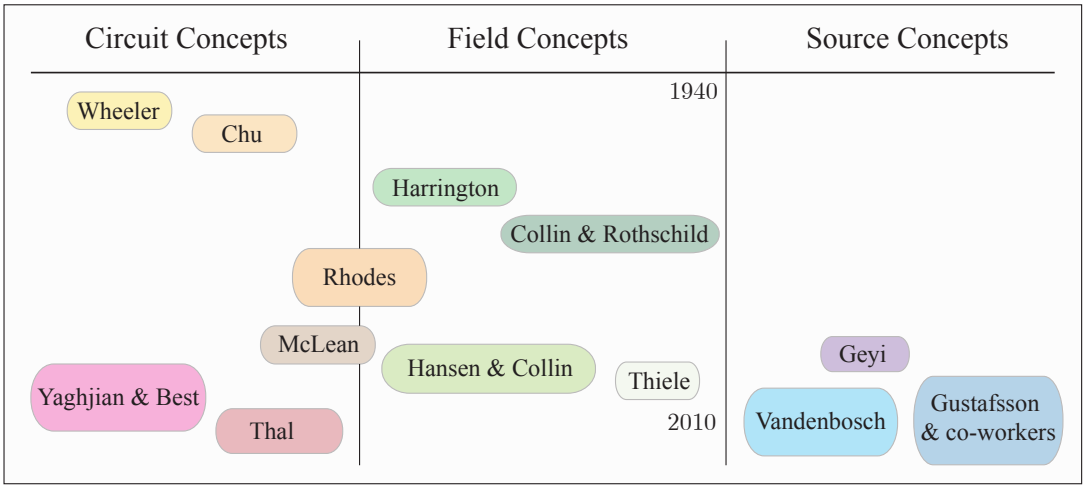

Figure 2.2: An overview of the most significant works dealing with the Q factor that are related to this thesis. Various definitions of Q are possible, depending on the choice of the fundamental quantity (impedance, fields, currents). In recent years, the source current has been widely used for defining the Q factor and its fundamental bounds, since this approach opens new possibilities in optimization and modal decomposition.

by Rhodes covers problems of stored energy and the Q factor. He extended the work of Levis [101] and Fante [100] and postulated the reactance theorem for antennas [102], which defines the relation between the frequency derivative of the reactance and five energy terms (electric and magnetic parts, heating losses, radiation and dispersion). He also introduced the concept of observable energy [103] and studied the Q factor of planar antennas and apertures calculated from stored energy [104, 105]. From the practical point of view, the principles and restrictions of small antennas are reviewed in [106] and [107], respectively.

After 15 years, the problem of radiation Q has been reopened. Another method for establishing the Q bounds was published by McLean [108], leading to the same results as in the work of Collin and Rothschild. Foltz and McLean [109] evaluated the Q bounds of a prolate spheroid by calculating the stored energy from the fields. These bounds have a better fit for practical antennas (e.g. a cylindrical dipole). The superdirective ratio was utilized by Thiele, Detweiler and Penno [110] making direct use of a far-field pattern separated into a visible part and an invisible part. No modal spherical wave expansion was needed, and two interesting hypotheses related to the realizable lower bound of Q were mentioned. At least one of them is still pending. Geyi and Jarmuszewski attempted to prove that Foster's theorem also holds for antennas. However, this observation has been widely criticised [111], or even refuted [112], since it contrasts with everyday antenna design experience. The same topic was recently reinvestigated in [113].

The spherical wave function is reused by Geyi in [114] to discuss the maximum possible ratios of gain to Q. His further contributions [115, 116] present pioneering work in terms of defining Q solely as a function of current. However, the expressions that were presented were only a quasi-static approximation. In [117] and [118] Kwon noted inconsistencies in some previous attempts to define the lower bound of Q and the maximum gain. Another critical review was written by Grimes and Grimes [119], and some other notes were added

by Sten and Hujanen in [120]. Thal used the ladder network [121] to extend Chu's limit by including energy inside Chu's sphere. Later, he extended his circuit approach towards the study of different radiation patterns, gain and Q characteristics [122], and for the Q bounds of ESA with arbitrary shape [123]. The same results as Thal in [121] were reported by Hansen and Collin [124], utilizing TM and TE spherical modes and including the energy stored inside the enclosing sphere.

A different concept of Q was proposed by Yaghjian and Best [83]. Exact and approximative formulas for Q were derived in terms of differentiation both the input impedance and of the electromagnetic field. The input impedance formula is very easy to evaluate or to measure. Their approach has been verified by numerous studies [125–128], in which practical ESA designs were benchmarked. This approach is nowadays widely used because of its simplicity and accuracy. The absence of a source current definition can be considered as a slight drawback of the method, and the presence of the frequency derivative unfortunately precludes a single point numerical calculation.

Following an approach similar to that of Geyi, Vandenbosch derived rigorous expressions for stored electric and magnetic energies [129]. A sophisticated method for extracting the far-field energy is used in the time-harmonic domain. Lower bounds of arbitrary shape can be found right from the resultant expressions [130, 131]. Only the source current has to be specified, which makes it possible to evaluate Q directly in modern electromagnetic solvers.

Another approach for providing Q and gain expressions for ESA of arbitrary shape is represented in work of Gustafsson and associates [10, 132]. The scattering theory [133] is utilized to define the polarizability dyadics. The concept of polarizability opens new ways to calculate the bounds of directivity over Q and gain over Q ratios for arbitrary shape, including complex scatterers [134]. Polarizability can be a subject of optimization [135].

In order to reach the lower bound of Q, magnetic materials and/or a combination of TE and TM modes are investigated, since the stored energy inside Chu's sphere has to be frozen out. The conditions that have to be satisfied are already known, for details see e.g. the work of Kim and Breinbjerg [136–139] or the work of Stuart and Yaghjian [140]. The latest papers deal with highly dispersive materials inside Chu's sphere [141]. According to preliminary results [142], these structures can embody significantly lower Q than non-dispersive structures. Finally, Sievenpiper and co-authors [143] compared 112 ESA designs and pointed out that current efforts are almost about reaching the fundamental bound of Q.

The major persisting flaws are related to the validity of Foster's theorem, a consistent definition and evaluation of stored electromagnetic energy, the interrelationship between all definitions of Q, and the the exact relationship between radiation Q and FBW. Although belief in the proportionality of Q to FBW is based on the theory of lumped circuits, and is actually not clarified for antennas, all definitions are numerically equal for Q reaching high values, making the proportion between Q and FBW exact for $Q \to \infty$.

2.4 Stored Electromagnetic Energy

The Q factor is traditionally defined as the ratio between 2π times the stored energy and the lost energy per cycle. The evaluation of lost energy does not pose any problems, but

stored energy has not yet been fully solved. Considering a radiation structure, the problem lies in not knowing which part of the total energy belongs to the radiated energy and which part belongs to the stored energy. Works closely related to the problem of stored energy are briefly introduced below.

The field radiated by an antenna consists of a radiation field carrying power to infinity, and a localized reactive (near) field. In the time-harmonic domain the electric or magnetic energy stored in the field is infinite [87], since the field pervades all space. Collin and Rothschild solved the problem with infinite energies in the time-harmonic domain by subtracting the radiation energy [98], assuming the radial energy velocity to be the speed of light.

Smith provided a lower estimate from the input impedance of a one-port [98]. The problem of stored energy for both non-dispersive and dispersive media was reported by Landau, Lifshitz and Pitaevskii [144]. Rhodes introduced the concept of observable stored energy [103], and expressed it as the sum of interior and exterior energies (i.e. the energy inside the material medium of the system, and the energy arising from the field in the exterior volume that surrounds the radiating system). More importantly, the subtraction technique proposed by Collin and Rothschild was disproved [103].

In his report [145], Cockrell treated planar antennas and their relative bandwidth. The divergent energetic integrals were solved by transferring them to distributions and omitting non-observable parts. A similar approach as in [104] was utilized, including the definition of FWB and Q. Carpenter tried to solve the problem of stored energy by utilizing potentials instead of fields [146]. However, as pointed out in comments [147] and [148], the resultant expressions suffer mainly from variance under the Lorenz gauge condition [99]. Thus, these expressions cannot be correct (the energy must be gauge invariant). Grimes and Grimes argued [149] that the complex Poynting theorem [87] forms an insufficient basis for a full description of the power in the radiation field. Some difficulties related to the complex Poynting theorem are presented in the technical report of White and Overfelt [150], including an evaluation of some basic circuits (both lumped and radiating) and their Q.

Since 2000, many authors have gone back to stored energy analysis in the time domain. Shlivinski and Heyman published a time domain approach to studying short-pulse antennas [151,152]. The spherical mode decomposition known from the frequency domain has been extensively utilized. Collardey, Sharaiha and Mahdjoubi employed a brute force Finite-Difference Time-Domain (FDTD) method [153,154]. The radiated energy was subtracted thanks to the definition of the complex Poynting vector in each Yee cell [155]. A very complete Ph.D. thesis by Direen [156] deals with various definitions of the stored energies and the corresponding Q factors. The concept of recoverable energy is incorporated into the definition of the Q factor.

Geyi [115] and Vandenbosch [129] tried to derive the stored energy in the time-harmonic domain. Geyi obtained only quasi-static energies, but Vandenbosch's comprehensive approach led to rigorous expressions. Since the expressions are of bilinear form and contain (convolution) integral operators, they can be a subject of advanced numerical methods, see e.g. the utilization of Lagrange multipliers [157] in [158], and the utilization of convex optimization [159] in [160,161]. In order to evaluate Vandenbosch's expressions, no feeding port has to be defined.

Later, Vandenbosch generalized his expressions for stored energy directly in the time domain [162, 163]. Considering the sinusoidal current, the expressions are reduced to those already derived in the time-harmonic domain [129]. Unfortunately, it was found by Gustafsson that these energies can be negative for certain modes [158]. This indicates either that the expressions are wrong (including those in the time domain), or that certain modal currents cannot exist separately (e.g. they cannot be fed so that no other mode is excited). Finally, Mikki and Antar presented a comprehensive theory of the antenna near-field [164,165], so that the energy exchange processes between various regions can be analysed, and the stored energy can be evaluated in terms of the TE and TM modes.

The problem of the stored energy in dispersive media has been attacked by many authors, e.g. by Landau [144] and Brillouin [166]. Unfortunately, the stored energy in a dispersive system is at present known only under certain conditions, see [167–169].

Nowadays, the closed-form, analytical and general definition of stored energy is still not known. From the recent perspective, the possible definition should be unique and invariant, and the results should be non-negative for any physically realizable current. If possible, the final expressions should be defined as functions of current only. These conditions enable quick evaluation of the stored energy in existing electromagnetic simulators and e.g. optimization of the structure by numerical optimization routines (see Section 2.7), or employment of modal decomposition.

The problem of stored energy evaluation is one of the author's key contributions, and is discussed in Chapter 3.

2.5 Input Impedance and Antenna Gain

Almost all ESAs can be considered as short dipoles and loops, which are both usually classified as superdirective antennas [5], since their directivity remains equal to 1.5 as their ka size decreases [6].

The fundamental matching limitations were found by Fano [170], and impedance matching is nowadays a well-understood technique [171], covering both Foster circuits and non-Foster circuits (producing negative resistance, inductance or positive capacitance) [5]. However, achieving good matching is a serious problem in ESAs, because of the load of 50Ω [7]. The challenge here is to modify the geometry of the antenna in such a way that it will come as near to self-resonance as possible, while keeping the other antenna parameters the same.

The radiation pattern of a ESA is often similar to the doughnut-shaped omni-directional pattern of the Hertzian dipole [6]. This observation comes from the fact that ESA usually works as a dominant TE (dipole) or TM (loop) spherical mode, or as a combination of these two modes. However, some other possible patterns were presented in [97, 117, 118]. When the source currents are available, the radiation fields can easily be calculated in both the near-field and the far-field [172] without any simplifications.

A critical topic for a small antenna is radiation efficiency, since it has been shown [97] that the radiation losses are extremely prominent for small values of ka. This is primarily due to the high concentrations of current density (in many cases, current filaments that are out-of-phase are placed close together, increasing the stored energy and lowering the radiation efficiency). Investigations of this topic usually start from analysis of a small

dipole antenna [5, 7]. The radiation efficiency can be calculated by employing IBC [89], e.g. in FEKO software [173], or can be measured by Wheeler cap method [174]. However, ESA stores a great deal of energy in the near-field (i.e. the near-field is wide-spread, containing a high-intensity field), and thus the cap has to be electrically large enough not to disturb the near-field [175], see also [176] and [177].

It is therefore clear that the gain of ESA is predominantly affected by the small radiation efficiency and the impedance mismatch, since the directivity is more or less constant, and the polarization losses can be minimized in almost all cases. For more details, see [5–7, 178] and references therein.

2.6 Fractal Antennas, Antennas With Highly Irregular Shapes

A fractal is any mathematical set that can be characterized by self-similar patterns. Some self-similar patterns have been well-known since mediaeval times, but they have been subject to rigorous treatment starting with mathematics of 17th century and continuing in the 19th century with the definition of the first analytical curve, which is continuous but nowhere differentiable [179]. The name fractal comes from Mandelbrot, who was the first to describe and provide a consistent definition of the fractals [180].

Any fractal set is typically described by the Hausdorff dimension [181] which, by definition, differs from the topological dimension [181]. This means that while fractal curve has topological dimension equal to one, the Hausdorff dimension can be different (e.g. equal to 2 or 3 for the space-filling curve defined in 2- or 3-dimensional Euclidean space). The Hausdorff dimension is sometimes called the fractal dimension, and for practical purposes it is usually replaced by the box-counting dimension, which can be easily computed, giving an estimation of the fractal dimension [179].

Having the self-similarity property in mind, some benefits for ESA can be determined. Fractal antennas are miniaturized, since currents are forced to flow around a significantly longer path than in the case of a smooth Euclidean geometry [182], [183]. Fractal antennas often embody multiband behaviour (the individual operational bands are distributed in spectra with respect to the iterations), which can be for a given Voltage Standing Wave Ratio (VSWR) considered as a broadband behaviour [184]. Thanks to modal decomposition, it was also realized that spectra of fractal shapes contain extraordinary modes that cannot in principle exist in the spectra of smooth Euclidean shapes (see e.g. localized eigenfunctions in [185] or localized modes in [186]). These high-order modes exhibit high directivity, since they mimic an antenna array. In addition, they are implicitly in-phased, and thus they can be easily fed. However, these modes are practically unobtainable for ESAs.

Unfortunately, the benefits of fractals are at the cost of serious disadvantages, i.e. poor radiation efficiency [187] and narrowband behaviour (high Q) in a single resonance operation [188]. From the practical point of view, there are problems with fractals of high iteration, mainly during discretization in computer-aided simulators, and with precise manufacturing.

Fractal antennas have attracted great interest and have become very popular in ESA

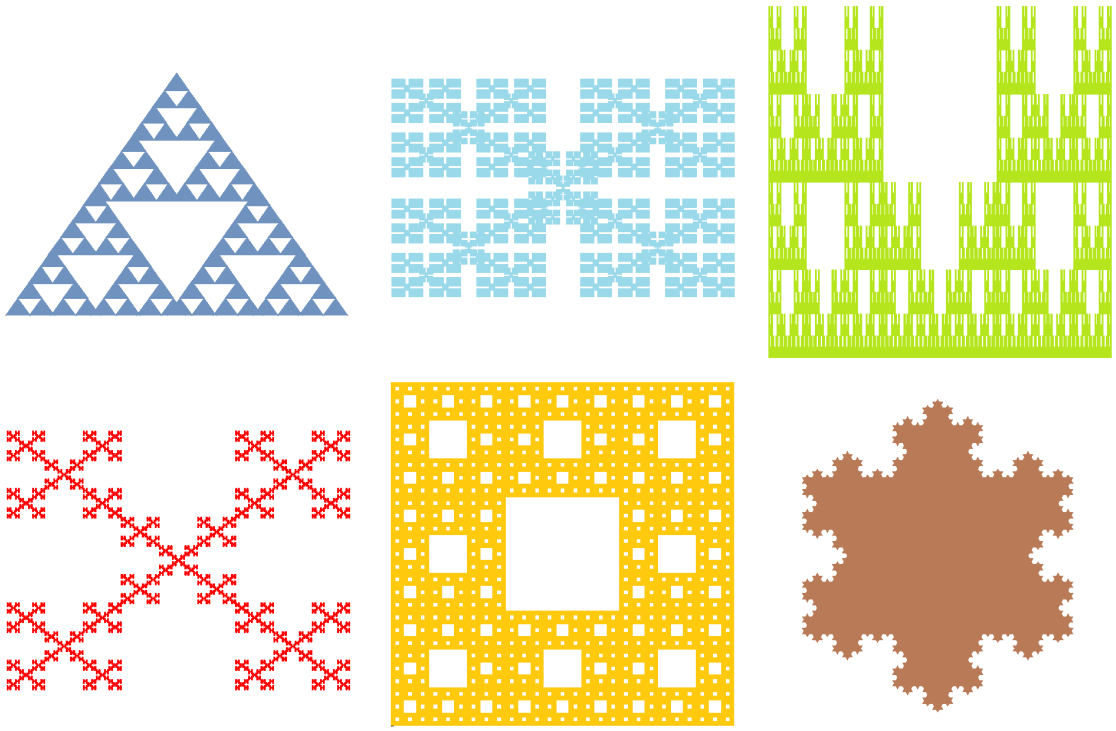

Figure 2.3: Selected representatives of the iterated function system (IFS). From left to right, from top to bottom: Sierpinski triangle, filled Minkowki curve, U-shape fractal, another Minkowski curve, Sierpinski gasket, Koch island. All shapes can be generated as wire structures, and some of them can be generated by an L-system grammar (e.g. Koch island).

design, see e.g. [5,9] and references therein. Following the standard division, fractal radiators are denoted as of fractal boundary (usually wire antennas) and of fractal mass (patch antennas). Space-filling curves, called Peano curves, are a special kind of a boundary 1D fractals [179]. These curves are one-dimensional objects, which however fill the whole space as the iteration goes to infinity.

Several classes of fractals are known in the literature, according to the way in which they were generated [179]. Only the Iterated Function System (IFS) and the Lindenmayer system (L-system) are used in this thesis. IFS is union of several copies of itself, each copy being transformed by a selected affine transformation with the contraction factor smaller than one, see Fig. 2.3. The IFS is based on the Banach contraction mapping principle [189], and is defined with the aid of the Hutchison operator [190]. L-system [191] is an iterative rewriting system with a formal grammar consisting of several strings which describe the initial primitives (i.e. basic curves) and a collection of production rules [189]. Both IFS and the L-system are considered as a synthetic fractals.

Practical antennas should be referred to as poly-fractals or pre-fractals since they are only of finite iteration. However, this distinction is usually neglected. The following representatives have been selected to document recent activities in fractal antennas: the Koch monopole antenna and its properties have been described in [192], [193], [194], the Sierpinsky triangle was utilized in [184], two space-filling curves were compared in [187],

fractal elements were utilized [195] for design of Frequency Selective Surface (FSS, [196]), the radiation from fractal apertures was investigated in [197], and the hexagonal multiband fractal antenna was presented in [198]. Extensive treatments of the whole topic of fractal antennas has been presented in theses from the Polytechnic University of Catalonia (UPC), where the Fractus company was founded, namely in the work by Borja Borau [186] and Pros [199]. Other notable theses [79, 200, 201] are mentioned for completeness.

Most fractal design has been performed by trial and error methods or by parametric studies of a selected motif. The reason is that the mathematics that should be able to provide a fully description of the fractal structures and their physical behaviour is still under development [185]. Some basics from fractional calculus are already known [202], making it possible to solve some specific partial differential equations [202]. However, for example, no solution is known for a wave equation of fractional dimension [203], since new functional spaces and new analytical tools are required [204]. Recent works deal with the fractional Laplacian of particular fractals [185]. Point our here that even the basic operations in vector calculus are extremely involved in fractal geometry [205]. Similarly, the phenomenon of localized modes is not yet fully explained, although it was reported a long ago by Berry [206].

Microstrip antennas are widely described in [178, 207] and in references therein, covering basic patch antenna theory, the advantages and limitations, numerical methods, an analysis of basic path radiators, feeding techniques, broadbanding, topics on active antennas and patch arrays. Microstrip fractal antennas are treated in [5, 9, 208]. Ingenious ESA designs can be found particularly in [5] and [7].

2.7 Optimization and Antenna Synthesis

Optimization allows the best element to be found from a set of available alternatives, so that the objective function is minimized or maximized [157]. Formally, variables from a decision space (or also a feasible space) are mapped into a objective space via an objective function which is sometimes called a fitness function [209]. Depending on the dimensions of the decision space, the optimization is denoted as one-dimensional or multi-dimensional. By analogy, depending on the dimension of the objective space, the optimization is denoted as single-objective (SOO) or multi-objective (MOO), [209]. For the theory of MOO, see [210], where all the important concepts are explained in detail. Mostly, the decision space is restricted to given dimensions (e.g. where the parameters allow practical realization). This type of optimization is constrained, and the boundary conditions have to be specified before it starts. According to the behaviour of the fitness function, optimization methods are linear and nonlinear. Any optimization is denoted as local if it seeks a point at which the objective function is smaller than at other feasible nearby points [157]. For convex and linear programming, all local solutions are also global solutions [157]. The optimization is called deterministic if the model is completely known. Otherwise, the optimization is stochastic. The minima of the fitness function that are reached during the optimization are denoted as the cost function. Typically, the optimization runs until the prescribed minimum is found or the maximum number of iterations has run out [209]. For a comprehensive review of all important optimization techniques, see [157, 159, 209, 210], which cover all methods from the simplest gradient Newton method, via Lagrange multi-

pliers, the trust region, convex optimization (CO) and the Nelder-Mead method (NMA) to complex (multi-objective) heuristic algorithms like Simulated Annealing, Genetic Algorithm (GA), Particle Swarm Optimization (PSO) and Ant Colony Optimization (ACO).

Practical antenna optimization problems are often formulated by non-analytical fitness function. It is therefore almost impossible even to estimate the fitness function behaviour. In such cases, it is appropriate to use more robust algorithms, which prevent a hang-up in the local minima. Probably the first widely used global heuristic method was GA. However, its implementation is quite involved and its overall performance is close to the performance of algorithms described below.

Today, the leading optimization method is PSO. It was synthesized by the psychologists Kennedy and Eberhart [211] for studying flocks of birds, see also [212] for additional details. PSO and its properties have been extensively studied on a large class of functions [213] and real-life problems [214]. PSO primarily depends on two variable parameters for which, depending on the problem, several recommendations exist [213]. They are supported by theoretical studies [215, 216]. PSO is most suitable for global constrained optimization [209] of highly irregular multi-dimensional functions (hundreds of dimensions have been successfully tested). It can be combined advantageously with other algorithms, e.g. NMA [217] and GA [218] into a hybrid method. It can be concluded that PSO is a safe choice for almost any complex optimization problem, especially if a robust hybrid PSO method is utilized [219].

The usage of PSO in electromagnetism is widely documented in the literature, see e.g. [220, 221]. The boundary conditions that are essential for antenna design optimization were revisited in [222]. Note also the interesting work of Mikki and Kishk, who established an analogy between PSO and Newtonian mechanics, and then modified PSO in accordance with quantum mechanics [223, 224].

Another interesting heuristic algorithm is the Self-Organizing Migrating Algorithm (SOMA, [225]). SOMA is a robust heuristic evolutionary algorithm with efficiency comparable to PSO. Like PSO, SOMA can easily be extended to MOO [226].

A boom in optimized antenna designs started in the 1990s, along with the new generation of powerful computers. Nowadays, most of the antenna community uses optimization as a tool only. The role of nature-inspired optimization algorithms was revisited in [227], and new optimization techniques are reviewed in [225]. Today, commercial simulators typically include a wide variety of optimization tools, to name a few: the CST Studio Suite [228] contains the interpolated quasi-Newton method, the trust region framework, NMA, GA, PSO; FEKO [78] contains NMA, GA and PSO. External optimizers can easily be connected to these softwares. Sensitivity analysis is another recently implemented feature.

Unfortunately, the onset of optimization techniques brought many antennas that were blindly optimized without any understanding of the basic physical principles. These attempts lack the necessary insight into antenna operation, and are thus correctly criticized by some authors [5, 69].

Chapter 3

Thesis Objectives and Solutions

Although characteristic modes, the Q factor and stored energy are topics that have been receiving a lot of attention in the proceedings of prestigious conferences (IEEE APS, EuCAP) and in prestigious journals in the field (IEEE Transactions on Antennas and Propagation), there are still many problems awaiting resolution.

The general aim of the thesis is to contribute to the theoretical as well as practical knowledge of electrically small antenna design. The particular goals are specified as:

- revision of the characteristic mode (CM) decomposition, elimination of the residual mode, resolution of problems with tracking, implementation of CM, see Section 3.2;
- superposition of modal quantities that are important for ESA design, see Section 3.3;
- feeding network synthesis, optimization of modal results, see Section 3.3;
- a consistent evaluation of stored electromagnetic energy, a source current definition of measurable Q, implementation of the calculation of Q during post-processing, see Section 3.4;
- utilization of fractal geometry, a study of its influence on the operation of an antenna, optimization of radiator geometry, see Section 3.5;
- practical verification of obtained results in commercial packages, and manufacturing promising antenna candidates, see Section 3.5.

Some of these issues are truly fundamental (e.g. modal superposition and optimization, the definition of stored energy), while other issues are rather particular (residual mode, tracking routine). In this Chapter, the original contribution of the author to the topic is briefly discussed, and is linked with the author's publications, which are enumerated in Section 3.1. For the sake of clarity, the original developments are divided into parts which are not sorted chronologically, but rather follow the structure of the previous chapter.

3.1 Author's Publications Related to Thesis Objectivities

All author's papers related to the thesis are listed below. They are systematically referenced in this Chapter which serves as an accompanying document. Selected papers of the author are included in Appendix A.1, and form the core of the thesis.

Journal Papers

- **M. Capek**, L. Jelinek, P. Hazdra, and J. Eichler, "The Measurable Q Factor and Observable Energies of Radiating Structures," *IEEE Transactions on Antennas and Propagation*, Vol. 62, No. 1, pp. 311–318, Jan. 2014.
- P. Hazdra, **M. Capek**, and J. Eichler, "Comments to "Reactive Energies, Impedance, and Q Factor of Radiating Structures" by G. Vandenbosch," *IEEE Transactions on Antennas and Propagation*, Vol. 61, No. 12, pp. 6266–6267, Dec. 2013.
- **M. Capek**, P. Hamouz, P. Hazdra, and J. Eichler, "Implementation of the Theory of Characteristic Modes in MATLAB," *IEEE Antennas and Propagation Magazine*, Vol. 55, No. 2, pp. 176–189, April 2013.
- **M. Capek**, P. Hazdra, and J. Eichler, "A Method for the Evaluation of Modal Radiation Q," *IEEE Transactions on Antennas and Propagation*, Vol. 60, No. 10, pp. 4556–4567, Oct. 2012.
- J. Eichler, P. Hazdra, **M. Capek**, and M. Mazanek, "Modal Resonant Frequencies and Radiation Quality Factors of Microstrip Antennas," *International Journal of Antennas and Propagation*, Vol. 2012, pp. 1–9.
- **M. Capek**, P. Hazdra, P. Hamouz, and J. Eichler: "A Method for Tracking Characteristic Numbers and Vectors," *Progress In Electromagnetics Research B*, Vol. 33, pp. 115–134, 2011.
- J. Eichler, P. Hazdra, **M. Capek**, T. Korinek, and P. Hamouz, "Design of a Dual Band Orthogonally Polarized L-probe Fed Fractal Patch Antenna Using Modal Methods," *IEEE Antennas and Propagation Letters*, Vol. 10, pp. 1389–1392, 2011.
- P. Hazdra, **M. Capek**, and J. Eichler, "Radiation Q-factors of Thin-Wire Dipole Arrangements," *IEEE Antennas and Wireless Propagation Letters*, Vol. 10, pp. 556–560, 2011.
- **M. Capek**, P. Hazdra, P. Hamouz, and M. Mazanek, "Software Tools for Efficient Generation, Modeling and Optimisation of Fractal Radiating Structures," *IET Microwaves, Antennas and Propagation*, Vol. 5, pp. 1002–1007, 2011.

Journal Papers (in review)

- **M. Capek**, J. Eichler, and P. Hazdra, "Evaluation of Radiation Efficiency from Characteristic Currents," submitted to *IET Microwaves, Antennas and Propagation*, after major revision.

- **M. Capek**, L. Jelinek, P. Hazdra, and J. Eichler, "An Analytical Evaluation of the Measurable Quality Factor Q_Z for Dominant Spherical Modes," submitted to *IET Microwaves, Antennas and Propagation*.
- **M. Capek**, L. Jelinek, G. A. E. Vandenbosch, and P. Hazdra, "Electromagnetic Energies and Radiation Q Factors," submitted to *IEEE Transactions on Antennas and Propagation*.
- P. Hazdra, **M. Capek**, J. Eichler, and M. Mazanek, "The Radiation Q-Factor of a $\lambda/2$ Dipole Above Ground Plane," submitted to *IEEE Antennas and Propagation Letters*, after major revision.
- J. Eichler, P. Hazdra, and **M. Capek**, "Aspects of Mesh Generation for Characteristic Mode Analysis," submitted to *IEEE Antennas and Propagation Magazine*.
- P. Hamouz, P. Hazdra, **M. Capek**, J. Eichler, A. Diallo, P. Ferrero, and C. Luxey, "Polarization Diversity in UMTS Mobile Phones analyzed with Characteristic Modes"," submitted to *IEEE Antennas and Propagation Letters*.

Conference Papers

- **M. Capek**, L. Jelinek, P. Hazdra, and J. Eichler, "The Source Definition of The Quality Factor Q_Z," *IEEE International Symposium on Antennas and Propagation and USNC-URSI Radio Science Meeeting*, Memphis, USA, 2014.
- L. Jelinek, **M. Capek**, P. Hazdra, and J. Eichler, "Lower Bounds of the Quality Factor Q_Z," *IEEE International Symposium on Antennas and Propagation and USNC-URSI Radio Science Meeeting*, Memphis, USA, 2014.
- **M. Capek**, J. Eichler, P. Hazdra, and M. Mazanek, "A Method for the Evaluation of Radiation Efficiency Based on Modal Approach," in *Proceedings of the 8th European Conference on Antennas and Propagation (EuCAP)*, Hague, Netherlands, 2014.
- F. Kozak, **M. Capek**, V. Jenik, P. Hudec, and Z. Skvor, "Simulation of Electromagnetic Field of a Fast Moving Target Close to Antennas," in *Proceedings of the 7th European Conference on Antennas and Propagation (EuCAP)*, pp. 294–298, Gothenburg, Sweden, April 2013.
- **M. Capek**, P. Hazdra, J. Eichler, P. Hamouz, and M. Mazanek, "Acceleration Techniques in Matlab for EM Community," in *Proceedings of the 7th European Conference on Antennas and Propagation (EuCAP)*, pp. 2639–2642, Gothenburg, Sweden, April 2013.
- J. Eichler, P. Hazdra, **M. Capek**, D. Segovia-Vargas, and V. González-Posadas, "Active Low Noise Dipole Antenna," in *10th International Symposium on Antennas, Propagation and EM Theory (ISAPE 2012)*, 2012.
- P. Hazdra, **M. Capek**, J. Eichler, T. Korinek, and M. Mazanek, "On the Modal Resonant Properties of Microstrip Antennas," in *Proceedings of the 6th European Conference on Antennas and Propagation (EuCAP 2012)*, pp. 1650–1654, 2012.

- **M. Capek**, P. Hazdra, J. Eichler, P. Hamouz, M. Mazanek, and V. Sobotikova, "The Evaluation of Total Radiation Q Based on Modal Approach," in *Proceedings of the 6th European Conference on Antennas and Propagation (EuCAP)*, pp. 883–885, Prague, Czech Republic, April 2012.
- P. Hazdra, J. Eichler, **M. Capek**, P. Hamouz, and T. Korinek, "Small Dual-band Fractal Antenna with Orthogonal Polarizations," in *Proceedings of the 5th European Conference on Antennas and Propagation (EuCAP)*, pp. 2733–2736, Rome, Italy, April 2011.
- P. Hazdra, **M. Capek**, J. Eichler, P. Hamouz, and M. Mazanek, "Radiation Q of Dipole Modal Currents," in *Proceedings of the 5th European Conference on Antennas and Propagation (EuCAP)*, IEEE, pp. 1578–1581, Rome, Italy, April 2011.
- P. Hamouz, P. Hazdra, M. Polivka, **M. Capek**, and M. Mazanek, "Radiation Efficiency and Q Factor Study of Franklin Antenna Using the Theory of Characteristc Modes," in *Proceedings of the 5th European Conference on Antennas and Propagation (EuCAP)*, IEEE, 2011, pp. 1974–1977, Rome, Italy, April 2011.
- P. Hazdra, **M. Capek**, P. Hamouz, and M. Mazanek, "Advanced Modal Techniques for Microstrip Patch Antenna Analysis," in *Conference Proceedings ICECom 2010*, Zagreb: KoREMA, pp. 1–6, 2010.
- **M. Capek**, and P. Hazdra, "Design of IFS Patch Antenna Using Particle Swarm Optimization," in *Proceedings of the 4th European Conference on Antennas and Propagation (EuCAP)*, IEEE, pp. 1–5, 2010.
- P. Hazdra, **M. Capek**, and J. Kracek, "Optimization Tool for Fractal Patches Based on the IFS Algorithm," in *Proceedings of the 3rd European Conference on Antennas and Propagation (EuCAP)*, IEEE, pp. 1837–1839, 2009.
- **M. Capek**, "PSO Optimalization of IFS Fractal Patch Antennas," in *Poster 2009*, Prague, CTU in Prague, 2009.
- P. Hazdra and **M. Capek**, "IFS Tool for Fractal Microstrip Patch Antenna Analysis," in *Proceedings of the 14th Conference on Microwave Techniques COMITE*, Prague, pp. 227–230, 2008.
- **M. Capek** and P. Hazdra, "PSO optimalizace v MATLABU," in *Technical Computing Prague 2008, 16th Annual Conference Proceedings*, Praha, Humusoft, 2008. (in Czech)

3.2 Revision of CM Theory, Interpretation of Modal Results

This topic is divided into parts covering theory, numerical issues, and implementation.

3.2.1 Theoretical Problems

An important theoretical problem in characteristic decomposition is its completeness and the hypothetical existence of the so-called residual mode. It has been presented [23, 42] that a residuum always exists, constituting the difference between the superposition of characteristic modes and the direct solution given by the Method of Moments (MoM). The existence of the residual mode was attributed to the presence of feeding. Based on the completeness of the CM decomposition, proved in [39], which was already mentioned by Harrington [16], no residual mode should however exist. It thus follows that the residuum should be a numerical issue only. After an analysis of several algebraic parameters (modal significance, condition numbers, etc.), the problem was found to reside in a wrong sign of the radiated power of high-order modes (thus typically almost non-radiating modes) [229•]. This also explains why the imaginary part of the residuum was significantly larger than the real part if the real excitation was considered. The same result was obtained by Lagrange multipliers, which were formally used to solve the GEP of the CM decomposition. As a result, a correction formula was proposed [229•]. The numerical verification was performed on an example of a thin-wire dipole [84] fed by a delta gap source [172]. For this purpose, the simple one-dimensional Galerkin formulation of the MoM was implemented [19], and the resultant symmetric impedance matrix was decomposed by the generalized Schur (QZ) decomposition [14] into the CM basis. Using the correction formula, the residual mode was suppressed to a level of numerical noise [229•]. It can be concluded that the issue of the residual mode can mainly be explained the numerically ill-conditioned matrix pencil of CM GEP [14].

An analytical prescription for the dominant CM mode on a half-wavelength dipole was investigated. Unfortunately, no such function is yet known. Determining this function would help to verify the meshing and decomposition techniques. It can be shown via the Fourier transform [230] and the Dirichlet-Poincaré inequality [231] that the CM functional has no solution in 1-dimensional Sobolev $\mathcal{W}^{1,2}$ space [232], when an infinitely thin wire is considered. Some 2-dimensional structures were analytically treated using spectral methods. However, this work remains unpublished, and is therefore not detailed in this thesis.

Finally, an attempt was undertaken to approximate the CM modes by analytical functions. This technique can be used especially in the case of small antennas at their natural resonance (only one mode is excited). Since the CM forms a variational solution, the current shape of the mode is extremely resistant to a change in geometry (the topology has to remain the same). This concept was successfully tested in [233∗] on an example of thin-wire full wavelength loop, which was miniaturized by two U-notches placed at the minima of the current density. The current density was approximated by a sine function, which not only proved to be a very precise approximation but also lead to a tremendous speed-up of the calculation (no need to repeat the CM decomposition). This allowed Q

to be optimized with respect to the geometry of the notches. The working frequency was selected exactly at the resonance of the dominant mode, and it was calculated from the (constant) electrical length of the wire. The results for the approximative current shape and the exact current shape were in excellent agreement.

3.2.2 Properties of Radiating and Non-Radiating Modes

Among other classifications, characteristic modes can be divided into two major groups: radiating modes and non-radiating modes [35]. Radiating modes and their properties were studied in [234•] on an example of a rectangular patch and fractal shapes. Non-radiating modes, often called inductive modes, radiate poorly at all frequencies. It has been widely accepted [35] that such modes have strictly inductive behaviour, so that they have no natural resonance. All these reasons let to other notation: static modes.

However, it can be shown that in special cases these modes are able to resonate. For example, consider a static mode on an electrically long cylinder (the current flows uniformly azimuthally along the angular coordinate). Then the eigennumber is positive for reasonably small ka (i.e. the mode is inductive). However, for large enough ka the eigennumber achieves a zero value (the mode resonates), and then the eigennumber starts to be negative. This effect usually occurs for a high values of ka, and only for certain structures. Note here that the value of the eigennumber reflects the amount of reactive power of the mode. As will be shown in Section 3.4, negativeness of the eigennumber is closely related to the problem of stored energy, since the electric energy of these modes is identical to zero (no charge is present), yielding a theoretically negative value for magnetic energy [158, 235]. Exactly the same problem was reported for an example of the dominant TE spherical mode in [236•]. It is important to stress that the inductive characteristic mode cannot, as is widely accepted, be excited alone.

3.2.3 Numerical Issues of the CM

A complete solution of GEP performed by generalized Schur decompostion is extremely time-consuming ($\propto \mathcal{O}\left(N^3\right)$, N is the number of unknowns). A further problem is that finer discretization leads to a bigger basis, which contains a lot of high-order (non-radiating) modes which are ill-posed. Both of these modes affect the decomposition [237•]. These problems can be significantly cut short by utilizing the implicitly restarted Arnoldi method [238]. Unfortunately, this method finds only the first few modes, and is therefore not suitable for subsequent modal superposition. No effective preconditioning of the CM decomposition that is valid for the whole basis is known at the present time.

Characteristic modes and numbers are theoretically continuous with respect to frequency. Unfortunately, due to the numerical solution (only a finite number of modes is found at each frequency [17]), both the modes and the numbers are disordered. This means that the resultant characteristic basis should be sorted (tracked) throughout the spectrum. Only simple correlation techniques have been used until now [23], and the sorting algorithm has therefore been significantly improved [237•], making the tracking procedure reliable and robust. Problems with tracking led to the development of the Adaptive Frequency Solver (AFS), which automatically determines what frequency points are calculated in the next iteration [239•].

CM can be calculated only for structures that radiate well at a given frequency. The consequences of violation of this condition are shown in Fig. 3 and Fig. 5 of [236•]. Numerical data is missing around the resonant frequencies of the internal (cavity) modes [87], and even the new tracking routine with AFS fails in these circumstances.

3.2.4 Practical Utilization of CM

Before implementing CM decomposition, it is first necessary to program the MoM. The software that has been developed is inspired by the Makarov code [240], which utilizes the RWG basis functions [241], and currents flowing in a vacuum are considered. Unfortunately, the Galerkin method [242] is affected by asymmetric evaluation of the source and observation regions, since a 9-point barycentric subdivision and centre point integration are used [240]. The points therefore do not coincide, which guarantees that no singularity occurs even for an evaluation of a self-term (all distances between the centre point of a triangle and the centres of 9 small triangles are nonzero). Some features (e.g. PEC mirroring [84]) are present, and the code is properly vectorized in Matlab [243]. The MoM code was verified against FEKO, and the input impedance of a thin-wire dipole is compared in [244•]. The agreement is almost excellent for electrically small and medium size structures ($ka < 10$), but it starts to vary for higher frequencies.

The in-house MeshGen mesh generator written by Jan Eichler can be used to discretize the structure properly [245•]. It is based on the distmesh package [246], which utilizes Delaunay triangulation [247]. All the antenna primitives are meshed subsequently. For further information, e.g. on the role of discretization in CM decomposition, see [245•]. Alternatively, the mesh can be imported from commercial softwares, e.g. Comsol Multiphysics [248] or FEKO.

The TCMapp CM analyser was developed during the author's Ph.D. studies [239•]. To date, the generalized Schur decomposition and the implicitly restarted Arnoldi method are available in TCMapp for impedance matrix factorization. After CM decomposition, a tracking procedure has to be performed. Several tracking methods are available, including the simple correlation method and the adaptive method described above [237•]. The slight asymmetry of the impedance matrix causes serious problems for CM decomposition (the standard symmetrization does not take quantifiable effect). Many pre-processing and post-processing routines are included in the TCMapp package, e.g. the mesh quality analyser, the near-field and far-field calculation, the evaluation of the radiation efficiency and the Q factor, and associated graphical plotting, see [249•] and also [239•]. TCMapp software was extensively used, e.g. for investigating the patch behaviour above the infinite ground plane, L-probe feeding and the design of a circularly polarized patch antenna [250•]. All studies in [234•] were also performed in TCMapp.

3.3 Superposition of Modal Quantities

Instead of simulating the entire antenna system (geometry, materials and feeding), only the PEC motive with no excitation is subjected to CM decomposition. The effect of different feeding scenarios and metallizations can be considered afterwards, during the post-processing step.

This approach is extremely fast, since the full-wave simulation runs only once. The feeding network can then easily be optimized. Thus these methods answer not only the common question "What is the overall value ...", but – more importantly – the question "What might be the overall value ...". Two novel methods are presented below, one for calculating the modal efficiencies, and the other for calculating the modal Q factors.

3.3.1 Modal Radiation Efficiency

If the electrical dimensions are small and a complex geometry is used, the radiation efficiency can be significantly decreased by closely situated out-of-phase currents of high amplitude [172]. This is often due to one specific mode. A proper understanding of modal radiation efficiency therefore makes it possible to optimize the feeding network and, for example, to eliminate a problematic (low-efficiency) mode.

A very simple method [251•] that precluded modal superposition was replaced by an advanced method, which is described in [252•] and [253•]. The key assumption here is that the current density distribution is almost the same for surface currents flowing on a PEC body and for volumetric currents flowing in a lossy body. Only simple model of the skin-effect [87] was utilized, thus the metallization is assumed to be thick enough to suppress the current wave (in practice, this assumption is usually fulfilled).

The approximative method was successfully tested against FEKO (only overall efficiency could be tested, since FEKO does not contain a calculation of modal radiation efficiency). The worst error was less than 1% for good conductors (copper, aluminium) and for standard metallization thickness (10-50 μm).

Since no modification of CM is needed, and since the feeding can be considered in post-processing, the definition of radiation efficiency can be generalized so that the modal efficiencies can be calculated, see [253•] for an exact derivation. The superposition is performed thanks to the so-called beta coupling matrix which concentrates all effects of feeding (various positions, amplitudes and phases). It is interesting that mutual lost powers between different modes occur, and potentially take negative values (the overall lost power is always positive).

3.3.2 Modal Quality Factor

While Harrington's definition of characteristic modal Q [80] is widely known, it is based solely on the behaviour of the associated eigenvalue. It is also known that this definition is correct only near to the natural resonances. A new definition of the modal radiation Q factor was therefore established, utilizing orthogonal and superposition relations of the characteristic modes and expressions derived in [129]. An exact definition, implementation and verification on examples is presented in [254•]. There is also a demonstration of how to obtain lower Q of a given meander dipole by synthesizing the feeding network via the heuristic PSO algorithm [212]. Another example is presented in [255•].

From the practical point of view, the expressions contains a singularity which has to be carefully treated [256], and care must be taken to include a sufficient number of modes since even poorly excited modes may store a considerable amount of energy. As in the case of modal efficiency, the mutual energies are nonzero, and this implies that the CM

equivalent network should be extended towards the mutual capacitance and inductance between all resonant RLC blocks.

3.4 Q factor and Stored Electromagnetic Energy

A recent breakthrough in the investigation of stored energy [129] has stimulated new research in this area. The expressions analytically derived in [129] were tested in [257•] on the example of two closely spaced dipoles, see [258•]. It was noticed [259•] that the whole derivation, as presented in [129], can be significantly simplified by an *ad hoc* assumption and by utilizing the dynamic potentials [99]. Thus, all resulting terms are finite, and no extraction technique is needed [257•].

However, it was observed [158] that under certain conditions, e.g. for an electrically long cylinder with dominant TM mode, the stored energy [129] can be negative. Further research will investigate whether the definition is incorrect or the currents are practically unfeasible[1] [235]. Another interesting but as yet unsolved question is whether these energies are invariant under the Lorenz gauge (similarly to the case of Carpenter's relations [146–148]).

3.4.1 Stored Energy in a Non-Stationary Electromagnetic Field

To resolve problems with the definition of stored energy, a new scheme for calculating it is proposed in [3•], yielding the true values for stored energy (at least for the tested structures). By definition, only positive values occur. The method is developed in the time domain, in which the circuit under study is brought to the steady state by a power supply which is switched off after one period. Two simulation runs are in principle necessary in a time domain simulator (e.g. in CST-MWS), and two runs are then needed during a post-processing step in which the currents recorded in the simulator are evaluated. In the first post-processing run, the transient current is used. Then, in the second run, the current is frozen right after the power supply is switched off. The difference between these two runs can extract the radiated energy. For a detailed description and discussion, see [3•]. The universality of this approach reopens the question about the energy stored in dispersive media [144].

3.4.2 Source Concept of the Q_Z Factor

The impedance Q factor, denoted as Q_Z, is based on the assumption that a small antenna can be modelled by a single resonant circuit [83]. Then Q_Z can be expressed from the frequency derivation of an input impedance near the resonance [83]. Q_Z is easy to evaluate, and is indeed widely used in practice. Interestingly, it has been shown that, thanks to the complex power balance theorem and the potential definition of electromagnetic fields [99], the original circuit definition of Q_Z can be expressed solely by the currents flowing on an antenna. For a detailed derivation, see [244•] or [260•].

[1] The problem of a static mode on a tall cylinder has been treated analytically in the spectral domain, and the results were numerically compared with the eigennumber of the static mode and with spatial integration of energetic expressions [129]. The results were in perfect agreement. Note that none of these approaches take the real excitation into consideration.

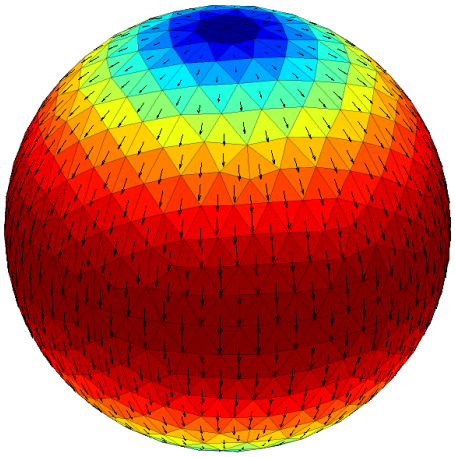

Figure 3.1: Normalized current distribution of the characteristic mode of a sphere PEC shell. The mode has the same shape as the dominant spherical TE mode.

Alternatively, Q_Z can be formulated as a function of several energetic terms, which are discussed in [244•]. Some of them emerge in the definition of the classical Q, compare [129, 261] with [3•]. In other words, classical Q and Q_Z differ, which is explicitly proved in [3•]. The difference is mainly due to the presence (or absence) of explicit derivative terms. This raises the question, whether the quality factor should be defined with or without terms containing the differentiation with respect to the angular frequency.

Since the proportionality between Q (Q_Z) and FBW should be unique, only one of these Q factors can be correct (or none of them). The three different definitions of Q are therefore tested [3•] on two non-trivial RLC circuits, which are analytically worked out by Cauchy's residue theorem and contour integration [262]. Surprisingly, better proportionality of Q_Z to FBW than of Q to FBW is questioned[2].

It is also demonstrated that the Q_Z formulation can be reduced in the vicinity of a resonance to a differentiation of reactance only [263•]. This is in accordance with observations made in [244•].

3.4.3 Fundamental Bounds of the Q_Z Factor

The newly derived source current formulation of Q_Z [244•] allows an analytical solution of Q_Z of any geometry for which the vector wave function is separable [95]. The technique is described in [236•] and [264•] on examples of dominant TM and TE spherical modes, see Fig. 3.1. The whole derivation is analytical, without any approximations. Exactly the same series expansion as for the limits of classical Q in [121] and [124] are found for $ka < 0.5$.

These results are important from both the theoretical and the practical point of view. Since Q_Z is often used in practice for estimating FBW, it is important to know its fundamental lower bounds (which, as has been shown, are in accordance with the lower bounds of Q).

[2]It can be proven on an example of a non-trivial RLC circuit that Q and Q_Z differ, and only Q_Z is proportional to FBW. This observation is yet to be published.

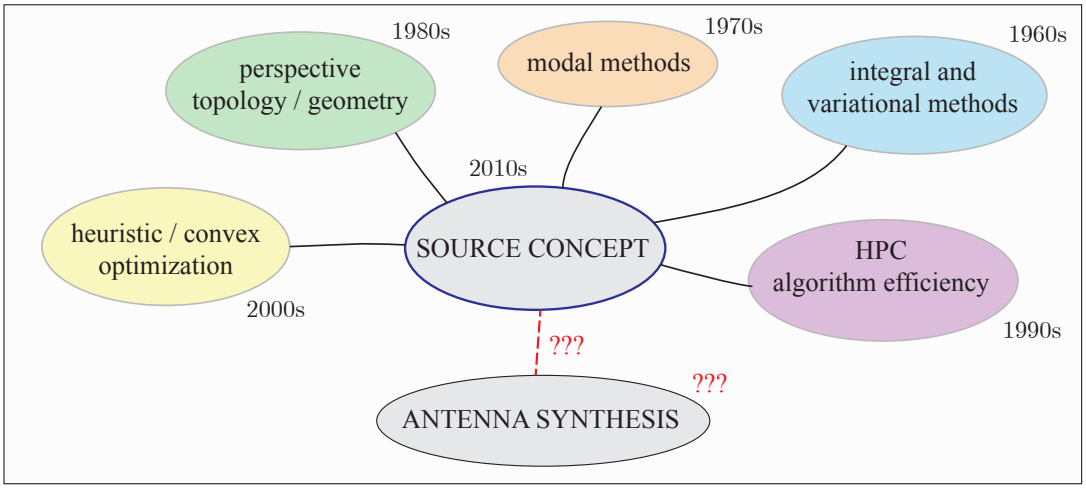

Figure 3.2: The source concept as a summary of a wide range of fields of mathematics, physics and engineering, which have to be properly combined. As depicted, it would also necessarily involve novel advanced techniques such as convex optimization of high performance computing.

3.5 Small Antenna Design

3.5.1 Source Concept Optimization, Utilization of Modal Methods

The expression "source concept" is used throughout this thesis. It labels a contemporary approach to antenna design, which exclusively utilizes source currents as an input or an output for subsequent numerical methods. A wide range of approaches need to be properly combined in order to establish the source concept, see Fig. 3.2. Some undisputed advantages of this approach have already been mentioned, or are clearly explained in the appended publications.

Optimization routines are an important step towards automatized design. For this purpose, the PSOptimizer PSO algorithm [212] was implemented in Matlab, see [265•]. The possible input is not restricted to a particular problem (i.e. any m-file containing a reasonable fitness function can be optimized), and the absorbing, reflecting and invisible boundary condition [220] are included. An invisible wall is greatly preferred since it saves computation time. The PSOptimizer was particularly tested in [266•].

The SOMA algorithm was coded in [267∗], using a set of novel walls. A new updating strategy was proposed, and was successfully tested on examples of some highly degenerate functions.

Note that the practical usage of any optimization routine is strictly limited by the No-free-lunch theorem [268, 269]. Mainly for this reason, some efficient hybrids were developed. A combination of the Nelder-Mead simplex method [157] and PSO was designed in [270∗]. The good global exploring property of a particle swarm is combined with the fast convergence of a simplex method. Formally, the motion equation of the PSO was extended by one additional term, which describes the behaviour of the simplex. Thus, three empirical parameters have to be properly set up before optimization starts.

All the algorithms mentioned above are single-objective optimizations [209]. This

means, that the fitness function has to be aggregated into a function of only one scalar variable [209]. However, the complete Pareto-optimal front is often needed. Multi-objective optimization (MOO) was employed for this purpose. MOO is based on a hybrid of PSO [271,272] and SOMA [226]. Elitism is utilized together with an external archive [210], which is adaptively maintained. The MOO algorithm is currently being tested on an example of an array of dipoles.

A complete framework consisting of a cavity model in Comsol Multiphysis, the IFS generator and the PSOptimizer is presented in [249•]. Its applicability for antenna design is documented on a example of fractal antenna, which was optimized and then fabricated [249•]. Another example can be found in [267∗], in which the in-house SOMA was used together with CM analysis to find an optimal shape of for a small antenna.

3.5.2 Influence of the Fractal Geometry on Radiation Properties

Dealing with modern small antennas, one quickly note that any geometry with a highly perturbed shape can exhibit resonances at low frequencies with respect to its size [182]. As a special case, fractal geometry [189] was utilized.

It order to study fractal structures, the IFSMaker IFS generator was implemented [273•]. The only inputs are: an initial set of points, generating transformations and required iterations. Fractal patch antennas were then studied in [234•] and [250•] via CM decomposition. The effects of fractal iteration, type of mode and height above the ground plane were investigated. Modal resonant properties of microstrip antennas are studied in [274•]. Note that optimization of the IFS does not produce random segment antennas, which have been criticized. They have still the prescribed topology, and only the geometry is optimized, see Fig. 3.3.

3.5.3 Acceleration Using High Performance Computing

Modal methods like generalized Schur decomposition are typically extremely time-consuming, and a great amount of memory and disk space is required. This is the ultimate price to be paid for the deeper physical insight provided by modal methods. Two ways can be used to reduce the computational effort. The first leads to alternative algorithms (usually iterative algorithms like the Arnoldi method [14]), while the second utilizes High Performance Computing. HPC usually means a simultaneous calculation on more than one CPU thread, more processors, more computers in a cluster, or even – especially in the last decade – calculation on GPU cards [275].

To accelerate the code in Matlab, Parallel Computing Toolbox (PCT, [276]), Distributive Computing Server (DCS, [277]) and the Jacket package [278] were used. PCT allows the use 8 or less cores simultaneously in parallel mode on a single machine[3]. The distributive Computing Server allows the use of significantly more threads (from tens to thousands). However, one has to start the scheduler (the simplest scheduler is the job manager), then prepare a job that contains individual tasks (e.g. decomposition for the selected frequency sample). The network latency should also be considered. The Jacket package enables GPU computing in high-level Matlab code.

[3]The limit has been improved to 12 cores from Matlab 2013a.

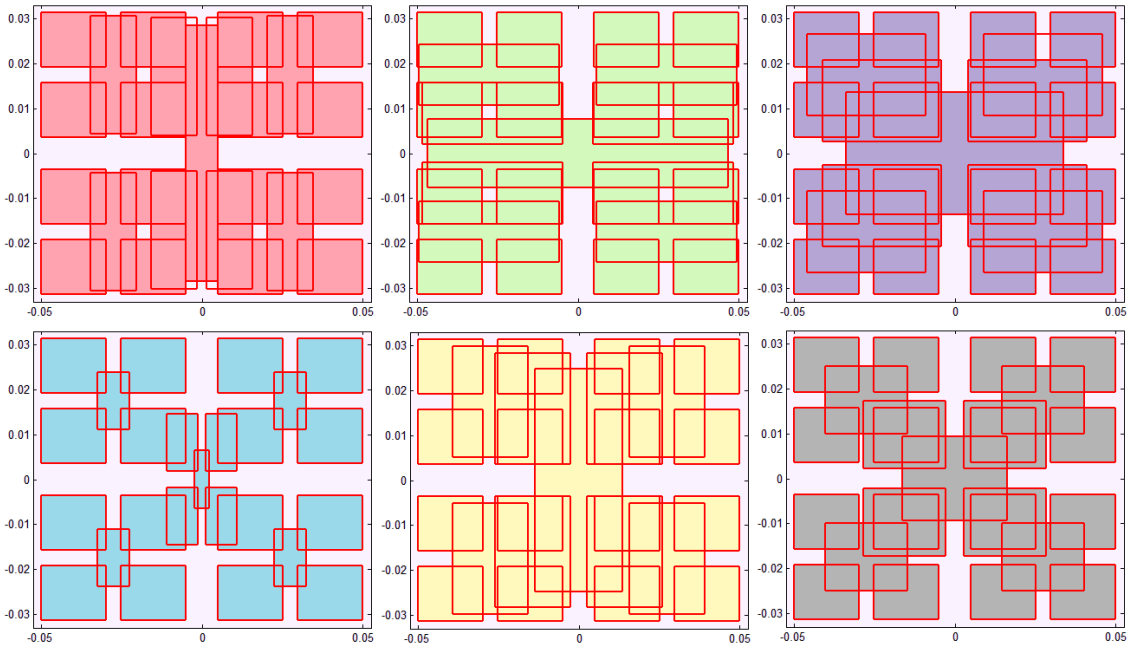

Figure 3.3: Six different particle swarm optimization agents generated by iterated function system radiators. These shapes are candidates for electrically small antenna. The geometry is created in the IFSMaker generator, properly meshed in the MeshGen and then evaluated in the TCMapp characteristic mode analyser. The radiation Q factor and the resonant frequency are then calculated. All steps are performed via in-house tools inside an optimization loop. The full-wave calculation and the post-processing are accelerated on CPU(s) and GPU(s), respectively.

Typically, it is better to accelerate complex tasks (matrix inversion, factorization) on CPU, while small atomized tasks are more suitable for GPU acceleration (e.g. massive numerical integrations performed during post-processing). The use of these packages is described in [279•], where the basic theory of HPC and benchmarking are also presented.

Together with other original Matlab functionality described in Sections 3.2-3.5, this completes the AtoM software (Antenna toolbox for Matlab), see Fig. 3.4 and Appendix A.2.

3.5.4 Practical Antenna Design, Manufacturing and Measuring

Finally, the ultimate benchmark for any physical theory must be to confront the predicted results with reality. This is especially true for theories postulated and the tools developed in this thesis.

The in-house simulations were systematically compared with modern full-wave simulators, e.g. CST-MWS [228], IE3D [280], FEKO [78] and Comsol Multiphysis [248], which are based on various numerical methods, e.g. MoM, FDTD, the Finite Integration Technique (FIT), and the Finite Element Method (FEM), see [242, 281, 282] for an extensive survey. This diversity minimizes all potential errors and makes it possible to choose the best simulator for a given purpose.

In addition, several antenna candidates were fabricated. A patch antenna with circular

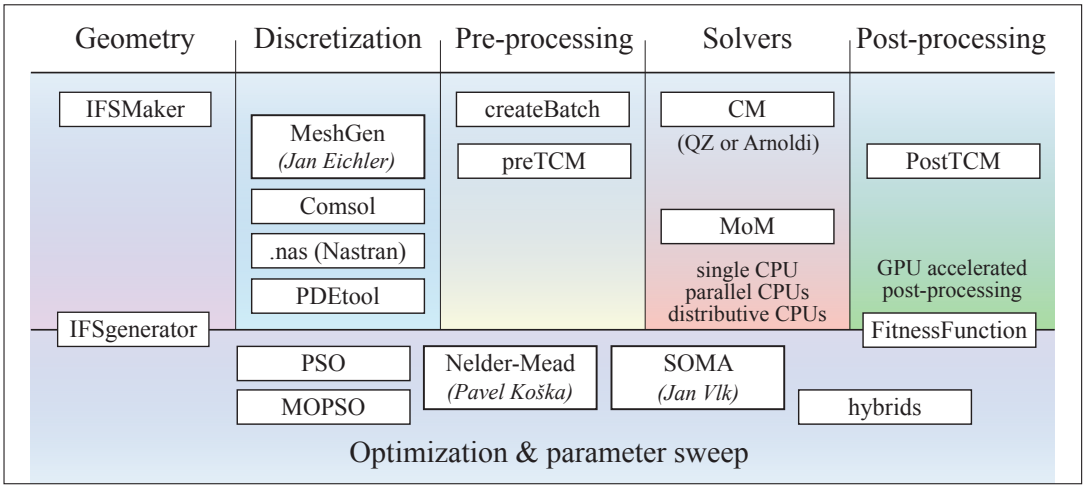

Figure 3.4: Tools already implemented that constitute the AtoM toolbox. Each box represents one functionality. All tools can be used together or separately.

polarization [283] is presented in [250•]. The dimensions of the antenna were found by modal analysis.

A dual-band antenna with a fractal motif was simulated both in the AtoM toolbox and in the CST-MWS commercial package [284•]. The fabricated antenna was measured in an anechoic chamber, see [284•] or [285•] for VSWR and radiation patterns.

Other potentialities of CM decomposition are presented in [4•]. The two-element array structure is designed for polarization diversity in UMTS mobile phones.

Finally, a full wavelength loop minimized by modal analysis of U-notches was manufactured and measured [267∗], see Fig. 3.5.

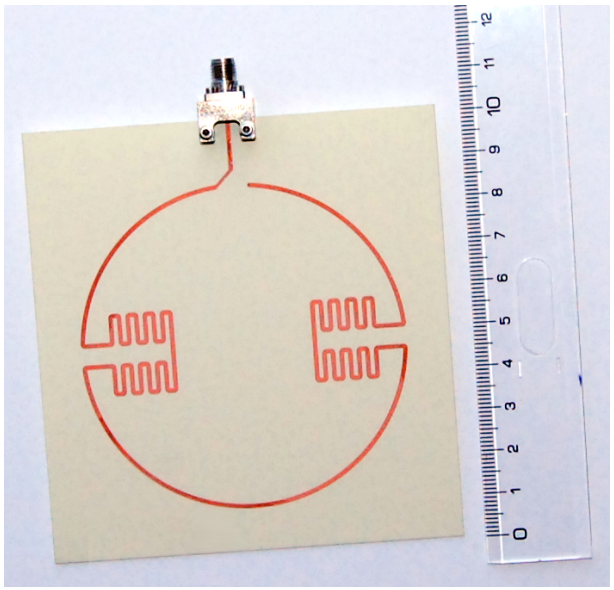

Figure 3.5: A manufactured sample of a dual-band antenna. The original full-wavelength loop was miniaturized using CM analysis and optimization techniques. The simulated values of Q_Z are 14.77 (first band) and 21.48 (second band), the measured values are 15.48 and 24.42, respectively. The antenna operates at $ka = 0.7$ (first band).

Chapter 4

Conclusion

4.1 What Has Already Been Done

This thesis dealt with an analysis and a synthesis of small antennas, and draw links between each topic and papers that have been published (or submitted). All objectives scheduled at the beginning of Section 3 have been solved, using various techniques involving analytical, algebraic and numerical mathematics, physics and computational methods.

The most important contributions of the thesis are:

- novel tracking method for CM analysis has been introduced,
- the adaptive frequency solver for CM decomposition has been developed,
- the "residual mode" has been explain and compensated,
- the dominant CM has been approximated by an analytic function, and size reduction has been achieved by modal optimization,
- the modal radiation efficiencies and their superposition formula have been derived,
- the modal radiation Q factors and their superposition formula have been derived,
- the source current definition of Q_Z has been derived,
- Q_Z of the dominant spherical TM and TE modes has been determined,
- stored electromagnetic energy has been evaluated in the time domain,
- PSO, SOMA and the Nelder-Mead simplex optimization methods have been implemented, and have been generalized towards a hybrid method with new boundary conditions, and the MOO PSO-SOMA framework with an adaptive external archive,
- a versatile IFS generator (IFSMaker), a CM analyzer (TCMapp) and relating post-processing have been developed, AtoM software have been completed,
- high performance computing in Matlab has been utilized,
- several small antennas of various geometries have been manufactured and measured.

It is essential not only to point out here what has already done, but also to indicate what can be done in the future. This plot is provided in two steps – near-term and long-term goals.

4.2 What Should be Done in the Near Future

Since it has been shown that the characteristic mode can be replaced by an approximative but analytical function, some basic structures may be investigated in details. For example, a loop miniaturized by two U-notches can be closely studied without the need to employ a time-consuming full-wave method. To date, very little is known about characteristic mode decomposition in the time domain, which may bring new applications. Implementing periodic boundary condition into characteristic modes would help with the design of frequency selective surfaces. Since spherical modes are known analytically, it may be useful to calculate a multipole expansion of characteristic radiation patterns into spherical modes. Attention should be paid to the utilization of multi-objective optimization for analysing modal quantities.

Although some progress has been made, the true shape of the dominant characteristic mode on a dipole is still not known. The related mathematics is extremely involved, making this task a true challenge.

The AtoM software needs further improvements. Utilization of Pearson's correlation may perfect the tracking procedure. The method of moments code has to be extended so that dielectrics can be involved. High-order basis functions and the utilization of a magnetic field integral equation together with electric field integral equation may significantly improve the accuracy. An analytical evaluation of potential integrals should be considered to avoid a non-symmetric impedance matrix. Convex optimization needs to be incorporated into the AtoM software, e.g. by using a third-party package. The concept of polarizability promises to solve many problems of small antenna design, and it should therefore be integrated into the source concept. This has only been partially done up to now thanks to the quasi-static calculation of polarizability, which is based on currents obtained from the method of moments.

Structural decomposition, already used in mechanical engineering, has somehow relation to modal methods. It assumes that the radiating structure can be separated into several parts which are connected through the matrix of coupling coefficients. Under certain conditions, these separated parts and their parameters can be evaluated independently. Note that the source concept offers a general principle that can be used in relatively distant fields of electrodynamics, e.g. for seeking new split ring resonator geometries.

The issue of negative energy need to be rigorously handled. The question of the invariance of the Vandenbosch expressions need to be addressed, in order to confirm whether they are correct. The novel technique presented here for calculating the stored energy should be simplified (both formally and numerically) and transformed to the spectral domain.

It is important to resolve what Q is directly proportional to FBW. A single formulation should be used consistently, and various definitions of Q should be unified. The relationship between the modal Q factors and the lower available Q should be closely investigated, and the hypothesis that the lower available Q is an infimum of modal Q factors needs to be

proven or refuted.

Implementation of the source definition of the Q_Z factor into the convex optimization may prevent difficulties with the potentially negative stored energy value. The source definition of Q_Z should be generalized for dispersive media. This will significantly simplify the present investigation of high-dispersive structures. It may also be of interest to determine the fundamental lower bounds of the Q_Z factor for an ellipsoid or for any other separable geometry. In comparison with the bounds for a sphere, these limits can be more predicative for common antennas such as dipole.

The true role of the Foster theorem for radiating structures should finally be explained.

4.3 A Long-term Vision

A complete synthesis is nearly impossible, but it is possible to make partially synthesis, with some simplifications. Hypothetically, the source concept, which combines modal and structural decomposition, optimization and other novel methods, e.g. polarizability may solve the problem of synthesis without any restrictions. This may be true at least for certain structures.

Another tedious problem is that antenna characteristics change significantly in the presence of a complex environment. This causes principal difficulties e.g. for analysing on-body wearable antennas or artificial materials. A major issue is how to evaluate the stored electromagnetic energy in this case. This is an as yet unsolved problem in physics. A recently-developed method could be a promising candidate for the evaluation scheme.

Finally, little is analytically known about source current distributions, especially in the case of fractal structures. Today, the wave equation cannot be solved analytically (and, of course, also not numerically) for any fractal structure. Collocation fractal electrodynamics is sometimes used, and it is argued that electromagnetism as a whole should be generalized to noninteger integro-differential calculus. However, only the future will decide whether fractals can be treated effectively in electrodynamics. This ambitious goal is more mathematical than physical. It is therefore necessary to stay prepared for new findings that can be utilized to promote developments in fractal antenna design.

All in all, it is clear that the book of electrically small antennas is still wide open ...

Bibliography

[1] J. C. Maxwell, *A Treatise on Electricity and Magnetism.* Clarendon Press, 1873, vol. 1.

[2] ——, *A Treatise on Electricity and Magnetism.* Clarendon Press, 1873, vol. 2.

[3] M. Capek, L. Jelinek, G. A. E. Vandenbosch, and P. Hazdra, "A scheme for stored energy evaluation and a comparison with contemporary techniques," *IEEE Trans. Antennas Propag.*, 2014, submitted (arXiv:1309.6122).

[4] P. Hamouz, P. Hazdra, M. Capek, J. Eichler, A. Diallo, F. Ferrero, and C. Luxey, "Polarization diversity in UMTS mobile phones analyzed with characteristic modes," *IEEE Antennas Wireless Propag. Lett.*, 2014, submitted.

[5] R. C. Hansen, *Electrically Small, Superdirective, and Superconductive Antennas.* John Wiley, 2006.

[6] J. L. Volakis, C. Chen, and K. Fujimoto, *Small Antennas: Miniaturization Techniques & Applications.* McGraw-Hill, 2010.

[7] K. Fujimoto and H. Morishita, *Modern Small Antennas.* Cambridge University Press, 2013.

[8] R. W. P. King, *The Theory of Linear Antennas.* Harvard University Press, 1956.

[9] F. Gross, Ed., *Frontiers in Antennas: Next Generation Design & Engineering.* McGraw-Hill Professional, 2011.

[10] M. Gustafsson, C. Sohl, and G. Kristensson, "Illustrations of new physical bounds on linearly polarized antennas," *IEEE Trans. Antennas Propag.*, vol. 57, no. 5, pp. 1319–1327, May 2009.

[11] G. Bachman and L. Narici, *Functional Analysis.* Dover, 2000.

[12] N. I. Akhiezer and I. M. Glazman, *Theory of Linear Operators in Hilbert Space*, 2nd ed. Dover, 1993.

[13] N. Dunford and J. T. Schwartz, *Linear Operators I – General Theory.* Wiley, 1988.

[14] J. H. Wilkinson, *The Algebraic Eigenvalue Problem.* Oxford University Press, 1988.

[15] R. J. Garbacz and R. H. Turpin, "A generalized expansion for radiated and scattered fields," *IEEE Trans. Antennas Propag.*, vol. 19, no. 3, pp. 348–358, May 1971.

[16] R. F. Harrington and J. R. Mautz, "Theory of characteristic modes for conducting bodies," *IEEE Trans. Antennas Propag.*, vol. 19, no. 5, pp. 622–628, Sept. 1971.

[17] ——, "Computation of characteristic modes for conducting bodies," *IEEE Trans. Antennas Propag.*, vol. 19, no. 5, pp. 629–639, Sept. 1971.

[18] W. C. Gibson, *The Method of Moments in Electromagnetics*, 1st ed. Chapman and Hall/CRC, 2007.

[19] R. F. Harrington, *Field Computation by Moment Methods*. John Wiley - IEEE Press, 1993.

[20] R. Weinstock, *Calculus of Variations*. Dover, 1974.

[21] H. Sagan, *Boundary and Eigenvalue Problems in Mathematical Physics*. Dover, 1989.

[22] E. Newman, "Small antenna location synthesis using characteristic modes," *IEEE Trans. Antennas Propag.*, vol. 27, no. 4, pp. 530–531, July 1979.

[23] M. Cabedo-Fabres, "Systematic design of antennas using the theory of characteristic modes," Ph.D. dissertation, UPV, Feb. 2007.

[24] B. D. Raines and R. G. Rojas, "Wideband characteristic mode tracking," *IEEE Trans. Antennas Propag.*, vol. 60, no. 7, pp. 3537–3541, July 2012.

[25] ——, "Wideband tracking of characteristic modes," in *Proceedings of the 5th European Conference on Antennas and Propagation (EUCAP)*, Rome, Italy, April 2011.

[26] D. J. Ludick, U. Jakobus, and M. Vogel, "A tracking algorithm for the eigenvectors calculated with characteristic mode analysis," in *Proceedings of the 8th European Conference on Antennas and Propagation (EUCAP)*, 2014, pp. 629–632.

[27] T. Tanaka, "Fast generalized eigenvector tracking based on the power method," *IEEE Signal Processing Letters*, vol. 16, no. 11, pp. 969–972, Nov. 2009.

[28] R. F. Harrington, J. R. Mautz, and Y. Chang, "Characteristic modes for dielectric and magnetic bodies," *IEEE Trans. Antennas Propag.*, vol. 20, no. 2, pp. 194–198, March 1972.

[29] R. F. Harrington and J. R. Mautz, "Characteristic modes for aperture problems," *IEEE Trans. Microwave Theory Tech.*, vol. 33, no. 6, pp. 500–505, June 1985.

[30] Y. Leviatan, "Low-frequency characteristic modes for aperture coupling problems," *IEEE Transactions on Microwave Theory and Techniques*, vol. 34, no. 11, pp. 1208–1213, Nov. 1986.

[31] R. J. Garbacz, "A generalized expansion for radiated and scattered fields," Ph.D. dissertation, The Ohio State Univ., 1968.

[32] E. Safin, R. Martens, and D. Manteuffel, "Modal source reconstruction based on radiated far-field for antenna design," in *Proc. 6th European Conference on Antennas and Propagation (EuCAP)*, 2012, pp. 1645–1649.

[33] E. Antonino-Daviu, "Analysis and design of antennas for wireless communications using modal methods," Ph.D. dissertation, UPV, Feb. 2008.

[34] B. A. Austin and K. P. Murray, "The application of characteristic-mode techniques to vehicle-mounted nvis antennas," *IEEE Antennas Propag. Magazine*, vol. 40, pp. 7–21, Feb. 1998.

[35] M. Cabedo-Fabres, E. Antonino-Daviu, A. Valero-Nogueira, and M. F. Bataller, "The theory of characteristic modes revisited: A contribution to the design of antennas for modern applications," *IEEE Antennas Propag. Magazine*, vol. 49, no. 5, pp. 52–68, Oct. 2007.

[36] J. Ethier and D. A. McNamara, "Modal significance measure in characteristic mode analysis of radiating structures," *Electronics Letters*, vol. 46, no. 2, pp. 107–108, Jan. 2010.

[37] R. Mittra, Ed., *Numerical and Asymptotic Techniques in Electromagnetics*, ser. Topics in Applied Physics. Springer - Verlag, 1975, vol. 3.

[38] J. G. Van Bladel, *Electromagnetic Fields*, 2nd ed. John Wiley - IEEE Press, 2007.

[39] P. Hazdra and P. Hamouz, "On the modal superposition lying under the MoM matrix equations," *Radioengineering*, vol. 17, no. 3, pp. 42–46, Sept. 2008.

[40] E. Safin and D. Manteuffel, "Reconstruction of the characteristic modes on an antenna based on the radiated far field," *IEEE Trans. Antennas Propag.*, vol. 61, no. 6, pp. 2964–2971, June 2013.

[41] J. J. Adams and J. T. Bernhard, "Broadband equivalent circuit models for antenna impedances and fields using characteristic modes," *IEEE Trans. Antennas Propag.*, vol. 61, no. 8, pp. 3985–3994, Aug. 2013.

[42] M. Cabedo-Fabres, E. Antonino-Daviu, D. S. Escuderos, and V. M. Rodrigo-Penarrocha, "On the application of characteristic modes for the analysis of large scale antenna problems," in *Proceedings of the 2nd European Conference on Antennas and Propagation (EUCAP)*, Edinburgh, UK, Nov. 2007.

[43] A. Andujar, J. Anguera, and C. Puente, "Ground plane boosters as a compact antenna technology for wireless handheld devices," *IEEE Trans. Antennas Propag.*, vol. 59, no. 5, pp. 1668–1677, May 2011.

[44] R. Martens, E. Safin, and D. Manteuffel, "Inductive and capacitive excitation of the characteristic modes of small terminals," in *Loughborough Antennas & Propagation Conference*, Nov. 2011, pp. 1–4.

[45] M. Cabedo-Fabres, E. Antonino-Daviu, A. Valero-Nogueira, and M. Ferrando-Bataller, "Optimization of the polarization of reflectarrays using characteristic modes," in *IEEE Antennas and Propagation Society International Symposium*, vol. 1, June 2004, pp. 13–16.

[46] Y. Chen and C.-F. Wang, "Synthesis of reactively controlled antenna arrays using characteristic modes and de algorithm," *IEEE Antennas Wireless Propag. Lett.*, vol. 11, pp. 385–388, 2012.

[47] J. Ethier, M. Chaharmir, J. Shaker, and D. Lee, "Development of novel low-cost reflectarrays," *IEEE Antennas Propag. Magazine*, vol. 54, no. 3, pp. 277–287, June 2012.

[48] S. Wang and H. Arai, "Analysis of an optimized notch array antenna by using the theory of characteristic modes," *IEEE Antennas Wireless Propag. Lett.*, vol. 13, pp. 253–256, 2014.

[49] J. Ethier and D. McNamara, "Multiband antenna synthesis using characteristic mode indicators as an objective function for optimization," in *IEEE International Conference on Wireless Information Technology and Systems (ICWITS)*, Aug 2010, pp. 1–4.

[50] E. Antonino-Daviu, M. Cabedo-Fabres, M. Gallo, M. F. Bataller, and M. Bozzetti, "Design of a multimode MIMO antenna using characteristic modes," in *Proceedings of the 3rd European Conference on Antennas and Propagation (EUCAP)*, Berlin, Germany, March 2009, pp. 1840–1844.

[51] A. Araghi and G. Dadashzadeh, "Oriented design of an antenna for mimo applications using theory of characteristic modes," *IEEE Antennas Wireless Propag. Lett.*, vol. 11, pp. 1140–1143, 2012.

[52] J. Ethier and D. McNamara, "The use of generalized characteristic modes in the design of mimo antennas," *IEEE Transactions on Magnetics*, vol. 45, no. 3, pp. 1124–1127, March 2009.

[53] ——, "An interpretation of mode-decoupled MIMO antennas in terms of characteristic port modes," *IEEE Transactions on Magnetics*, vol. 45, no. 3, pp. 1128–1131, March 2009.

[54] A. Krewski, W. Schroeder, and K. Solbach, "Bandwidth limitations and optimum low-band LTE MIMO antenna placement in mobile terminals using modal analysis," in *Proceedings of the 5th European Conference on Antennas and Propagation (EUCAP)*, April 2011, pp. 142–146.

[55] H. Li, Z. Miers, and B. K. Lau, "Generating multiple characteristic modes below 1GHz in small terminals for MIMO antenna design," in *IEEE Antennas and Propagation Society International Symposium (APS/URSI)*, July 2013, pp. 180–181.

[56] R. Martens, J. Holopainen, E. Safin, J. Ilvonen, and D. Manteuffel, "Optimal dual-antenna design in a small terminal multiantenna system," *IEEE Antennas Wireless Propag. Lett.*, vol. 12, pp. 1700–1703, 2013.

[57] Y. Chen and C.-F. Wang, "Synthesis of platform integrated antennas for reconfigurable radiation patterns using the theory of characteristic modes," in *In proceedings of 10th International Symposium on Antennas, Propagation & EM Theory*, Oct. 2012, pp. 281–285.

[58] ——, "Electrically small UAV antenna design using characteristic modes," *IEEE Trans. Antennas Propag.*, vol. 62, no. 2, pp. 535–545, Feb. 2014.

[59] J. J. Adams and J. T. Bernhard, "A modal approach to tuning and bandwidth enhancement of an electrically small antenna," *IEEE Trans. Antennas Propag.*, vol. 59, no. 4, pp. 1085–1092, April 2011.

[60] ——, "Tuning method for a new electrically small antenna with low Q," *IEEE Antennas Wireless Propag. Lett.*, vol. 8, pp. 303–306, 2009.

[61] F. Gallee, T. Bernabeu, M. Cabedo-Fabres, E. Daviu, and A. Nogueira, "Application of the theory of characteristic modes to the design of compact metallic strip antenna with multilayer technology (LTCC)," in *Proceedings of the 7th European Conference on Antennas and Propagation (EUCAP)*, April 2013, pp. 1891–1895.

[62] M. Hilbert, M. Tilston, and K. Balmain, "Resonance phenomena of log-periodic antennas: characteristic-mode analysis," *IEEE Trans. Antennas Propag.*, vol. 37, no. 10, pp. 1224–1234, Oct, 1989.

[63] K. Obeidat, B. Raines, R. Rojas, and B. Strojny, "Design of frequency reconfigurable antennas using the theory of network characteristic modes," *IEEE Transactions on Antennas and Propagation*, vol. 58, no. 10, pp. 3106–3113, Oct. 2010.

[64] W. Wu, B.-Z. Wang, X.-S. Yang, and Y. Zhang, "A pattern-reconfigurable planar fractal antenna and its characteristic-mode analysis," *IEEE Antennas Propag. Magazine*, vol. 49, no. 3, pp. 68–75, June 2007.

[65] Y. Chen and C.-F. Wang, "Characteristic-mode-based improvement of circularly polarized U-slot and E-shaped patch antennas," *IEEE Antennas Wireless Propag. Lett.*, vol. 11, pp. 1474–1477, 2012.

[66] W. Wu and Y.-P. Zhang, "Analysis of ultra-wideband printed planar quasi-monopole antennas using the theory of characteristic modes," *IEEE Antennas Propag. Magazine*, vol. 52, no. 6, pp. 67–77, Dec. 2010.

[67] M. Sonkki, "Wideband and multi-element antennas for mobile applications," Ph.D. dissertation, University of Oulu, 2009.

[68] K. A. Obeidat, "Design methodology for wideband electrically small antennas based on the theory of characteristic modes," Ph.D. dissertation, Univ. of Illinois, 2010.

[69] J. J. Adams, "Characteristic modes for impedance matching and broadbanding of electrically small antennas," Ph.D. dissertation, Univ. of Illinois, 2011.

[70] B. D. Raines, "Systematic design of multiple antenna systems using characteristic modes," Ph.D. dissertation, The Ohio State Univ., 2011.

[71] B. T. Strojny, "Excitation and analysis of characteristic modes on complex antenna structures," Ph.D. dissertation, The Ohio State Univ., 2011.

[72] J. Ethier, "Antenna shape synthesis using characteristic mode concepts," Ph.D. dissertation, University of Ottawa, 2012.

[73] D. Liu, R. J. Garbacz, and D. M. Pozar, "Antenna synthesis and optimization using generalized characteristic modes," *IEEE Trans. Antennas Propag.*, vol. 38, no. 6, pp. 862–868, June 1990.

[74] N. N. Lebedev, *Special Functions & Their Applications*. Dover, 1972.

[75] C. Baum, "The singularity expansion method: Background and developments," *IEEE Antennas Propag. Society Newsletter*, vol. 28, no. 4, pp. 14–23, Aug. 1986.

[76] S. M. Mikki and Y. Antar, "A theory of antenna electromagnetic near field – part I," *IEEE Trans. Antennas Propag.*, vol. 59, no. 12, pp. 4691–4705, Dec. 2011.

[77] ——, "A theory of antenna electromagnetic near field – part II," *IEEE Trans. Antennas Propag.*, vol. 59, no. 12, pp. 4706–4724, Dec. 2011.

[78] EM Software & Systems-S.A. FEKO. [Online]. Available: www.feko.info

[79] P. Hazdra, "Planární fraktálové anténní struktury," Ph.D. dissertation, CTU in Prague, 2009, (in Czech).

[80] R. F. Harrington and J. R. Mautz, "Control of radar scattering by reactive loading," *IEEE Trans. Antennas Propag.*, vol. 20, no. 4, pp. 446–454, July 1972.

[81] G. W. Stewart and J. Sun, *Matrix Perturbation Theory*. Academic Press, 1990.

[82] J. Ethier and D. A. McNamara, "Through the looking glass: A characteristic mode view of electromagnetic modeling & design," in *ANTEM-AMEREM*, July 2010, pp. 1–4.

[83] A. D. Yaghjian and S. R. Best, "Impedance, bandwidth and Q of antennas," *IEEE Trans. Antennas Propag.*, vol. 53, no. 4, pp. 1298–1324, April 2005.

[84] C. A. Balanis, *Antenna Theory Analysis and Design*, 3rd ed. John Wiley, 2005.

[85] R. F. Harrington and J. R. Mautz, "Pattern synthesis for loaded N-port scatterers," *IEEE Trans. Antennas Propag.*, vol. 22, no. 2, pp. 184–190, March 1974.

[86] P. Hamouz, M. Polivka, and P. Hazdra, "Efficiency treatment of two closely spaced metal sheets by characteristic mode theory," in *Proceedings of the 3rd European Conference on Antennas and Propagation (EUCAP)*, March 2009, pp. 178–181.

[87] R. F. Harrington, *Time-Harmonic Electromagnetic Fields*, 2nd ed. John Wiley - IEEE Press, 2001.

[88] E. Safin and D. Manteuffel, "Influence of the impedance matching on the characteristic wave modes," in *Proceedings of the 8th European Conference on Antennas and Propagation (EUCAP)*, 2014, pp. 1323–1327.

[89] Z. G. Qian, W. C. Chew, and R. Suaya, "Generalized impedance boundary condition for conductor modeling in surface integral equation," *IEEE Trans. Microwave Theory Tech.*, vol. 55, no. 11, pp. 2354–2364, 2007.

[90] J. Ethier and D. McNamara, "Sub-structure characteristic mode concept for antenna shape synthesis," *Electronics Letters*, vol. 48, no. 9, pp. 471–472, April 2012.

[91] R. M. Fano, L. J. Chu, and R. B. Adler, *Electromagnetic Fields, Energy, and Forces.* MIT Press, 1968.

[92] H. A. Wheeler, "Fundamental limitations of small antennas," *Proc. of IRE*, vol. 35, no. 12, pp. 1479–1484, 1947.

[93] E. Hallen, *Electromagnetic Theory.* Chapman & Hall, 1962.

[94] S. A. Schelkunoff and H. T. Friis, *Antennas: Theory and Practice.* John Wiley, 1952.

[95] P. M. Morse and H. Feshbach, *Methods of Theoretical Physics.* McGraw-Hill, 1953.

[96] L. J. Chu, "Physical limitations of omni-directional antennas," *J. Appl. Phys.*, vol. 19, pp. 1163–1175, 1948.

[97] R. F. Harrington, "Effects of antenna size on gain, bandwidth, and efficiency," *J. Nat. Bur. Stand.*, vol. 64-D, pp. 1–12, 1960.

[98] R. E. Collin and S. Rothschild, "Evaluation of antenna Q," *IEEE Trans. Antennas Propag.*, vol. 12, pp. 23–27, 1964.

[99] J. D. Jackson, *Classical Electrodynamics*, 3rd ed. John Wiley, 1998.

[100] R. L. Fante, "Quality factor of general ideal antennas," *IEEE Trans. Antennas Propag.*, vol. 17, no. 2, pp. 151–157, 1969.

[101] C. A. Levis, "A reactance theorem for antennas," *Proc. of IRE*, vol. 45, no. 8, pp. 1128–1134, Aug. 1957.

[102] D. R. Rhodes, "A reactance theorem," *Proc. R. Soc. Lond. A.*, vol. 353, pp. 1–10, Feb. 1977.

[103] ——, "Observable stored energies of electromagnetic systems," *J. Franklin Inst.*, vol. 302, no. 3, pp. 225–237, 1976.

[104] ——, "On the stored energy of planar apertures," *IEEE Trans. Antennas Propag.*, vol. 14, no. 6, pp. 676–684, Nov. 1966.

[105] ——, "On the quality factor of strip and line source antennas and its relationship to superdirectivity ratio," *IEEE Trans. Antennas Propag.*, vol. 20, no. 3, pp. 318–325, May 1972.

[106] H. A. Wheeler, "Small antennas," *IEEE Trans. Antennas Propag.*, vol. 23, no. 4, pp. 462–469, July 1975.

[107] R. C. Hansen, "Fundamental limitations in antennas," *Proc. of IEEE*, vol. 69, no. 2, pp. 170–182, 1981.

[108] J. S. McLean, "A re-examination of the fundamental limits on the radiation Q of electrically small antennas," *IEEE Trans. Antennas Propag.*, vol. 44, no. 5, pp. 672–675, May 1996.

[109] H. D. Foltz and J. S. McLean, "Limits on the radiation Q of electrically small antennas restricted to oblong bounding regions," in *IEEE International Symposium on Antennas and Propagation*, vol. 4, July 1999, pp. 2702–2705.

[110] G. A. Thiele, P. T. Detweiler, and R. P. Penno, "On the lower bound of the radiation Q for electrically small antennas," *IEEE Trans. Antennas Propag.*, vol. 51, no. 6, pp. 1263–1269, June 2003.

[111] J. B. Andersen and S. Berntsen, "Comments to 'The Foster Reactance Theorem for Antennas and Radiation Q'," *IEEE Trans. Antennas Propag.*, vol. 55, no. 3, pp. 1013–1014, March 2007.

[112] S. R. Best, "The foster reactance theorem and quality factor for antennas," *IEEE Antennas Wireless Propag. Lett.*, vol. 3, no. 1, pp. 306–309, Dec. 2004.

[113] W. Geyi. (2014) On stored energies and radiation Q. arXiv:1403.3129. [Online]. Available: http://arxiv.org/abs/1403.3129

[114] Y. Geyi, "Physical limitation of antenna," *IEEE Trans. Antennas Propag.*, vol. 51, no. 8, pp. 2116–2123, Aug. 2003.

[115] ——, "A method for the evaluation of small antenna Q," *IEEE Trans. Antennas Propag.*, vol. 51, no. 8, pp. 2124–2129, Aug. 2003.

[116] W. Geyi, *Foundations of Applied Electrodynamics*. John Wiley, 2010.

[117] D. H. Kwon, "On the radiation Q and the gain of crossed electric and magnetic dipole moments," *IEEE Trans. Antennas Propag.*, vol. 53, no. 5, pp. 1981–1987, May 2005.

[118] ——, "Radiation Q and gain of TM and TE sources in phase-delayed rotated configurations," *IEEE Trans. Antennas Propag.*, vol. 56, no. 8, pp. 2783–2786, Aug. 2008.

[119] D. M. Grimes and C. A. Grimes, "Minimum Q of electrically small antennas: A critical review," *Microwave and Optical Technology Letters*, vol. 28, no. 3, pp. 172–177, Feb. 2001.

[120] J. C.-E. Sten and A. Hujanen, "Notes on the quality factor and bandwidth of radiating systems," *Electrical Engineering*, vol. 84, no. 4, pp. 189–195, May 2002.

[121] H. L. Thal, "New radiation Q limits for spherical wire antennas," *IEEE Trans. Antennas Propag.*, vol. 54, no. 10, pp. 2757–2763, Oct. 2006.

[122] ——, "Polarization, gain, and Q for small antennas," *IEEE Trans. Antennas Propag.*, vol. 59, no. 12, pp. 4844–4848, Dec. 2011.

[123] ——, "Q bounds for arbitrary small antennas: A circuit approach," *IEEE Trans. Antennas Propag.*, vol. 60, no. 7, pp. 3120–3128, July 2012.

[124] R. C. Hansen and R. E. Collin, "A new Chu formula for Q," *IEEE Antennas Propag. Magazine*, vol. 51, no. 5, pp. 38–41, Oct. 2009,

[125] S. R. Best, "The radiation properties of electrically small folded spherical helix antennas," *IEEE Trans. Antennas Propag.*, vol. 52, no. 4, pp. 953–960, April 2004.

[126] ——, "A discussion on the quality factor of impedance matched electrically small wire antennas," *IEEE Trans. Antennas Propag.*, vol. 53, no. 1, pp. 502–508, Jan. 2005.

[127] ——, "Low Q electrically small linear and elliptical polarized spherical dipole antennas," *IEEE Trans. Antennas Propag.*, vol. 53, no. 3, pp. 1047–1053, March 2005.

[128] S. R. Best and D. L. Hanna, "A performance comparison of fundamental small-antenna designs," *IEEE Antennas Propag. Magazine*, vol. 52, no. 1, pp. 47–70, Feb. 2010.

[129] G. A. E. Vandenbosch, "Reactive energies, impedance, and Q factor of radiating structures," *IEEE Trans. Antennas Propag.*, vol. 58, no. 4, pp. 1112–1127, Apr. 2010.

[130] ——, "Simple procedure to derive lower bounds for radiation Q of electrically small devices of arbitrary topology," *IEEE Trans. Antennas Propag.*, vol. 59, no. 6, pp. 2217–2225, June 2011.

[131] ——, "Explicit relation between volume and lower bound for Q for small dipole topologies," *IEEE Trans. Antennas Propag.*, vol. 60, no. 2, pp. 1147–1152, Feb. 2012.

[132] M. Gustafsson, C. Sohl, and G. Kristensson, "Physical limitations on antennas of arbitrary shape," *Proc. of Royal Soc. A: Math., Phys. and Engineering Sciences*, vol. 463, pp. 2589–2607, 2007.

[133] R. G. Newton, *Scattering Theory of Waves and Particles.* Dover, 1982.

[134] D. H. Kwon, "Bandwidth limitations of phased array elements," in *IEEE Antennas and Propagation Society International Symposium*, 2013, pp. 97–98.

[135] M. Shahpari, D. V. Thiel, and A. Lewis, "An investigation into the Gustafsson limit for small planar antennas using optimization," *IEEE Trans. Antennas Propag.*, vol. 62, no. 2, pp. 950–955, Feb. 2014.

[136] O. S. Kim, O. Breinbjerg, and A. D. Yaghjian, "Electrically small magnetic dipole antennas with quality factors approaching the Chu lower bound," *IEEE Trans. Antennas Propag.*, vol. 58, pp. 1898–1906, 2010.

[137] O. S. Kim, "Low-Q electrically small spherical magnetic dipole antennas," *IEEE Trans. Antennas Propag.*, vol. 58, no. 7, pp. 2210–2217, July 2010.

[138] O. S. Kim and O. Breinbjerg, "Reaching the Chu lower bound on Q with magnetic dipole antennas using a magnetic-coated PEC core;;," *IEEE Trans. Antennas Propag.*, vol. 59, no. 8, pp. 2799–2805, Aug. 2011.

[139] O. S. Kim, "Minimum Q electrically small antennas," *IEEE Trans. Antennas Propag.*, vol. 60, no. 8, pp. 3551–3558, Aug. 2012.

[140] H. R. Stuart and A. D. Yaghjian, "Approaching the lower bounds on Q for electrically small electric-dipole antennas using high permeability shells," *IEEE Trans. Antennas Propag.*, vol. 58, no. 12, pp. 3865–3872, December 2010.

[141] A. D. Yaghjian, M. Gustafsson, and B. L. G. Jonsson, "Minimum Q for lossy and losseless electrically small dipole antenna," *Progress In Electromagnetics Research*, vol. 143, pp. 641–673, 2013.

[142] ——, "Quality factor for lossy and lossless antennas," in *Proceedings of the 8th European Conference on Antennas and Propagation (EUCAP)*, 2014, pp. 3768–3771.

[143] Sievenpiper, D. F., et al., "Experimental validation of performance limits and design guidelines for small antennas," *IEEE Trans. Antennas Propag.*, vol. 60, no. 1, pp. 8–19, Jan. 2012.

[144] L. D. Landau, E. M. Lifshitz, and L. P. Pitaevskii, *Electrodynamics of Continuous Media*, 2nd ed. Butterworth-Heinemann, 1979.

[145] C. R. Cockrell, "Finite part electric and magnetic stored energies for plannar antennas," Langley Research Center, Hampton, Virginia, NASA 81955, Feb. 1981.

[146] C. J. Carpenter, "Electromagnetic energy and power in terms of charges and potentials instead of fields," *Proc. of IEE A*, vol. 136, no. 2, pp. 55–65, March 1989.

[147] V. G. Endean and C. J. Carpenter, "Comments to 'electromagnetic energy and power in terms of charges and potentials instead of fields'," *Proc. of IEE A*, vol. 139, no. 6, pp. 338–342, Nov. 1992.

[148] M. Uehara, J. E. Allen, and C. J. Carpenter, "Comments to 'electromagnetic energy and power in terms of charges and potentials instead of fields'," *Proc. of IEE A*, vol. 139, no. 1, pp. 42–44, Jan. 1992.

[149] C. A. Grimes and D. M. Grimes, "The Poynting theorems and the potential for electrically small antennas," in *IEEE Proceedings of Aerospace Conference*, vol. 3, February 1997, pp. 161–176.

[150] D. J. White and P. L. Overfelt, "Poynting's theorems and their relationship to antenna power, Q, and bandwidth," Naval Air Warfare Center Weapons Division, China Lake, CA, Tech. Rep. NAWCWPNS 8419, 1999.

[151] A. Shlivinski and E. Heyman, "Time-domain near-field analysis of short-pulse antennas - part I: Spherical wave (multipole) expansion," *IEEE Trans. Antennas Propag.*, vol. 47, no. 2, pp. 271–279, Feb. 1999.

[152] ——, "Time-domain near-field analysis of short-pulse antennas - part II: Reactive energy and the antenna Q," *IEEE Trans. Antennas Propag.*, vol. 47, no. 2, pp. 280–286, Feb. 1999.

[153] S. Collardey, A. Sharaiha, and K. Mahdjoubi, "Calculation of small antennas quality factor using FDTD method," *IEEE Antennas Wireless Propag. Lett.*, vol. 5, pp. 191–194, 2006.

[154] ——, "Evaluation of antenna radiation Q using FDTD method," *Electronics Letters*, vol. 41, no. 12, pp. 675–677, June 2005.

[155] A. Taflove and S. C. Hagness, *Computational Electrodynamics: The Finite-Difference Time-Domain Method*. Artech House, 2004.

[156] R. H. Direen, "Fundamental limitations on the terminal behavior of antennas and nonuniform transmission lines," Ph.D. dissertation, University of Colorado, 2010.

[157] J. Nocedal and S. Wright, *Numerical Optimization*. Springer, 2006.

[158] M. Gustafsson, M. Cismasu, and B. L. G. Jonsson, "Physical bounds and optimal currents on antennas," *IEEE Trans. Antennas Propag.*, vol. 60, no. 6, pp. 2672–2681, June 2012.

[159] S. Boyd and L. Vandenberghe, *Convex Optimization*. Cambridge University Press, 2004.

[160] M. Gustafsson and S. Nordebo, "Optimal antenna currents for Q, superdirectivity, and radiation patterns using convex optimization," *IEEE Trans. Antennas Propag.*, vol. 61, no. 3, pp. 1109–1118, March 2013.

[161] M. Cismasu and M. Gustafsson, "Antenna bandwidth optimization with single freuquency simulation," *IEEE Trans. Antennas Propag.*, vol. 62, no. 3, pp. 1304–1311, March 2014.

[162] G. A. E. Vandenbosch, "Radiators in time domain, part I: Electric, magnetic, and radiated energies," *IEEE Trans. Antennas Propag.*, vol. 61, no. 8, pp. 3995–4003, Aug. 2013.

[163] ——, "Radiators in time domain-part II: Finite pulses, sinusoidal regime and Q factor," *IEEE Trans. Antennas Propag.*, vol. 61, no. 8, pp. 4004–4012, Aug. 2013.

[164] S. M. Mikki and Y. Antar, "The antenna current Green's function formalism – part I," *IEEE Trans. Antennas Propag.*, vol. 61, no. 9, pp. 4493–4504, September 2013.

[165] ——, "The antenna current Green's function formalism – part II," *IEEE Trans. Antennas Propag.*, vol. 61, no. 9, pp. 4505–4519, September 2013.

[166] L. Brillouin, *Wave Propagation and Group Velocity*. Academic Press, 1960.

[167] R. Loudon, "The propagation of electromagnetic energy through an absorbing dielectric," *J. Phys. A.*, vol. 3, no. 3, pp. 233–245, 1970.

[168] V. G. Polevoi, "Maximum energy extractable from an electromagnetic field," *Radiophysics and Quantum Electronics*, vol. 33, no. 7, pp. 603–609, 1990.

[169] R. Ruppin, "Electromagnetic energy density in a dispersive and absorptive material," *Physics Letters A*, vol. 299, pp. 309–312, 2002.

[170] R. M. Fano, "Theoretical limitations on the broadband matching of arbitrary impedances," *Journal of the Franklin Inst.*, vol. 249, no. 1–2, pp. 57–83, 139–154, 1950.

[171] R. E. Collin, *Foundations for Microwave Engineering*, 2nd ed. John Wiley - IEEE Press, 1992.

[172] C. A. Balanis, *Advanced Engineering Electromagnetics*. John Wiley, 1989.

[173] (2013, February) Feko, user's manual, suite 6.2.2. EM Software & Systems-S.A. (Pty) Ltd. 32 Techno Avenue, Technopark, Stellenbosch, 7600, South Africa. [Online]. Available: www.feko.info

[174] H. A. Wheeler, "The radiansphere around a small antenna," *Proc. of IRE*, vol. 47, no. 8, pp. 1325–1331, 1959.

[175] Y. Huang, R. M. Narayanan, and G. R. Kadambi, "On Wheeler's method for efficiency measurement of small antennas," in *IEEE Antennas and Propagation Society International Symposium*, vol. 3, 2001, pp. 346–349.

[176] E. H. Newman, P. Bohley, and C. H. Walter, "Two methods for the measurement of antenna efficiency," *IEEE Trans. Antennas Propag.*, vol. 23, no. 4, pp. 457–461, July 1975.

[177] G. Smith, "An analysis of the Wheeler method for measuring the radiating efficiency of antennas," *IEEE Trans. Antennas Propag.*, vol. 25, pp. 552–556, 1977.

[178] R. Garg, P. Bhartia, I. Bahl, and A. Ittipiboon, *Mictrostrip Antenna Design Handbook*. Artech House, 2001.

[179] H.-O. Peitgen, H. Jürgens, and D. Saupe, *Chaos and Fractals: New Frontiers of Science*. Springer, 2004.

[180] B. B. Mandelbrot, *The Fractal Geometry of Nature*. Freeman, 1982.

[181] G. Edgar, *Measure, Topology and Fractal Geometry*, 2nd ed. Springer, 2008.

[182] S. R. Best and J. D. Morrow, "The effectiveness of space-filling fractal geometry in lowering resonant frequency," *IEEE Antennas Wireless Propag. Lett.*, vol. 1, no. 1, pp. 112–115, 2002.

[183] ——, "On the significance of current vector alignment in establishing the resonant frequency of small space-filling wire antennas," *IEEE Antennas Wireless Propag. Lett.*, vol. 2, pp. 201–204, 2003.

[184] C. Puente-Baliarda, J. Romeu, R. Pous, and A. Cardama, "On the behavior of the Sierpinski multiband fractal antenna," *IEEE Trans. Antennas Propag.*, vol. 46, no. 4, pp. 517–524, April 1998.

[185] J. Kigami, *Analysis on Fractals.* Cambridge University Press, 2001.

[186] M. C. Borja-Borau, "Fractal microstrip patch antennas with fractal perimeter and self-affine properties," Ph.D. dissertation, UPC, 2001.

[187] J. Zhu, A. Hoorfar, and H. Engheta, "Peano antennas," *IEEE Antennas and Wireless Propag. Letters*, vol. 3, no. 1, pp. 71–74, Dec. 2004.

[188] S. R. Best, "Operating band comparison of the perturbed Sierpinski and modified Parany Gasket antennas," *IEEE Antennas Wireless Propag. Lett.*, vol. 1, no. 1, pp. 35–38, 2002.

[189] K. J. Falconer, *Fractal Geometry – Mathematical Foundations and Applications.* John Wiley, 2003.

[190] J. Hutchinson, "Fractals and self-similarity," *Indiana Univ. J. Math.*, vol. 30, pp. 713–747, 1981.

[191] A. Lindenmayer, "Mathematical models for cellular interactions in development," *Journal of Theoretical Biology*, vol. 18, no. 3, pp. 280–299, March 1968.

[192] C. Puente, J. Romeu, R. Pous, and J. Ramis, "Small but long Koch fractal monopole," *Electronics Letters*, vol. 34, no. 1, pp. 9–10, January 1998.

[193] C. Puente-Baliarda, J. Romeu, and A. Cardama, "The Koch monopole: A small fractal antenna," *IEEE Trans. Antennas Propag.*, vol. 48, no. 11, pp. 1773–1781, November 2000.

[194] C. Puente-Baliarda, C. B. Borau, M. N. Rodero, and R. J. R., "An iterative model for fractal antennas: Application to the Sierpinski gasket antenna," *IEEE Trans. Antennas Propag.*, vol. 48, no. 5, pp. 713–719, May 2000.

[195] J. Romeu and Y. Rahmat-Samii, "Fractal elements and their applications to frequency selective surfaces," *IEEE Proc. Aerospace Conference*, vol. 5, pp. 77–81, Mar. 2000.

[196] B. A. Munk, *Frequency Selective Surfaces.* Wiley, 2000.

[197] B. Ghosh, S. N. Sinha, and M. V. Kartikeyan, "Radiation from rectangular waveguide-fed fractal apertures," *IEEE Trans. Antennas Propag.*, vol. 58, no. 6, pp. 2088–2093, June 2010.

[198] P. W. Tang and P. F. Wahid, "Hexagonal fractal multiband antenna," *IEEE Antennas and Wireless Propagation Letters*, vol. 3, no. 1, pp. 111–112, December 2004.

[199] J. A. Pros, "Fractal and broadband techniques on miniature, multifrequency, and high-directivity mictrostrip patch antennas," Ph.D. dissertation, UPC, 2003.

[200] A. K. S. Salem, "Fractal surfaces and the Kirchhoff approximation for modeling quasi-specular surface scattering: Theory and applications," Ph.D. dissertation, Stanford, 2006.

[201] J. S. Petko, "Ultra-wideband and interleaved polyfractal antenna arrays," Ph.D. dissertation, The Pennsylvania State University, 2008.

[202] K. B. Oldham and J. Spanier, *The Fractional Calculus.* Dover, 2006.

[203] R. S. Strichartz, *Differential Equations on Fractals.* Princeton University Press, 2006.

[204] H. Triebel, *Fractals and Spectra.* Birkhäuser Verlag, 2007.

[205] M. Giona, "Contour integrals and vector calculus on fractal curves and interfaces," *Chaos, Solitons & Fractals*, vol. 10, no. 2, pp. 1349–1370, 1999.

[206] M. V. Berry, "Distribution of modes in fractal resonators," *Struct. Stability in Phys.*, vol. 4, pp. 51–53, 1979.

[207] K. F. Lee and W. Chen, Eds., *Advances in Microstrip and Printed Antennas.* John Wiley, 1997.

[208] D. A. Sánchez-Hernández, Ed., *Multiband Integrated Antennas for 4G Terminals.* Artech House, 2008.

[209] A. P. Engelbrecht, *Fundamentals of Computational Swarm Intelligence.* John Wiley, 2007.

[210] K. Deb, *Multi-Objective Optimization using Evolutionary Algorithms.* John Wiley, 2001.

[211] J. Kennedy and R. Eberhart, "Particle swarm optimization," in *IEEE International Conference on Neural Networks*, vol. 4, Nov. 1995, pp. 1942–1948.

[212] J. Kennedy and R. C. Eberhart, *Swarm Intelligence.* Academic Press, 2001.

[213] K. E. Parsopoulos and M. N. Vrahatis, "Recent approaches to global optimization problems through particle swarm optimization," *Natural Computing*, vol. 1, pp. 235–306, 2002.

[214] F. T. S. Chan and M. K. Tiwari, *Swarm Intelligence – Focus on Ant and Particle Swarm Optimization.* I-Tech Education and Publishing, 2007.

[215] D. N. Wilke, S. Kok, and A. A. Groenwold, "Comparison of linear and classical velocity update rules in particle swarm optimization: Notes on diversity," *Int. J. Numer. Math. Eng.*, vol. 70, pp. 962–984, Nov. 2007.

[216] ——, "Comparison of linear and classical velocity update rules in particle swarm optimization: Notes on scale and frame invariance," *Int. J. Numer. Math. Eng.*, vol. 70, pp. 985–1008, Nov. 2007.

[217] A. Liu and Y. M.-T., "A new hybrid nelder-mead particle swarm optimization for coordination optimization of directional overcurrent relays," *Mathematical Problems in Engineering*, vol. 2014, pp. 1–18, 2012.

[218] A. Gandelli, F. Grimaccia, M. Mussetta, P. Pirinoli, and R. E. Zich, "Genetical swarm optimization: An evolutionary algorithm for antenna design," *Automatika*, vol. 47, no. 3-4, pp. 105–112, 2006.

[219] M. Wu, T. Hu, and J. D. Weir, "An adaptive particle swarm optimization with multiple adaptive methods," *IEEE Trans. Evolut. Comp.*, vol. 17, no. 5, pp. 705–720, October 2013.

[220] J. Robinson and Y. Rahmat-Samii, "Particle swarm optimization in electromagnetics," *IEEE Trans. Antennas Propag.*, vol. 52, no. 2, pp. 397–407, Feb. 2004.

[221] N. Jin and Y. Rahmat-Samii, "Advances in particle swarm optimization for antenna designs: Real-number, binary, single-objective and multiobjective implementations," *IEEE Trans. Antennas Propag.*, vol. 55, no. 3, pp. 556–567, March 2007.

[222] S. Xu and Y. Rahmat-Samii, "Boundary conditions in particle swarm optimization revisited," *IEEE Trans. Antennas Propag.*, vol. 55, no. 3, pp. 760–765, March 2007.

[223] S. M. Mikki and A. A. Kishk, "Quantum particle swarm optimization for electromagnetics," *IEEE Trans. Antennas Propag.*, vol. 54, no. 10, pp. 2764–2775, Oct. 2006.

[224] ——, "Physical theory for particle swarm optimization," *Progress In Electromagnetics Research*, vol. 75, pp. 171–207, 2007.

[225] G. C. Onwubolu and B. V. Babu, *New Optimization Techniques in Engineering*. Springer, 2004.

[226] P. Kadlec and Z. Raida, "A novel multi-objective self-organizing migrating algorithm," *Radioengineering*, vol. 20, no. 4, pp. 804–816, Dec. 2011.

[227] Y. Rahmat-Samii, J. M. Kovitz, and H. Rajagopalan, "Nature-inspired optimization techniques in communication antenna design," *Proc. of IEEE*, vol. 100, no. 7, pp. 2132–2144, July 2012.

[228] CST Computer Simulation Technology. http://www.cst.com/.

[229] M. Capek, P. Hazdra, and J. Eichler, "Complex power-ratio functional for radiating structures with applications to the characteristic mode theory," 2014, prepared for publication.

[230] H. F. Davis, *Fourier Series and Orthogonal Functions*. Dover, 1989.

[231] L. C. Evans, *Partial Differential Equations: Second Edition.* American Mathematical Society, 2010.

[232] W. Rudin, *Functional Analysis.* McGraw-Hill, 1991.

[233] V. Zavada, "Energetic functional of U-notched loop antenna," Master's thesis, CTU in Prague, 2014, (in Czech).

[234] P. Eichler, J. andHazdra, M. Capek, and M. Mazanek, "Modal resonant frequencies and radiation quality factors of microstrip antennas," *International J. of Antenas and Propag.*, vol. 2012, pp. 1–9, 2012.

[235] G. A. E. Vandenbosch, "Reply to "Comments on 'Reactive energies, impedance, and Q factor of radiating structures'"," *IEEE Trans. Antennas Propag.*, vol. 61, no. 12, p. 6268, Dec. 2013.

[236] M. Capek, L. Jelinek, P. Hazdra, and J. Eichler, "An analytical evaluation and the lower bounds of the measurable quality factor Q_Z," *IEEE Trans. Antennas Propag.*, pp. 1–9, 2014, submitted (arXiv: 1311.1750v1).

[237] M. Capek, P. Hazdra, P. Hamouz, and J. Eichler, "A method for tracking characteristic numbers and vectors," *Progress In Electromagnetics Research B*, vol. 33, pp. 115–134, 2011.

[238] D. J. Ludick, E. Lezar, and U. Jakobus, "Characteristic mode analysis of arbitrary electromagnetic structures using FEKO," in *ICEAA*, 2012, pp. 208–211.

[239] M. Capek, P. Hamouz, P. Hazdra, and J. Eichler, "Implementation of the Theory of Characteristic Modes in Matlab," *IEEE Antennas Propag. Magazine*, vol. 55, no. 2, pp. 176–189, April 2013.

[240] S. N. Makarov, *Antenna and EM Modeling with Matlab.* John Wiley, 2002.

[241] S. M. Rao, D. R. Wilton, and A. W. Glisson, "Electromagnetic scattering by surfaces of arbitrary shape," *IEEE Trans. Antennas Propag.*, vol. 30, no. 3, pp. 409–418, May 1982.

[242] M. N. O. Sadiku, *Numerical Techniques in Electromagnetics with Matlab*, 3rd ed. CRC Press, 2009.

[243] The MathWorks. The Matlab. [Online]. Available: www.mathworks.com

[244] M. Capek, L. Jelinek, P. Hazdra, and J. Eichler, "The measurable Q factor and observable energies of radiating structures," *IEEE Trans. Antennas Propag.*, vol. 62, no. 1, pp. 311–318, Jan. 2014.

[245] J. Eichler, P. Hazdra, and M. Capek, "Aspects of mesh generation for characteristic mode analysis," *IEEE Antennas Propag. Magazine*, 2014, submitted.

[246] P.-O. Persson, "Mesh generation for implicit geometries," Ph.D. dissertation, MIT, 2006.

[247] M. De Berg, O. Cheong, M. Van Kreveld, and M. Overmars, *Computational Geometry – Algorithms and Applications*. Springer, 2008.

[248] COMSOL Multiphysics. [Online]. Available: www.comsol.com

[249] M. Capek, P. Hazdra, J. Eichler, and M. Mazanek, "Software tools for efficient generation, modelling and optimisation of fractal radiating structures," *IET Microw. Antennas Propag.*, vol. 5, no. 8, pp. 1002–1007, 2011.

[250] P. Hazdra, M. Capek, P. Hamouz, and M. Mazánek, "Advanced modal techniques for microstrip patch antenna analysis," in *ICECom*, Dubrovnik, 2010, pp. 1–6.

[251] P. Hamouz, P. Hazdra, M. Polivka, M. Capek, and M. Mazanek, "Radiation efficiency and Q factor study of franklin antenna using the theory of characteristic modes," in *Proceedings of the 5th European Conference on Antennas and Propagation (EUCAP)*, Rome, Italy, April 2011, pp. 1974–1977.

[252] M. Capek, J. Eichler, P. Hazdra, and M. Mazanek, "A method for the evaluation of radiation efficiency based on modal approach," in *Proceedings of the 8th European Conference on Antennas and Propagation (EUCAP)*, 2014.

[253] M. Capek, J. Eichler, and P. Hazdra, "Evaluation of radiation effciency from characteristic currents," *IET Microw. Antennas Propag.*, 2014, submitted.

[254] M. Capek, P. Hazdra, and J. Eichler, "A method for the evaluation of radiation Q based on modal approach," *IEEE Trans. Antennas Propag.*, vol. 60, no. 10, pp. 4556–4567, Oct. 2012.

[255] M. Capek, P. Hazdra, J. Eichler, P. Hamouz, M. Mazanek, and V. Sobotikova, "The evaluation of total radiation Q based on modal approach," in *Proceedings of the 6th European Conference on Antennas and Propagation (EUCAP)*, Prague, Czech Republic, April 2012.

[256] P. Arcioni, M. Bressan, and L. Perregrini, "On the evaluation of the double surface integrals arising in the application of the boundary integral method to 3-D problems," *IEEE Trans. Microwave Theory Tech.*, vol. 44, no. 3, pp. 436–438, March 1997.

[257] P. Hazdra, M. Capek, and J. Eichler, "Radiation Q-factors of thin-wire dipole arrangements," *IEEE Antennas Wireless Propag. Lett.*, vol. 10, pp. 556–560, 2011.

[258] P. Hazdra, M. Capek, J. Eichler, P. Hamouz, and M. Mazanek, "Radiation Q of dipole modal currents," in *Proceedings of the 5th European Conference on Antennas and Propagation (EUCAP)*, Rome, Italy, April 2011, pp. 1578–1581.

[259] P. Hazdra, M. Capek, and J. Eichler, "Comments to 'Reactive Energies, Impedance, and Q Factor of Radiating Structures' by G. Vandenbosch," *IEEE Trans. Antennas Propag.*, vol. 61, no. 12, pp. 6266–6267, Dec. 2013.

[260] M. Capek, L. Jelinek, P. Hazdra, and J. Eichler, "The source definition of the quality factor Q_Z," in *IEEE International Symposium on Antennas and Propagation and USNC-URSI Radio Science Meeting*, 2014, accepted.

[261] M. Gustafsson and B. L. G. Jonsson. Stored electromagnetic energy and antenna Q. eprint arXiv: 1211.5521. [Online]. Available: http://adsabs.harvard.edu/abs/2012arXiv1211.5521G

[262] K. Cahill, *Physical Mathematics*. Cambridge University Press, 2013.

[263] P. Hazdra, M. Capek, J. Eichler, and M. Mazanek, "The radiation Q-factor of a $\lambda/2$ dipole above ground plane," *IEEE Antennas Wireless Propag. Lett.*, 2014, submitted.

[264] L. Jelinek, M. Capek, P. Hazdra, and J. Eichler, "Lower bounds of the quality factor Q_Z," in *IEEE International Symposium on Antennas and Propagation and USNC-URSI Radio Science Meeting*, 2014, accepted.

[265] M. Capek, "PSO optimization of IFS fractal patch antennas," in *Poster*, Prague, Czech Republic, 2009, (student conference).

[266] P. Hazdra, M. Capek, and J. Kraček, "Optimization tool for fractal patches based on the IFS algorithm," in *Proceedings of the 3rd European Conference on Antennas and Propagation (EUCAP)*, Berlin, Germany, 2009.

[267] J. Vlk, "Design of electrically small antenna," Master's thesis, CTU in Prague, 2012, (in Czech). [Online]. Available: http://mtt.ieee.cz/studentska-soutez/soutez2012/Diplomov%C3%A1%20pr%C3%A1ce%20(A0M17DIP).pdf

[268] D. H. Wolpert and W. G. Macready, "No free lunch theorems for search," Santa Fe Institute, Santa Fe, Tech. Rep. 95-02-010, 1995.

[269] ——, "No free lunch theorems for optimization," *IEEE Trans. Evolut. Comp.*, vol. 1, no. 1, pp. 67–82, April 1997.

[270] P. Koška, "Hybrid nelder-mead - particle swarm optimization," Master's thesis, CTU in Prague, 2014, (in Czech).

[271] C. A. Coello Coello and M. S. Lechuga, "Mopso: A proposal for multiobjective particle swarm optimization," *Proc. of Evolut. Comp.*, vol. 2, pp. 1051–1056, 2002.

[272] C. A. Coello Coello, G. T. Pulido, and M. S. Lechuga, "Handling multiple objectives with particle swarm optimization," *IEEE Trans. Evolut. Comp.*, vol. 8, no. 3, pp. 256–279, June 2004.

[273] P. Hazdra and M. Capek, "IFS tool for microstrip patch antenna analysis," in *COMITE*, 2008.

[274] P. Hazdra, M. Capek, J. Eichler, T. Korinek, and M. Mazanek, "On the modal resonant properties of microstrip antennas," in *Proceedings of the 6th European Conference on Antennas and Propagation (EUCAP)*, March 2012, pp. 1650–1654.

[275] J. D. Owens, M. Houston, D. Luebke, S. Green, J. E. Stone, and J. C. Phillips, "GPU computing," *Proc. of IEEE*, vol. 96, no. 5, pp. 879–899, May 2008.

[276] The MathWorks, *Parallel Computing Toolbox*, 2012.

[277] ——, *Distributed Computing Server (Installation Guide)*, 2012.

[278] The Jacket (ArrayFire). [Online]. Available: http://www.accelereyes.com/

[279] M. Capek, P. Hazdra, J. Eichler, P. Hamouz, and M. Mazanek, "Acceleration techniques in Matlab for EM community," in *Proceedings of the 7th European Conference on Antennas and Propagation (EUCAP)*, Gothenburg, Sweden, April 2013.

[280] IE3D. [Online]. Available: http://www.rfglobalnet.com/doc/full-wave-3-d-em-simulator-for-both-planar-an-0001

[281] J.-M. Jin, *Theory and Computation of Electromagnetic Fields*. John Wiley, 2010.

[282] R. Garg, *Analytical and Computational Methods in Electromagnetics*. Artech House, 2008.

[283] S. Gao, Q. Luo, and F. Zhu, *Circularly Polarized Antennas*. John Wiley, 2014.

[284] J. Eichler, P. Hazdra, M. Capek, T. Korinek, and P. Hamouz, "Design of a dual-band orthogonally polarized l-probe-fed fractal patch antenna using modal methods," *IEEE Antennas Wireless Propag. Lett.*, vol. 10, pp. 1389–1392, 2011.

[285] P. Hazdra, J. Eichler, M. Capek, P. Hamouz, and T. Korinek, "Small dual-band fractal antenna with orthogonal polarizations," in *Proceedings of the 5th European Conference on Antennas and Propagation (EUCAP)*, 2011.

[286] M. Capek and P. Hazdra, "Design of IFS patch antenna using Particle Swarm Optimization," in *Proceedings of the 4th European Conference on Antennas and Propagation (EUCAP)*, Barcelona, Spain, April 2010.

Chapter 5

Appendix A.1 – Selected author's publications

Selected author's journal, magazine and conference papers (first author only) that are related to the thesis are chronologically listed bellow.

1. M. Capek, "PSO optimization of IFS fractal patch antennas," in *Poster*, Prague, Czech Republic, 2009. [265]

2. M. Capek and P. Hazdra, "Design of IFS patch antenna using Particle Swarm Optimization," in *Proceedings of the 4th European Conference on Antennas and Propagation (EUCAP)*, Barcelona, Spain, April 2010. [286]

3. M. Capek, P. Hazdra, J. Eichler, and M. Mazanek, "Software tools for efficient generation, modelling and optimisation of fractal radiating structures," *IET Microw. Antennas Propag.*, vol. 5, no. 8, pp. 1002–1007, 2011. [249]

4. M. Capek, P. Hazdra, P. Hamouz, and J. Eichler, "A method for tracking characteristic numbers and vectors," *PIER-B*, vol. 33, pp. 115–134, 2011. [237]

5. M. Capek, P. Hazdra, J. Eichler, P. Hamouz, M. Mazanek, and V. Sobotikova, "The evaluation of total radiation Q based on modal approach," in *Proceedings of the 6th European Conference on Antennas and Propagation (EUCAP)*, Prague, Czech Republic, April 2012. [255]

6. M. Capek, P. Hazdra, and J. Eichler, "A method for the evaluation of radiation Q based on modal approach," *IEEE Trans. Antennas Propag.*, vol. 60, no. 10, pp. 4556–4567, Oct. 2012. [254]

7. M. Capek, P. Hamouz, P. Hazdra, and J. Eichler, "Implementation of the Theory of Characteristic Modes in Matlab," *IEEE Antennas Propag. Magazine*, vol. 55, no. 2, pp. 176–189, April 2013. [239]

8. M. Capek, P. Hazdra, J. Eichler, P. Hamouz, and M. Mazanek, "Acceleration techniques in Matlab for EM community," in *Proceedings of the 7th European Conference on Antennas and Propagation (EUCAP)*, Gothenburg, Sweden, April 2013. [279]

9. M. Capek, L. Jelinek, P. Hazdra, and J. Eichler, "The measurable Q factor and observable energies of radiating structures," *IEEE Trans. Antennas Propag.*, vol. 62, no. 1, pp. 311–318, Jan. 2014. [244]

10. M. Capek, J. Eichler, P. Hazdra, and M. Mazanek, "A method for the evaluation of radiation efficiency based on modal approach," in *Proceedings of the 8th European Conference on Antennas and Propagation (EUCAP)*, 2014, accepted. [252]

11. M. Capek, L. Jelinek, P. Hazdra, and J. Eichler, "The source definition of the quality factor Q_Z," in *IEEE International Symposium on Antennas and Propagation and USNC-URSI Radio Science Meeting*, 2014, accepted. [260]

12. M. Capek, J. Eichler, and P. Hazdra, "Evaluation of radiation effciency from characteristic currents," *IET Microw. Antennas Propag.*, 2014, after major revision. [253]

13. M. Capek, L. Jelinek, P. Hazdra, and J. Eichler, "An Analytical Evaluation of the Measurable Quality Factor Q_Z for Dominant Spherical Modes," *IET Microw. Antennas Propag.*, pp. 1–8, 2014, submitted (arXiv: 1311.1750v1). [236]

14. M. Capek, L. Jelinek, G. A. E. Vandenbosch, and P. Hazdra, "Electromagnetic energies and radiation Q factor," *IEEE Trans. Antennas Propag.*, 2014, submitted (arXiv:1309.6122). [3]

One more paper was attached at the end of the thesis:

M. Capek, P. Hazdra, and J. Eichler, "Complex power-ratio functional for radiating structures with applications to the characteristic mode theory," *rejected from IEEE Trans. Antennas Propag.*

This paper has unfortunately been rejected from publication in IEEE Transactions on Antennas and Propagation. The main criticism concerns about incomplete text of sections II and III. The manuscript has been attached since some particular information are mentioned in the text above. The manuscript is being rewritten and will be once more submitted.

PSO optimalization of IFS fractal patch antennas

Miloslav ČAPEK[1]

[1]Dept. of Electromagnetic Field, Czech Technical University, FEE, Technická 2, 166 27 Praha, Czech Republic

capekm6@fel.cvut.cz

Abstract. *Paper describes the use of IFS (Iterated Function System) fractals employed as a planar microstrip patch antennas. The fractal shapes have some interesting features when used as a radiator - like reduction of resonant frequencies or multiband behaviour. To generate the IFS fractals, versatile tool named IFSMaker (based on Matlab Object-Oriented Programming), has been evolved. After fractal predesign, one can start to optimize the IFS collage by using the PSO algorithm. This procedure is managed by the PSOptimizer tool. Optimalization loop (which includes IFS generator, cavity model solver and PSO evaluation) may works generally with any number of optimalization conditions. This feature is provided by IFSLimiter tool. The resonant frequencies are calculated with cavity model in Comsol Multiphysics environment.*

Keywords

Iterated function system, Particle swarm optimization, Cavity model, Modal analysis, Microstrip patch antenna

1. IFS fractal as a microstrip antenna

Self-similarity, the major feature of fractal, can be decribed with the aid of the Hutchison operator:

$$\mathbf{w}(X) = \bigcup_{i=1}^{m} w_i(X), X \subseteq \mathbb{R}^n \tag{1}$$

Transformations w_i (for i-th iteration) are applied to a point matrix X. There are some restrictions like that the objects from next iteration must be smaller than object from previous (contraction factor < 1). The object size is measured by the means of distance function (alias metric), for Euclidean measure: $d = \sqrt{x^2 + y^2}$. For example of new fractal creating, see Fig. 1.

The IFS transformations are defined by a matrix equation:

$$x(w) = \mathbf{A}W + \mathbf{B}. \tag{2}$$

In details:

$$w \begin{pmatrix} x_{new} \\ y_{new} \end{pmatrix} = \begin{pmatrix} a & b \\ c & d \end{pmatrix} \begin{pmatrix} x_{old} \\ y_{old} \end{pmatrix} + \begin{pmatrix} e \\ f \end{pmatrix} \tag{3}$$

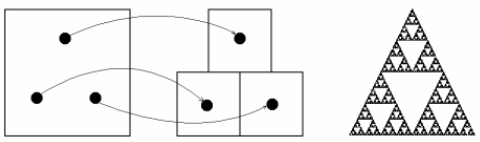

Fig. 1. Creating a new iteration of IFS (Sierpinski triangle)

Eq. (3) is one of the so-called affine transformation:

- Point translation by vector $[p_x, p_y]$
- Scale change with coefficient M_s
- Horizontal scale change M_x
- Vertical scale change M_y
- Horizontal skew S_x
- Vertical skew S_y
- Rotation by angle α

For IFS storage purpose, we utilize our own FRC format, consisting of FRC.base, FRC.tran, FRC.iter and FRC.type fields. Generation of the IFS as shown above, is the main

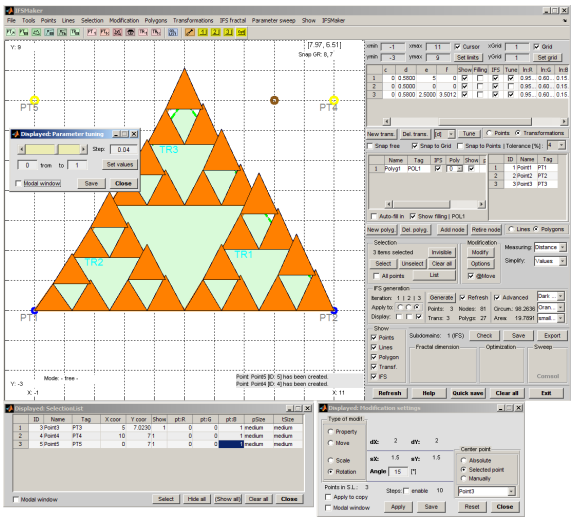

Fig. 2. IFSMaker

issue of the IFSMaker, programmed in OOP paradigm. It is possible to load/save the FRCs as well as interactively edit and modify points and transformations. Another functions

include area/perimeter calculation and fractal dimension estimation. All functions work "on the fly", so it's possible to dynamically change all properties at any time. Screenshot of IFSMaker is on the fig. 2.

2. Solving resonant frequency using the Cavity Model

Cavity Model (CM) consider patch antenna as a 2D cavity with perfect magnetic condition (PMC) and perfect electric condition (PEC) as shown at fig. 3. Mathematically,

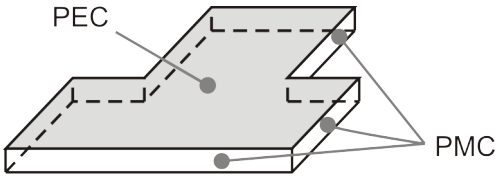

Fig. 3. CM conditions

the conditions are defined as:

$$\mathbf{E} \times z = 0, \ \mathbf{H}.\mathbf{z} = 0; \ \text{for } z = 0, z = h, \tag{4}$$

$$\mathbf{H} \times n = 0, \ \mathbf{E}.\mathbf{n} = 0; \ \text{boundary of antenna.} \tag{5}$$

After some manipulation, the scalar Helmholtz equation can be derived:

$$\left(\nabla_t + k_n^2\right) E_{z,n} = 0 \tag{6}$$

where $\nabla_t = \left(\frac{\partial^2}{\partial x^2} + \frac{\partial^2}{\partial y^2}\right)$ and k_n^2 are eigenvalues. Resonant frequencies are obtained from the condition $\lambda_n = k_n^2$. We assume that no magnetic material is present under the patch.

$$f_n = \frac{c_0}{2\pi\sqrt{\epsilon_r}}\lambda_n, k_n^2 = \omega^2\mu_0\epsilon. \tag{7}$$

Closed-form solution is known only for special cases, thus FEM is used for solving eq. (6). Early version utilized Matlab's PDE toolbox, in the future we would like to use in-house characteristic mode solver, which is much more precise. Eq. (6) may be written in compact form in terms of linear operator equation:

$$L\psi_n = \lambda_n\psi_n. \tag{8}$$

Unfortunately, CM approximation has some prepotent restrictions, for instance the height of antenna is limited to $h \ll \lambda$. Further information can be found in [3].

3. Particle swarm optimization

Particle swarm optimization (PSO) is based on swarm intelligence. This kind of optimization is highly stable, fast and very robust mainly because of low risk of local minima hangup.

Basic principle of the PSO rely on swarm of agents moving over the given's function space. During every algorithm iteration, fitness functions (f.f.) for all the agents is determined. Behavior of the swarm may be described by the following equation:

$$v_{id}^{n+1} = wv_{id}^n + c_1 r_1^n (p_{id}^n - \chi_{id}^n) + c_2 r_2^n (p_{gd}^n - \chi_{id}^n) \tag{9}$$

Values p_{id}^n (every agent individual minimum) p_{gd}^n (global minimum of the whole swarm, that is the best value of p_{id}^n) are weighted by random values r_1^n a r_2^n. Contribution of these is influenced by the constants c_1 and c_2, which affects the swarm behavior (cognitive vs social). Once we know the speed of agents, their position is updated:

$$\chi_{id}^{n+1} = \chi_{id}^n + \Delta_t v_{id}^{n+1} \tag{10}$$

Δ_t is a discrete time which can be chosen arbitrarily (generally, we suppose that $\Delta_t = 1$). At χ positions, new $gbest$ and $pbest$ are updated.

If the agents are not limited in space, there is a risk of their leaving the solution space s.s. (i.e. the space where the problem has physical meaning). Thus, proper wall has to be introduced - according to [5], invisible wall has been chosen. For agents outside the s.s, fitness function isn't evaluated and agents slowly returns back to proper physical space. Consequently, computational time is effectively saved.

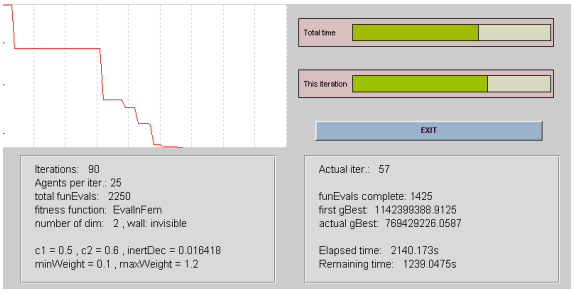

Fig. 4. PSOptimizer GUI

Algorithm described above was implemented into PSOptimizer application. Our optimizer is coded in a very general way and thus is able to optimize any m-file function which returns f.f. Then, p_{id}^n is accordingly updated. Cost function (c.f.) is shown during the process, see fig. 4 at left. [7] gives examples of Rosenbrock and Levy No. 5 functions optimization.

It's very useful to know the physical nature of the given problem so proper choosing of the swarm size and maximum number of iterations may speed-up the optimization process.

4. Results

Flowchart of the whole optimization loop is shown at fig. 5. We will now demonstrate the optimization of a fractal-patch fundamental resonant mode frequency. Motif

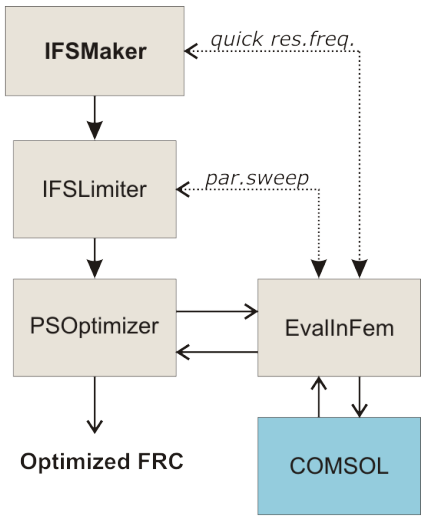

Fig. 5. Optimization loop

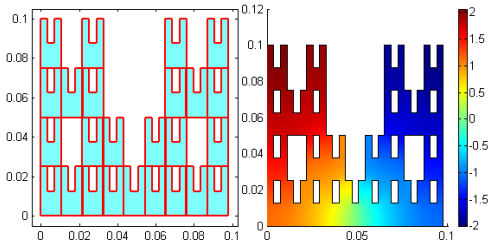

Fig. 6. Initial fractal motif to be optimized

we choosed (fig. 6) is easily created with the IFS maker.

Modal frequencies of this structure, (with the maximum x- size being constant 100mm) is at Tab. 1 left and Tab. 2 respectively.

Now the optimization conditions and bounds has to be defined and stored into the PsoData structure. For this purpose, IFSLimiter tool reads the FRC and exports the PsoData, see fig. 7.

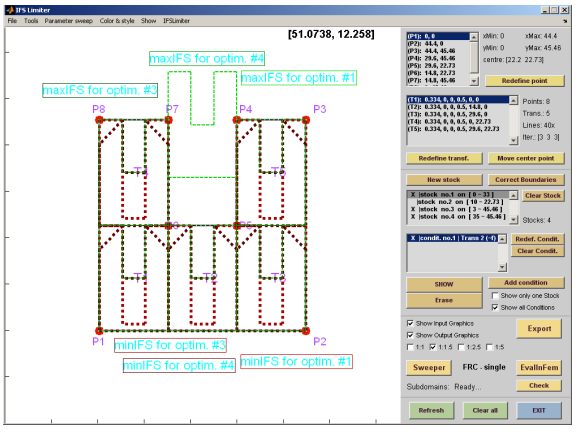

Fig. 7. PSO conditions in the IFSLimiter

The optimization is now initiated with the choose of 25 agents, 175 iterations and constants c1, c2 = 2:

- ResTb = PSOptimizer(PsoData,'EvalInFem',25,175)

or

- ResTb = EvalInFem('pso',PsoData,25,175)

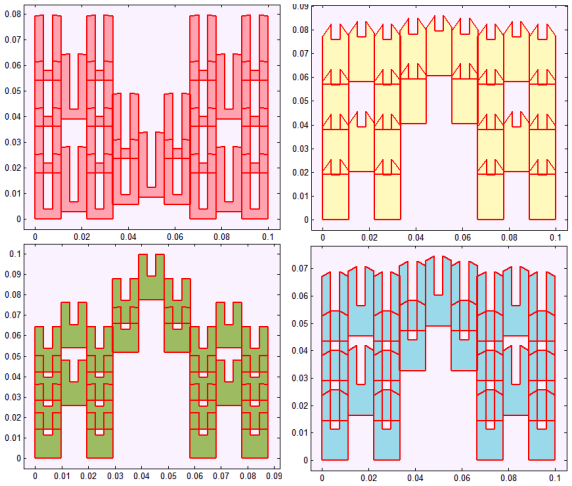

Fig. 8. The optimized collages

During the optimization, Comsol's cavity model is called through the EvalInFem function which receives current data from the optimizer, generates the IFS collage, performs meshing (+sets boundary conditions etc.). Finally, the solver (femeig) is called and after some postprocessing steps, resonant frequencies are returned back to the PSOptimizer for evaluation. EvalInFem also handles geometry exceptions

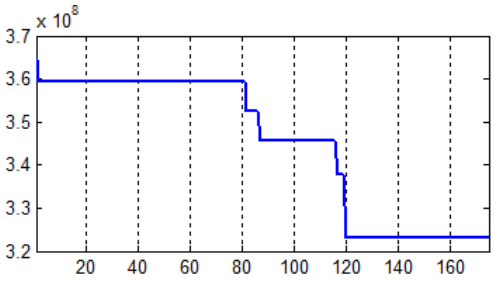

Fig. 9. Cost function of the IFS optimization

(disconnected parts of the patch..), problems with meshing, Comsol connection loose etc. This is very important to keep the optimization process fluent. From Tab. 1 it is observed

	not optimized	optimized
$c_1 = 2.0, c_2 = 2.0, w_{min} = 0.4, w_{max} = 0.9$		
1. mode	638.403 MHz	323.049 MHz
2. mode	1308.741 MHz	811.961 MHz
3. mode	1651.183 MHz	1532.101 MHz
4. mode	1751.222 MHz	1782.136 MHz
5. mode	2253.036 MHz	1843.199 MHz

Tab. 1. Resonant frequency for the first five modes

that dominant mode of the optimized patch is almost 50%

lower than the original structure. Of course, we should treat such values as estimation only, because CM doesn't include all the phenomenons like the internal coupling. It's recommended to refine this results with full-wave simulation (CST MWS) or with characteristic modes.

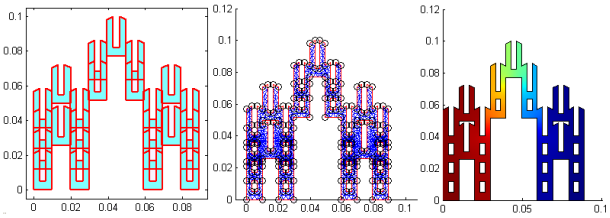

Fig. 10. Optimized fractal

	not optimized	optimized
0. iter.	902.701 MHz	499.581 MHz
1. iter.	746.830 MHz	529.672 MHz
2. iter.	638.404 MHz	323.045 MHz
3. iter.	543.919 MHz	–(∗)
	∗ multiple subdomains	

Tab. 2. Resonant frequency vs. iteration

5. Conslusion

This paper presented set of in-house tools for effective work with microstrip patch antennas based on fractal concept. We are able to design, edit and optimize fractal structures described by the Iterated function systems. Further work will be aimed to calculate and optimize radiation patterns (using the electric currents flowing along the patch), improving the PSO speed and multiband antenna synthesis.

References

[1] JAMES, J., R., HALL, P., S. *Handbook of Microstrip Antennas vol.1*. London: Peter Peregrinus Ltd., 1989.

[2] KENNEDY, J., EBERHART R. *Particle Swarm Optimization*. IEEE, 1995

[3] The Comsol Multiphysics, http://www.comsol.com/

[4] TIŠNOVSKÝ, P. *Interaktivní editor afinních transformací*. Brno: VUT, 1999.

[5] ROBINSON J., RAHMAT-SAMII Y. *Particle Swarm Optimization in Electromagnetics*. IEEE Trans-AP, vol. 52, no. 2, pgs. 397-407, 2004

[6] HAZDRA P., ČAPEK M. *IFS Tool for Fractal Microstrip Patch Antenna Analysis* in COMITE, Prague, 2008.

[7] ČAPEK M., HAZDRA P. *PSO optimalizace v Matlabu*. Technical Computing Prague, 2008.

[8] HAZDRA P., ČAPEK M., KRAČEK J. *Optimization Tool for Fractal Patches Based on the IFS Algorithm*. EuCAP, 2009.

[9] ČAPEK, M. *Modální analýza mikropáskových patch antén*. Prague: CTU-FEE, 2007.

About Authors...

Miloslav ČAPEK was born in České Budějovice, Czech republic, in March 1985. He recieved the B.S. degree in Telecommunication and radio engeneering from the Czech Technical University (CTU), Prague, in 2007. He is currently working toward the M.S. degree. He focuse on development and implementation of particle swarm optimization, iterated function system and other techniques. His favourite programming environment is Matlab.

Design of IFS Patch Antenna Using Particle Swarm Optimization

Miloslav Capek
Czech Technical University in Prague, FEE
Technicka 2, 166 27 Prague, Czech Republic
capekmi2@fel.cvut.cz

Pavel Hazdra
Czech Technical University in Prague, FEE
Technicka 2, 166 27 Prague, Czech Republic

***Abstract*—Paper describes usage of the IFS (Iterated Function System) fractals employed as a planar microstrip patch antennas. To generate the IFS fractals, versatile tool named IFSMaker has been evolved. Efficient design of patches will be shown. After fractal pre-design, one can start to optimize the IFS collage by using the PSO algorithm. This procedure is managed by the PSOptimizer tool. Optimalization loop (which includes IFS generator, cavity model (CM) solver and PSO evaluation) works generally with any number of optimalization conditions. This feature is provided by IFSLimiter tool. Resonant frequencies (eigenvalue problem) are calculated with cavity model in Comsol Multiphysics environment. Finally we discuss the radiation pattern calculation and usage of theory of characteristic modes as well.**

I. Introduction

The fractal shapes [1] have some interesting features when used as a planar radiator [3] – like reduction of resonant frequencies or multiband behaviour. It is necessary to keep in mind both benefits of fractal geometry and antenna parameters. Our motivation is to minimize fundamental resonant frequency and to calculate the radiation pattern of the selected fractal patch antennas (section VI) while preserving the minimum patch area. We use benefits of different approaches for IFS, Cavity Model, PSO, electric and magnetics sources etc.

II. IFS Fractal as a Microstrip Antenna

Briefly, the major feature of fractal is self-similarity, which can be decribed with the aid of the Hutchison operator:

$$\mathbf{w}(X) = \bigcup_{i=1}^{m} w_i(X), X \subseteq \mathbb{R}^n \tag{1}$$

Transformations w_i (for i-th iteration) are applied to a point matrix X. There are some restrictions like that the objects from next iteration must be smaller than object from previous (contraction factor < 1). Object size is measured by the means of distance function (alias metric), for Euclidean measure: $d = \sqrt{x^2 + y^2}$, [1]. See for example Sierpinski triangle generation in Fig. 1. The IFS transformations are defined by a matrix equation:

$$x(w) = \mathbf{A}W + \mathbf{B}. \tag{2}$$

In details:

$$w \begin{pmatrix} x_{new} \\ y_{new} \end{pmatrix} = \begin{pmatrix} a & b \\ c & d \end{pmatrix} \begin{pmatrix} x_{old} \\ y_{old} \end{pmatrix} + \begin{pmatrix} e \\ f \end{pmatrix} \tag{3}$$

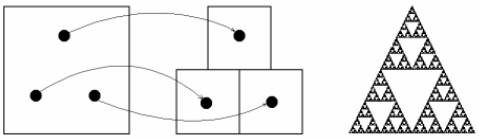

Fig. 1. Creating a new iteration of IFS (Sierpinsky triangle)

Eq. (3) is one of the so-called affine transformation which can provide:

- Point translation by vector $[p_x, p_y]$
- Scale change with coefficient M_s
- Horizontal scale change M_x
- Vertical scale change M_y
- Horizontal skew S_x
- Vertical skew S_y
- Rotation by angle α

Next sections will focus on utilizing of these structures as a microstrip patch antenna.

A. IFSMaker

At first, it is necessary to develop a tool for IFS patches generation. This task is performed by IFSMaker programmed in Matlab environment [2]. For IFS storage purpose, we utilize our own FRC format consisting of:

- FRC.base (base points of IFS)
- FRC.tran (affine transformations)
- FRC.iter (number of iteration)
- FRC.type (type of data structure)

It is possible to load/save the FRCs as well as interactively edit and modify points and transformations. Another functions include area/perimeter calculation and fractal dimension estimation. All functions work "on the fly", so we can dynamically change all properties at any time. Screenshot of IFSMaker is shown in Fig. 2.

B. IFS Design

First step is to define some points to establish the base object. The transformations are determined by the [a–f] coefficients. Because the modification of transformation is frequent and useful operation, the sweep utility has been included, see Fig. 4. There are many other features, like the modification tool (Fig. 5). Final fractal geometry can be saved in native

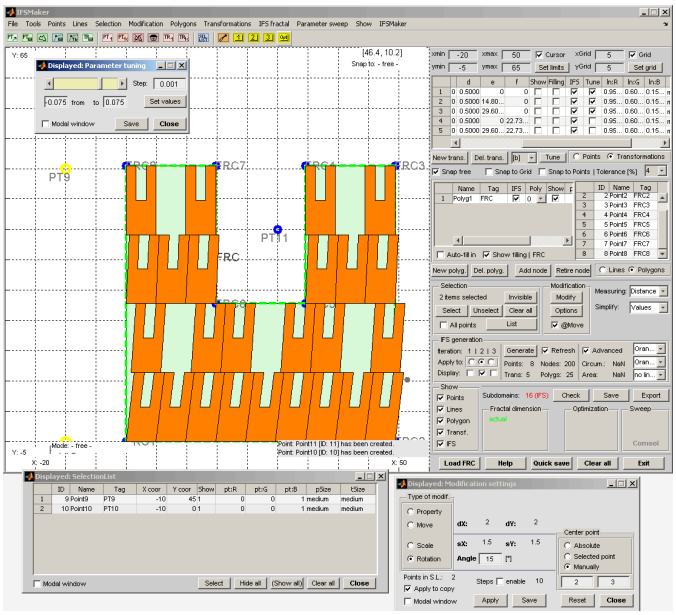

Fig. 2. IFSMaker tool based on Matlab Object-Oriented Programming

FRC format. Alternatively one can export fractal to the txt and/or 3dt file.

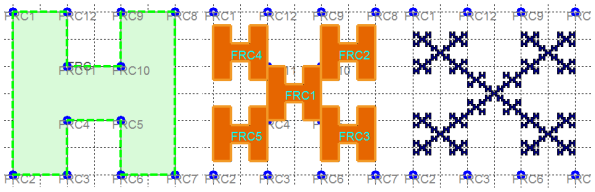

Fig. 3. Fractal creation in IFSMaker (base object with points, transformations and finished fractal, FRC_K)

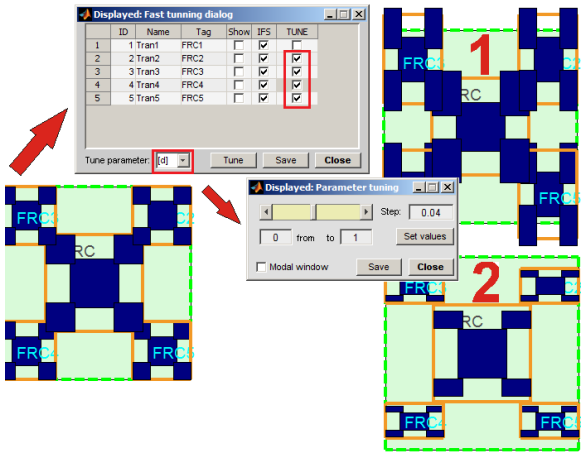

Fig. 4. IFSMaker: transformation tuning (FRC_J)

In more detail we focus now on fractal named FRC_K. Its parameters are:

- FRC.base = $[-x_1\, x_1; -x_1\ -x_1; -x_2\ -x_1; -x_2\ -x_2; x_2\ -x_2; x_2\ -x_1; x_1\ -x_1; x_1\, x_1; x_2\, x_1; x_2\, x_2; -x_2\, x_2; -x_2\, x_1]$,
- FRC.tran = $[a\,0\,0\,d\,0\,0;\ a\,0\,0\,d\,e\,f;\ a\,0\,0\,d\,e\,-f;\ a\,0\,0\,d\,-e\,f;\ a\,0\,0\,d\,-e\,-f]$,
- FRC.iter = 1 or 2,
- FRC.type = 'pntstrns',

where $x_1 = 0.75$, $x_2 = 0.25$ and $a = d = 0.334$, $e = 0.5$ and $f = 0.375$. Whole process is outlined in the Fig. 3.

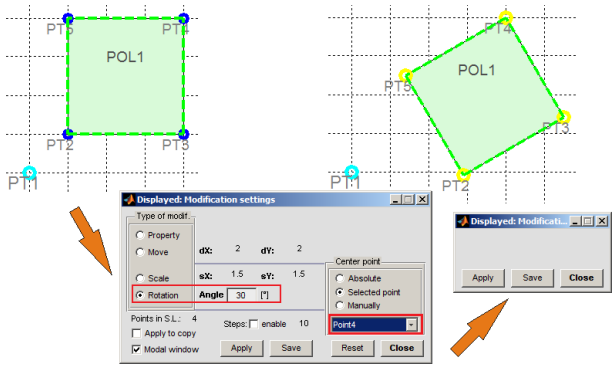

Fig. 5. IFSMaker: base object modification

III. Solving Resonant Frequency Using the Cavity Model

Cavity Model (CM) consider patch antenna as a 2D cavity with perfect magnetic condition (PMC) and perfect electric condition (PEC) as shown in Fig. 6. Mathematically, the conditions are defined as:

$$\mathbf{E} \times z = 0,\ \mathbf{H}.\mathbf{z} = 0;\ \text{for } z = 0, z = h, \tag{4}$$

$$\mathbf{H} \times n = 0,\ \mathbf{E}.\mathbf{n} = 0;\ \text{boundary of antenna.} \tag{5}$$

After some manipulation, the scalar Helmholtz equation can

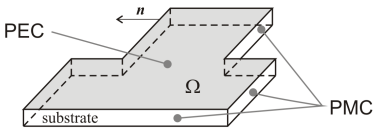

Fig. 6. CM conditions

be derived:

$$(\nabla_t + k_n^2)\, E_{z,n} = 0 \tag{6}$$

where $\nabla_t = \left(\frac{\partial^2}{\partial x^2} + \frac{\partial^2}{\partial y^2}\right)$ and k_n^2 are eigenvalues. Resonant frequencies are obtained from the equation $\lambda_n = k_n^2$. It's assumed that there's no magnetic material under the patch:

$$f_n = \frac{c_0}{2\pi\sqrt{\epsilon_r}}\lambda_n, k_n^2 = \omega^2\mu_0\epsilon. \tag{7}$$

Closed-form solution is known only for special (canonical) cases, thus FEM (Comsol Multiphysics, [5]) is used for solving eq. (6). Early version utilized Matlab's PDE toolbox, in the future we would like to use our in-house characteristic mode

solver (TCM, [4]), which is much more accurate. TCM solver is used for reference purpose currently.

Eq. (6) may be written in compact form in terms of linear operator equation:

$$L\psi_n = \lambda_n \psi_n. \tag{8}$$

Unfortunately, CM approximation has some prepotent restrictions, for instance the height of antenna is limited to $h \ll \lambda$. Further details can be found in [3].

A. EvalInFem Application

The EvalInFem call has to be performed every time. This is very important to keep the optimization process fluent. It is, therefore, necessary to handle geometry exceptions (disconnected parts of the patch..), problems with meshing, Comsol connection loose etc.

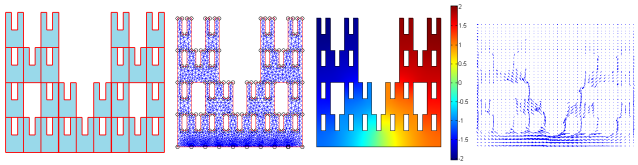

Fig. 7. Cavity model procedure (IFS patch, mesh, eigenvalue problem, current distribution; FRC_C)

Some of the resulting modes (usually 1-2 modes) are incorrect due to the numerical noise and have to be cutted off. Whole structure is updated to keep constant size (5cm or 10cm for example), thus agents results can be compared each other. EvalInFem function is relatively fast (approximately 4-7 second per count).

IV. Particle Swarm Optimization

Particle swarm optimization (PSO) is based on swarm intelligence. This kind of optimization is highly stable, fast and very robust mainly because of low risk of local minima hangup.

Basic principle of the PSO rely on swarm of agents moving over the given's function space, [6]. During every algorithm iteration, fitness functions (f.f.) for all the agents is evaluated. Behavior of the swarm is described by the following equation:

$$v_{id}^{n+1} = w v_{id}^{n} + c_1 r_1^n (p_{id}^n - \chi_{id}^n) + c_2 r_2^n (p_{gd}^n - \chi_{id}^n) \tag{9}$$

Values p_{id}^n (every agent individual minimum) p_{gd}^n (global minimum of the whole swarm – best value of p_{id}^n) are weighted by a random values r_1^n a r_2^n. Their contribution is influenced by the constants c_1 and c_2, which affects the swarm behavior (cognitive vs social). Once we know the speed of agents, their position is updated:

$$\chi_{id}^{n+1} = \chi_{id}^{n} + \Delta_t v_{id}^{n+1} \tag{10}$$

Δ_t is a discrete time which can be chosen arbitrarily (generally, we suppose that $\Delta_t = 1$). At χ positions, new $gbest$ and $pbest$ are updated.

If the agents are not limited in space, there is a risk of their leaving the solution space s.s. (i.e. the space where the problem has physical meaning). Thus, proper wall has to be introduced – according to [7], invisible wall has been chosen. For agents outside the s.s, fitness function isn't evaluated and agents slowly returns back to a proper physical space. Consequently, computational time is effectively saved.

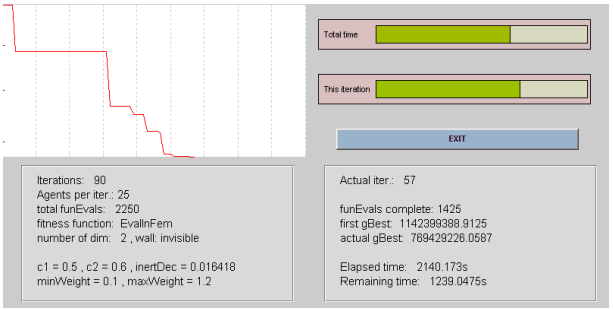

Fig. 8. PSOptimizer GUI

Algorithm described above was implemented into PSOptimizer application. Our optimizer is coded in a very general way and is able to optimize any m-file function which returns f.f. Then, p_{id}^n is accordingly updated. Cost function (c.f.) is depicted during the process, see Fig. 8.

It's very useful to know the physical nature of the given problem so proper choosing of the swarm size and maximum number of iterations may speed-up the optimization process. In principle it is impossible to find the best solution in finite time. Still we can locate a solution which is very good.

V. Current Distribution and Radiation Pattern

There are two ways to calculate the radiation pattern – using electric or magnetic current as complementary sources. The coordinate system, which fits to our case, is shown in Fig. 9. The magnetic currents on the edges of the patch is

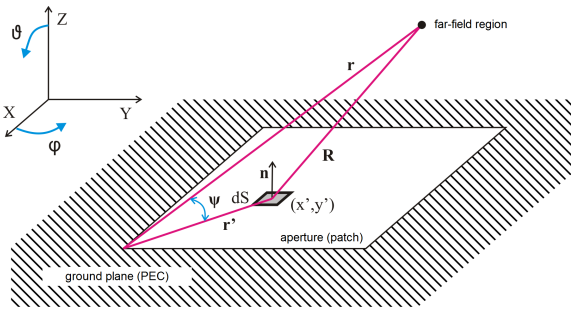

Fig. 9. Coordinate system for patch analysis

conventional source, because we compute less elements (edges elements only). On other hand, determination of outer normal vector is hard task. Hence, we use surface electric currents.

The spherical far-field components can be expressed as:

$$E_\theta = \frac{jk\eta e^{-jkr}}{4\pi r} \iint_{(x,y)} (J_x \cos\phi + J_y \sin\phi) \cos\theta \, e^{jkr'} \mathrm{d}x\mathrm{d}y \tag{11}$$

$$E_\phi = \frac{jk\eta e^{-jkr}}{4\pi r} \iint_{(x,y)} (-J_x \sin\phi + J_y \cos\phi) e^{jkr'} \mathrm{d}x\mathrm{d}y, \tag{12}$$

where $r' = x' \sin\theta\cos\phi + y' \sin\theta \sin\phi$, $\eta = \sqrt{\frac{\mu}{\epsilon}} = Z_0$ and $\beta = \omega\sqrt{\mu\epsilon}$. The remaining component $E_r \cong 0$. Finally, the directional pattern is given by:

$$D(\theta,\phi) = \frac{4\pi E^2(\theta,\phi)}{\int_0^\pi \int_0^{2\pi} E^2(\theta,\phi)\mathrm{d}\Omega}, \tag{13}$$

where $E^2(\theta,\phi) = E_\theta^2 + E_\phi^2$. More details could be found at [8] and [11].

VI. Results

Flowchart of the whole optimization loop is shown in Fig. 10. We will now demonstrate the optimization of a fractal-patch fundamental resonant mode frequency.

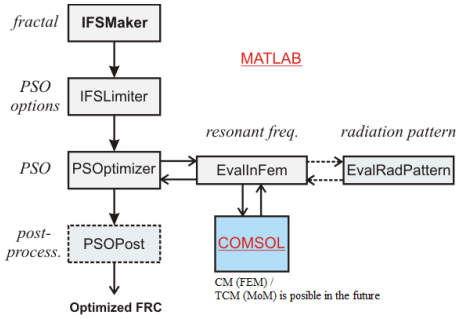

Fig. 10. Project workflow

Modal frequencies of the selected structure (FRC_K, Fig. 3), (with the maximum x- size being kept constant 100mm) is at Tab. I left and Tab. II respectively.

Now the optimization conditions and bounds has to be defined and stored into the PsoData structure. For this purpose, IFSLimiter tool reads the FRC and exports the PsoData, see Fig. 11.

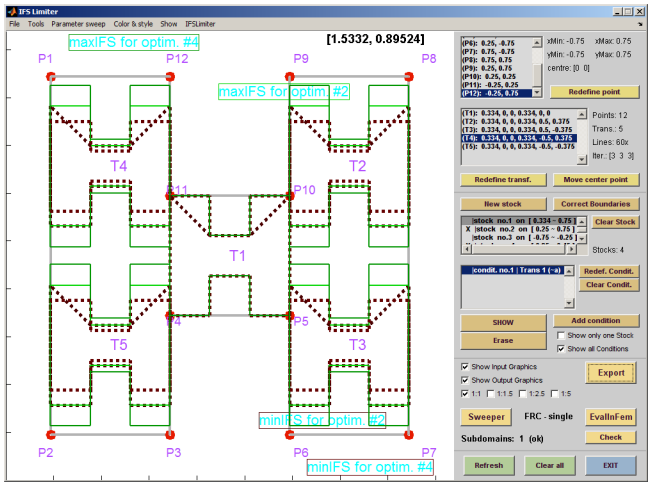

Fig. 11. PSO conditions in the IFSLimiter (FRC_K)

The optimization is now initiated with the choose of 45 agents, 200 iterations and constants c1, c2 = 2:

or
- ResTb = PSOptimizer(PsoData,'EvalInFem',45,200)
- ResTb = EvalInFem('pso',PsoData,45,200)

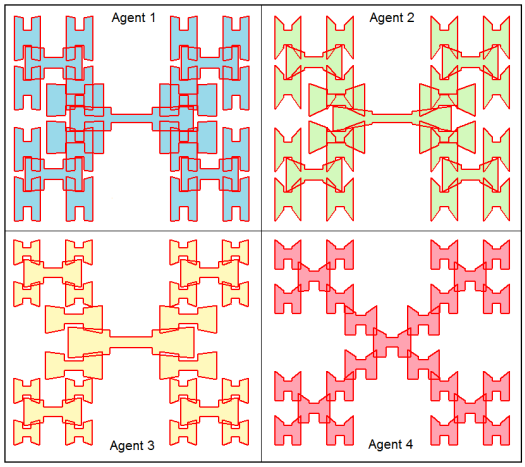

Fig. 12. A few agents of PSO algorithm

During the optimization, Comsol's cavity model is processed through the EvalInFem function which receives current data from the optimizer, generates the IFS collage, performs meshing (+sets boundary conditions etc.). Finally, the solver (femeig) is called and after some postprocessing steps, resonant frequencies are returned back to the PSOptimizer for evaluation.

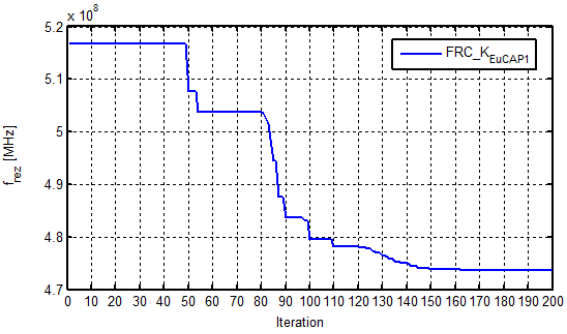

Fig. 13. Cost function for optimization

From Tab. I it is observed that dominant mode of the optimized patch is roughly 30% lower than the original structure. Of course, we should treat such values as estimation only, because CM doesn't include all the phenomenons like the internal coupling. It's recommended to refine this results with full-wave simulation (CST MWS) or with characteristic modes.

Resonant frequencies for first four modes in TCM solver are higher (about 20%, hold generally). Nevertheless, the current distributions are similar for CM and TCM, see Fig. 15. Next table (Tab. II) shows the trend of frequency reduction with increasing iteration. This phenomenon is very well known in literature. In addition, the same trend is valid to both source and optimized patch.

www.ietdl.org

Published in IET Microwaves, Antennas & Propagation
Received on 30th June 2010
doi: 10.1049/iet-map.2010.0269

Special Issue on RF/Microwave Communication Subsystems for Emerging Wireless Technologies

ISSN 1751-8725

Software tools for efficient generation, modelling and optimisation of fractal radiating structures

M. Capek P. Hazdra P. Hamouz M. Mazanek

Department of Electromagnetic Field, Czech Technical University in Prague, Technicka 2, Prague, 16627, Czech Republic, Europe
E-mail: hazdrap@fel.cvut.cz

Abstract: This study describes in-house developed software tools for designing micro-strip patch fractal antennas. As the fractal geometry is quite complex, IFSMaker application was developed purposely for an easy definition and maintaining of planar fractal structures. In the next step, the authors use the cavity model technique for modal analysis of internal fields of the patch. This simplified model is reasonably fast, so that the optimisation loop may be employed in order to reduce the fundamental mode resonant frequency. This is accomplished with the EvalInFEM, PSOoptimizer and IFSLimiter applications. The theory of characteristic modes is then used to refine the results and finally the antenna is simulated with a full-wave CST simulator, built and measured.

1 Introduction

Micro-strip patches with fractal geometry are in focus of many researchers, see, for example, [1]. The reasons are both practical and purely scientific. Sapoval [2] studied the properties of fractal resonators concluding that atypical resonant modes exist on them. In an electromagnetic area, modes on fractal micro-strip patches exhibit similar properties. In our work we are mainly interested in the lowest (fundamental) mode of whose resonant frequency we try to minimise using the particle swarm optimisation (PSO) [3, 4]. Resonant frequencies are evaluated through the cavity model (CM) simplification [5] and the scalar Helmholtz equation is numerically solved by the finite-element method (FEM) utilising the COMSOL Multiphysics software [6]. Further refinement of modal properties is accomplished by the usage of the characteristic modes [7].

2 Generation of planar fractal structures

For the purpose of generating planar fractal structures in a very general way, the so-called iterated function systems (IFS) algorithm [8] has been employed. It is defined as the following union

$$\boldsymbol{w}(X) = \bigcup_{i=1}^{m} w_i(X), X \subseteq R^n \tag{1}$$

Where the affine transformations w_i are given by

$$w: \begin{pmatrix} x_{\text{new}} \\ y_{\text{new}} \end{pmatrix} = \begin{pmatrix} a & b \\ c & d \end{pmatrix} \begin{pmatrix} x_{\text{old}} \\ y_{\text{old}} \end{pmatrix} + \begin{pmatrix} e \\ f \end{pmatrix} \tag{2}$$

In the equation above, a and d control scale, b and c rotation and e and f translation of the given x and y points set. This contractive linear transformation is iteratively applied to every point of the base object [8]. An intuitive application IFSMaker (Fig. 1) has been coded in MATLAB allowing us to design the base object and set of required transformations easily. All the parameters could be interactively tuned to see their effect on the resulting fractal of chosen iteration immediately.

IFSMaker can export fractal geometry in .txt (set of points), .3dt (IE3D [9]) format as well as in our MATLAB structure (FRC) containing a, b, c, d, e, f coefficients, base object and iteration stage.

3 Cavity model analysis

Cavity model (CM) [5] is a well-known simplification for micro-strip patch antennas based on treating the patch as 2D cavity with perfect magnetic walls on boundary. We search for a set of eigenfields and related resonant frequencies by solving the scalar Helmholtz equation

$$L E_{z,n} = 0 \tag{3}$$

with boundary conditions $(\partial E_z/\partial \boldsymbol{n}) = 0$, where $\boldsymbol{n}$ is outer normal to the patch. The operator L is defined as

$$L = \left(\frac{\partial^2}{\partial x^2} + \frac{\partial^2}{\partial y^2} + \lambda_n \right) \tag{4}$$

and it is assumed that the patch is lying in the XY-plane. Equation (3) is solved by the FEM with the help of

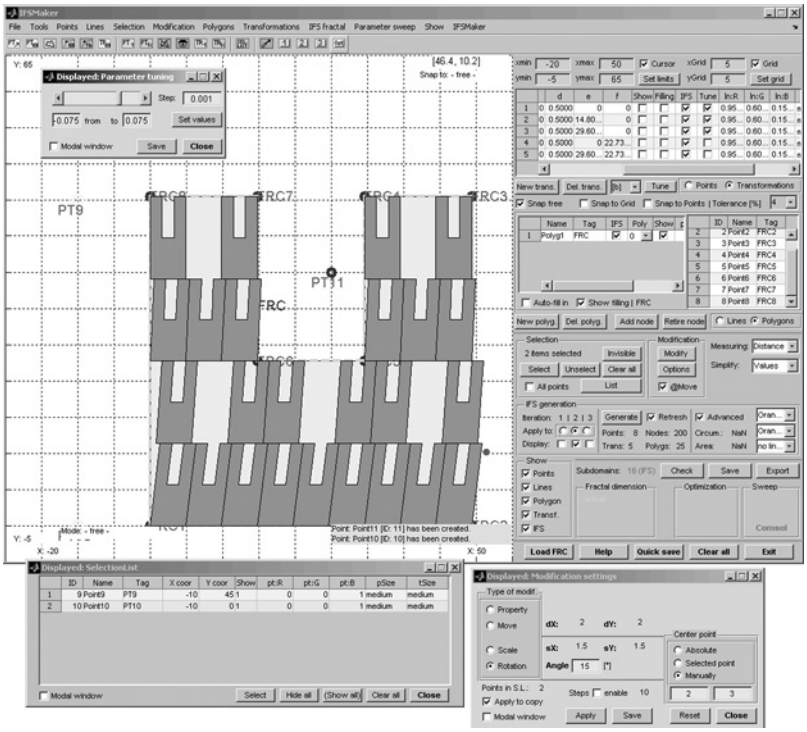

Fig. 1 *IFSMaker*

COMSOL Multiphysics [6]. Results are resonant frequencies

$$f_n = \frac{c_0}{2\pi\sqrt{\varepsilon_{\text{reff}}}}\sqrt{\lambda_n} \tag{5}$$

where c_0 is the speed of light in free space, $\varepsilon_{\text{reff}}$ effective permittivity of the substrate and λ_n are eigenvalues. Every resonant frequency is associated with specific modal field distribution $E_{z,n}$ from which the surface electric currents are calculated through [10]

$$\boldsymbol{J} = \frac{-1}{j\omega\mu}\nabla E_{z,n} \tag{6}$$

The FRC structure exported from IFSMaker is an input for the CM solver incorporated in quite complex MATLAB's function EvalInFEM. Below is a list of tasks programmed in this function (see Fig. 2):

- polygon processing (scale), unification
- structure discretisation
- setting appropriate physics for COMSOL
- calling COMSOL for solution, postprocessing, resonant frequencies calculation.

4 Characteristic mode analysis

Characteristic modes for perfectly conducting bodies of area S are defined through the electric field integral equation (EFIE) [11] in our case. After applying the method of moments method, we arrive at the complex impedance matrix $\boldsymbol{Z} = \boldsymbol{R} + \mathrm{j}\boldsymbol{X}$ and following functional is defined

$$F(\boldsymbol{J}) = \frac{\langle \boldsymbol{J}, X\boldsymbol{J}\rangle}{\langle \boldsymbol{J}, R\boldsymbol{J}\rangle} = \frac{\text{power stored}}{\text{power radiated}} \tag{7}$$

which we intend to minimise; this means to maximise the radiated power. Current distributions that fulfil $F(\boldsymbol{J}) = \min$ on the PEC structure are called the external (characteristic) modes and depend only on the shape and frequency [12].

Associated Euler's equation for (7) is a standard weighed eigenvalue equation

$$X\boldsymbol{J}_n = \lambda_n R\boldsymbol{J}_n \tag{8}$$

Solution of (8) leads to the set of characteristic eigencurrents $\boldsymbol{J}_n$ and associated eigenvalues λ_n. The properties of eigenvalues are described in [13]; at this moment it is important to note that λ_n reflects the amount of reactive power (thus $\lambda_n = 0$ presents the nth mode resonance). Instead of eigenvalues, the so-called characteristic angles α_n are introduced to show more visible behaviour with frequency [14]. Characteristic

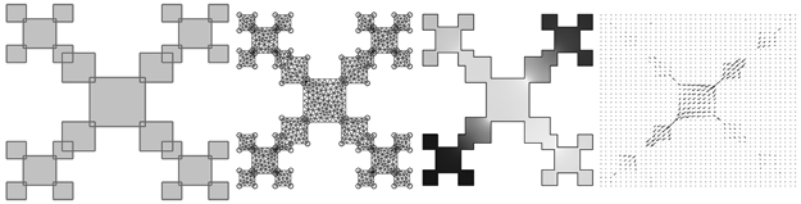

Fig. 2 *EvallInFEM workflow (IFS shape, mesh, solution of the eigenvalue problem – Ez and current distribution J)*

currents form a complete orthogonal set and hence the total current on a conducting body may be expressed as a linear superposition of these mode currents [13] (at a given frequency for which the $\boldsymbol{Z}$ matrix is calculated)

$$\boldsymbol{J} = \sum_n a_n \boldsymbol{J}_n = \sum_n \frac{\langle \boldsymbol{J}_n, \boldsymbol{E}^i \rangle}{1 + \mathrm{j}\lambda_n} \boldsymbol{J}_n \tag{9}$$

The expansion coefficients a_n comprise the $\langle \boldsymbol{J}_n, \boldsymbol{E}^i \rangle$ reaction term (responsible for coupling between the impressed field and current modes) and of the so-called modal amplitude factor $1/|1 + \mathrm{j}\lambda_n|$ reflecting a relative dominance of modes.

There is also relation of the modal superposition (9) and 'classical' direct matrix inversion employed in EM simulators, see Fig. 3. Advantage of the modal approach is gaining of additive useful information (characteristic modes and eigenvalues/characteristic angles).

The modal decomposition process has been implemented in the MATLAB environment using Makarov EFIE codes [15] with the RWG basis functions [16]. The usage is restricted to arbitrary 3D PEC structures with air dielectrics.

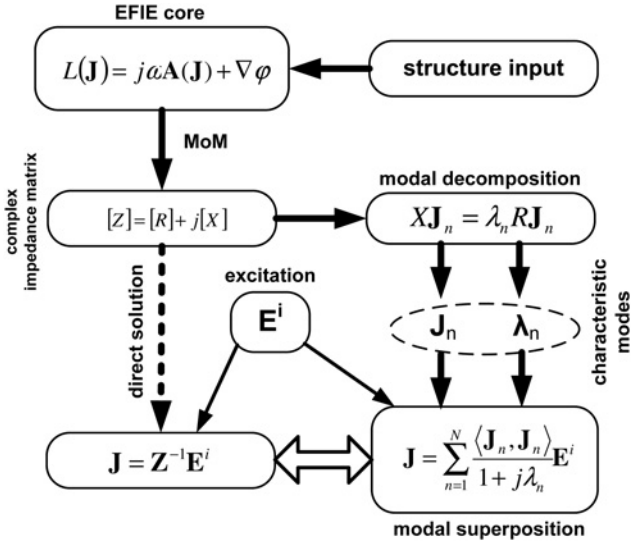

Fig. 3 *Relation between direct matrix inversion and the modal superposition*

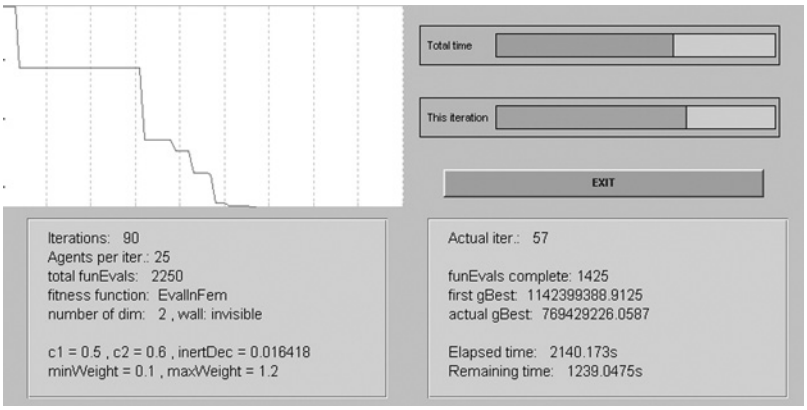

Fig. 4 *PSO tool interface*

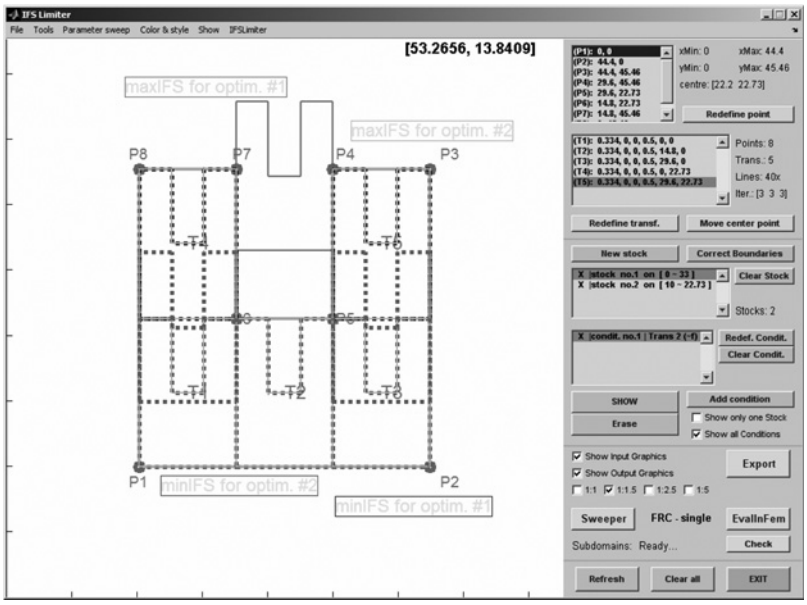

Fig. 5 *Screenshot of the IFSlimiter*

doi: 10.1049/iet-map.2010.0269

Our developed TCMtool has the main following advantages:

- comsol Multiphysics [6]/PDETOOLbox [17] mesh import, direct FRC format input
- optional Green's function for infinite ground plane simulations
- single solver/multicore solver/distributed solver (along a computer network with Matlab installed)

5 Particle swarm optimisation

The idea of the PSO algorithm [18] is based on nature swarm (bees etc.) behaviour. The PSO is initialised with a group of random particles (solutions) and then searches for optima by updating generations. In every iteration n, each particle is updated by following two 'best' values. The first one p_{id} is the best solution (fitness) it has achieved so far. Another 'best' value that is tracked by the particle swarm optimiser is the best global value p_{gd}, obtained so far by any particle in the population. After finding the two best values, the particle updates its velocity v

$$v_{id}^{n+1} = wv_{id}^{n} + c_1 r_1^n (p_{id}^n - x_{id}^n) + c_2 r_2^n (p_{gd}^n - x_{id}^n) \quad (10)$$

Furthermore, w is the weighting factor (which eliminates the oscillations along the global best), c_1, c_2 are constants and r_1, r_2 are randomly generated numbers with normal distribution from (0, 1) interval [19].

Once the direction and speed of agents is known, their new position is calculated according to

$$x_{id}^{n+1} = x_{id}^{n} + v_{id}^{n} \Delta t \quad (11)$$

where $\Delta t = 1$ is discrete time.

The above-described PSO algorithm has been implemented in the MATLAB environment (Fig. 4). Generally, it is able to

Table 1 FCL-2 IFS base set

N	X_n	y_n
1	−25	−25
2	25	−25
3	25	25
4	−25	25

Table 2 FCL-2 IFS T1–T5 transformations data

Transformation	a	b	c	d	e	f
T1	0.48	0	0	0.48	0	0
T2	0.48	0	0	0.48	13	13
T3	0.48	0	0	0.48	13	−13
T4	0.48	0	0	0.48	−13	13
T5	0.48	0	0	0.48	−13	−13

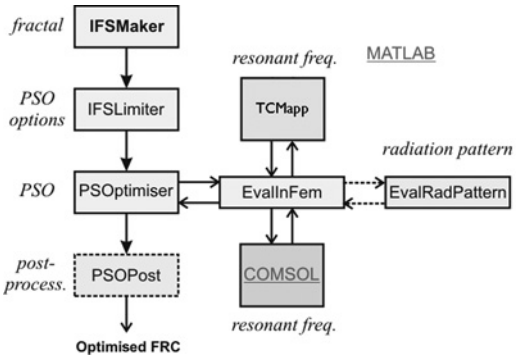

Fig. 6 *Optimisation workflow*

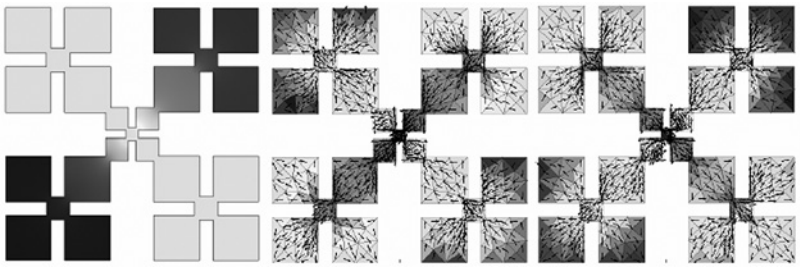

Fig. 7 *Optimised FCL-2 structure*
Dominant mode Ez (left) and first two degenerated characteristic currents J1 and J1′

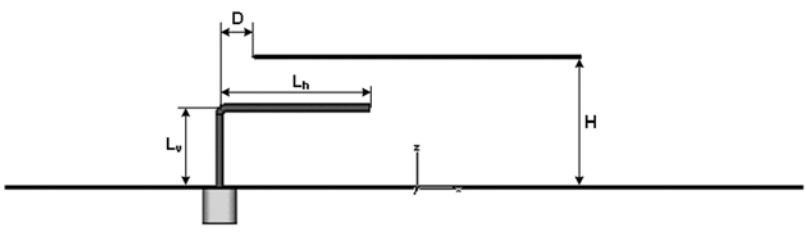

Fig. 8 *Layout of the L-probe fed patch*

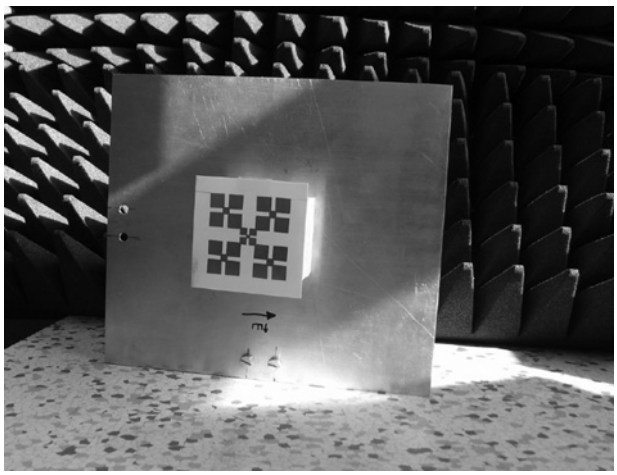

Fig. 9 *Manufactured sample of the FCL-2 antenna*

optimise any problem with fitness function given by the m-file.

6 Optimisation of the fractal patches

In this part we will discuss the optimisation of fractal patch structures created by the IFSMaker focusing on minimising the fundamental mode resonant frequency f_1. During the iteration loop, EvalInFEM evaluates (5) and its output f_1 is fitness function for PSO. For a given fractal structure (described by the FRC format variable), bounds for IFS parameters has to be set first. For this purpose, an interactive tool named IFSlimiter has been coded – see its screenshot at Fig. 5.

6.1 Example of miniaturised fractal patch antenna

The structure of our interest is the so-called FCL-2 (Fractal Clover Leaf of the 2nd iteration), which appeared in [20]

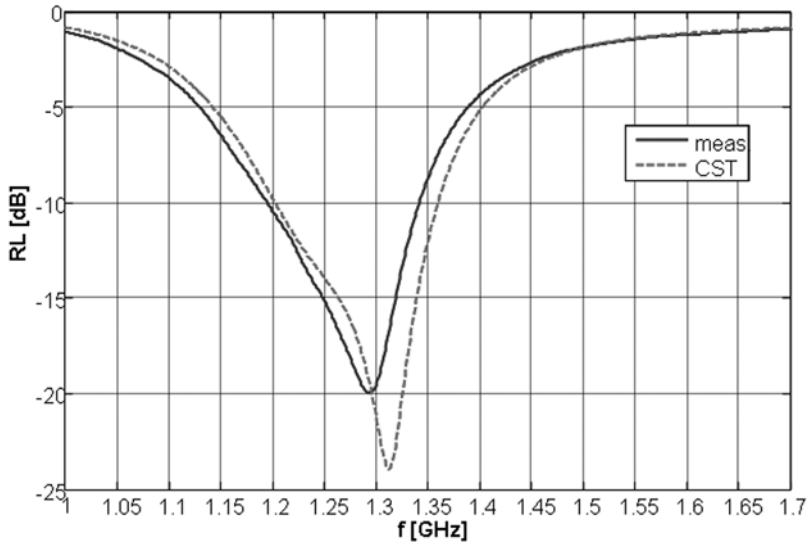

Fig. 10 *Simulated and measured return loss of the FCL-2*

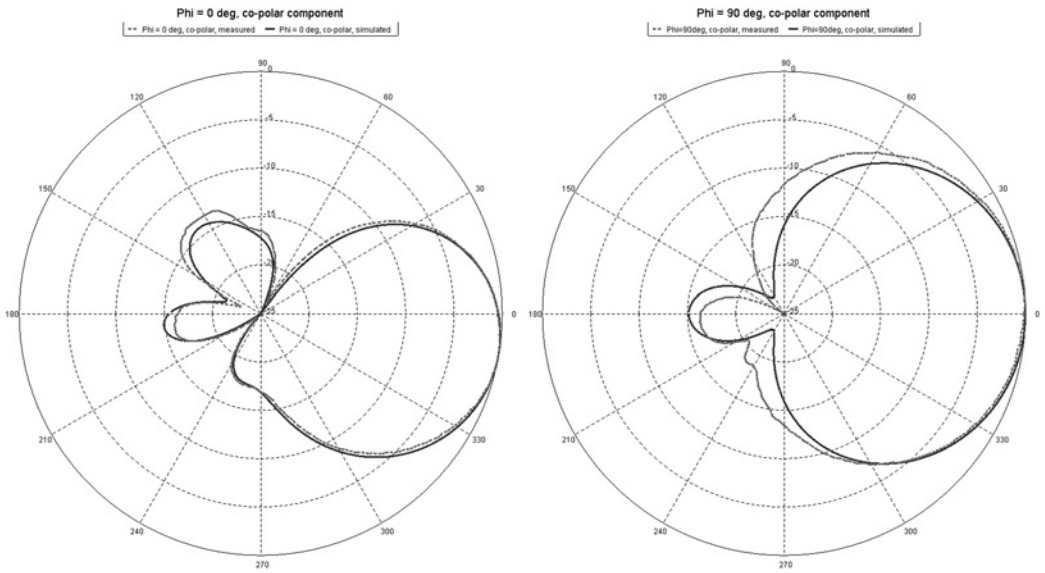

Fig. 11 *Simulated and measured radiation pattern cuts at centre frequency*
E-plane (left), H-plane (right)

doi: 10.1049/iet-map.2010.0269

and is described by the IFS coefficient shown in Tables 1 and 2.

The outer dimensions are fixed at 50 mm $\times$50 mm and kept constant through the whole optimisation. The set-up for the PSO is as follows:

- $c_1 = c_2 = 2$
- weighting coefficient w linearly varies from $w_{min} = 0.4$ to $w_{max} = 0.9$ through the PSO run
- 20 agents and 250 iterations (Comsol called 5000 times)
- Scale factors of $T1-T5$ transformations will be bounded to $T1$: $a \in \langle 0.2;\ 0.6\rangle$, $d \in \langle 0.2,\ 0.6\rangle$, $T2-T5$: $a \in \langle 0.4,\ 0.6\rangle$, $d \in \langle 0.4,\ 0.6\rangle$ (six parameters optimised in total)

After 250 iterations the dominant frequency was reduced from 1.35 to 1 GHz as obtained from CM calculation (see optimalisation workflow at Fig. 6). Characteristic modes give similar value – 1.19 GHz for the patch's height above infinite ground $H = 1$ mm. Fig. 7 shows the dominant mode field distributions – electric field from the CM and related characteristic currents $\boldsymbol{J}_1$ and $\boldsymbol{J}_1'$ (first two modes are degenerated). Note that 50 mm $\times$50 mm rectangular patch (iteration 0 of the FCL) has resonant frequency $f_{rect} = 3.3$ GHz, and so there is remarkable frequency reduction caused by the fractal geometry.

6.2 Feeding the patch and measurement

Because of broadband operation required, the patch is fed by the L-probe mechanism (Fig. 8), [21].

The height of the FCL-2 is set to $H = 36$ mm for which it resonates at 1.45 GHz according to the characteristic mode analysis. L-probe parameters were optimised by the CST Microwave Studio [22] to obtain wideband behaviour (loop around the Smith chart): $L_h = 41.5$ mm, $L_v = 19$ mm, $D = 0$. A manufactured sample of the antenna has been built and measured (Fig. 9). The holding substrate is made from foam and in simulations $\varepsilon_r = 1$ is considered. Antenna is etched on Rogers RO4350B substrate of thickness 0.762 mm $\varepsilon_r = 3.66$. The effective permittivity of this combination is estimated to be around $\varepsilon_{reff} = 1.4$.

Comparison of return loss (Fig. 10) shows good agreement between the simulation and the actual measurement. The relative frequency bandwidth (RL < -10 dB) is 13% with centre frequency $f_c = 1.3$ GHz.

Radiation pattern cuts (normalised, in dB) are shown at Fig. 11, simulated gain is 8 dBi with radiation efficiency $> 95\%$. The electrical size of the antenna is $0.213\lambda \times 0.213\lambda \times 0.153\lambda$.

7 Conclusions

This paper has described our effort in developing MATLAB codes for modal field decomposition and its applications in the design and optimisation of fractal-shaped micro-strip patch antennas. We started from the IFSMaker, a tool for the easy creation of planar IFS fractals. Analysis of generated fractal patches is then performed either by the Cavity Model, or by more accurate Characteristic Modes. Using the IFSLimiter together with the PSO optimiser, we are now able to optimise the IFS parameters in order to minimise the fundamental resonant frequency. L-probe feeding then allows us to design a miniaturised wideband fractal patch antenna as demonstrated by the IKS-2 patch.

Near-future plans are to employ multi-objective particle swarm optimisation (MOPSO) towards automating the antenna design under given conditions for resonant frequencies, radiation Q and radiation patterns. That would need to fully employ the characteristic modal analyser into the optimisation loop.

8 Acknowledgments

This research and publication have been supported by the Czech Ministry of Education, Youth and Sports in the frame of the project modelling and simulation of fields OC08018 (COST IC0603) and by the grant SGS10/170/OHK3/2 T/13.

9 References

1 Anguera, J.: 'Fractal and broadband techniques on miniature, multifrequency and high-directivity microstrip patch antennas'. PhD thesis, UPC, 2003
2 Sapoval, B., Gobron, T., Margolina, A.: 'Vibrations of fractal drums', *Phys. Rev. E*, 1991, **67**, (21), pp. 2974–2977
3 Kennedy, J., Eberhart, R.: 'Particle swarm optimization', *IEEE Neural Netw.*, 1995, **40**, pp. 1942–1948
4 Robinson, J., Rahmat-Samii, Y.: 'Particle swarm optimization in electromagnetics', *IEEE Trans. AP*, 2004, **52**, pp. 397–407
5 James, J.R., Hall, P.S., Wood, C.: 'Microstrip antenna theory and design' (Peter Peregrinus, London, UK, 1981)
6 http://www.comsol.com, accessed May 2010
7 Garbacz, R.J.: 'A generalized expansion for radiated and scattered field'. PhD thesis, Ohio State University, Columbus, OH, 1968
8 Falconer, K.: 'Fractal geometry: mathematical foundations and applications' (John Wiley, USA, 2003, 2nd edn.)
9 http://www.zeland.com, accessed May 2010
10 Balanis, C.A.: 'Advanced engineering electromagnetics' (John Wiley, USA, 1989)
11 Harrington, R.F.: 'Field computation by moment methods' (John Wiley, IEEE Press, USA, 1993)
12 Daviu, E.A.: 'Analysis and design of antennas for wireless communications using modal methods'. PhD thesis, UPV, Valencia, 2008
13 Cabedo, M., Antonino, E., Valero, A., Ferrando, M.: 'The theory of characteristic modes revisited: a contribution to the design of antennas for modern applications', *IEEE Antennas Propag. Mag.*, 2007, **49**, (5), pp. 52–68
14 Hazdra, P., Hamouz, P.: 'On the modal superposition lying under the MoM matrix equations', *Radio Eng.*, 2008, **17**, (3), pp. 42–46
15 Makarov, S.N.: 'Antenna and EM modeling with Matlab' (John Wiley, USA, 2002)
16 Rao, S.M., Wilton, D.R., Glisson, A.W.: 'Electromagnetic scattering by surfaces of arbitrary shape', *IEEE Trans. AP*, 1982, **30**, (3), pp. 409–418
17 http://www.mathworks.com, accessed May 2010
18 Eberhart, R.C., Shi, Y., Kennedy, J.: 'Swarm intelligence' (Morgan Kaufmann, USA, 2001)
19 Engelbrecht, A.P.: 'Fundamentals of computational swarm intelligence' (John Wiley, USA, 2006)
20 Tayefeh, M., Aligodarz, K.: 'Wideband miniaturized L-probe fed fractal clover leaf microstrip patch antenna' (Jina, France, 2004)
21 Mak, C., Luk, K., Lee, K., Chow, Y.: 'Experimental study of a microstrip patch antenna with an L-shaped probe', *IEEE Trans. AP*, 2000, **48**, (5), pp. 777–783
22 http://www.cst.com, accessed April 2010

Progress In Electromagnetics Research B, Vol. 33, 115–134, 2011

A METHOD FOR TRACKING CHARACTERISTIC NUMBERS AND VECTORS

M. Capek*, P. Hazdra, P. Hamouz, and J. Eichler

Department of Electromagnetic Field, Faculty of Electrical Engineering, Czech Technical University in Prague, Technicka 2, 16627 Prague 6, Czech Republic

Abstract—A new method for tracking characteristic numbers and vectors appearing in the Characteristic Mode Theory is presented in this paper. The challenge here is that the spectral decomposition of the moment impedance-matrix doesn't always produce well ordered eigenmodes. This issue is addressed particularly to finite numerical accuracy and slight nonsymmetry of the frequency-dependent matrix. At specific frequencies, the decomposition problem might be ill-posed and non-uniquely defined as well. Hence an advanced tracking procedure has been developed to deal with noisy modes, non-continuous behavior of eigenvalues, mode swapping etc. Proposed method has been successfully implemented into our in-house Characteristic Mode software tool for the design of microstrip patch antennas and tested for some interesting examples.

1. INTRODUCTION

Eigenmodes and eigenvalues are valuable characteristics of important electromagnetic operators like Electric Field Integral Equation EFIE [1]. After necessary numerical processing (as the analytical solution is available for only few canonical cases, [2]), those functional operators become discrete and are conventionally represented by a matrix [3]. Diagonalization techniques like the spectral matrix decomposition [4] or the Singular Value Decomposition (SVD) [5] are capable to obtain an orthogonal set of eigenmodes which are of great physical importance [6]. In the following text, spectral eigen-decomposition of the EFIE complex impedance matrix is performed in the frequency domain over a relatively broadband sweep (through several resonances).

Received 2 June 2011, Accepted 18 July 2011, Scheduled 28 July 2011

* Corresponding author: Miloslav Capek (capekmi2@fel.cvut.cz).

Unfortunately, it is found that modes and eigenvalues are not generally sorted properly with frequency. Mode order might be switched, or an unphysical solution arises. Moreover, some modes could turn up (or disappear) at any frequency step. We recognize the proper manipulation and tracking of the modes as the main problem when dealing with modal decomposition, namely the Theory of Characteristic Modes (TCM) [7]. Straightforward method used so far, based on simple eigenvector correlation, has been found insufficient for complex structures.

2. MATHEMATICAL FORMULATION OF THEORY OF CHARACTERISTIC MODES

The tangential electric field on a Perfect Electrical Conductor (PEC) satisfies the equation

$$\mathbf{E}^s_{\tan} + \mathbf{E}^i_{\tan} = 0, \tag{1}$$

where index s represents the scattered field and index i the incident field respectively. Since the radiated field $\mathbf{E}^s_{\tan}$ is a function of the induced surface current density $\mathbf{J}$, the following integral operator L is introduced:

$$L(\mathbf{J}) = \mathbf{E}^s_{\tan}. \tag{2}$$

Combining 1 and 2 we arrive at the so-called EFIE (Electric Field Integral Equation) [8]:

$$\left[L(\mathbf{J}) - \mathbf{E}^i\right]_{\tan} = 0. \tag{3}$$

The potential structure of the $L(\mathbf{J})$ operator is well-known and may be found e.g., in [9]. Since L relates field and current quantities, it has a character of impedance:

$$Z(\mathbf{J}) = [L(\mathbf{J})]_{\tan} \tag{4}$$

and in discrete form the above is known as the Method of Moments complex impedance matrix $\mathbf{Z} = \mathbf{R} + j\mathbf{X}$. For TCM modal-decomposition purposes, this matrix has to be symmetrical with its real and imaginary Hermitian parts [10]. Thus, the Galerkin method [11] is required for the construction of $\mathbf{Z}$.

Let us consider the following functional relation:

$$F(\mathbf{J}) = \frac{\langle \mathbf{J}, X\mathbf{J} \rangle}{\langle \mathbf{J}, R\mathbf{J} \rangle} = \frac{\text{power stored}}{\text{power radiated}}. \tag{5}$$

There exists a set of modal currents (called the characteristic ones) that minimize the above functional. These characteristic currents are thus maximizing the power radiated by the structure. It is known

that (5) could be minimized by solving the associated Euler's equation (weighted eigen-equation):

$$X\mathbf{J}_n = \lambda_n R\mathbf{J}_n, \tag{6}$$

where $\mathbf{J}_n$ are real characteristic currents and λ_n their associated eigenvalues [12]. Instead of eigenvalues, characteristic angles are being used often thanks to their steeper change:

$$\alpha_n = 180 - \arctan(\lambda_n). \tag{7}$$

Characteristic angles are (theoretically) continuous through the values of 90–270, resonance of the nth mode occurs when $\alpha_n = 180$. An illustration example of λ_n and α_n for a simple strip dipole antenna is shown at Fig. 1, the pink horizontal line marks the resonance. Half-wave dipole has been simulated as 300 mm long strip dipole of 5 mm width.

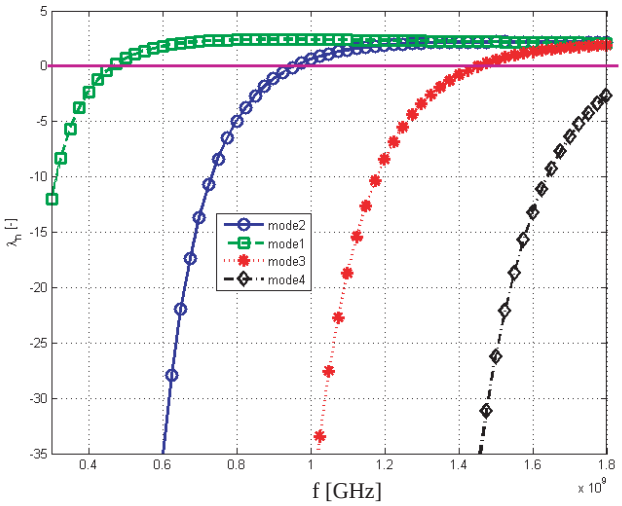

Figure 1. Eigenvalues and characteristic angles for simple strip dipole 300×5 mm, 6 modes.

The TCM has been implemented into Matlab's code. The EFIE core is based on the RWG elements [13].

3. THE TRACKING PROBLEM

By the numerical solution of (6) in Matlab (particularly by the eig function that make use of the LAPACK [14] package), eigenvalues and eigenvectors are obtained. The sorting problem is schematically depicted at Fig. 2 — during sequential frequency steps, mode order swaps (red arrows) or modes arise or vanish. This quite typical behavior is illustrated on an example of rectangular perfectly

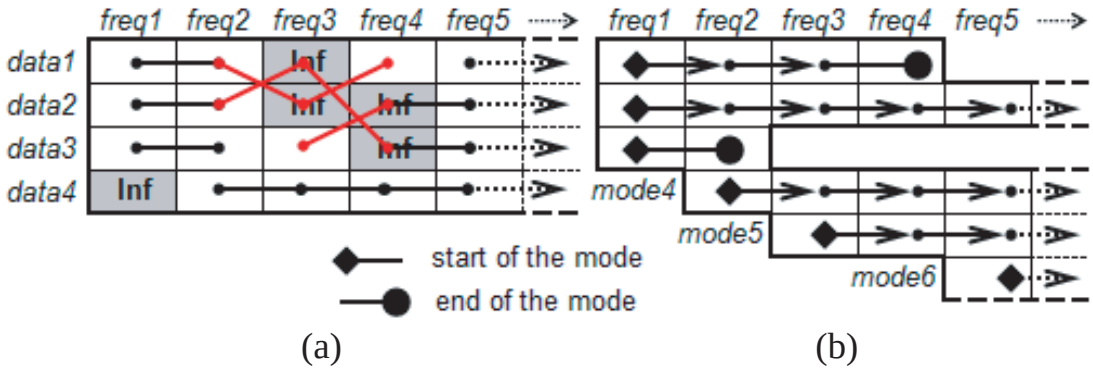

Figure 2. The tracking problem. Original data from TCM (a) and ideally sorted results (b).

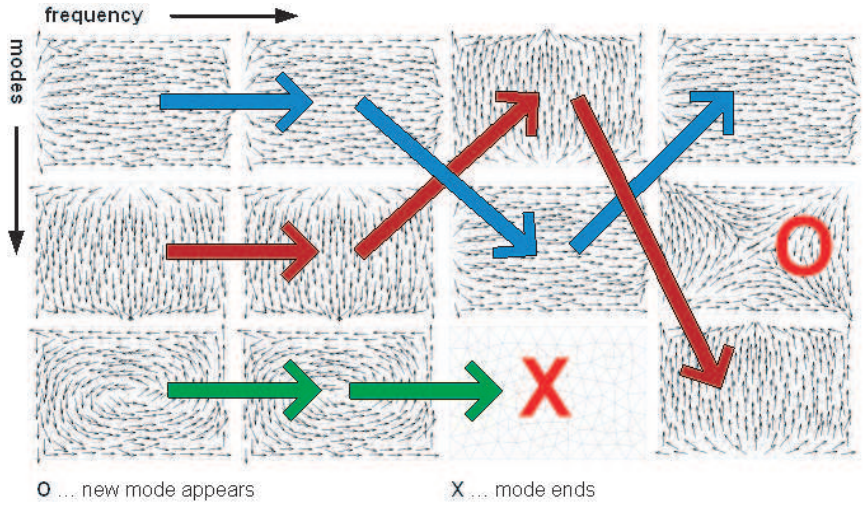

Figure 3. Unsorted characteristic currents for rectangular plate (modes 1. and 2. are swapping at 2nd and 3rd sample, mode 3 at 3rd position is corrupted).

conductive plate — see a few unsorted modes at Fig. 3. Clearly, the eigenvalues are swapped, so there are physically different current distributions along the frequency.

Let's demonstrate our effort on three examples of different structural and computational complexity. First is a 100 × 60 mm rectangle (further noted as Rec100 × 60, Fig. 4(a)), discretized with 244 triangular RWG elements. Eigenvalues have been calculated for frequencies 1 GHz–4 GHz with 50 MHz steps. For this simple case there are no serious sorting problems. The second example is represented by 110 × 30 mm U-slot patch antenna [15] (Fig. 4(b)) with 722 triangles and 161 frequency steps between 0.5 GHz and 4.5 GHz. The last (and

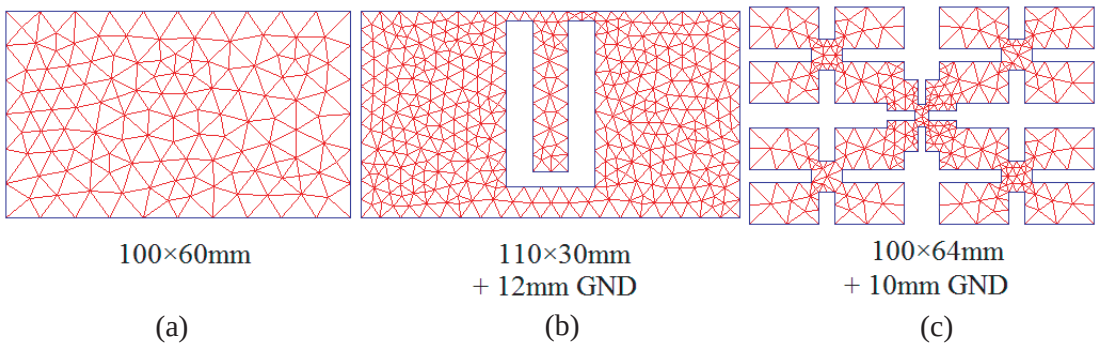

Figure 4. Demonstration examples (rectangle plate, U slot patch antenna and fractal antenna).

probably most interesting) example that will be discussed is the fractal patch antenna of 2nd iteration. Fractal motif is based on the "X" motif [16] (further noted as FRC_B2, Fig. 4(c)). The FRC_B2 fractal is discretized into 518 elements and computed at frequencies 0.7 GHz–2.8 GHz with 20 MHz steps. For the U-slot antenna and fractal patch antenna, infinite ground plane was considered (height of patches above the ground plane is 12 mm and 10 mm, respectively). It will be shown that initial simple eigenvector correlation approach (described later in Section 3.2) fails for such complex structures as this fractal one.

3.1. The Tracking Problem Definition

As already shown at Fig. 2 and Fig. 3, eigenvalues and eigenvectors are more or less randomly swapped and they need to be properly sorted. There are also other, accuracy-related, problems: matrix numerical noise (rounding errors) and matrix symmetry.

3.1.1. Eigenvalues

These numerical issues lead to $\pm\infty$ or 0 valued eigenvalues at certain frequencies. But fortunately, the frequency behaviour of eigenvalues could be interpolated later. Occasionally, some eigenvalues suddenly changes their sign (see later). Although the MoM code is based on the Galerkin testing procedure, the Z-matrix is not purely symmetrical [17]. As a result, some eigenvalues have unphysical imaginary parts which should be cut off. Another complication originates from the fact that the user may request more modes than are available at a given frequency. Such empty positions are replaced by the "NaN" values for further manipulation and user notification.

3.1.2. Eigenvectors

Problems with eigenvectors are weaker because they are directly used as the input data for tracking. Three main complications were recognized in eigenvectors context: zero vectors, numerical noise (chaotic modes) and degenerated modes.

All the above described numerical problems significantly complicate the respective tracking. Fig. 5 and Fig. 6 shows raw unsorted characteristic angles for Rec100 × 60, U-slot antenna and FRC_B2. It could be seen that there are frequent leaps as sketched at Fig. 2. Abrupt jumps to values of 90 or 270 are due to the +/− sign changes of characteristic numbers.

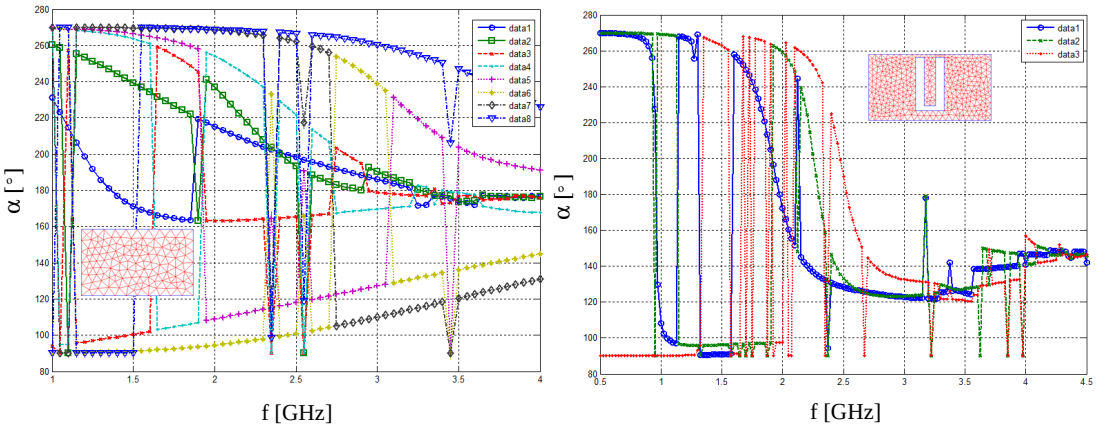

Figure 5. Unsorted raw characteristic angles ((a) Rec100 × 60, (b) U-slot).

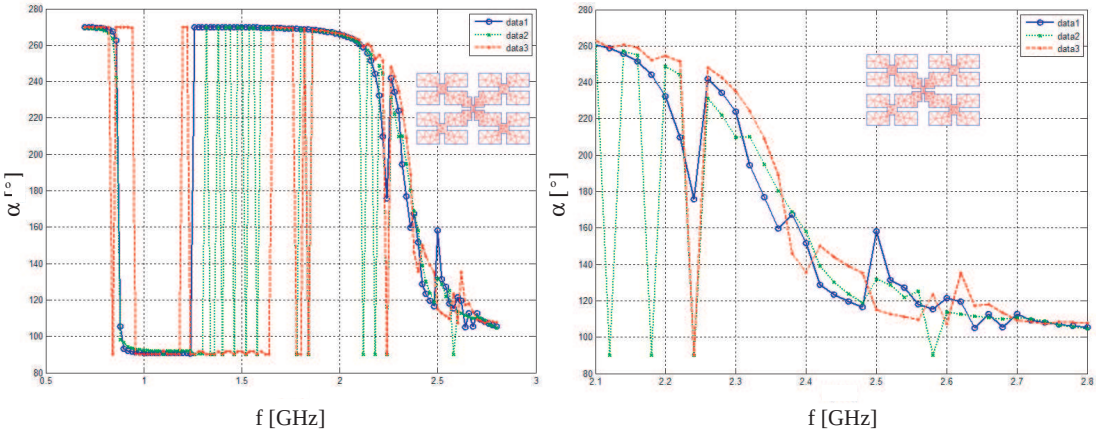

Figure 6. Unsorted raw characteristic angles ((a) FRC_B2 and (b) the detail at 2.1 GHz–2.8 GHz), only the first three modes are shown for clarity.

3.2. Previous Tracking Method

Previous tracking method was based on the correlation of the characteristic vectors (corrcoef in Matlab). Modes are sorted in eigenvalue-ascending order from the lowest frequency. Initially, modes from the first frequency are simply copied from the unsorted array to the sorted one. For all the combinations of modes on the first frequency and subsequent (yet unsorted) frequencies, the correlation coefficients of eigenvectors are calculated. For each mode on the first frequency, we find its next frequency pair with the highest respective correlation coefficient. Modes are then copied into an array dedicated for sorted modes and this procedure is repeated for all the frequencies in ascending order (see Fig. 7).

The above method is very simple because there is no need for any preprocessing — we work with eigenvectors directly obtained from the

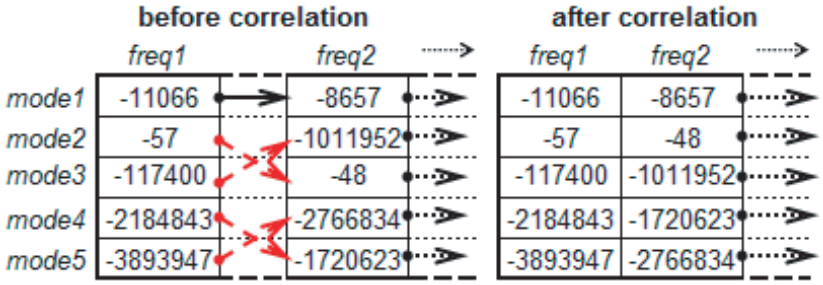

Figure 7. The schematic procedure for sorting using the correlation method and assigning the mode with the min. correlation coefficient (modes are represented by the char. number).

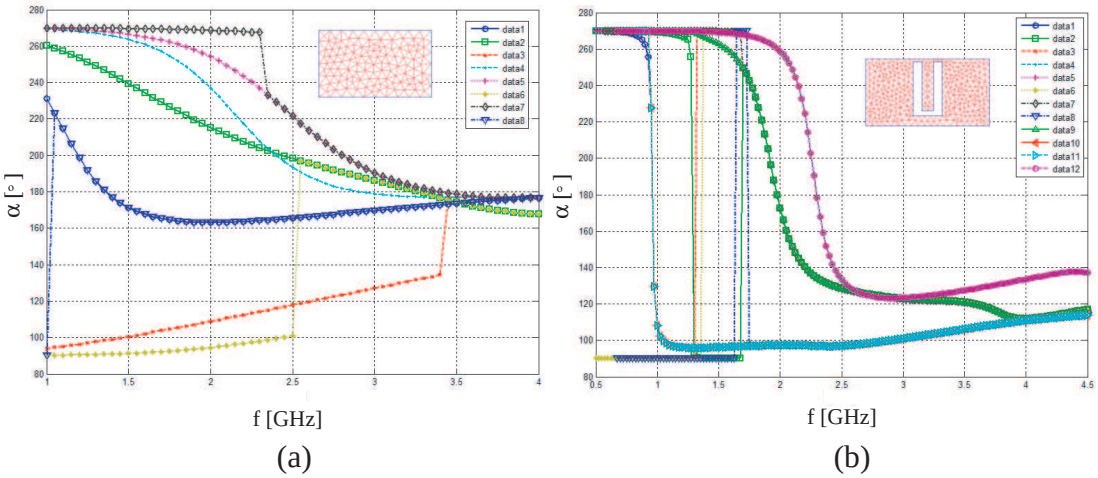

(a) (b)

Figure 8. (a) The sorted characteristic angles (correlation method) for Rec100 × 60 and (b) U-slot antenna.

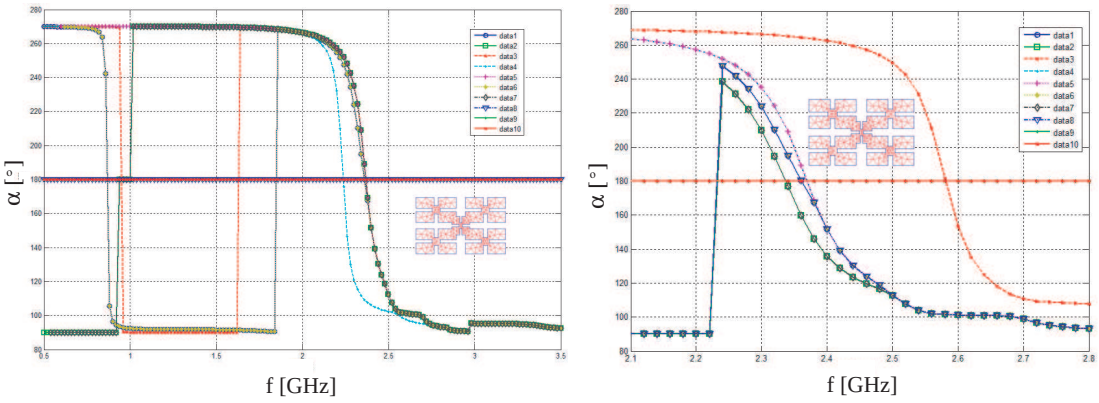

Figure 9. (a) The sorted characteristic angles (correlation method) for FRC_B2 and (b) the detail at 2.1 GHz–2.8 GHz, same structure. Compare these results with the unsorted data at Fig. 6 to notice swapping and missing modes.

eig function. All modes are treated as existing from the 1st frequency sample to the end of the tracking process. For simple structures, this approach is quite satisfactory (see Fig. 8 for rectangle without and with U-slot). For advanced structures, however, modes can easily "swap", or one mode might merge with another one; thereupon the mode goes missing on the remaining frequencies (Fig. 9, FRC_B2 (b)).

3.3. New Method

The new proposed tracking method is split into three stages — preprocessing of raw data from the eig function, main sorting and postprocessing (mode discrimination, eigenvalue interpolation and refining). Contrary to the correlation method described in Section 3.2, more tricks have had been employed, one of the basic precautions is that the Z-matrix is now calculated in double-precision. A slight increase in solving time (5–10%) is compensated by much precise sorting. Since the new tracking method algorithm is rather extensive, please follow the flowchart of the whole procedure shown at Fig. 10.

3.4. New Method: Preprocessing

While in the preprocessing stage, a number of operations are performed in order to prepare and optimize raw data from the eig function for main tracking routine. At first, eigenvalue and eigenvector matrices of dimension (Modes × Frequencies) are allocated, the Z-matrix is decomposed at all the frequency points and if all the requested modes are not found, relevant empty entries are filled with NaNs. After

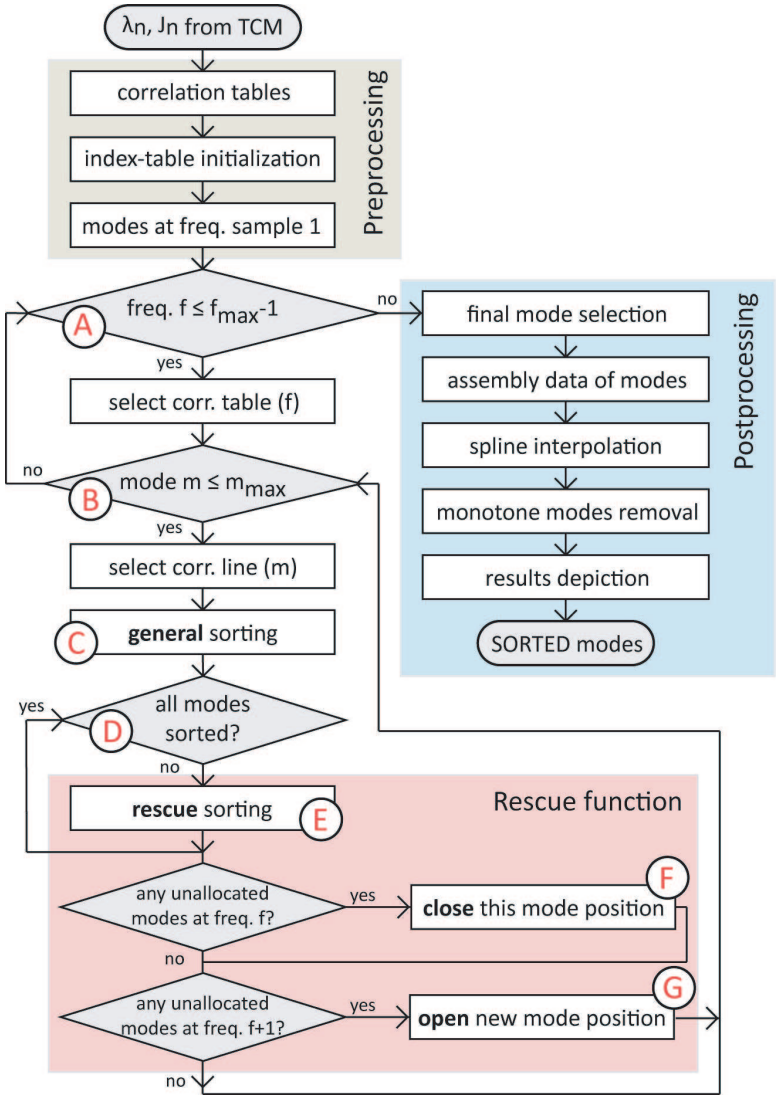

Figure 10. New sorting method flowchart.

necessary zeroing the imaginary part of the eigenvectors, correlation tables for all of the frequency samples and unsorted modes are computed.

For each single frequency we have to deal with rectangular matrix of dimension $E \times M$, where E is the number of triangle-edges and M is the number of modes.

Next, a similarity limit is calculated for every mode m (VEC_m) at a given frequency F with all the modes n at subsequent frequency $F+1$ (VEC_n). The similarity limit is based on a correlation between eigenvectors (note that the absolute value makes opposite oriented modes equal):

$$\rho_{m,n} = |\mathrm{corr}(\mathrm{VEC}_m, \mathrm{VEC}_n)|. \tag{8}$$

Sufficient number of mesh elements generally differs and depends on structure topology, desired accuracy of the modal shapes, number of requested modes and frequency. Convenient number of triangles is in order of hundreds for electrically small antennas.

At this point, the input data are correctly prepared and after the necessary Matlab allocations, we continue with the main tracking process.

3.5. New Method: Tracking Procedure

Tracking is performed sequentially through frequency samples. At every step, prearranged correlation table for corresponding frequency is loaded. Example of ordinary correlation table for sample frequency indexes 5 and 6 is depicted in Fig. 11(a).

We demonstrate our effort on an example depicted at Figs. 11–13. Typical correlation table is shown at Fig. 11(a). Higher freq. samples (namely 5th and 6th) have been advantageously chosen because of better clearness (mode *m3* is already closed at this frequency, so the Index Table could be used also for description of the Rescue Function). Correlations between all accessible (unsorted) modes at 5th and 6th frequency were calculated. Then the IT contains only sorted modes (from previous frequencies) and modes that are sorted in the Primary Sorting Routine (see Section 3.6). Because the meaning of IT is a little intricate, diagram at the bottom of Fig. 11 represents the sorted modes in more intuitive graphical form.

Right side of Fig. 11 depicts the index table of the sorted modes. The index table (IT, in Fig. 11(b)) is allocated in the preprocessing part and treated during both sorting process and post processing part. Each column of IT matches one sorted mode. Obviously, at the end of the tracking there could be more columns of the index table than the number of computed modes from the TCM decomposition.

During the sorting process, one of the three cases could occur:

(i) Primary sorting: Mode from frequency $F + 1$ (6th sample at Fig. 11(a)) sufficiently correlates with some mode from freq. F (5th sample at Fig. 11(a)). See Section 3.6 later.

(ii) Rescue function: Mode from frequency $F + 1$ doesn't correlate with any mode from frequency F, but sufficiently correlates with mode from lower freq. sample (and which is already closed). More detail in Sections 3.7 and 3.8.

(iii) Opening new mode: Mode from frequency $F + 1$ doesn't correlate with any mode from frequency F, or from lower frequencies (where are the closed modes, for example the cell $F3$-*m3* at Fig. 11(b)), see Section 3.8.

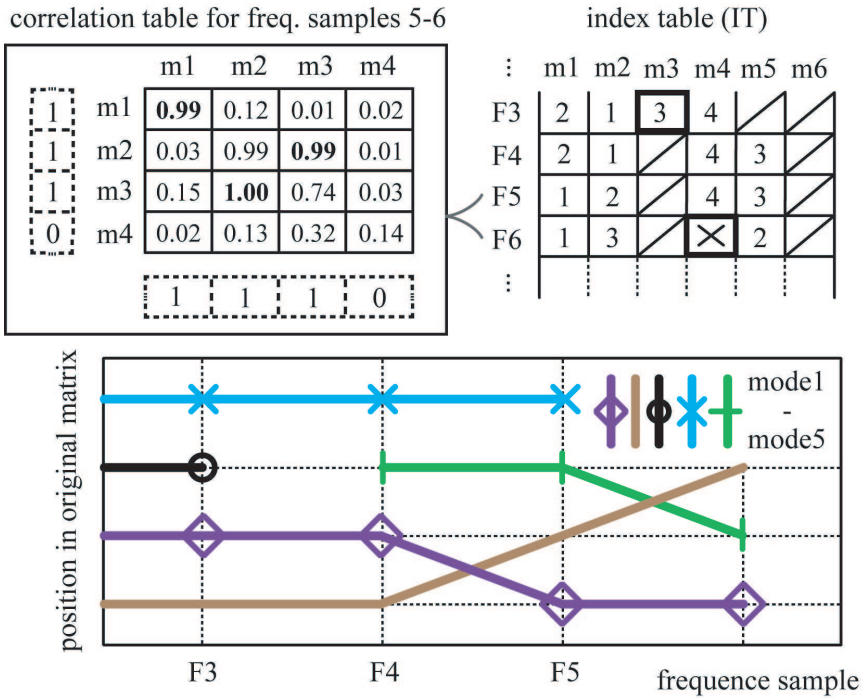

Figure 11. Treatment of correlation table at given frequency step ($m1$–$m4$ — modes from original matrix) and the sorted modes represented by table of indexes (IT); bottom part shows data from IT as a "trajectory" of modes during the sorting process (X — mode is closed, O — new mode is opened.).

Of course, as noted above, any mode can arise, vanish or rearise spontaneously anywhere. Thus, the algorithm has to be able to recognize all the cases mentioned hereinbefore.

3.6. New Method: Primary Tracking Routine

The desired tracking procedure is the ideal case stated as the number one — selected mode from previous frequency sample simply continues in the next frequency step (even though its position is different). It means that the correlation value is sufficient enough to join these modes together. The optimal value of minimal correlation depends on task type, as a rule we adopt the value of 0.8. Such mode is then internally marked as the employed mode (see the logical ones in dashed frames at Fig. 11(a)) and its position in the original matrix is saved to the IT.

Index table contains entries that points to real data stored in original matrix. We shortly recall that the original matrix is obtained from the eig runtime and it is unsorted and could be particularly damaged from the numerical point of view. Thus, for example at

Fig. 11, mode at position 3 in original matrix and at 5th frequency sample perfectly correlates ($\rho_{32} = 1$) with mode at position 2 at next (6th) frequency step.

It often happens that certain mode doesn't correlate sufficiently with any other mode (e.g., *m4* at Fig. 11 — no value exceeds 0.8). More sophisticated method, as described in part 3.7, should be used (see Ⓔ in the flowchart).

3.7. New Method: Rescue Function

The rescue function (ReF, Ⓔ in the flowchart) is employed when there's no regular solution found for one or more modes. In principle, this automatically occurs when null or chaotic eigenvectors appear, or when there are fundamental changes of currents with frequency so minimum similarity limit is not reached. It has been found suitable to find out all modes that are already closed and recalculate new correlations between these (closed) modes and modes awaiting allocation into the index table. The ReF maintains its local stack for this purpose. We try to demonstrate the ReF concept at Fig. 12(a). This figure refers again to data at Fig. 11. Output of the ReF is just binary and will be stated as "success" and "fail".

It is possible that some mode existed for several frequencies, than disappeared and after several more samples rearises. It would be appropriate to interconnect these parts because they represent the same mode. For instance, mode *m4* with low correlation at Fig. 11 failed in primary sorting and this is why the ReF is employed. The ReF algorithm collects all modes that are already closed. It is mode *m3* at frequency $F3$ at Fig. 11(a). Now, the ReF computes the correlation between mode *m4* at frequency $F6$ and mode *m3* at freq. $F3$. If the computed correlation satisfy the minimum correlation limit, closed mode *m3* will be reopened and linked with mode *m4* (Fig. 12(a)). Of course, because one mode was restored, another one has to be closed. ReF then finds the last mode that used the 4th index (mode *m4* in Fig. 12) and closes it (see the bold slash in cell *m4*-$F6$ at Fig. 12). For purposes of localization of the first and the last valid sample of mode, auxiliary vectors S and E have been implemented — see Fig. 12. Vector S denotes starting position and E denotes ending position of modes.

If ReF failed, most likely the new mode has been found (see Fig. 12(b)). Then task from the Section 3.8 is performed.

It was observed that about 30 percent of all modes in rescue function can be relinked (restored). This value, although generally dependent on numerical quality of the impedance matrix, was found almost constant for number of tested planar structures.

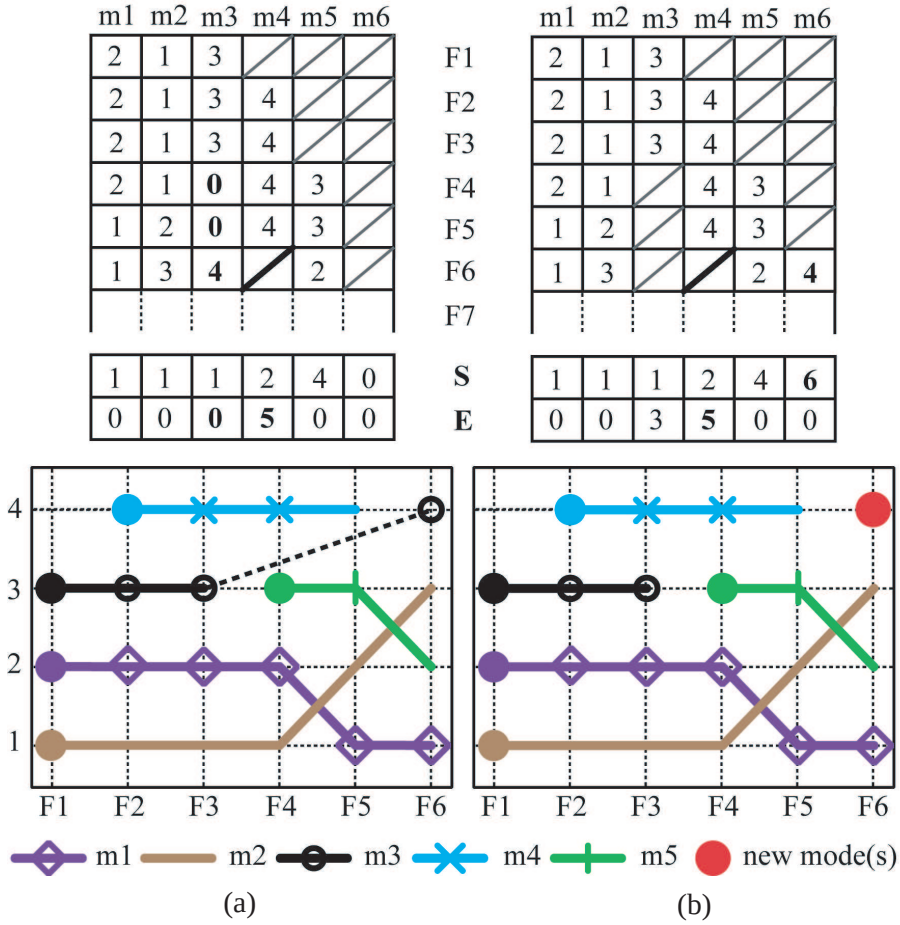

Figure 12. Example of the rescue function and opening modes at freq. sample $F + 1$ and closing modes at freq. sample F (rescue function succeeds at (a) and fails at (b)).

3.8. New Method: Opening New Mode(s)

An opening procedure is called whenever both primary tracking and the ReF break down. One or more new modes have to be established — see Fig. 12(b) where the Rescue Function fails in saving mode *m4* from Fig. 11. Then mode *m3* stays unopened and new mode *m6* is created. Starting position is equal to 6 (at the 6th frequency sample, see matrix S at Fig. 12(b)). The mode *m4* in index table is closed (the same bold slash as before), because it continues as the mode *m6*.

3.9. New Method: Post-processing

With the help of original data matrix and the information from IT, modes are assigned to their correct positions. Modes have different length and their number is greater than the size of the source matrix.

To improve the quality of the sorted results, automated post processing tools were developed and consist of:

(i) Mode pruning: Great number of modes found is especially caused by NaN or chaotic vectors. These modes have usually only one element in the index table. In post processing part it is possible to prune these ones (length of modes is optional).

(ii) Final mode assignment: All remaining modes in the index table IT are subsequently fulfilled with the real data stored in original (source) matrix. Indexes from the index table show the actual data position in original matrix.

(iii) Spline interpolation of empty places for rescued modes: It is convenient (e.g., for resonant frequency evaluation) to interpolate the empty places between the connected parts of modes that were rescued. Such places are zero-filled (for instance, see zeros in rescued mode *m3* in Fig. 12(a)). The spline interpolation is optional.

(iv) Monotonous modes removal: Several modes have negligible meaning within the computed frequency range; see Fig. 14 (modes with $\alpha \approx 90°$). This implies that these modes could be deleted to make the characteristic angles graph more transparent. Both limits (blue dashed lines in Fig. 14) are optional.

(v) Displaying results: All required variables are allocated and returned to the Matlab workspace. The set of requested sorted modes can be depicted and further manipulated (zoom, export).

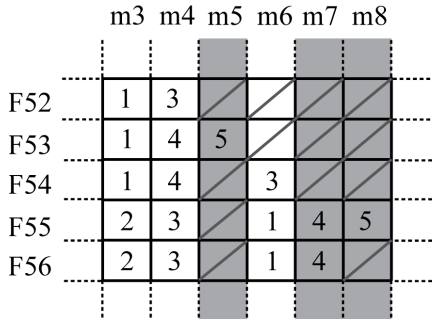

Figure 13. Example of pruning of the index table (all modes existing less than 3 frequency samples will be wiped off as shown by grey columns.

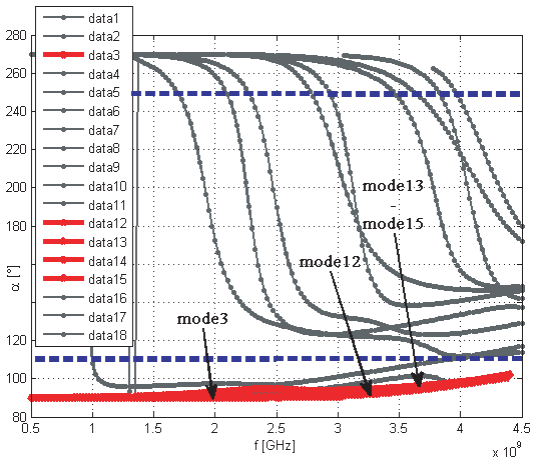

Figure 14. Removal of monotonic modes.

Figures 15 and 16 show the sorted characteristic angles by the method described above — no mode converges into itself nor swaps to another (compare with unsorted data at Figs. 5 and 6).

Finally, the storage matrices for eigenvalues and eigenvectors contain only real-valued entries now. Moreover, the eigenvalues were interpolated to present smooth behavior. This helps to easily find resonant frequencies, estimate modal radiation Q [18] and so on.

Unfortunately, one truly tough (but not crucial) problem still remains — managing degenerated modes. Example of degenerated modes is shown at Fig. 19. They are the same modes, but rotationally

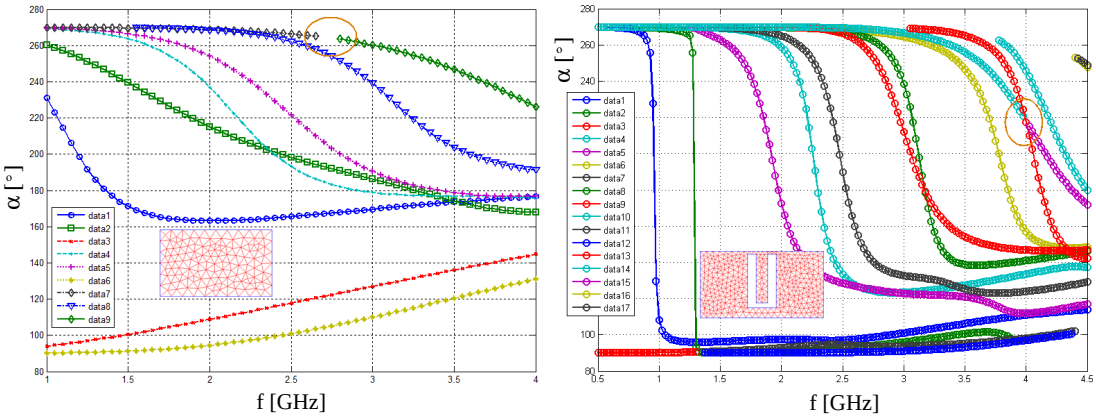

Figure 15. New sorting method: (a) Char. angles for Rec100 × 60 and (b) U-slot antenna.

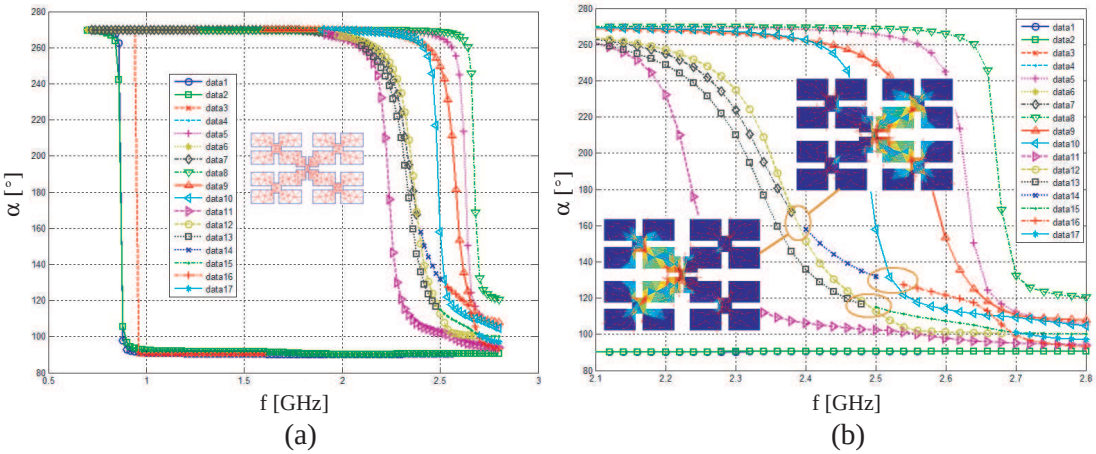

Figure 16. New sorting method: Char. angles for FRC_B2 (a) and the expanded part for 2.1 GHz–2.8 GHz (two degenerated modes at 2.38 GHz and 2.4 GHz are depicted).

symmetric. Degenerated modes can be identified at Figs. 15 and 16 as well and their appearance is marked by orange ellipses. To remedy this issue, some additional information has to be taken into the account (like the area occupied by currents), but this is subject for future work.

4. SOME LIMITATIONS

Proposed method has some limitations discussed below. The so-called split-ring [19] is introduced at Fig. 17. This structure shows a complex behavior (the thin-strip coupled elements). Even here, however, the suggested tracking method achieves favorable results (not comparable with ordinary correlation). Nevertheless, the individual modes are not tracked perfectly, see Fig. 18.

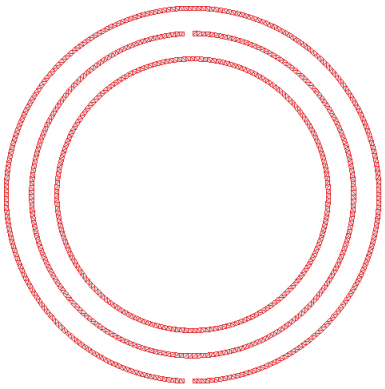

Figure 17. The split-ring example.

The correct selection of frequency samples is also important — fine step is very time consuming, very rough step leads to errors in the tracking algorithm (which can give bad results). As a compromise, it is advisable to select at least two samples between two nearest modal resonant frequencies. A better solution is to use iterative modal solver, which adaptively adds the frequency samples in places that have large mode distribution changes.

The correlation coefficient has an important role in the method and cannot be removed. It determines the degree of (non-) similarity where the selected mode is marked as a new (so far non-existing). This threshold cannot be determined analytically, since the input data contain numerical noise and their appearance is not known in advance.

Some examples (typically fractal structures) are still not sorted correctly. This could be due to degenerate modes or due to a large set of modes that are similar. Finer mesh would be better in this case.

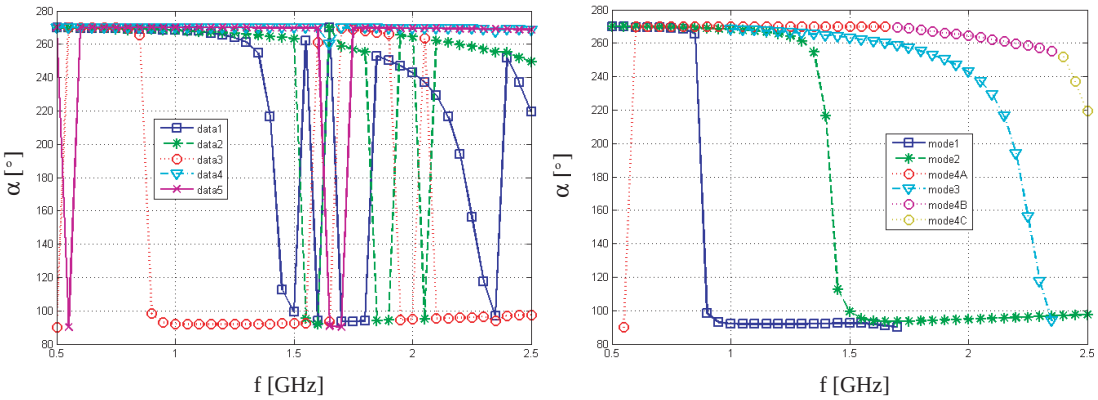

Figure 18. Char. angles for split-ring: (a) unsorted data and (b) new tracking method.

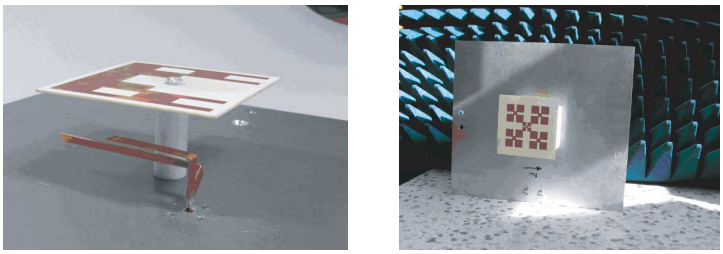

Figure 19. Manufactured fractal patch antennas ((a) FRC_C1 with double L-probe at and (b) FRC_B2).

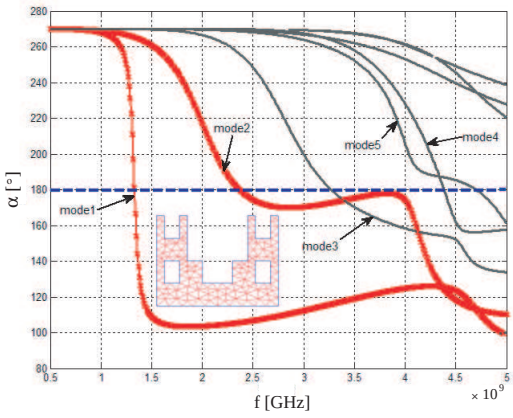

Figure 20. Sorted numbers of the FRC_C1 structure from Fig. 19(a). First two modes were used. Resonant frequency is marked as thick dashed line.

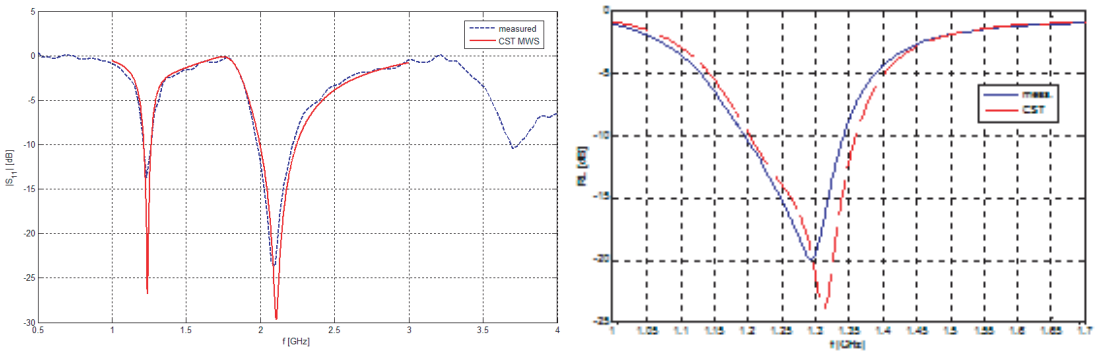

Figure 21. Simulated and measured return loss of antennas from Fig. 19.

5. APPLICATIONS

In this part we will briefly discuss practical applications of the new sorting method. Two planar antennas with fractal geometry are used for this purpose. Manufactured fractal antennas based on the U-shaped IFS and the FRC_B2 motif (mentioned above) are shown at Fig. 19. In case of the U-shaped antenna, two dominant modes at frequencies 1.35 GHz and 2.34 GHz can be easily identified by the TCM with the new sorting method incorporated, see Fig. 20. Because of need for dual-band antenna behavior, both modes were employed (it means that they are excited by a properly located double L-probe structure) [20]). Infinite ground plane has been included during the TCM analysis and height of the patch was set to $H = 29\,\text{mm}$. CST-MWS full-wave FIT simulator was applied at the very end of the design process for verification purposes of the TCM results. Comparison between simulated and measured return loss is shown in Fig. 21 and the agreement is obvious. Second antenna is shown at Fig. 19(b). Study of properly sorted modes again enables us to find the right place of feeding. More details about these particular antennas can be found in [21].

6. CONCLUSION

Eigenvalue decomposition of the moment impedance matrix produces not well ordered eigenmodes. It is needed for characteristic currents to be properly linked to their according eigenvalues in ascending order. Because the eigendecomposition might not be well numerically posed at all frequencies of interest, additional advanced sorting process has been developed and implemented into an already existing Characteristic mode analyzer. It is observed that proposed method is obviously

more efficient than the previous one that sorted just by correlation of eigenvectors. Still, there is need for further improvements before MoPSO could be subjoined in a robust way.

ACKNOWLEDGMENT

This research and publication have been supported by the grants DG102/08/H018 Modeling and simulation of fields, OC08018 (COST IC0603) and by the Grant Agency of the Czech Technical University in Prague, grant No. SGS11/065/OHK3/1T/13.

REFERENCES

1. Harrington, R. F., *Field Computation by Moment Methods*, John Wiley — IEEE Press, USA, 1993.
2. Hussein, K. F. A., "Fast computational algorithm for efie applied to arbitrarily-shaped conducting surfaces," *Progress In Electromagnetics Research*, Vol. 68, 339–357, 2007.
3. Harrington, R. F., "Matrix methods for field problems," *Proceedings of the IEEE*, Vol. 55, No. 2, 1967.
4. Davis, H. and K. Thomson, *Linear Algebra and Linear Operators in Engineering*, Vol. 3, Academic Press, 2000.
5. Press, W. H., S. A. Teukolsky, W. T. Vetterling, and B. P. Flannery, *Numerical Recipes in C*, Cambridge Univ. Press, U.K., 1992.
6. Liu, Y., F. Safavi, S. Chadhuri, and R. Sabry, "On the determination of resonant modes of dielectric objects using surface integral equations," *IEEE Transactions on Antennas and Propagation*, Vol. 52, No. 4, 2004.
7. Hazdra, P. and P. Hamouz, "On the modal superposition lying under the MoM matrix equations," *Radioengineering*, Vol. 17, No. 3, 2008.
8. Harrington, R. F. and J. R. Mautz, "Theory of characteristic modes for conducting bodies," *IEEE Transactions on Antennas and Propagation*, Vol. 19, No. 5, 1971.
9. Balanis, C. A, *Advanced Engineering Electromagnetics*, John Wiley, USA, 1989.
10. Abadir, K. and J. Magnus, *Matrix Algebra*, Cambridge Univ. Press, U.K., 2005.
11. Chari, M. and S. Salon, *Numerical Mathods in Electromagnetism*, Academic Press, 2000.

12. Cabedo, M. F., E. D. Antonino, A. N. Valero, and M. F. Bataller, "The theory of characteristic modes revisited: A contribution to the design of antennas for modern applications," *IEEE Antennas and Propagation Magazine*, Vol. 49, No. 5, 2007.
13. Makarov, S. N., *Antenna and EM Modeling with Matlab*, John Wiley, USA, 2002.
14. Anderson, E., et al., *LAPACK Users' Guide*, Society for Industrial and Applied Mathematics (SIAM), USA, 1999.
15. Lee, K. F., S. L. S. Yang, A. A. Kishk, and M. L. Kwai, "The versatile u-slot patch antenna," *IEEE Antennas and Propagation Magazine*, Vol. 52, No. 1, 2010.
16. Peitgen, H. O., H. Jrgens, and D. Saupe, *Chaos and Fractals*, Springer, USA, 2004.
17. Arajo, M. G., J. M. Brtolo, F. Obelleiro, and J. L. Rodrguez, "Geometry based preconditioner for radiation problems involving wire and surface basis functions," *Progress In Electromagnetics Research*, Vol. 93, 29–40, 2009.
18. Gustafsson, M. and S. Nordebo, "Bandwidth, Q factor, and resonance models of antennas," *Progress In Electromagnetics Research*, Vol. 62, 1–20, 2006.
19. Fan, J.-W., C. H. Liang, and X.-W. Dai, "Design of cross-coupled dual-band filter with equal-length split-ring resonators," *Progress In Electromagnetics Research*, Vol. 75, 285–293, 2007.
20. Chen, Y., H.-J. Sun, and X. Lv, "Novel design of dual-polarization broad-band and dual-band printed L-shaped probe fed microstrip patch antenna," *Journal of Electromagnetic Waves and Applications*, Vol. 23, No. 2–3, 297–308, 2009.
21. Hazdra, P., "Fractal patch antennas," Ph.D. thesis, CTU in Prague, Czech Republic, 2009.

The Evaluation of Total Radiation Q Based on Modal Approach

Miloslav Capek*, Pavel Hazdra*, Jan Eichler*, Pavel Hamouz*, Milos Mazanek*, Veronika Sobotikova†
*Department of Electromagnetic Field
Faculty of Electrical Engineering
Czech Technical University in Prague, Prague, Technicka 2, 166 27
Email: miloslav.capek@fel.cvut.cz
†Department of Mathematics
Faculty of Electrical Engineering
Czech Technical University in Prague, Prague, Technicka 2, 166 27

***Abstract*—The total Q of selected structures is to be calculated from the set of eigenmodes with associated eigen-energies and eigen-powers. Thanks to the analytical expression of these quantities, the procedure is highly accurate, respecting arbitrary current densities flowing along the radiating device. The electric field integral equation, Delaunay triangulation, method of moments, Rao-Wilton-Glisson basis function and the theory of characteristic modes constitute the underlying theoretical background. Calculation of the modal energies and Q factors enable us to study the effect of the radiating shape separately to the feeding. To outline some benefits of proposed method, the total radiation Q of a Huyghens source is calculated for several distances between a loop and an dipole.**

***Index Terms*—Antenna theory, eigenvalues and eigenfunctions, electromagnetic theory, Q factor.**

I. Introduction

The radiation Q factor has long been discussed as one of the most significant parameter of the radiating system, especially in the field of the electrically small antenna (ESA) theory [1]. For each structure, we can locate the minimum possible Q which is related to the maximum possible bandwidth (BW) potential [2].

The total Q of selected structure is calculated from the set of eigenmodes with associated eigen-Q factors. Modal approach is very helpful in antenna design because the entire procedure extracts the feeding from the given structure.

The main objective of this paper is to demonstate the validity of new expression for the summation of modal Q's. All algorithms are coded in Matlab R2011 and employed in our in-house antenna tool. Note that bold symbol denotes matrix (vector) form.

II. Modal Radiation Q

For modal analysis purposes Theory of Characteristic Modes (TCM) is utilized [3]. TCM is based on Electric Field Integral Equation (EFIE) [4], [5] with Rao-Wilton-Glisson (RWG) basis functions [6], [7]. Resulting eigenmodes must be properly sorted (tracked) [8].

Main output of the TCM is the matrix of eigenvectors which represent the current distribution on the given structure. It is thus appropriate to use the calculation method based directly on the sources (currents). These requirements have been fulfilled by G.Vandenbosch [9]. The derived expressions are rigorous, widely useable and easy to implement.

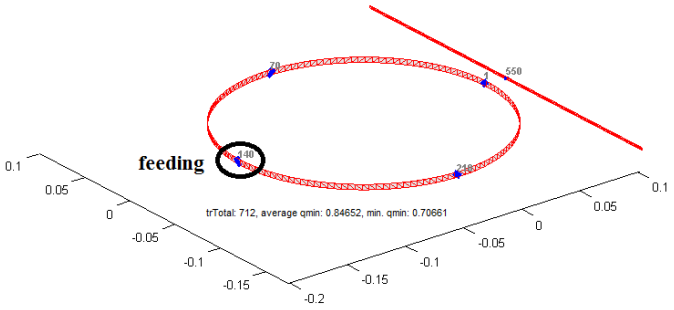

Fig. 1. RWG model of Huyghens source

General radiation Q definition could be also introduced in case of modal approach:

$$Q_{u,v} = 2\omega_0 \frac{\max\left\{\tilde{W}_e^{u,v}, \tilde{W}_m^{u,v}\right\}}{\tilde{P}_r^{u,v}} \tag{1}$$

where u and v are indexes of selected modes. Because of normalization, the radiated power $P_r^{u,u}$ is identically equal to one. However, radiated power $P_r^{u,v}$ and energies $W_{e/m}^{u,v}$ must be numerically calculated using the expressions in [9]. The above-mentioned integration is carefully performed, especially for overlaping elements (self-coupling terms), for detailed information see [10].

III. Sum of Modal Q Factors

Based on [10], the total radiation Q factor can be expressed as

$$Q_M = 2\omega_0 \frac{\max\left\{\sum_u^M \sum_v^M \beta_{u,v}\tilde{W}_e^{u,v}, \sum_u^M \sum_v^M \beta_{u,v}\tilde{W}_m^{u,v}\right\}}{\sum_u^M \sum_v^M \beta_{u,v}\tilde{P}_r^{u,v}}. \tag{2}$$

Note that we still assume the TCM approach with the Perfect Electric Conductor (PEC). Then the "beta" matrix is

$$\boldsymbol{\beta} = \frac{\langle \mathbf{j}_u, \mathbf{E}^i \rangle \langle \mathbf{j}_v, \mathbf{E}^i \rangle (1 + \lambda_u \lambda_v)}{(1 + \lambda_u^2)(1 + \lambda_v^2)}, \tag{3}$$

where $\mathbf{j}_u$ is u-th eigenvector, $\mathbf{E}^i$ is incident electric field and λ_u is u-th eigennumber.

Equation (2) can be further simplified. Considering unitary radiated power $P_r^{u,u}$, the denominator of (2) is

$$\sum_u^M \sum_v^M \beta_{u,v} \tilde{P}_r^{u,v} = \mathrm{tr}(\boldsymbol{\beta}). \tag{4}$$

Then the total Q_M is

$$Q_M = 2\omega_0 \langle \tilde{\mathbf{W}}_{e/m}, \boldsymbol{\beta}_0 \rangle \tag{5}$$

where $\boldsymbol{\beta}_0 = \boldsymbol{\beta}/\mathrm{tr}(\boldsymbol{\beta})$, $\langle A, B \rangle$ is general inner product and

$$\tilde{\mathbf{W}}_{e/m} = \begin{cases} \tilde{\mathbf{W}}_e & \text{if } \langle \tilde{\mathbf{W}}_e, \boldsymbol{\beta}_0 \rangle > \langle \tilde{\mathbf{W}}_m, \boldsymbol{\beta}_0 \rangle \\ \tilde{\mathbf{W}}_m & \text{if } \langle \tilde{\mathbf{W}}_m, \boldsymbol{\beta}_0 \rangle > \langle \tilde{\mathbf{W}}_e, \boldsymbol{\beta}_0 \rangle \end{cases} \tag{6}$$

To study the contribution of each mode, the following modification can be of interest:

$$Q_M = 2\omega_0 C \sum_u^M \sum_v^M S_{u,v}, \tag{7}$$

where C is

$$C = ||\tilde{W}_{e/m}^{u,v} \beta_0^{u,v}||_F \tag{8}$$

and

$$\mathbf{S} = \frac{\tilde{W}_{e/m}^{u,v} \beta_0^{u,v}}{C}. \tag{9}$$

Relation $||\mathbf{A}||_F$ denotes the Frobenius norm of matrix $\mathbf{A}$.

Resulting matrix $\mathbf{S}$ has unitary Frobenius norm $||\mathbf{S}||_F = 1$, all terms of $\mathbf{S} \in (-1, 1)$, in addition the diagonal terms are $\mathbf{S} \in (0, 1)$. Very interesting is also stand-alone scalar number $Q_M^* = 2\omega C$ where it is assuming, that the sum of $\mathbf{S}$ is identically equal to one.

IV. Evaluation of Total Q

We demonstate our effort on a Huyghens source [12], see Fig. 1. Planar Huyghens source consists of a loop with radius r and a dipole with length $2L$ and width w. Both of them are self-resonant at the same frequency (dipole: $2L = \lambda/2$, loop: $2\pi r = \lambda$). The distance between center of the loop and the dipole is d. The dipole is discretized into 432 triangles. The loop is discretized into 280 triangles and is fed by a voltage gap at the place highlighted at Fig. 1. Modal analysis is performed for distances $d \in r + \left\{\frac{\lambda}{32}; \frac{\lambda}{16}; \frac{\lambda}{8}; \frac{\lambda}{4}\right\}$ between a center of the loop and a middle of the dipole.

At first, the set of eigenmodes is computed and then the modal radiation Q_u factors are determined. For example of the modal Q factors of standalone loop see Fig. 2 (distance d is theoretically infinite). Similar results are obtained for case of the dipole. Corresponding eigennumbers are depicted in terms of eigenangles at Fig. 3. The eigenangles are defined as

$$\delta_u = 180 - \arctan(\lambda_u). \tag{10}$$

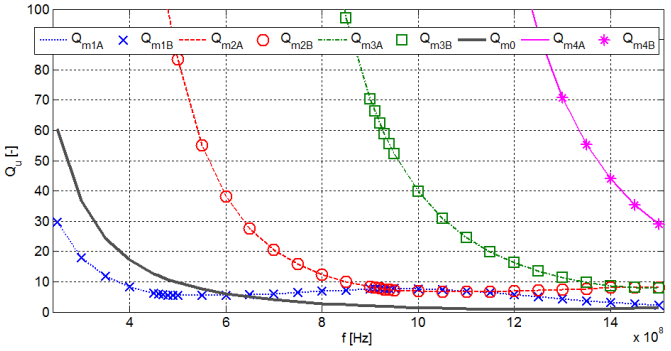

Fig. 2. Modal radiation Q_u of a loop

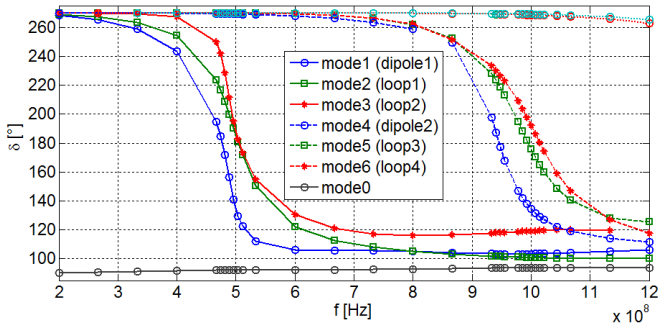

Fig. 3. Eigenangles of Huyghens source for distance $d = r + \lambda/16$

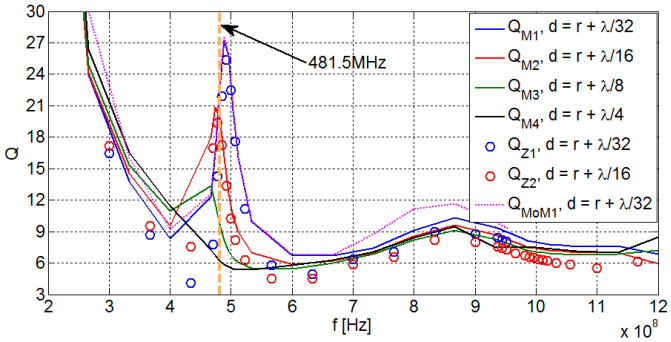

Fig. 4. Total Q_M computed for distances $d \in r + \left\{\frac{\lambda}{32}; \frac{\lambda}{16}; \frac{\lambda}{8}; \frac{\lambda}{4}\right\}$

Modal currents on loop, orthogonal two by two, are shown for instance in [11] and the behaviour of dipole is depicted in [10], respectively.

Second step considers the feeding positions – see voltage gap at Fig. 1. Proposed method is able to predict the lowest possible Q, but – in practice – the final Q_M is always (significantly) higher.

For future development some numerical issues must be taken into account – e.g. improved singularity handling, unstable EFIE round about resonance frequencies.

But even through the problems mentioned above, the radiation factor Q_M respects deeper matters than the circuit-like parameter Z_{in} whose derivation is the principle of Q_Z calculation, [2].

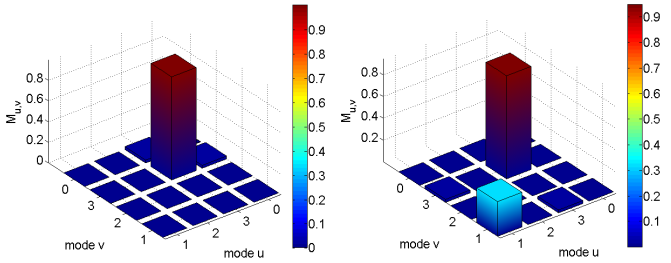

Fig. 5. Matrices $\mathbf{S_1}$ and $\mathbf{S_2}$ at $f = 481.5$MHz that form total Q_{M1} and Q_{M2} respectively

V. Conclusion

Rigorous expressions for electric and magnetic stored energies are utilized for the evaluation of the radiation Q factor based on the superposition of the characteristic mode currents.

The method stated above can be used for effective design of multiband and broadband ESAs. It also provides a deep physical insight into the studied structures. The commonly used Q_Z factor gives a nice estimation of the radiation Q, but it only answers the question "what is the overall Q?". In turn, the Q_M approach is much more general since answers also on important question "what might the overall Q be?" The presented concept opens novel possibilities for lowering the Q by using multipoint feeds and the design of MIMO antennas. The presented method has been successfully employed in the optimisation loop as well.

Acknowledgment

This work was supported by the Grant Agency of the Czech Technical University in Prague, grant No. SGS12/142/OHK3/2T/13 and by the project MSM6840770014. The authors would like to thank Dr. J. Kral for his comments. The authors are also grateful for fruitful discussion with Prof. G. Vandenbosch.

References

[1] J. L. Volakis, Ch.-Ch. Chen and K. Fujimoto, "Survey of Small Antenna Theory," in *Small Antennas: Miniaturization Techniques & Applications*, 1st ed. McGraw-Hill, 2010, ch.2, pp.3-100.

[2] A. D. Yaghjian and S. R. Best, "Impedance, Bandwidth and Q of Antennas," *IEEE Trans. Antennas Propag.*, vol. 53, no. 4, pp. 1298-1324, Apr., 2005.

[3] R. F. Harrington and J. R. Mautz, "Theory of Characteristic Modes for Conducting Bodies," *IEEE Trans. Antennas Propag.*, vol. 19, no. 5, pp. 622-628, Sept., 1971.

[4] R. F. Harrington, *Field Computation by Moment Methods*, John Wiley - IEEE Press, 1993.

[5] W. C. Gibson, *The Method of Moments in Electromagnetics*, 1st ed. Chapman & Hall, 2008.

[6] S. M. Rao, D. R. Wilton and A. W. Glisson, "Electromagnetic Scattering by Surfaces of Arbitrary Shape," *IEEE Trans. Antennas Propag.*, vol. 30, no. 3, pp. 409-418, May, 1982.

[7] S. N. Makarov, *Antenna and EM Modeling with Matlab*, 1st ed. John Wiley, 2002.

[8] M. Capek, P. Hazdra, P. Hamouz and J. Eichler, "A method for tracking characteristic numbers and vectors," *Progress In Electromagnetics Research B*, vol. 33, pp. 115-134, 2011.

[9] G. A. E. Vandenbosch, "Reactive Energies, Impedance, and Q Factor of Radiating Structures," *IEEE Trans. Antennas Propag.*, vol. 58, no. 4, pp. 1112-1127, Apr., 2010.

[10] M. Capek, P. Hazdra and J. Eichler, "A Method for Evaluation of Modal Radiation Q," submitted to *IEEE Trans. Antennas Propag.*

[11] M. Cabedo-Fabres, "Systematic Design of Antennas Using the Theory of Characteristic Modes," *PhD thesis*, UPV, Feb., 2007.

[12] S. R. Best, "Progress in the Design and Realization of an Electrically Small Huygens Source," *5th European Conference on Antennas and Propagation*, Rome, Italy, 2011.

A Method for the Evaluation of Radiation Q Based on Modal Approach

Miloslav Capek, *Student Member, IEEE*, Pavel Hazdra, *Member, IEEE*, and Jan Eichler, *Student Member, IEEE*

***Abstract*—A new formula for the evaluation of the modal radiation Q factor is derived. The total Q of selected structures is to be calculated from the set of eigenmodes with associated eigen-energies and eigen-powers. Thanks to the analytical expression of these quantities, the procedure is highly accurate, respecting arbitrary current densities flowing along the radiating device. The electric field integral equation, Delaunay triangulation, method of moments, Rao-Wilton-Glisson basis function and the theory of characteristic modes constitute the underlying theoretical background. In terms of the modal radiation Q, all necessary relations are presented and the essential points of implementation are discussed. Calculation of the modal energies and Q factors enable us to study the effect of the radiating shape separately to the feeding. This approach can be very helpful in antenna design. A few examples are given, including a thin-strip dipole, two coupled dipoles a bowtie antenna and an electrically small meander folded dipole. Results are compared with prior estimates and some observations are discussed. Good agreement is observed for different methods.**

***Index Terms*—Antenna theory, eigenvalues and eigenfunctions, electromagnetic theory, Q factor.**

I. Introduction

THE radiation Q factor has long been discussed as one of the most significant and interesting parameter of the radiating system, especially in the field of the electrically small antenna (ESA) theory [1]. Each radiating shape has a minimum possible Q which is related to the maximum possible bandwidth potential [2].

There are many methods for estimating Q approximately (chronologically Wheeler [3], Chu [4], Harrington [5], Collin and Rotschild [6], McLean [7], Geyi [8]). Earlier work [3]–[7] do not consider actual current distribution, so they have to deal only with bounds related to dimensions of the enclosing sphere. The first attempt to include source distribution (current/charge) was presented by Geyi [8], but these energies are still quasistatic. Different approach taking the actual shape into account (based on static polarizability), was presented by Gustafsson *et al.* [9].

For effective ESA design as well as for the rigorous study of radiating structures, it is appropriate to use the calculation method based directly on the sources (currents), respecting their topology. These requirements have been fulfilled by G. Vandenbosch [10]. The derived expressions are rigorous, widely usable and easy to implement. They have been verified and successfully tested for simple examples in [11].

We extend this theory for modal analysis purposes, based on the theory of characteristic modes (TCM) [12] and then utilize them for the investigation of radiation Q for some canonical antennas. This approach allows us to study the behaviour of the shape of the radiating structure and its feeding separately. This means that the modal quantities have only to be calculated once and then the effect of the feeding port on superposition is studied through the coupling matrix, later denoted as $\boldsymbol{\beta}$. In addition, understanding the behaviour of modal energies assists in effective ESA design as will be shown in the case of optimization of the meander folded dipole.

The main objective of this paper is to derive the expression for the summation of modal energies and powers in order to obtain total Q. The comparison between the final expressions (24), (25) and some estimations of Q are given in Section V. All algorithms were coded in Matlab R2011a and employed in our in-house antenna tool. The described method could be used for arbitrary (triangularized) surface antennas with air dielectric.

II. The Radiation Q-Factor

The radiation Q factor is usually defined for antennas as [1]

$$Q = \frac{2\omega_0 \max\{W_e, W_m\}}{P_r}, \tag{1}$$

where W_e and W_m are the time averaged stored electric and magnetic energies and P_r is radiated power. The (1) assumes that the antenna is tuned to the resonance at angular frequency ω_0 by an ideal lossless reactive element so that the input impedance is pure real, [6]. Moreover, it is known that Q is inversely proportional to the antenna (fractional) bandwidth and for the constant $\mathrm{VSWR} < s$

$$\mathrm{FBW} \approx \left(\frac{s-1}{\sqrt{s}}\right)\frac{1}{Q}, \tag{2}$$

where the Q factor in (2) is assumed to be much greater than one.

The following expressions for W_e, W_m and P_r are analytically derived in [10] and generalized to a suitable form for the sake of the proposed method (note that the indexes u and v will be associated with the mode indexes in subsequent sections)

$$W_e^{u,v} = \frac{1}{16\pi\omega_0^2\epsilon_0}\left(I_{We}^{u,v} - I_{Wr}^{u,v}\right) \tag{3}$$

Manuscript received August 17, 2011; revised March 21, 2012; accepted May 11, 2012. Date of publication July 10, 2012; date of current version October 02, 2012. This work was supported by the Grant Agency of the Czech Technical University in Prague, under Grants SGS12/142/OHK3/2T/13 and COST IC0803 (RFCSET).

The authors are with the Department of Electromagnetic Field, Faculty of Electrical Engineering, Czech Technical University in Prague, Technicka 2, 16627, Prague, Czech Republic (e-mail: miloslav.capek@fel.cvut.cz).

Color versions of one or more of the figures in this paper are available online at http://ieeexplore.ieee.org.

Digital Object Identifier 10.1109/TAP.2012.2207329

and

$$W_m^{u,v} = \frac{1}{16\pi\omega_0^2\epsilon_0}\left(I_{Wm}^{u,v} - I_{Wr}^{u,v}\right) \tag{4}$$

where

$$I_{We}^{u,v} = \int_{\Omega_1}\int_{\Omega_2} q_u(\mathbf{r_1}) q_v^*(\mathbf{r_2}) \frac{\cos(k_0 r_{21})}{r_{21}} \mathrm{d}\Omega_1 \mathrm{d}\Omega_2, \tag{5}$$

$$I_{Wm}^{u,v} = k_0^2 \int_{\Omega_1}\int_{\Omega_2} \left(\mathbf{J}_u(\mathbf{r_1}) \cdot \mathbf{J}_v^*(\mathbf{r_2})\right) \frac{\cos(k_0 r_{21})}{r_{21}} \mathrm{d}\Omega_1 \mathrm{d}\Omega_2, \tag{6}$$

$$I_{Wr}^{u,v} = \frac{k_0}{2} \int_{\Omega_1}\int_{\Omega_2} \Big[k_0^2 \left(\mathbf{J}_u(\mathbf{r_1}) \cdot \mathbf{J}_v^*(\mathbf{r_2})\right) - q_u(\mathbf{r_1}) q_v^*(\mathbf{r_2})\Big] \sin(k_0 r_{21}) \mathrm{d}\Omega_1 \mathrm{d}\Omega_2. \tag{7}$$

Finally, the radiated power is determined as

$$P_r^{u,v} = \frac{1}{8\pi\omega_0\epsilon_0} \int_{\Omega_1}\int_{\Omega_2} \Big[k_0^2 \left(\mathbf{J}_u(\mathbf{r_1}) \cdot \mathbf{J}_v^*(\mathbf{r_2})\right) - q_u(\mathbf{r_1}) q_v^*(\mathbf{r_2})\Big] \frac{\sin(k_0 r_{21})}{r_{21}} \mathrm{d}\Omega_1 \mathrm{d}\Omega_2. \tag{8}$$

$W_e^{u,v}$, $W_m^{u,v}$ and $P_r^{u,v}$ define the energies and the total radiated power based on uth source (J_u or q_u) on domain Ω_1 and vth source (J_v or q_v) on domain Ω_2. In the $\mathcal{R}^3$ Euclidean space, the distance r_{21} is 2-norm distance $r_{21} = |\mathbf{r}_2 - \mathbf{r}_1|$.

Note that for wavelength λ_0 the angular wavenumber $k_0 = 2\pi/\lambda_0$ and the charge density is defined as $q_u = \nabla \cdot J_u$. In most studied cases the domains Ω_1 and Ω_2 are equal ($\Omega = \Omega_1 = \Omega_2$), for $\Omega_1 \neq \Omega_2$ see [11].

III. Modal Q Formulation

In order to obtain modal Q's, we have to introduce a proper modal method to obtain eigenmodes and eigenvalues. This method is, in our case, the Theory of Characteristic Modes.

Eigenmodes $\mathbf{j}_u$ and eigenvalues λ_u are physically vivid and valuable characteristics of electromagnetic operators such as the electric field integral equation (EFIE) [13], [14]. In the following text, spectral eigen-decomposition of the EFIE complex impedance matrix is performed in the frequency domain. The next section briefly summarizes the mathematical formulation of the EFIE as well as the TCM since it is crucial to know all the properties of relevant variables.

A. The Electric Field Integral Equation

The EFIE can be formulated by employing a boundary condition for the tangential incident ($\mathbf{E}^i$) and a scattered electric field on the perfect electric conductor (PEC)

$$\left[L(\mathbf{J}) - \mathbf{E}^i\right]_{\tan} = 0. \tag{9}$$

The operator $L(\mathbf{J})$ is defined as

$$L(\mathbf{J}) = \mathrm{j}\omega\mathbf{A}(\mathbf{J}) + \nabla\phi(\mathbf{J}), \tag{10}$$

where $\mathbf{A}(\mathbf{J})$ and $\phi(\mathbf{J})$ are vector and scalar potentials respectively [15]. Physically, $-L(\mathbf{J})$ gives the scattered electric field intensity. Therefore, L has the characteristics of impedance

$$Z(\mathbf{J}) = \left[L(\mathbf{J})\right]_{\tan}. \tag{11}$$

The solution of (11) can be treated directly

$$\mathbf{J}_{MoM} = \mathbf{Z}^{-1}\mathbf{E}^i \tag{12}$$

as usually employed in the method of moments (MoM) [17] or by the superposition of the characteristic currents [12], [18]. This knowledge is important for our later expectations.[1]

In both cases, the impedance matrix and the (unknown) surface induced current density have to be expanded by appropriate basis functions (the most suitable are the well-known RWG basis functions $\mathbf{f}_s$ [19]); Galerkin's method is used.

The Q factor based on total current density from MoM has already been successfully calculated in [10] and [11] (MoM in Matlab with a thin-wire reduced kernel). However, to the knowledge of the authors, modal Q factors and stored energies have never been rigorously computed.

B. Theory of Characteristic Modes

The TCM evaluates the total surface current density as a sum of characteristic (eigen-) currents. They depend only on the shape and frequency, not on excitation. Details can be found in [12] and [20].

The impedance matrix $\mathbf{Z} = \mathbf{R} + \mathrm{j}\mathbf{X}$ is complex and symmetric (but not Hermitian), its parts $\mathbf{R}$ and $\mathbf{X}$ are real and symmetric. After a little manipulation we get the associated Euler's equation (a generalized eigenvalue problem)

$$\mathbf{X}\mathbf{j} = \lambda\mathbf{R}\mathbf{j}. \tag{13}$$

A solution of (13) may easily be obtained using the `eig` routine in Matlab [21]. The square impedance matrix $\mathbf{Z}$ of order U (the number of inner edges) produces U eigen-pairs $(\lambda_u, \mathbf{j}_u)$. Each eigenvector $\mathbf{j}_u$ together with the RWG functions forms the vector modal current density

$$\mathbf{J}(\mathbf{r}) = \sum_{u=1}^{U} j_u \mathbf{f}_u(\mathbf{r}), \tag{14}$$

where the basis functions $\mathbf{f}_u$ are defined in [19].

The total current density can be expressed as a linear combination of these modal currents

$$\mathbf{J}_{tot} = \sum_{u=1}^{U} \alpha_u \mathbf{J}_u = \sum_{u=1}^{U} \frac{\langle \mathbf{j}_u, \mathbf{E}^i \rangle}{1 + \mathrm{j}\lambda_u} \mathbf{J}_u. \tag{15}$$

The expansion coefficient α_u is obviously the modal amplitude. The result of $\langle \mathbf{j}_u, \mathbf{E}^i \rangle = \mathbf{j}_u^T \mathbf{E}^i$ is a scalar value called the modal excitation factor [20]. Remember that the $\mathbf{E}^i$ and $\mathbf{J}_{tot}$ have the same meaning in both MoM and TCM. Without the loss of generality, we consider only real feeding of $\mathbf{E}^i$ for the rest of the paper. It should be pointed out, that the sum (15) is in fact incomplete. There is certain portion of evanescent imaginary cur-

[1]To get more insight on the relationship between the direct MoM and the TCM see [16].

rent arising from the voltage-gap [22], contributing to the stored energies. This is reason why there are slight discrepancies between Q_M and Q_{Jtot} as will be seen later. Such residual current could be obtained as

$$\mathbf{J}_{res} = \mathbf{J}_{MoM} - \mathbf{J}_{tot} = \mathbf{Z}^{-1}\mathbf{E}^i - \sum_{u=1}^{U} \frac{\langle \mathbf{j}_u, \mathbf{E}^i \rangle}{1 + \mathrm{j}\lambda_u} \mathbf{J}_u \tag{16}$$

and its contribution included. Since its effect is not crucial, it is omitted here, however this issue is currently under study.

Thanks to the linearity of the divergence operator, the total charge density $q = \nabla \cdot \mathbf{J}$ is

$$q(\mathbf{r}) = \sum_{u=1}^{U} j_u \nabla \cdot \mathbf{f}_u(\mathbf{r}), \tag{17}$$

and

$$\nabla \cdot \mathbf{f}_u(\mathbf{r}) = \begin{cases} \frac{l_u}{A_u^{\pm}} & \mathbf{r} \text{ in } \Omega_u^{\pm} \\ 0 & \text{otherwise} \end{cases} \tag{18}$$

On the basis of (15)–(17) we have

$$\mathbf{q}_{tot} = \sum_{u=1}^{U} \alpha_u \mathbf{q}_u = \sum_{u=1}^{U} \frac{\langle \mathbf{j}_u, \mathbf{E}^i \rangle}{1 + \mathrm{j}\lambda_u} \mathbf{q}_u. \tag{19}$$

The modal decomposition (`eig` function) is time-consuming but can be parallelized.[2] Even thought the TCM forms the orthogonal set of modes, the eigencurrents are of yet indetermined amplitudes. This problem is handled by normalization to unit radiated power for each frequency of interest [12]

$$\langle \mathbf{J}_u^*, \mathbf{R}\mathbf{J}_u \rangle = 1 \text{ W} = P_r^{u,u}. \tag{20}$$

C. Calculation of Modal Energies

Let us consider only (the first) two modes ($M = 2, u \in \{1, 2\}$) for simplicity and write out the current summation

$$\mathbf{J}_{tot} = \sum_{1,2} \alpha_u \mathbf{J}_u = \alpha_1 \mathbf{J}_1 + \alpha_2 \mathbf{J}_2. \tag{21}$$

The total charge density is obtained in the same way. Because variables $\mathbf{f}_s, \mathbf{j}_u$ and $\mathbf{q}_u$ are real, both modal currents and charge densities are real. However, the coefficients $\alpha_u = \langle \mathbf{j}_u, \mathbf{E}^i \rangle / 1 + \mathrm{j}\lambda_u$ are still complex and thus both the total current and charge densities are complex-valued.

If we take a look at (5)–(8), only parts $\mathbf{J}_u(d) \cdot \mathbf{J}_v^*(d)$ and $q_u(d) q_v^*(d)$ have to be worked out at a given frequency f_0 and on a triangularized shape Ω (or just a selected triangle T). Using (21)

$$\begin{aligned} \mathbf{J}_u(d) \cdot \mathbf{J}_v^*(d) &= \mathbf{J}_{tot}(d) \cdot \mathbf{J}_{tot}^*(d) \\ &= (\alpha_1 \mathbf{J}_1(d) + \alpha_2 \mathbf{J}_2(d)) (\alpha_1^* \mathbf{J}_1(d) + \alpha_2^* \mathbf{J}_2(d)) \\ &= \underbrace{\alpha_1 \alpha_1^* \mathbf{J}_1 \cdot \mathbf{J}_1}_{\sim \text{INT11}} + \underbrace{(\alpha_1^* \alpha_2 + \alpha_1 \alpha_2^*) \mathbf{J}_1 \cdot \mathbf{J}_2}_{\sim \text{INT12, INT21}} \\ &\quad + \underbrace{\alpha_2 \alpha_2^* \mathbf{J}_2 \cdot \mathbf{J}_2}_{\sim \text{INT22}} \end{aligned} \tag{22}$$

[2]This has been done via the Matlab Distributed Computing toolbox gaining a speed-up of about 9 for 12 nodes.

and analogously for the $q_u(d) q_v^*(d)$ part. Parts INT11/INT22 and INT12/INT21 are recognized as self and mutual interactions respectively. All discussed integrals may be divided in M^2 subintegrals (22) with corresponding modes u, v as the input data. For clarity, the "summation matrix" is introduced for electric/magnetic energy

$$\mathbf{W}_{e/m}^{M=2} = \begin{bmatrix} W_{e/m}^{11} & W_{e/m}^{12} \\ W_{e/m}^{21} & W_{e/m}^{22} \end{bmatrix} \sim \begin{bmatrix} \text{INT11} & \text{INT12} \\ \text{INT21} & \text{INT22} \end{bmatrix} \tag{23}$$

The above procedure can be generalized to any number of modes (for proof see the Appendix). The total number of M modes form the energy matrices $W_{e/m}$ of $M \times M$ size. Then the radiation Q is expressed by a novel relation

$$Q_M = 2\omega_0 \frac{\max \left\{ \sum_u^M \sum_v^M \beta_{u,v} W_e^{u,v}, \sum_u^M \sum_v^M \beta_{u,v} W_m^{u,v} \right\}}{\sum_u^M \sum_v^M \beta_{u,v} P_r^{u,v}}, \tag{24}$$

where the coupling matrix β is written as

$$\beta_{u,v} = \frac{\langle \mathbf{j}_u, \mathbf{E}^i \rangle \langle \mathbf{j}_v, \mathbf{E}^i \rangle (1 + \lambda_u \lambda_v)}{(1 + \lambda_u^2)(1 + \lambda_v^2)}. \tag{25}$$

Using the Hadamard product $(A \circ B)_{u,v} = (A)_{u,v}(B)_{u,v}$ [23]

$$Q_M = 2\omega_0 \frac{\max \left\{ \sum_{u,v} (\boldsymbol{\beta} \circ \mathbf{W}_e)_{uv}, \sum_{u,v} (\boldsymbol{\beta} \circ \mathbf{W}_m)_{uv} \right\}}{\sum_{u,v} (\boldsymbol{\beta} \circ \mathbf{P}_r)_{uv}}. \tag{26}$$

Modal energies $W_e^{u,v}$ and $W_m^{u,v}$ respect (3) and (4) with input current and charge densities (14) and (17) respectively. $\mathbf{W}_{e/m}$ and $\boldsymbol{\beta}$ are in matrix form (23). At a given frequency, eigenvectors $\mathbf{j}_{u,v}$, eigenvalues $\lambda_{u,v}$ and stored modal energies $W_{e/m}^{u,v}$ are known. Therefore, the total Q_M factor can be tuned by just a single parameter—the actual feeding $\mathbf{E}^i$. In Section V we will verify that (24) is close to the total Q and is suitable for use in antenna design[3]. Both modal (3), (4) and total (23) energies give important additional information about the radiating structure. It is worth noting that the total Q factor can only be calculated from the modal stored energies and powers—direct superposition of modal Q factors is impossible.

IV. Software Implementation

The EFIE core is based on the RWG elements [24]. Thus, proper discretization has to be employed. The Matlab PDE toolbox usually creates mesh of poor quality (particularly for complex shapes like fractals), better results are obtained by the Comsol Multiphysics mesh generator. In order to control meshing, the authors work on an in-house mesh generator that employs the `distmesh` code from MIT [25]. In this paper we assume that the analysed geometry Ω is properly triangularized into T triangles with U inner edges. Note that the quality and number of triangles are crucial for the resulting convergence of the solution.

[3]For $M \to \infty$, the Q_∞ in (24) is simply equal to total Q. In practice, however, it is sufficient to sum only finite (low) numbers of modes $M \approx 5$.

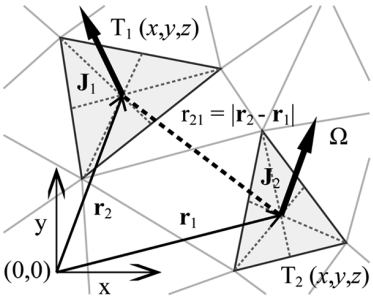

Fig. 1. Distance between non-overlapping current elements.

MoM solutions of thin-strip structures are usually assumed to be fed by the delta-gap [15]. Some planar structures are fed by the incident plane wave—usually only the x- or y-component $\mathbf{E}^i = [E_x, E_y, E_z]$ is used, [24]. The respective eigenproblem is solved in Matlab and all modes are sorted (tracked) and represented in terms of the characteristic angles [26]

$$\delta_u = 180 - \arctan(\lambda_u). \tag{27}$$

The characteristic angles are continuous through the values of 90-270, resonance of the uth mode occurs when $\delta_u = 180$. An illustrating example is shown in Section V.

A. Numerical Evaluation of $W_{e,m}$ and P_r—Distant Elements

The key expressions (5)–(8) consist of double surface integrals over a given planar structure Ω. In our case, Ω is discretized using the Delaunay triangulation, Fig. 1. Hence the integration is now performed via the compact set of triangles T.

The modal current matrices $\mathbf{J}_{u/v}$ are calculated from eigenvectors and the RWG basis function via (14). The order of $\mathbf{j}_{u/v}$ is $1 \times U$, but the order of the modal current $\mathbf{J}_{u/v}$ is $3 \times T$. Similarly, the modal charge distributions are calculated from (17) and each matrix $\mathbf{q}_{u/v}$ is of order $1 \times T$. Thus, one current vector $[J_x, J_y, J_z]$ and charge density q are assigned to each triangle. These values are considered constant throughout the triangle area and are assumed to be located at the centre of the triangles [27]. It will be shown later that this centroid approximation is accurate enough. However, it could fail e.g. for patch antennas at very small heights above the ground plane.

B. Numerical Evaluation of $W_{e,m}$—Overlapping Elements

As one can see, there are singularities in (5) and (6) for overlapping triangles ($T_1 = T_2$). The so-called self-coupling term [28] plays a major role in Q factor calculation and therefore it should be treated carefully. We are looking for a fast and sufficiently accurate solution to the following problem:

$$I_1(T_1 = T_2) = \int_{T_1}\int_{T_2} \frac{\cos(k_0 r_{21})}{r_{21}} \mathrm{d}t_1 \mathrm{d}t_2, \tag{28}$$

where $r_{21} = \sqrt{(x_2 - x_1)^2 + (y_2 - y_1)^2 + (z_2 - z_1)^2}$. The (28) is expanded in a Maclaurin series and since $k_0 R_{21} \to 0$ (R_{21} is the longest side of the triangle T_1) is satisfied, one can only use its first term. Then the cosine function $\cos(k_0 r_{21})$ from (28) reduces to the static singular part $1/r_{21}$. There is still a problem with the triangular region of integration.

TABLE I
CONVERGENCE OF THE SELECTED MODES, RECT. PLATE 30 × 20 cm

	1st mode				2nd mode	
edges	P_r [W]	Q_1	e_1 [%]	t [s]	Q_2	e_2 [%]
42	1.0041	0.738	87.23	0.015	–	–
180	1.0007	0.804	95.04	0.016	0.666	77.99
412	1.0002	0.814	96.25	0.031	0.789	92.39
926	0.9999	0.853	100.83	0.125	0.830	97.19
1691	0.9998	0.854	100.95	0.390	0.825	96.60
4704	0.9997	0.846	100	2.621	0.854	100

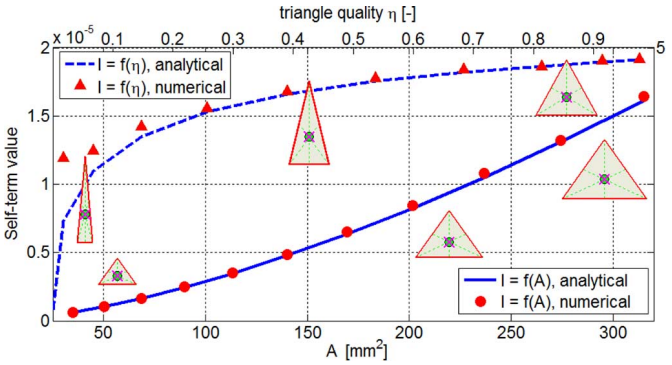

Fig. 2. Self-term values depending on the quality and area of the triangle.

The above issue was solved e.g. in [28] and the result was simplified in accordance with [29]

$$I_2 = -\frac{4}{3}A^2 \left(\frac{\ln\left(1 - \frac{2|\mathbf{h}_{12}|}{O}\right)}{|\mathbf{h}_{12}|} + \frac{\ln\left(1 - \frac{2|\mathbf{h}_{13}|}{O}\right)}{|\mathbf{h}_{13}|} + \frac{\ln\left(1 - \frac{2|\mathbf{h}_{23}|}{O}\right)}{|\mathbf{h}_{23}|} \right), \tag{29}$$

where $|\mathbf{h}_{12/13/23}|$ denote the length of the edges of the triangle and O is its perimeter. The computational cost of evaluating (29) is mainly determined by the $\ln$ functions (see fifth column in Table I).

Fig. 2 shows the behaviour of (29) while varying the triangle area and the triangle quality which is defined as

$$\eta = \frac{4\sqrt{3}A}{|\mathbf{P}_1 - \mathbf{P}_2|^2 + |\mathbf{P}_1 - \mathbf{P}_3|^2 + |\mathbf{P}_2 - \mathbf{P}_3|^2}. \tag{30}$$

The coefficient η is between 0 (three points on a line) and 1 (equilateral triangle). When varying the triangle area, quality is fixed (at value $\eta = 0.98$, solid line at Fig. 2) and when varying the triangle quality, area is fixed (dashed line at Fig. 2).

Finally note that the term $\sin(k_0 r_{21})/r_{21}$ in (8) is not singular and changes negligible within the triangle

$$\lim_{r_{21}\to 0} \frac{\sin(k_0 r_{21})}{r_{21}} = k_0 \lim_{k_0 r_{21}\to 0} \frac{\sin(k_0 r_{21})}{k_0 r_{21}} = k_0 \tag{31}$$

C. Convergence Analysis

It is very important that the algorithm is convergent with an increasing number of RWG basis functions (the parameter U). To verify this assumption, we consider a 30 × 20 cm rectangular plate in free space. This plate is discretized with a different number of triangles and analyzed using the TCM solver. Then,

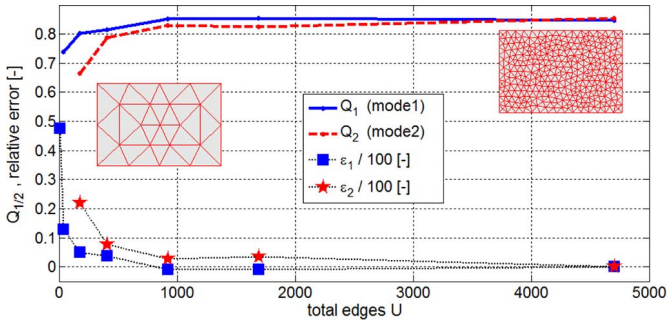

Fig. 3. Algorithm convergence, rect. plate 30 × 20 cm.

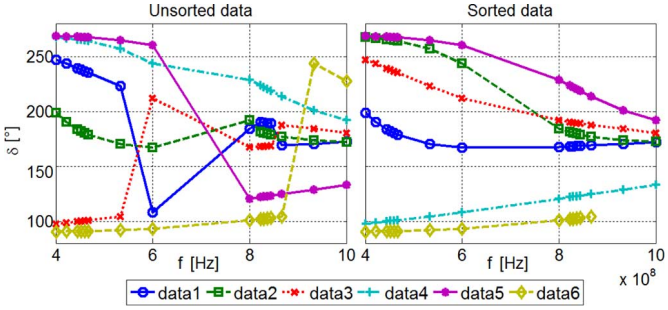

Fig. 4. The original data from the TCM (left) and the sorted ones (right), rec. plate 30 × 20 cm (634 triangles, 926 edges).

modal radiated power and Q factors are calculated for the 1st and 2nd modes, see Table I.

In terms of convergence, (8) is very interesting since from (20) it is observed that the modal radiated power should be equal to one (in case of 1st mode $u = v = 1$). Table I confirms that the modal radiated power P_r is very close to 1 W.

It can therefore be assumed that the numerical integration of radiated power (8) as well as the stored energies (3) and (4) are performed correctly. Singularity treatment can be illustrated at Fig. 3, which shows the convergence of modal Q factors for the 1st and 2nd modes of the rectangular plate. Note, that the inaccurate Q results for low values of U (typically fewer than 150 edges) are caused by a poorly conditioned TCM task. In the case of 42 edges the resonant frequency of the second mode was not found.

Given that energies $W_e^{u,v}$ and $W_m^{u,v}$ are very small (ranging in the order of $10^{-7} \div 10^{-9}$ relative to the unit radiated power), we can conclude that the convergence is sufficient.

Run-time complexity: The complexity of the TCM solution for F frequency samples is $\mathcal{O}(FU^3)$. Considering just one mode at a single frequency, the modal energy computation has a quadratic time complexity $\mathcal{O}(T^2)$ (see the 5th column in Table I). Finally, the complexity of (24) is $\mathcal{O}(Q_M) \propto \mathcal{O}(M^2T^2)$. Because it is sufficient to calculate only half of all the energies $W_e^{u,v}$ and $W_m^{u,v}$ (see Appendix), the time-complexity is $\mathcal{O}(Q_M) \propto \mathcal{O}((M^2/2)T^2)$. And since in practice $M \ll U$, the total calculation time is strongly dominated by the eigen-decomposition, see Section V-D2. Fortunately, in the frequency domain both (13) and (24) can be parallelized (at most F nodes may be employed).

D. Tracking of Eigenvalues and Eigenvectors

The spectral decomposition of the moment impedance matrix $\mathbf{Z}$ doesn't always produce well ordered eigenmodes (see Fig. 4 left). This issue is particularly caused by finite numerical accuracy and slight asymmetry of the frequency-dependent matrix (although the MoM code is based on the Galerkin testing procedure, the Z-matrix is not purely symmetrical). At specific frequencies, the decomposition issue might be ill-posed and non-uniquely defined as well.

Proper manipulation and tracking of the modes is the key to preventing physically different current distributions along the frequency samples. Many matrix preconditioners could be used but the resulting modes still need tracking. There are many issues that have to be considered and therefore a specific heuristic method was coded and implemented. Detailed description is beyond the scope of this paper although further information can be found in [30].

Another problem is caused by slight asymmetry of the TCM solution (currents are not ideally orthogonal to each other) and the fact that the current $\mathbf{J_{u/v}}$ can be computed with random sign. To explain this matter, we extend (13) to a formally correct form $C\mathbf{Xj} = C\lambda\mathbf{Rj}$. While the magnitude of the constant C can be removed by normalization to unit radiated power $\widehat{\mathbf{j}} = \mathbf{j}/\sqrt{\langle \mathbf{j}, \mathbf{Rj} \rangle}$, the sign of C remains unchanged.[4]

Fig. 4 shows that the frequency samples aren't spaced equidistantly. This is because that an adaptable frequency solver (AFS) is used in our tool. The AFS starts with an initial set of samples (specified by the user) and then dynamically adds additional samples to the locations with large changes in eigenvalues. This technique significantly saves computational time and helps the tracking of modes.

V. Application: Numerical Results

In this section we demonstrate our efforts on some selected problems. To validate the above mentioned approach, several Q estimates are compared.

The radiation Q factor may be estimated from the input impedance $\mathbf{Z}$ variation around the resonant frequency f_0 [2]

$$Q_Z = \omega_0 \frac{\left|\frac{\partial Z(\omega)}{\partial \omega}\right|}{2R(\omega_0)}. \tag{32}$$

The above equation could be converted to the modal form Q_{Zu}. Let us expand both the numerator and the denominator by current $|I|^2/2$ and suppose that Ω is PEC

$$\begin{aligned} Q_Z &= \omega_0 \frac{\left|\frac{\partial R(\omega)}{\partial \omega} + \mathrm{j}\frac{\partial X(\omega)}{\partial \omega}\right| \frac{|I|^2}{2}}{2R(\omega)\frac{|I|^2}{2}} \\ &= \frac{\omega_0 \left|\frac{\partial (P_r)}{\partial \omega} + \mathrm{j}\frac{\partial (2\omega(W_m - W_e))}{\partial \omega}\right|}{2P_r} \end{aligned} \tag{33}$$

Since from (20) $P_r = 1$ W, implying that $\partial(P_r)/\partial\omega = 0$, then

$$Q_{Zu} = \frac{\omega_0}{2} \left| \frac{\partial \left(2\omega \left(W_m^u(\omega) - W_e^u(\omega)\right)\right)}{\partial \omega} \right| \tag{34}$$

[4]This causes problems on adjacent frequencies. For example the current orientation at frequency F is $\{J_u, J_v\} \sim \{+,+\}$ and at freq. $F+1$ is $\{J_u, J_v\} \sim \{+,-\}$. Then, due to the slight non-orthogonality, the results at F and $F+1$ are significantly different.

TABLE II
COMPARISON OF ALL DEFINED Q THAT CONSIDER FEEDING

	Q_Z	Q_{MoM}	Q_{Jtot}	Q_M
Equation	(32)	(11)	(15)	(37)
Source	Z_{in}	$\mathbf{J}_{MoM}, \mathbf{q}_{MoM}$	$\mathbf{J}_{tot}, \mathbf{q}_{tot}$	$\boldsymbol{\beta}$, $\mathbf{W}_{e/m}$
Reference	[2]	[10]	×	×
Based on solver	MoM	MoM	TCM	TCM
Comp. speed	+++	++	+	+++
Information	+	++	++	+++

TABLE III
COMPARISON OF MODAL APPROACHES TO CALCULATION OF Q

	Q_n	$Q_{u,v}$	$\mathbf{W}_{e/m}$
Equation	(35)	(1)	(3), (4)
Source	λ_n	$\mathbf{W}_{e/m}$	$\mathbf{J}_u, \mathbf{q}_u$
Reference	[31]	×	[10]
Based on solver	TCM	TCM	×
Comp. speed	++	+++	+
Information	+	+++	++

The second modal-approach relation is based on the Rayleigh quotient formula for eigenvalue λ_n, [31]

$$Q_n = \frac{\omega_0}{2} \left| \frac{\partial \lambda_n(\omega)}{\partial \omega} \right|, \tag{35}$$

where $\partial\lambda_n/\partial\omega$ is the slope of the nth eigenvalue. Expressions (34) and (35) are equal, provided that

$$2\omega \left(W_m^u(\omega) - W_e^u(\omega) \right) = \lambda_u(\omega). \tag{36}$$

It can be proven that at resonance $Q_n = Q_{Zu}$. The above derived (24) can be formally simplified by using the Frobenius product, [23]. Because the Frobenius product is an inner product of the vector space, we use the same notation as in (15) or (20)

$$Q_M = 2\omega_0 \frac{\max\left\{ \langle \boldsymbol{\beta}, \mathbf{W}_e \rangle, \langle \boldsymbol{\beta}, \mathbf{W}_m \rangle \right\}}{\langle \boldsymbol{\beta}, \mathbf{P}_r \rangle}. \tag{37}$$

It has to be noted that (37) is the total Q factor calculated from M selected modes. However, if we consider only one mode u (without any feeding, $\beta_u = 1$), the corresponding Q factor will be referred to as the Q_u factor.

In many cases it isn't necessary to consider the whole matrix $\boldsymbol{\beta}$ because only the diagonal terms $u = v$ are relevant (the others are typically in the order of 10^{-20}, see Section V-B). We denote the diagonal terms as β_u.

Finally, for the comparison of Q_M, we introduce two more radiation factors Q_{MoM} and Q_{Jtot}. Both are also calculated using (3)–(8). The input current distribution $\mathbf{J}_{MoM}$ of factor Q_{MoM} is obtained directly from MoM, the total current $\mathbf{J}_{tot}$ of factor Q_{Jtot} is calculated by (15). See Table II and Table III for comparison of all defined radiation factors.

All the following examples are chosen in order to clarify the presented results. At first, we verify the modal method (RWG, TCM), then we calculate (32)–(37) and compare them with each other.

A. The Thin-Strip Dipole

The first antenna is a dipole in a free space. The length $2L$ is 300 mm and the width d is 2 mm. The dipole was discretized into 432 triangles (534 inner edges) and fed by a voltage gap

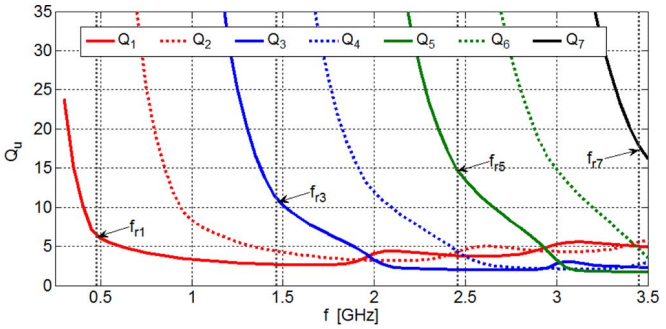

Fig. 5. The first seven modal Q_u factors of the 300 × 2 mm dipole.

TABLE IV
MODAL Q FACTORS IN RESONANCE AND THE β_u FACTORS FOR DIPOLE

u	f_r [MHz]	Q_n	Q_{Zu}	Q_u	$\beta_{u(1/2)}$	$\beta_{u(1/4)}$
1	475.9	6.78	6.20	6.62	93.29	50.03
2	969.0	9.15	8.28	8.93	$8 \cdot 10^{-23}$	95.31
3	1463.7	11.16	10.02	11.09	84.72	40.04
4	1959.3	12.93	11.53	13.00	$3 \cdot 10^{-24}$	0.20
5	2455.5	14.52	12.88	14.91	78.76	44.50
6	2952.4	16.00	14.09	16.43	$2 \cdot 10^{-22}$	76.44
7	3449.9	22.11	19.41	19.37	70.26	33.23

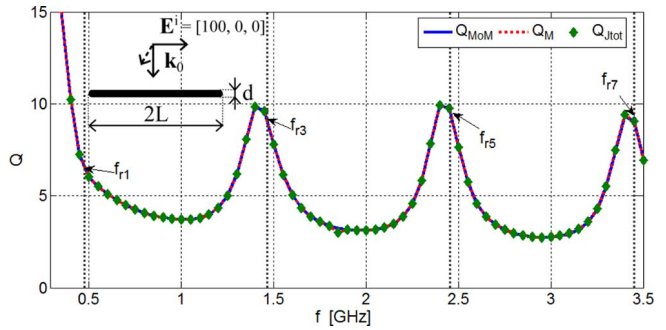

Fig. 6. Q_{MoM}, Q_M and Q_{Jtot} for the dipole 300 × 2 mm fed by an incident plane wave.

[15]. This structure is analyzed over a large frequency band (including the small antenna regime).

Let us look first at the modal Q_u factors that form the total Q_M. The first seven modal Q_u factors ($u \in \{1, \ldots, 7\}$) are depicted at Fig. 5. It is worth mentioning that all modes cyclically intertwine with each other in the lower right corner of Fig. 5. Table IV shows all modal Q factors compared numerically at the resonant frequency of each mode. Modal Q approximations (34), (35) and the exact Q_u factor agree quite well.

Further analysis assumes that the dipole is being excited. We consider an incident plane wave as well as two different feed edge positions.

At first, the total Q_M with incident plane wave feeding is shown at Fig. 6. The incident wave is polarized in the x-direction ($\mathbf{E}^i = [100, 0, 0]$). In this case, the agreement of Q_{MoM}, Q_M and Q_{Jtot} is excellent.

1) Central Feeding: The dipole is fed by a voltage gap ($E^i = 100$ V) located at the middle edge. The modal factors Q_u are not changed as they describe the intrinsic behaviour of the radiator. Due to symmetry, only odd modes are excited (see column $\beta_{u(1/2)}$ in Table IV).

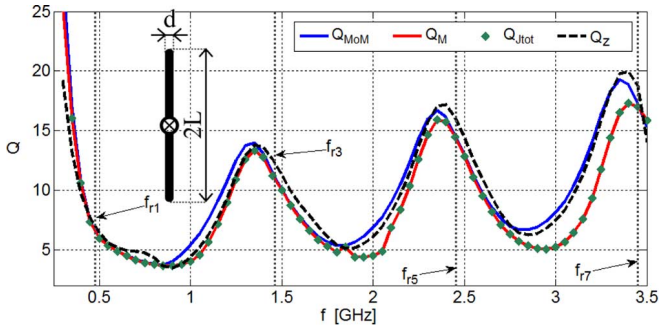

Fig. 7. Q_{MoM}, Q_M, Q_{Jtot} and Q_Z of the dipole 300 × 2 mm, feeding is placed in the middle of the dipole.

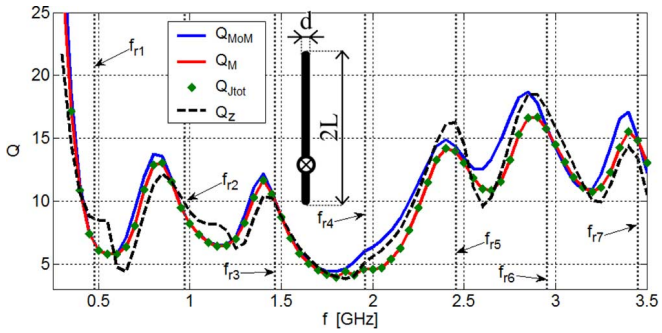

Fig. 8. Q_{MoM}, Q_M, Q_{Jtot} and Q_Z of the dipole 300 × 2 mm, feeding is placed at one quarter of the dipole length.

This explains why total Q factors at Fig. 7 are affected only by odd modal Q_u factors (see solid lines at Fig. 5). Comparison between Fig. 6 and Fig. 7 shows that the voltage gap case converges relatively poorly because of issues mentioned at Section III-B.

The total Q factor is an oscillating function with an absolute minimum of $f/f_{r1} \doteq 1.76$, see Fig. 7. It can be seen, that the agreement of the Q_{MoM} with the Q_Z approximations (directly derived from impedance matrix $\mathbf{Z}$) is quite good. Slight differences between Q_M and Q_{Jtot} at higher frequencies are also (except for the voltage gap issue) addressed by the fact that Q_M is calculated only for the first few modes M, which may no longer be effective at higher frequencies.

2) Feeding at 1/4 of the Dipole Length: Now the dipole is fed at the 1/4 of its length, more modes can be now excited and accordingly, the coefficients β_u changed significantly (see column $\beta_{u(1/4)}$ in Table IV). Hence the total Q factors at Fig. 8 are notably different as well—compare to Fig. 7. With the exception of the fourth mode (which cannot be excited), all modes somehow contribute to the total Q_M.

This example shows how the modal approach is effective and illuminating. The eigenproblem is calculated only once, after that we consider only the arrangement of the excitation.

B. The Mutually Coupled Dipoles—In-Phase Currents

The second example studies the Q factor of two side-by-side coupled dipoles. Both are 100 mm long and 1 mm wide, spaced by the distance d and fed in the middle of the antenna(s) with the same amplitude and phase ($E^i = 100$ V, $\mathbf{J}_1 = \mathbf{J}_2$). Dipoles

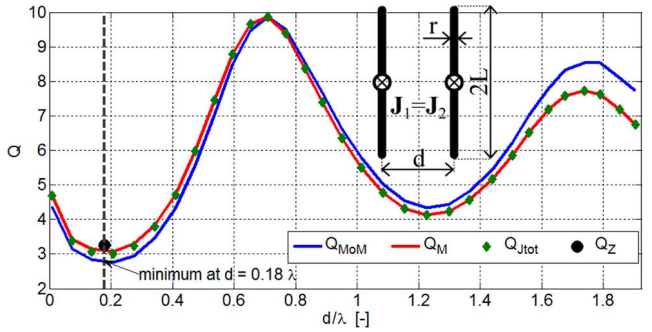

Fig. 9. Q_{MoM}, Q_M, Q_{Jtot} and Q_Z for in-phase fed dipoles of distance d.

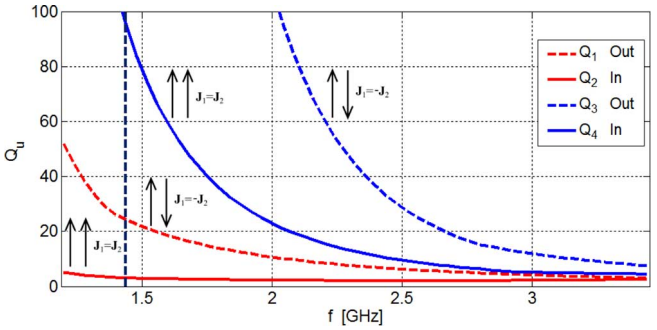

Fig. 10. The first four modal Q_u factors (two dipoles of distance $d = 0.18\lambda$).

TABLE V
MODAL Q FACTORS IN RESONANCE FOR TWO COUPLED THIN-STRIP DIPOLES OF DISTANCE $d = 0.18\lambda$ (MINIMAL TOTAL Q)

u	f_r [MHz]	Q_n	Q_{Zu}	Q_u
1	1386.5	31.40	27.21	26.74
2	1437.2	3.39	3.12	**3.01**
3	2816.3	15.52	13.98	15.17
4	2980.2	5.72	5.07	5.09

were discretized into 576 triangles (718 inner edges). This scenario is equivalent to a single horizontal dipole lying $d/2$ above a perfect magnetic infinite plane (PMC).

The total Q_M factor was calculated as a function of distance d. Comparison with other total Q factors is depicted at Fig. 9. Again, the total Q_M is an oscillating function with an absolute minimum of $d = 0.18\lambda$. While the case of out-of-phase currents was analytically verified in [11] ($d(\min(Q)) = 0.716\lambda$), for in-phase currents a similar study is more complicated.

Nevertheless, this behaviour can be easily explained by the TCM. Resonant frequencies and modal quality factors are displayed in Table V, Fig. 10 shows the first four modal Q_u factors ($u \in \{1, 2, 3, 4\}$); current orientation is schematically depicted as well. Table V shows that the in-phase modes have significantly lower Q_u than the out-of-phase modes.

Obviously, the total in-phase current is formed by the dominant in-phase mode at a given frequency (which is the frequency of the second mode with $f_{r2} = 1437.2$ MHz and $Q_u = 3.01$). Let us consider summation of four modes at frequency $f = f_{r2}$ and for distance $d = 0.18\lambda$. Then we obtain the values in Table VI. For Q_M calculation at this point, we can omit all coefficients and energies of an order less than 10^{-10}. In this case that is all except the second mode ($u = v = 2$), see Table VI).

TABLE VI
SUMMATION DATA AT RESONANCE FOR 2ND MODE ($f_{r2} = 1437.2$ MHz, IN-PHASE CURRENT) OF TWO COUPLED THIN-STRIP DIPOLES WITH DISTANCE $d = 0.18\lambda$ (MINIMAL TOTAL Q)

u	$\beta_{u,u}$ [-]	λ_u [-]	$2\omega(W_m^u - W_e^u)$	Q_u
1	$7 \cdot 10^{-24}$	1.72	1.94	24.42
2	**156**	**0.01**	**0.04**	**3.01**
3	$5 \cdot 10^{-29}$	-759.38	-680.53	902.10
4	$2 \cdot 10^{-27}$	-80.54	-72.64	95.48

Also all products of $\beta_{u,v} W_{e/m}^{u,v}$ for $u \neq v$ are negligible. As a result, only the second mode contributes to the total Q

$$Q_M = 2\omega_0 \frac{\max\left\{\beta_2 W_e^{2,2}, \beta_2 W_m^{2,2}\right\}}{\beta_2 P_r^{2,2}}. \tag{38}$$

Since $P_r^{2,2} \doteq 1$, we simplify (38) by extracting β_2

$$\begin{aligned} Q_M &= 2(2\pi f_{r2}) \max\left\{W_e^{2,2}, W_m^{2,2}\right\} \\ &= 4\pi 1.437 \cdot 10^9 \max\{1.642 \cdot 10^{-10}, 1.663 \cdot 10^{-10}\} \\ &= 3.01 \end{aligned}$$

It is seen that the minimal $Q_M = 3.01$ is directly equal to the modal Q_u of the second mode.

Note that the above described behaviour is also valid for the folded dipole with sufficient conductor coupling and a separation distance of $d \ll 0.05\lambda$.

C. The Bowtie Antenna

The next antenna under study is a bowtie in a free space. Its length L is 100 mm, width d is 60 mm and gap width t is 4 mm, see Fig. 13. The structure is discretized into 309 triangles with 436 inner edges (these values are doubled in the case of an infinite ground plane as described later). Two feeding scenarios have been considered—incident plane waves with polarizations $\mathbf{E}_1^i = [100, 0, 0]$ and $\mathbf{E}_2^i = [100, 100, 0]$.

The first step is the modal analysis of the bowtie without a ground plane. Characteristic angles are shown at Fig. 11 (solid lines), Fig. 12 depicts schematically the main current paths of these modes. For clarity we show only the first five modes, but in fact we analyze the first ten significant modes at a given frequency range. Nonetheless the results may be inaccurate at the end of the frequency spectrum (about $3.5 \div 4$ GHz).

Polarization of the incident plane wave dramatically affects the total sum for Q—Fig. 13. Total Q factors are the same for both polarizations up to a frequency of about 2.3 GHz. For higher frequencies, results start to strongly depend on the excitation of modes 2–10.

An interesting study is presented at Fig. 14, only $\mathbf{E}_1^i$ polarization is assumed. All the first ten modes are divided into four groups (see Fig. 14 left), while each group contains similar modes (regarding current distributions). Fig. 14 shows the effects on the total Q_M depending on which groups are summed up. It is clearly seen that the inductive (non-radiating, group D at Fig. 14 left) modes significantly affect the behaviour of the antenna (compare sum $A + B + C$ and $A + B + C + D$ at Fig. 14 right).

Then the bowtie is placed above an infinite ground plane at a height of h. Changes in eigen-angles are depicted at

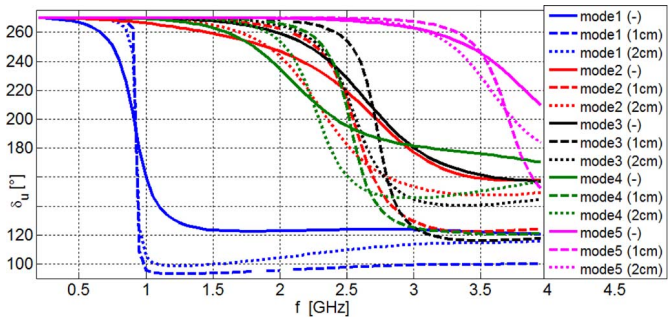

Fig. 11. The first five modes represented by the eigen-angles δ_u as a function of frequency, the bowtie antenna (solid line: no ground plane; dashed lines: infinite ground planes of height 1 cm and 2 cm, respectively).

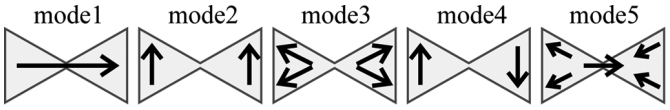

Fig. 12. Schematic depiction of the first five modes of the bowtie antenna.

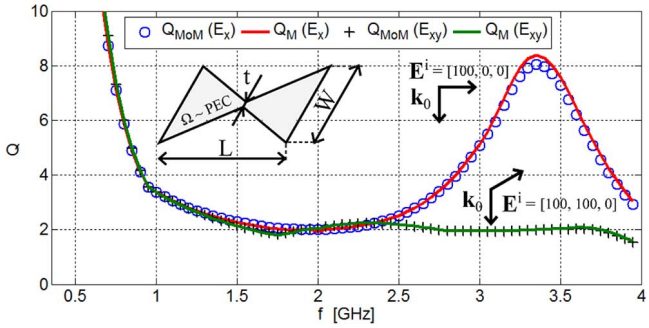

Fig. 13. Q_{MoM} and Q_M of the bowtie (two incident plane wave polarizations are considered).

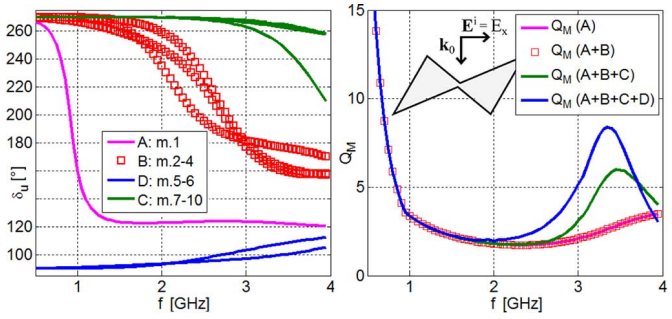

Fig. 14. The first ten modes of bowtie with associated four scenarios of Q_M factors (E_x polarization).

Fig. 11. With increasing height above the ground, the slope of eigen-angles decrease. Because of a minimum (and more or less constant) resonant frequency, only the dominant mode TM_{01} (without any feeding) will be studied. Using the image theory [15], the radiator in the $x - y$ plane placed h above the infinite electric ground plane is modeled as two bowties separated by the distance $2h$, see Fig. 15. In the TCM analyzer, proper out-of-phase mode is selected and analysed.

The modal factors Q_u and Q_n of the first mode are depicted at Fig. 16. These were obtained at resonance ($\delta_u = 0$) as a func-

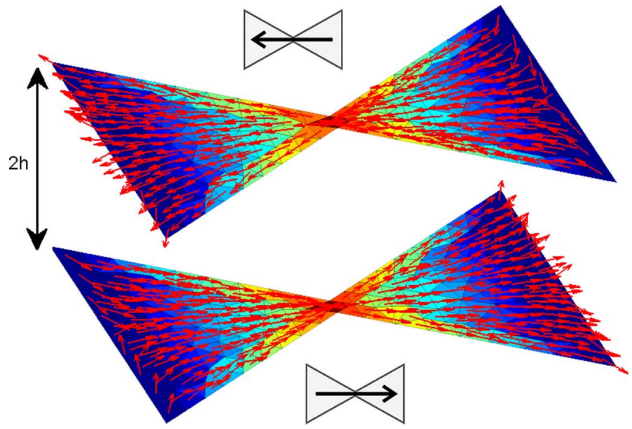

Fig. 15. Bowtie above infinite ground plane $h = 5$ mm, dominant mode TM_{01} shown.

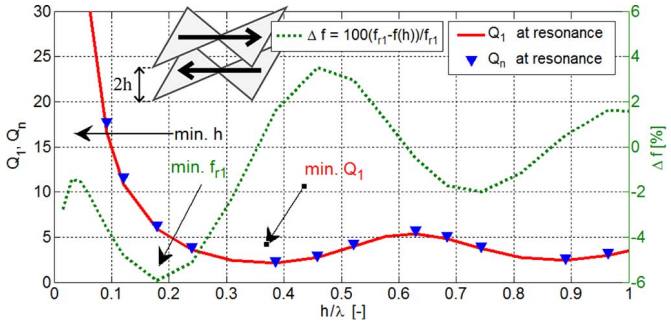

Fig. 16. The modal radiation Q_u and the resonant frequency for dominant mode of bowtie antenna as a function of height h.

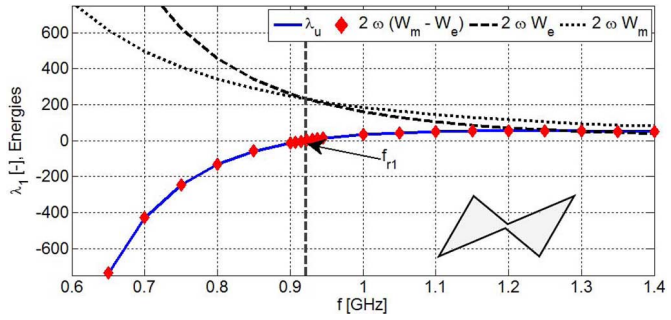

Fig. 17. The eigenvalues, electric and magnetic stored energies of the first mode at height 5 mm, bowtie.

tion of height h. For larger values of h the Q_u factor becomes smaller. The second curve at Fig. 16 (green dashed line) represents changes in the resonance frequency of the first mode, calculated as

$$\Delta f_{\%} = 100\frac{f_{r1}(\infty) - f_{r1}(h)}{f_{r1}(\infty)} \tag{39}$$

and displayed in [\%]. This allows us to locate zones with minimum values of h and Q_u and to find a compromise between them for a specific application. For comparison, the reactive energies of the 1st mode for height $h = 5$ mm ($f_{1r} = 927$ MHz) are plotted at Fig. 17. It is obvious that resonance occurs when the stored energies are equal and so the eigenvalue $\lambda_1 = 0$, (36).

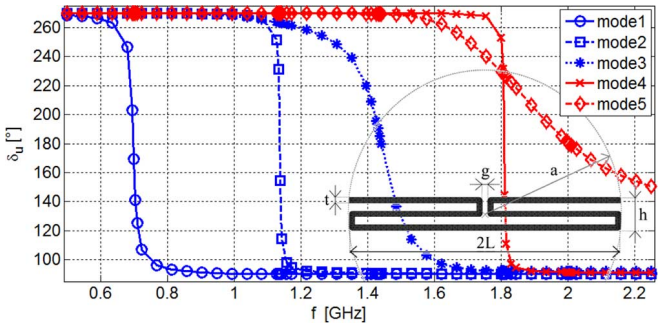

Fig. 18. The first five characteristic angles of meander folded dipole.

TABLE VII
MODAL Q FACTORS IN RESONANCE FOR MEANDER FOLDED DIPOLE (THE FIRST FIVE MODES ARE CONSIDERED)

u	f_r [MHz]	ka	Q_n	Q_u
1	697.8	0.736	43.34	43.54
2	1136.5	1.199	196.67	195.83
3	1442.2	1.521	13.76	13.82
4	1809.2	1.908	357.40	355.52
5	2005.1	2.115	3.45	3.41

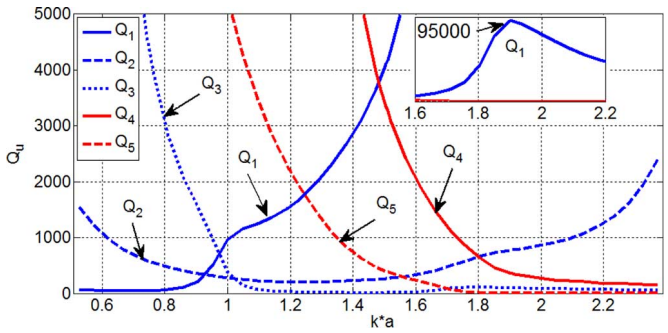

Fig. 19. The modal Q_u of the first five modes of meander folded dipole.

D. The Meander Folded Dipole

The last example is an electrically small meander folded dipole. Length $2L$ is 100 mm, overall width h is 12 mm (so enclosing a sphere of radius $a = \sqrt{L^2 + (h/2)^2} = 50.35$ mm), the width of strip t is 2 mm and the gap width g is also 2 mm. The dipole is discretized into 736 triangles with 929 inner edges. All the outer corners are bent with radius 1 mm and refined—see the lower right corner of Fig. 18. The frequency range for analysis is chosen from 0.5 GHz ($ka = 0.527$) to 2.25 GHz ($ka = 2.373$).

Modal analysis is performed with an adaptable frequency solver. The initial frequency step is set to 50 MHz (36 samples) with two additional iterations (60 samples are obtained at the end of calculation). Eigen-numbers are successfully sorted and converted to the eigenangles, see Fig. 18. There are five modes that are dominant in the selected frequency range.

The modal radiation factors Q_n (only at resonance) and Q_u were calculated for each mode, see Table VII and Fig. 19. The difference between Q_n and Q_u is caused primarily by numerical evaluation of derivation in (35), so the calculation of Q_n gets more inaccurate with higher values of Q. Also in this case the AFS solver is very useful. Note that the first mode is purely inductive at mid-range frequencies, thus the Q_1 rises very fast

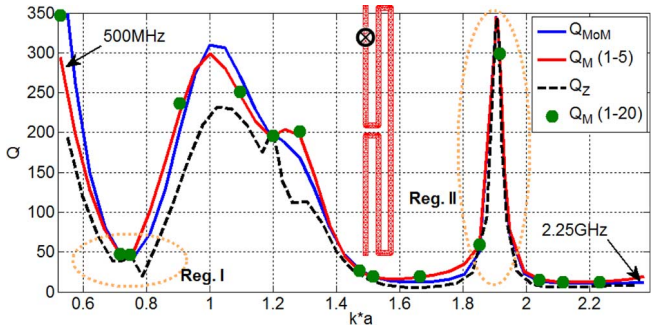

Fig. 20. Q_{MoM}, Q_M and Q_Z of meander folded dipole.

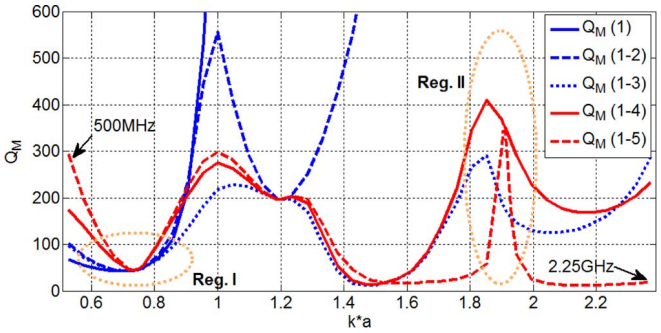

Fig. 21. Total Q_M calculation based on various number of modes (numbers in the legend characterize what modes have been summarized).

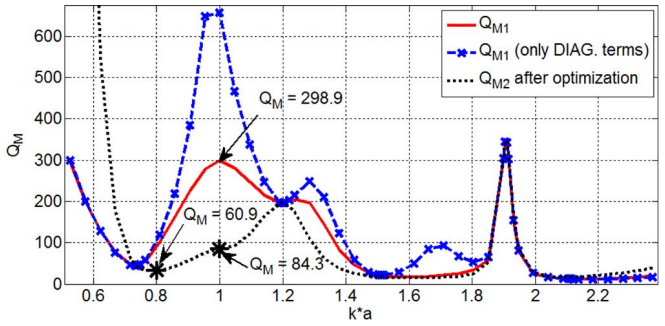

Fig. 22. Comparison between full Q_M and Q_M based only on diagonal terms in matrix $\boldsymbol{\beta}$, minimalized Q_M is displayed as an asterisk.

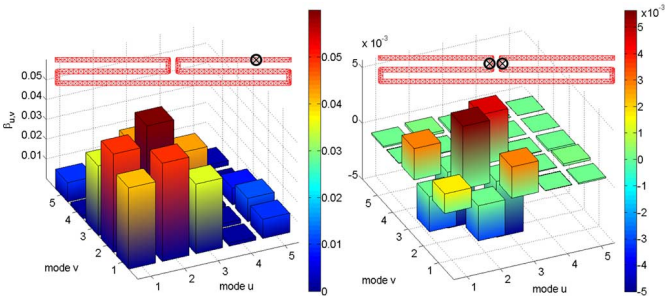

Fig. 23. $\boldsymbol{\beta}$ matrix for two feeding scenarios: the original feeding ($Q_M = 298.9$ at $ka = 1$) and the optimized feeding ($Q_M = 84.3$ at the same ka), first five modes are considered.

(reaching a value of 95000). A detailed description of the modal currents is beyond the scope of this paper.

1) Total Q_M Calculation: To obtain the total Q (both Q_M, Q_Z and Q_{MoM}), feeding has to be incorporated. For this purpose a voltage gap generator ($E^i = 100$ V) was placed at the inner edge of no. 39, highlighted at Fig. 20. Then the total Q factors are calculated and are shown at Fig. 20. Some observations are listed as follows.

- The course of Q_M is smooth and more or less equal with Q_{MoM}. On the other hand, Q_Z doesn't match very well, especially in locations distant from the modal (natural) resonances, [2].
- Q_M (1–5) for the first five modes is close to Q_M (1–20) for the first 20 modes (Q_M (1–20) is considered only at some frequencies to keep the figure readable).
- The fact that Q_M (1–5) is very close to Q_{MoM} is very interesting from the engineering point of view-no matter where the feeding is located, the summation of the first five modes is sufficient enough to obtain accurate Q_M in the "low ka" region.

One minimum of total Q is located in the small antenna regime (for $ka = 0.736$, that is the resonant frequency of the first mode). Then the total Q rises to a value of about 350. As will be shown later, total Q can be effectively reduced in relatively broadband regions.

From Fig. 21 is also obvious that the total Q_M for a growing number of modes ($M = 1, \ldots, M = 5$) is increasingly better matched with Q_{MoM}. In fact, the Q_M factor is perfectly adjusted at natural resonances because there is only one significant entry of the $\boldsymbol{\beta}$ matrix (for example it is β_2 for $ka = 1.2$ at Fig. 21).

Including all β entries (not only the diagonal ones) is generally necessary for correct calculation. Compare the red solid line at Fig. 22 (which shows full summation where all members are used) with blue dashed lines (which consider only the diagonal terms of the $\boldsymbol{\beta}$ matrix). For simple structures (like a dipole), it is usually sufficient to use the self coupling diagonal terms, but generally energies produced by eigencurrents seem to be non orthogonal (unlike radiated powers).

2) Total Q_M Minimization: The following subsection draws out some benefits of the proposed method. We choose $ka = 1$ with $Q_M = 298.9$, see Figs. 20–22. Using optimization we now try to minimize the Q_M factor in the neighborhood of the selected point $ka = 1$ (which is the boundary value of ESA).

A significant advantage is that the TCM solution and ergo the modal energies $\mathbf{W}_e$ and $\mathbf{W}_m$ are computed only once. All single-calculated operations (eigensolution (13), 60 freq. samples, time: 229 s; tracking [30], 20 modes, time: 10 s; and modal energies calculation (3), (4), 5 modes, time: 62 s) took totally[5] 301 s. Our in-house Particle Swarm Optimization algorithm [32] is utilized to find optimal feeding scenarios—we consider two (voltage) gaps with independent magnitudes $E^i_{1/2} \in (0, 100)$V that may be located at any inner edges.

Equations (25) and (37) form the so-called fitness function (f.f.) which was evaluated for 50 agents and 300 iterations. Optimization takes a total of 1741 seconds which is only 0.116 second per f.f. call.

The original and the optimized feeding points are depicted at Fig. 23, together with the $\boldsymbol{\beta}$ matrices before and after optimization. Note here that the modal energies as well as the radi-

[5]All calculations presented in this paper were performed at computer with i7-X980 3.33 GHz processor, 24 GB RAM and SDD disc. As mentioned above, some processes were parallelized (with 8 threads).

ated power matrices are the same in both cases. The resulting impressed gap magnitudes are identical 80 V. The total Q_M is significantly decreased to the value $Q_M = 84.3$ at $ka = 1$. The optimized Q_M is shown at Fig. 22 as a black dashed line with an asterisk mark at the studied value of ka.

VI. Conclusion

Rigorous expressions for electric and magnetic stored energies are utilized for the evaluation of the radiation Q factor based on the superposition of the characteristic mode currents. It is demonstrated that the newly derived coupling matrix $\beta_{u,v}$ (that includes the frequency and the feeding effects) determines the total radiation factor Q_M. This matrix may be viewed as a connection between the intrinsic behaviour of the antenna (described by the set of characteristic currents) and the external world, represented by feeding.

The presented algorithm is implemented and verified for several examples. An up-to-date tracker is applied for sorting the modal data obtained from paralleled eigen-decomposition. Good agreement between the proposed summation technique and conventional methods is observed. All the examples clearly illustrate that the novel expressions together with the robust modal method can be used for the investigation of the modal and total Q factors.

The method stated above can be used for effective design of multiband and broadband ESAs. It also provides a deep physical insight into the studied structures. The commonly used Q_Z factor gives a nice estimation of the radiation Q, but it only answers the question "what is the overall Q?" In turn, the Q_M approach is much more general since answers also on important question "what might the overall Q be?" The presented concept opens novel possibilities for lowering the Q by using multipoint feeds and the design of MIMO antennas. The presented method has been successfully employed in the optimization loop as well. Further work is aimed to study complex planar geometries and detailed analysis of the exact relationship between (modal) radiation factors and maximum bandwidth.

Appendix
Sum of Modal Energies

Consider (23) with M modes expressed as a double sum

$$W_{e/m}^{M} = \sum_{u=1}^{M}\sum_{v=1}^{M} \alpha_u \alpha_v^* W_{e/m}^{u,v}(\mathbf{J}_u, \mathbf{J}_v, q_u, q_v) \tag{40}$$

where modal energies $W_{e/m}^{u,v}(\ldots)$ are calculated by (3), (4). In the following, the arguments of energies $W_{e/m}^{u,v}$ are omitted. The (40) may be divided into two parts

- $u = v$
  The term $\alpha_u \alpha_v^*$ is real and equal (see (15)) to

$$\alpha_u \alpha_v^* = \frac{\langle \mathbf{j}_u, \mathbf{E}^i \rangle^2}{1 + \lambda_u^2}. \tag{41}$$

  If we expand the product (41) by $(1 + \lambda_u^2)$, then

$$W_{e/m}(u,u) = \sum_{u=1}^{M} \frac{\langle \mathbf{j}_u, \mathbf{E}^i \rangle^2 \left(1 + \lambda_u^2\right)}{\left(1 + \lambda_u^2\right)^2} W_{e/m}^{u,u}. \tag{42}$$

- $u \neq v$
  Since $\Re\{\alpha_u \alpha_v^*\} = \Re\{\alpha_u^* \alpha_v\}$, $\Im\{\alpha_u \alpha_v^*\} = -\Im\{\alpha_u^* \alpha_v\}$ and $W_{e/m}^{u,v} = W_{e/m}^{v,u}$ we can sum two terms at a time

$$W_{e/m}(u,v) + W_{e/m}(v,u) = \left(\alpha_u \alpha_v^* + \alpha_u^* \alpha_v\right) W_{e/m}^{u,v} \tag{43}$$

  and from (15) after several manipulations

$$W_{e/m}(u,v) + W_{e/m}(v,u) = \frac{2\langle \mathbf{j}_u, \mathbf{E}^i \rangle \langle \mathbf{j}_v, \mathbf{E}^i \rangle (1 + \lambda_u \lambda_v)}{\left(1 + \lambda_u^2\right)\left(1 + \lambda_v^2\right)} W_{e/m}^{u,v}. \tag{44}$$

Using (42) and (44)

$$W_{e/m}^{M} = \sum_{u=1}^{M}\sum_{v=1}^{M} \frac{\langle \mathbf{j}_u, \mathbf{E}^i \rangle \langle \mathbf{j}_v, \mathbf{E}^i \rangle (1 + \lambda_u \lambda_v)}{\left(1 + \lambda_u^2\right)\left(1 + \lambda_v^2\right)} W_{e/m}^{u,v}. \tag{45}$$

Acknowledgment

The authors would like to thank N. Bell, P. Hamouz, Dr. V. Sobotikova and Dr. J. Kral for their comments. The authors are also grateful for fruitful discussion with Prof. G. Vandenbosch. Also, we would like to thank three anonymous reviewers who suggested valuable improvements to the paper.

References

[1] J. L. Volakis, Ch.-Ch. Chen, and K. Fujimoto, "Survey of small antenna theory," in *Small Antennas: Miniaturization Techniques & Applications*, 1st ed. New York: McGraw-Hill, 2010, ch. 2, pp. 3–100.
[2] A. D. Yaghjian and S. R. Best, "Impedance, bandwidth and Q of antennas," *IEEE Trans. Antennas Propag.*, vol. 53, no. 4, pp. 1298–1324, Apr. 2005.
[3] H. A. Wheeler, "Fundamental limitations of small antennas," in *Proc. IRE*, Dec. 1947, vol. 35, pp. 1479–1484.
[4] L. J. Chu, "Physical limitations of omni-directional antennas," *J. Appl. Phys.*, vol. 19, pp. 1163–1175, Dec. 1948.
[5] R. F. Harrington, "Effect of antenna size on gain, bandwidth, and efficiency," *J. Res. Nat. Bur. Standards*, vol. 64D, pp. 1–12, Jan.–Feb. 1960.
[6] R. E. Collin and S. Rotchild, "Evaluation od antenna Q," *IEEE Trans. Antennas Propag.*, vol. 12, pp. 23–27, Jan. 1964.
[7] J. S. McLean, "A re-examination of the fundamental limits on the radiation q of electrically small antennas," *IEEE Trans. Antennas Propag.*, vol. 44, pp. 672–675, May 1996.
[8] Y. Geyi, "A method for the evaluation of small antenna Q," *IEEE Trans. Antennas Propag.*, vol. 51, pp. 2124–2129, Aug. 2003.
[9] M. Gustafsson, C. Sohl, and G. Kristensson, "Physical limitations on antennas of arbitrary shape," in *Proc. Royal Society A: Mathematical, Physical and Engineering Sciences*, 2007, vol. 463, no. 2086, pp. 2589–2607.
[10] G. A. E. Vandenbosch, "Reactive energies, impedance, and Q factor of radiating structures," *IEEE Trans. Antennas Propag.*, vol. 58, no. 4, pp. 1112–1127, Apr. 2010.
[11] P. Hazdra, M. Capek, and J. Eichler, "Radiation Q-factors of thin-wire dipole arrangements," *IEEE Antennas Wireless Propag. Lett.*, vol. 10, pp. 556–560, May 2011.
[12] R. F. Harrington and J. R. Mautz, "Theory of characteristic modes for conducting bodies," *IEEE Trans. Antennas Propag.*, vol. 19, no. 5, pp. 622–628, Sept. 1971.
[13] R. F. Harrington, *Field Computation by Moment Methods*. New York: John Wiley—IEEE Press, 1993.
[14] K. F. Warnick, *Numerical Analysis for Electromagnetic Integral Equations*. Norwood, MA: Artech House, 2008.
[15] C. A. Balanis, *Advanced Engineering Electromagnetics*. New York: Wiley, 1989.
[16] P. Hazdra and P. Hamouz, "On the modal superposition lying under the MoM matrix equations," *Radioengineering*, vol. 17, no. 3, pp. 42–46, Sep. 2008.
[17] W. C. Gibson, *The Method of Moments in Electromagnetics*, 1st ed. London, U.K.: Chapman & Hall, 2008.
[18] R. F. Harrington and J. R. Mautz, "Computation of characteristic modes for conducting bodies," *IEEE Trans. Antennas Propag.*, vol. 19, no. 5, pp. 629–639, Sept. 1971.

[19] S. M. Rao, D. R. Wilton, and A. W. Glisson, "Electromagnetic scattering by surfaces of arbitrary shape," *IEEE Trans. Antennas Propag.*, vol. 30, no. 3, pp. 409–418, May 1982.
[20] M. Cabedo-Fabres *et al.*, "The theory of characteristic modes revisited: A contribution to the design of antennas for modern applications," *IEEE Antennas Propag. Mag.*, vol. 49, no. 5, pp. 52–68, Oct. 2007.
[21] E. Anderson *et al., LAPACK Users' Guide*. Philadelphia, PA: Society for Industrial and Applied Mathematics (SIAM), 1999.
[22] M. Cabedo-Fabres, "Systematic Design of Antennas Using the Theory of Characteristic Modes," Ph.D. dissertation, UPV, Spain, Feb. 2007.
[23] R. A. Horn and C. R. Johnson, *Topics in Matrix Analysis*. Cambridge, U.K.: Cambridge Univ. Press, 1994.
[24] S. N. Makarov, *Antenna and EM Modeling with Matlab*, 1st ed. New York: John Wiley, 2002.
[25] P.-O. Persson, "Mesh Generation for Implicit Geometries," PhD. Thesis, MIT, , 2005.
[26] E. H. Newman, "Small antenna location synthesis using characteristic modes," *IEEE Trans. Antennas Propag.*, vol. 27, no. 4, pp. 530–531, July 1979.
[27] J. F. Shaeffer, MOM3D Method of Moments Code Theory Manual Denmar, Marietta, Georgia, Contract NAS1-18603, Rep. 189594, Mar. 1992.
[28] T. F. Eibert and V. Hansen, "On the calculation of potential integrals for linear source distributions on triangular domains," *IEEE Trans. Antennas Propag.*, vol. 43, no. 12, pp. 1499–1502, Dec. 1995.
[29] P. Arcioni, M. Bressan, and L. Perregrini, "On the evaluation of the double surface integrals arising in the application of the boundary integral method to 3-D problems," *IEEE Trans. Microwave Theory Tech.*, vol. 45, no. 3, pp. 436–439, Mar. 1997.
[30] M. Capek, P. Hazdra, P. Hamouz, and J. Eichler, "A method for tracking characteristic numbers and vectors," *Progr. Electromagn. Res. B*, vol. 33, pp. 115–134, 2011.
[31] R. F. Harrington and J. R. Mautz, "Control of radar scattering by reactive loading," *IEEE Trans. Antennas Propag.*, vol. 20, no. 4, pp. 446–454, Jul. 1972.
[32] M. Capek, P. Hazdra, P. Hamouz, and M. Mazanek, "Software tools for efficient generation, modeling and optimisation of fractal radiating structures," *IET Microw., Antennas Propag.*, vol. 5, no. 8, pp. 1002–1007, Jun. 2011.

Miloslav Capek (S'09) received the M.Sc. degree in electrical engineering from the Czech Technical University, Prague, Czech Republic, in 2009, where he is currently working towards the Ph.D. degree.

His research interests are in the area of electrically small antennas, numerical techniques, fractal geometry and optimalization.

Pavel Hazdra (M'03) received the M.S. and Ph.D. degrees in electrical engineering from the Czech Technical University in Prague, in 2003 and 2009, respectively.

He is a Research and Teaching Assistant with the Department of Electromagnetic Field, CTU-FEE. His research interests are in the area of electromagnetic theory, computational electromagnetics, fractal geometry, planar antennas and special prime-feed antennas.

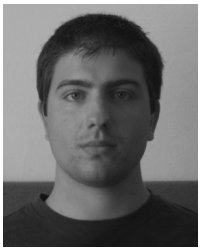

Jan Eichler (S'10) received the B.Sc. and M.Sc. degrees in electrical engineering from the Czech Technical University in Prague, in 2008 and 2010, respectively, where he is currently working towards the Ph.D. degree.

His research interests include multiband antennas, their simulation (full-wave or modal), fractal motifs and the quality factor of an antenna.

David B. Davidson
Dept. E&E Engineering
University of Stellenbosch
Stellenbosch 7600, South Africa
Tel: +27 21 808 4458;
Fax: +27 21 808 4981
E-mail: davidson@sun.ac.za

Foreword by the Editor

From time to time, advances in both algorithms and computational capability result in the "re-discovery" of a method that was originally described many years back. The theory of characteristic modes (first published over forty years back) is a current case in point, with the topic receiving a lot of attention recently again in computational electromagnetics. This month's contribution discusses a *MATLAB* implementation of the method, illustrated by application to some interesting antenna structures. As always, we thank the authors for their interesting contribution.

Implementation of the Theory of Characteristic Modes in *MATLAB*

Miloslav Capek, Pavel Hamouz, Pavel Hazdra, and Jan Eichler

Department of Electromagnetic Field
Czech Technical University in Prague
Czech Republic
E-mail: capekmi2@fel.cvut.cz; hamoupav@fel.cvut.cz; hazdrap@fel.cvut.cz; eichljan@fel.cvut.cz

Abstract

This paper describes the implementation of a complex *MATLAB* tool to calculate the characteristic modes and associated antenna parameters. The first code, written in *FORTRAN*, was presented in the early seventieths by Harrington and Mautz. Here, we utilize *MATLAB*, which is widely known and used in the antenna community these days. Because eigen-decomposition is time consuming, parallel and distributed computing is used. Thanks to the hundreds of built-in functions in *MATLAB*, computation of the surface currents from the eigenvectors obtained, as well as other important characteristics, are very easy and effective. The practical features are discussed with two examples.

Keywords: Computational electromagnetics; eigenvalues and eigenfunctions; MATLAB; electromagnetic theory

1. Introduction

The antenna tool presented in this paper is based on the well-known Method of Moments (MoM) [1] with the Rao-Wilton-Glisson (RWG) [2] basis functions. Used together with the modal decomposition formulated by Harrington [3], it constitutes a powerful tool for antenna analysis and synthesis. The input for the methods is an arbitrary three-dimensional surface "triangularized" by Delaunay triangularization [4]. The surface is assumed to be made of a perfect electric conductor (PEC) [5]; however, it is possible to include the effects of finite metal thickness and conductivity in post processing (see below). The metal surface must be placed in a vacuum, since the modal approach has been developed for a lossless surrounding medium, with relative permittivity $\varepsilon_r = 1$.

The electric-field integral equation (EFIE) is formulated for the metal surface [6]. Two possible treatments of the electric-field integral equation were implemented in the tool: the direct solution by MoM, and the modal decomposition in terms of characteristic modes. Both methods work with the same discretization, and therefore with the same impedance matrix, **Z**. As was proven in [7], if all modes on the structure are considered, both methods will give equal results. Former problems with the residual mode were solved recently in [8]. The direct MoM solution is therefore beneficial for checking the TCM (Theory of Characteristic Modes) solution.

In recent years, *MATLAB* [9] has also provided useful new and perspective features, like OOP (object-oriented programming, [10]), GPU computing (see, e.g., [11]), etc. All the presented algorithms were coded and successfully tested in *MATLAB Versions R2011b-R2012a*. All possible exceptions are caught correctly, so the presented version is stable. Some routines are included in the *LAPACK* package [12]. Those who are interested in the application presented here should see [13] for the compiled version, which is free.

2. An Overview of the Background Theory

All necessary theoretical issues are split into three parts:

- Calculation of the impedance matrix,
- Solution of the generalized eigenvalue problem, and
- Post processing.

Based on electric-field-integral-equation formulation [1], an impedance operator, **Z**, is defined by

$$\mathbf{n}_0 \times \mathbf{E}_1^i(\mathbf{r}') = -\mathbf{n}_0 \times \mathbf{E}_1^s(\mathbf{r}') = \mathbf{n}_0 \times \mathbf{Z}\left[\mathbf{J}(\mathbf{r}')\right], \quad (1)$$

where $\mathbf{r}' \in \Omega$, and Ω is the selected structure to be analyzed.

For an arbitrary shape, the impedance operator in Equation (1) can be obtained only in a numerical way. The structure Ω is therefore discretized to M triangles that share N inner – RWG – edges. For details about the calculation of the RWG basis functions, we refer to the classic paper [2]. Our impedance matrix is constructed in accordance with [14].

The discretized impedance operator **Z** can be separated as

$$\mathbf{Z} = \mathbf{R} + j\mathbf{X}, \quad (2)$$

where **R** and **X** have to be real and symmetrical matrices. The following expressions thus hold:

$$\mathbf{R} = \frac{1}{2}\left(\mathbf{Z} + \mathbf{Z}^*\right), \quad (3)$$

$$\mathbf{X} = \frac{1}{2j}\left(\mathbf{Z} - \mathbf{Z}^*\right), \quad (4)$$

where $\mathbf{Z}^*$ means the complex conjugate of **Z**. Matrix **Z** is therefore non-Hermitian but symmetrical.

The generalized eigenvalue problem of the form

$$\mathbf{X}\mathbf{J}_n = \lambda_n \mathbf{R}\mathbf{J}_n \quad (5)$$

was derived in [3]. The above-stated decomposition constitutes the characteristic basis of eigencurrents $\{\mathbf{J}_n\}$, with associated eigenvalues $\{\lambda_n\}$. This formulation is known as the Theory of Characteristic Modes (TCM), which can also be formulated in terms of an energetic functional

$$\mathcal{F}(\mathbf{J}_n) = \frac{\langle \mathbf{J}_m, \mathbf{X}\mathbf{J}_n \rangle}{\langle \mathbf{J}_m, \mathbf{R}\mathbf{J}_n \rangle} = \frac{2\omega\left(W_m^n - W_e^n\right)}{P_r^n} = \lambda_n. \quad (6)$$

It is obvious that such a functional minimizes the total net power, and maximizes the radiated power.

Because Equation (4) forms an orthogonal system, we apply the following normalization immediately after decomposition:

$$\langle \mathbf{J}_m, \mathbf{R}\mathbf{J}_n \rangle = \delta_{mn}, \quad (7)$$

$$\langle \mathbf{J}_m, \mathbf{X}\mathbf{J}_n \rangle = \delta_{mn}\lambda_n, \quad (8)$$

$$\langle \mathbf{J}_m, \mathbf{Z}\mathbf{J}_n \rangle = (1 + j\lambda_n)\delta_{mn}, \quad (9)$$

to obtain the orthonormal basis with respect to the radiated power. Of course, the above-mentioned normalization not only has benefits, but also some disadvantages (such as extreme scaling of nonradiating modes, etc.). In the following, we denote the modal radiated power as P_r^n, and the total net stored power as $2\omega\left(W_m^n - W_e^n\right)$ for the nth mode.

3. *MATLAB* Implementation

At this point, we start with a description of the schematic diagram depicted in Figure 1. For convenience, the setup of all necessary input data, the GUI, `preTCM`, of the software `TCMapp` was coded (see Figure 2). The `preTCM` routine stores the `pTCMproject` native format that contains all the necessary information to prepare the Theory of Characteristic Modes (TCM) task. For better understanding, we added a schematic code for the simplest Theory of Characteristic Modes decomposition of a thin-wire half-wavelength dipole in *MATLAB* (see Figure 3).

There are also other interfaces connected to the core of the application. These interfaces are fully automatic, and make it possible to perform optimization or the parametric sweep. Both `preTCM`, optimization, and the parametric sweep are directly connected to `createJob`. This part verifies all input data, finds computational resources, generates the `pTCMin` (see Figure 1) batch, and then sends the created job to the solver manager, `runSolver`. The `runSolver` part of the program is independent of low-level solvers (which can be placed, for example, on remote machines). It also makes it possible to add new solvers independently of each other (currently, the authors are working on a novel GPU solver in *MATLAB*).

The frequency samples for which the calculation will be performed have to be specified before the start of the calculation. It is possible to enter a fixed list of frequencies (see the top of Figure 4). This option is useful in all cases where the modal resonant frequencies are more or less known. Unfortunately, such frequencies are not usually known *a priori* for most of the optimization tasks, nor for complicated shapes. Therefore, the adaptive frequency sampler was developed (see the bottom of Figure 4). This powerful feature makes it possible to automatically refine all results near to modal resonances ($\lambda_n = 0$).

The low-level solvers can be directly chosen by the user (see Figure 5 for particular dialogs), or can be selected by the optimizer/parameter-sweep utility. The solution of Equation (4) may then be easily obtained using the `eig` routine in *MATLAB* (in fact, *MATLAB* calls some *LAPACK* functions: QR decomposition, reduction to Hessenberg matrix, etc.). After decomposition, all data are sent back to the `runSolver` service, which performs normalization, Equation (9), `tracking`, and sorting (in descending order).

The tracking routine [15] is somewhat delicate, because it can only be executed in a heuristic way (for details, see [15-16]). The available tracking methods are simple correlation (top of Figure 6), improved correlation (middle of Figure 6),

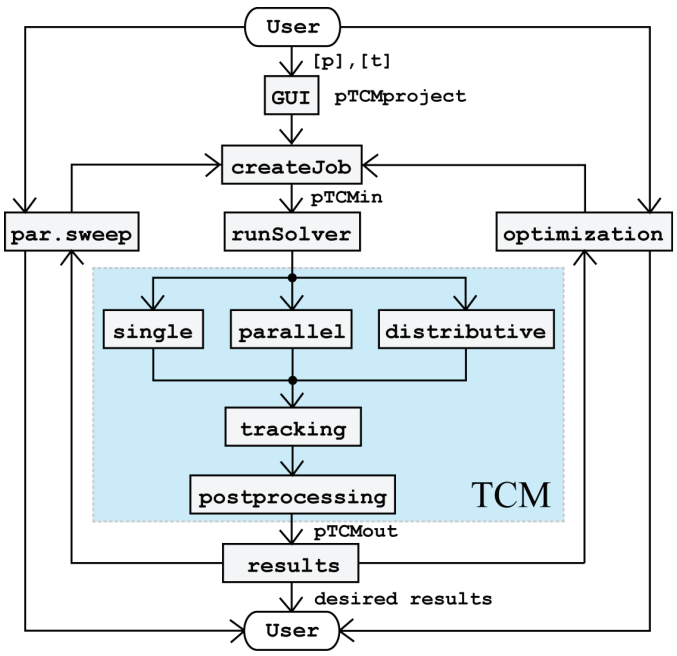


```
pTCMin =

      meshStruct: [1x1 struct]
       adaptFreq: [1x1 struct]
           freqs: [500000000 ··· ]
         mAnalyse: [1x1 struct]
          sorting: [1x1 struct]
          options: [1x1 struct]
     acceleration: [1x1 struct]
         postproc: [1x1 struct]
              def: [1x1 struct]
```

```
pTCMout =

        unsorted: [1x1 struct]
             def: [1x1 struct]
         results: [1x1 struct]
         options: [1x1 struct]
         freqList: [1x12 double]
       adaptFreq: [1x1 struct]
      meshStruct: [1x1 struct]
    condNumbers: [1x1 struct]
        postproc: [1x1 struct]
         zmatrix: [1x1 struct]
         history: [1x1 struct]
         sorting: [1x1 struct]
        mAnalyse: [1x1 struct]
          sorted: [1x1 struct]
```

Figure 1. (top) A schematic diagram of the Theory of Characteristic Modes application, and (bottom) the structure of the `pTCMin` and `pTCMout` variables.

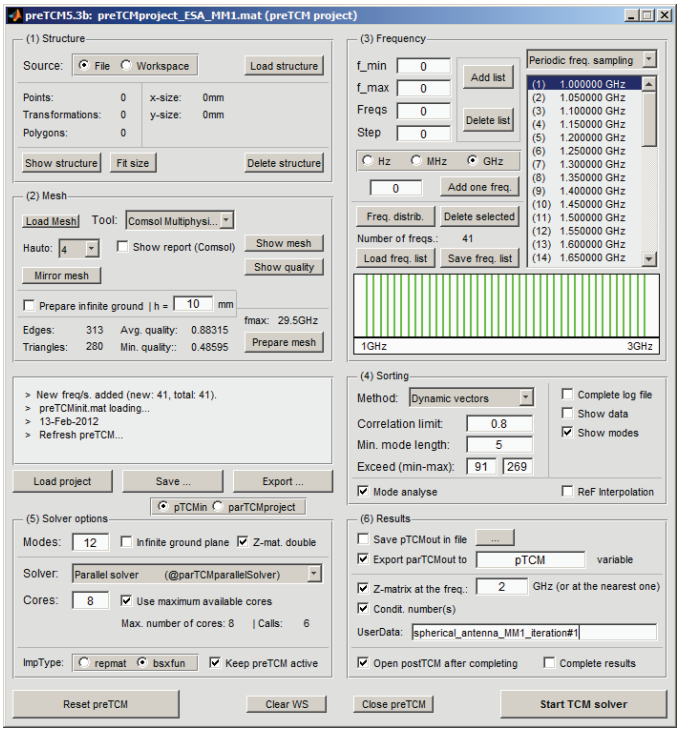

Figure 2. A screenshot of the `preTCM` tool in *MATLAB*.

```
L             = 0.1;    % dipole length [m]
a             = 1e-6;   % dipole radius [m]
N             = 101;    % number of segments
feed          = 51;     % feeding position
f             = 1.5e9;  % operational frequency
% ----------------------------------------------
Zin         = zeros(1,length(f));    % allocation
[Z,J,E]     = dipole(f,L,a,N,feed); % MoM
ReZ         = real(Z);               % Re(Z)
ImZ         = imag(Z);               % Im(Z)
[Vec,Num]   = eig(ImZ, ReZ);         % naive TCM
Num         = diag(Num);             % (NxN)->(N,1)
[V0,N0]     = quickSort(Vec,Num,0.8); % tracking
[V0,N0]     = signifSort(V0,N0);     % sort in ...
    desc. order
V0n         = zeros(size(V0));       % allocation
gamma       = zeros(N,1);            % ...
for j = 1:N  % "trivial" normalization
    V0n(:,j) = V0(:,j)/...
        sqrt(abs(V0(:,j)'*(ReZ*V0(:,j))));
    gamma(j) = dot(V0n(:,j),E)/(1 + 1j*N0(j));
end
Jtot        = zeros(size(J));     % allocation
for k = 1:N  % Jdif = J - Jtot  (check)
    Jtot  = Jtot + gamma(k)*V0n(:,k);
end
Jdif        = imag(J) - imag(Jtot); % evan.mode?
% Results:
figure; plot(V0n); grid on; xlim([0 N]);
figure; plot(Jdif); grid on; xlim([0 N]);
```

Figure 3. Simple Theory of Characteristic Modes code for the thin-wire half-wavelength dipole.

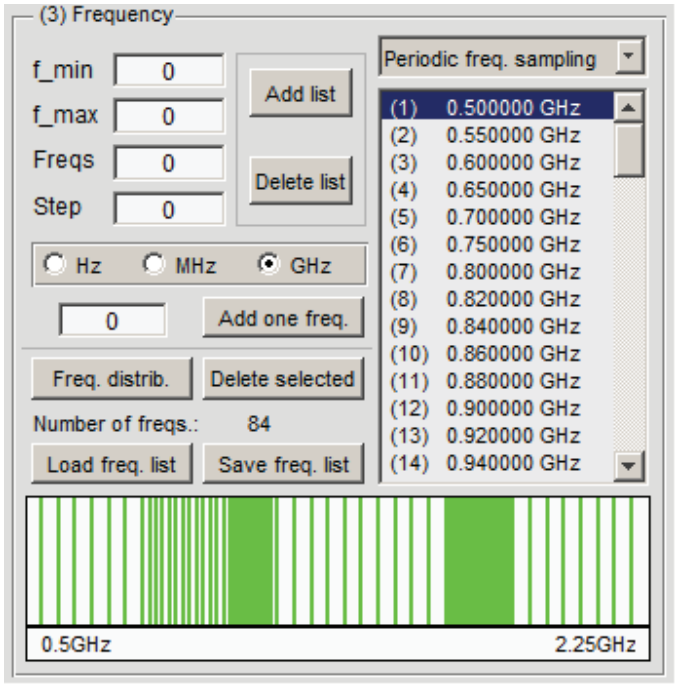

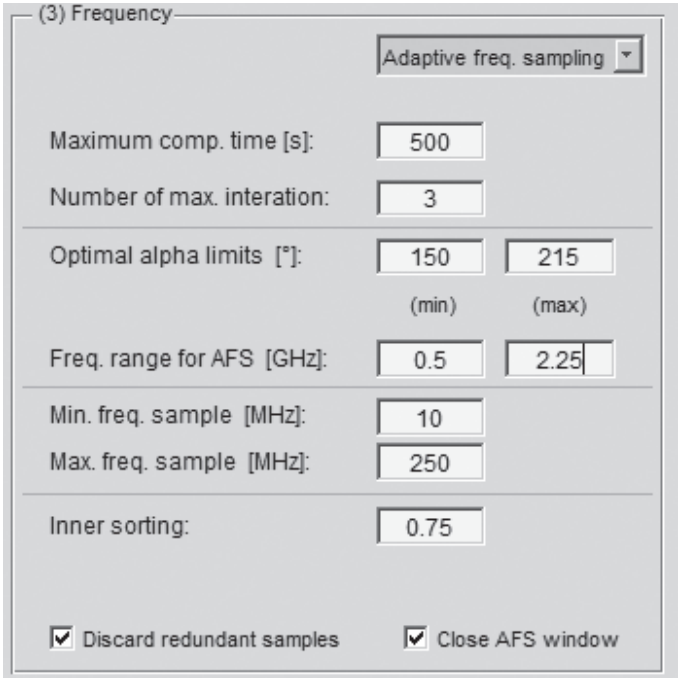

Figure 4. Screenshots of the Theory of Characteristic Modes tool in *MATLAB*: (top) manual frequency sampler, and (bottom) adaptive frequency sampler.

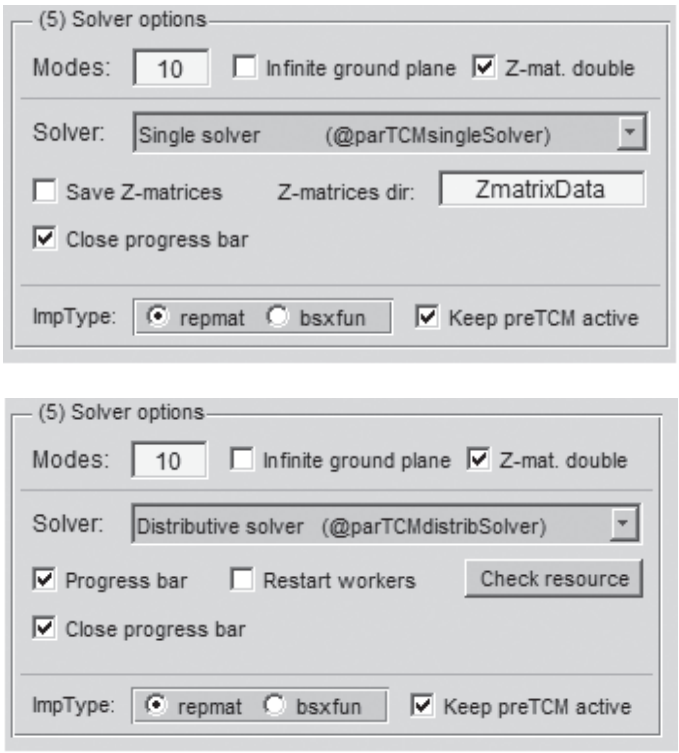

Figure 5. Screenshots of the Theory of Characteristic Modes tool in *MATLAB* showing the available solvers: (top) single, (middle) parallel, and (bottom) distributive.

and complex tracking with spline interpolation of missing data (bottom of Figure 6). The complex tracking method is schematically depicted in Figure 7 as a pseudocode. This part of the code is explicitly presented for the first time.

Finally, N modes have to be found in *MATLAB* and sent to the `postprocessing` part. However, due to numerical noise and the fact that the Theory of Characteristic Modes is ill-conditioned for nonradiating modes, we usually find far fewer modes than N. Fortunately, in practice, only five to 10 modes are needed for the correct analysis of antenna behavior in the selected frequency range. In the case of analysis of an electrically small antenna (ESA), only the first one or two modes are necessary.

The problems of time-consuming inversion and decomposition of the matrix $\mathbf{Z}$ were treated by parallel and distributive computing in *MATLAB* [17]. In parallel mode, only up to eight (12 in *R2012b*) threads can be simultaneously used on a single machine. An example of a typical speedup of a mid-sized task (in terms of the size of the mesh and the number of frequency samples) is depicted in Figure 8. The distributive mode allows the use of a large number of cores (or nodes) to be connected through the LAN at a time, e.g., the initial part of the distributed solver is depicted in Figure 9. This piece of code can be generalized for any cluster calculations in *MATLAB*.

Note that the *MATLAB* cluster can easily be established thanks to the *MATLAB* AdminCenter\footnote (however, of course, one must own the *MATLAB Distributed Computing Server* and/or *Parallel Computing Toolbox*). To achieve the best possible speedup, the code also has to be properly modified in terms of Amdahl's law [19]. This means that the parallelized part of the software has to be maximized.

4. Results Processing

The tools for characteristic-modes computation of an arbitrary three-dimensional PEC surface antenna were described in the previous section. The next step is a post processing of these results. The eigenvalues and eigenvectors are regarded as primary results, since all other modal properties can be computed from them. Primary results (including eigenvalues, eigenvectors, the frequency list, the mesh structure, solver options, etc.) are stored in the `pTCMout` variable (see Figure 1), which can be saved to a file and then used for the following operation.

To give a short summary, we provided two tables (Table 1 and Table 2), containing the most important post-processing functions. In spite of the fact that we briefly describe them,

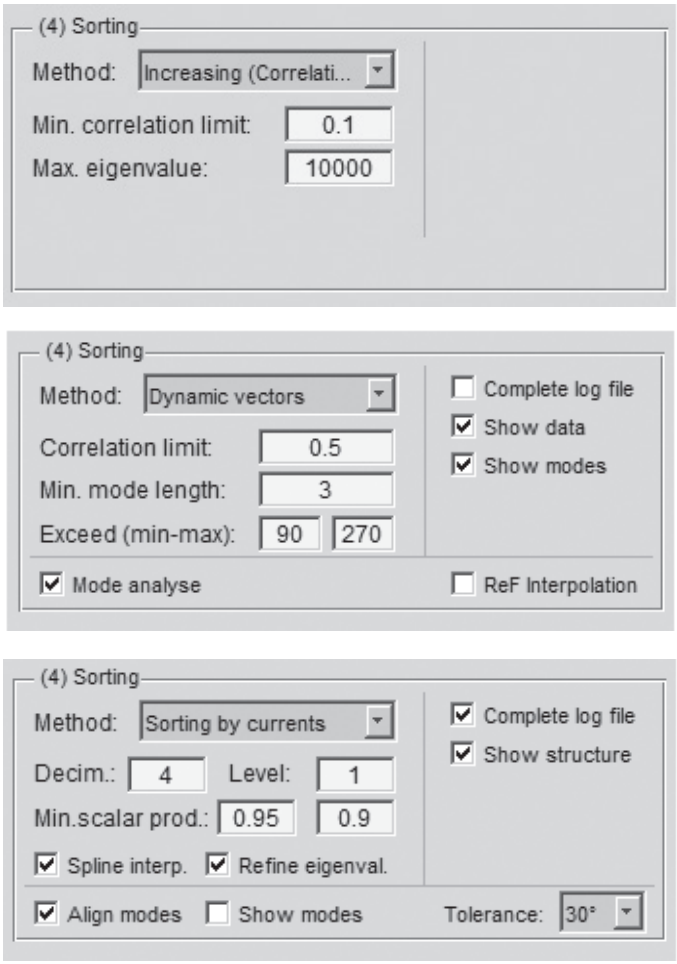

Figure 6. Screenshots of the Theory of Characteristic Modes tool in *MATLAB* showing tracking: (top) simple correlation, (middle) method #1, and (bottom) method #2.

```
corrTable = zeros(totNum,totNum,totFreq-1);
for thisFreq = 1:(totFreq-1)
    for thisMode = 1:totNum
% calculation of correlation tables (corrTable)
    end
end
%% ---INIT-------------------------------------
for initMode = 1:totNum
% set up index2Modes, startOfModes & totalModes
end % ---INIT/END/-----------------------------
for sortFreq = 1:(totFreq-1)
% allocation (allocModesAtFr0, allocModesAtFr1)
%% ---GENERAL_CORR-----------------------------
    for sortMode = 1:totNum
% primary function for modes that are ok
        if nextCorrValue > minCorrLimit && ...
                nextCorrValue >= checkCorrValue
            if nextModePosit <= totNum && ...
                    nextCorrValue >= ...
                        checkCorrValue
% make some tags and assign correct mode
            end
        end
    end % ---GENERAL_CORR/END/----------------
% find modes that are uncomplete and try ...
%% ---RESCUE_CORR-----------------------------
    if numOfFinisModes > 0
        for tryCompleteThisOne = ...
            1:length(uncomplModes)
% for every unfinished mode
            for thisRescueMode = ...
                1:numOfFinisModes
% try to find finshed mode
            end
            if rescModeValue > minCorrLimit
% if correlation is OK and ...
                if endOfModes(rescPosit) ~= 0
% ... original mode is closed: connect
                end
            end
        end
    end % ---RESCUE_CORR/END/-----------------
%% ---MODE_CLOSING----------------------------
    for thisCloseMode = 1:length(closeModesPos)
        % close every mode that is unused
    end % ---MODE_CLOSING/END/----------------
%% ---MODE_OPENING----------------------------
    for thisOpenMode = 1:length(openModesPos)
        % and, if necessary, open new ones
    end % ---MODE_OPENING/END/----------------
%% ---CHECK_NUMBER_OF_MODES_ACTUALLY_OPENED---
    if totalModes(sortFreq+1) > totalModes_limit
    end % ---CHECK_NUMBER_OF_MODES_ACT.../END/
end
```

Figure 7. Pseudo-code of the tracking procedure.

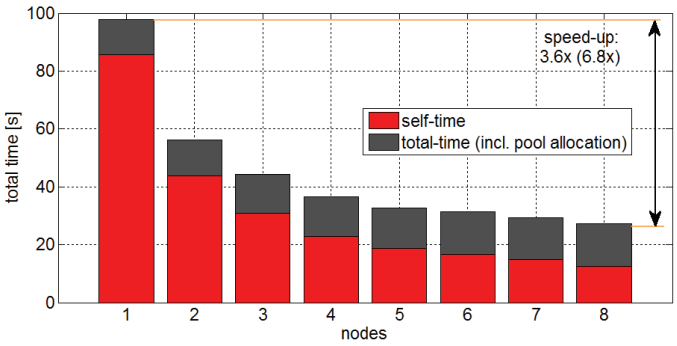

Figure 8. A typical parallel speedup of a medium-sized Theory of Characteristic Modes job.

```
% ... some distributive solver allocation
res             = findResource();
if strcmp(res.Type,'local')
    % RETURN
end
workers       = res.ClusterSize;
j             = createJob();
options.Zprec = opt.Zprecis; % single/double p.
if opt.infGround % Green's function for inf. GND
    set(j,'FileDependencies',...
        {'distBatch.m','distMeshStruct.mat',...
        'private/eigFcn.m','private/impGFcn.m'});
    options.gnd = true;
else
    set(j,'FileDependencies',...
        {'distBatch.m','distMeshStruct.mat',...
        'private/eigFcn.m','private/impFcn.m'});
    options.gnd = false;
end
delete('distMeshStruct.mat'); % del. temp file
if opt.restartWorkers % restart of all workers
    set(j,'RestartWorker',true);
end
fiOpt.starTime  = clock;
for k = 1:FreqSize % prepare all tasks
    fiOpt.freqs = k;
    createTask(j,@distBatch,8,...
        {freqList(k),options},'FinishedFcn',...
        @(scr,event)distBatchCompleted(fiOpt));
end
submit(j); % upload job to the cluster
waitForState(j,'finished');
results = getAllOutputArguments(j);
destroy(j); % destroy computed job
% results processing ...
```

Figure 9. The start of the distributed solver.

Table 1. Selected post-processing functions.

Function	Description
`resCurDistrib`	Calculates the modal current density
`resCharge`	Calculates the modal charge density
`resCoeff`	Calculates the modal coefficients
`resFF`	Calculates the modal radiated patterns
`resVoltageGap`	Connects the voltage gap
`resPlaneWave`	Generates the incident plane wave
`resSumCur`	Summarizes the selected modal currents
`resSumCharge`	Summarizes the selected modal charge density
`resQeig`	Estimates the modal radiation Q from a slope of λ_n
`resQz`	Calculates radiation Q factor from input impedance
`resQM`	Calculates radiation Q according to [18]

Table 2. Selected special display functions.

Function	Description
`plotMesh`	plots mesh, quality, tr./pt. numbers
`plotEigCur`	displays modal currents
`plotEigCharge`	displays charge densities
`plotEigNum`	displays eigenvalues
`plotFF`	displays modal radiated patterns

each function has complete help, which can be accessed via the *MATLAB* `help` command, if necessary.

Note also that many operations can be performed via standard built-in functions (such as `plot`, `surf`, etc.).

4.1 Selected Examples

Let us briefly discuss the application of `TCMapp` via two illustrative examples.

The first example is the Minkowski fractal in free space (see Figure 10). The `preTCM` accepts our in-house iterated function system (IFS) fractal [20] format, `FRC` [21], which represents any iterated function system in a compact form with base points, a list of affine transformations, and the iteration for fractal generation. For simplicity, we analyzed the above-mentioned fractal generated only for the first iteration. The initial size was 100 mm × 60 mm (see Figure 11 for three various triangularizations).

The second example consists of a Franklin antenna [22], depicted in Figure 12. This structure was considered only for the post-processing calculation of modal efficiencies and radiation Q factors. However, of course the Franklin antenna has to be analyzed first in the Theory of Characteristic Modes tool.

4.2 Geometry and Discretization

There are many possibilities for discretization of the selected structure, because only matrices with all vertex points `[p]` and with all triangles `[t]` are necessary for the computation of the characteristic modes. One can utilize the *MATLAB* PDE toolbox [23]. However, the PDE toolbox usually creates a mesh of poor quality. From the authors' point of view, the Comsol *Multiphysics* [24] option is better: it has an excellent mesh generator.

In order to improve the control of meshing even more, the authors are about to complete an in-house mesh generator based on the `distmesh` code [25]. We thus will be able to generate any required three-dimensional structure, including periodic

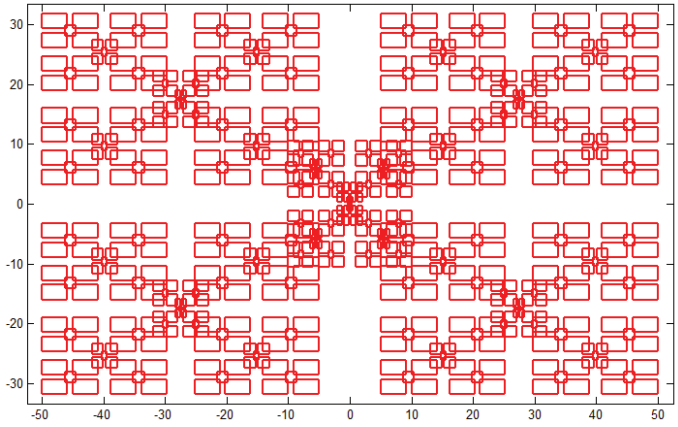

Figure 10. The Minkowski iterated function system fractal, fourth iteration.

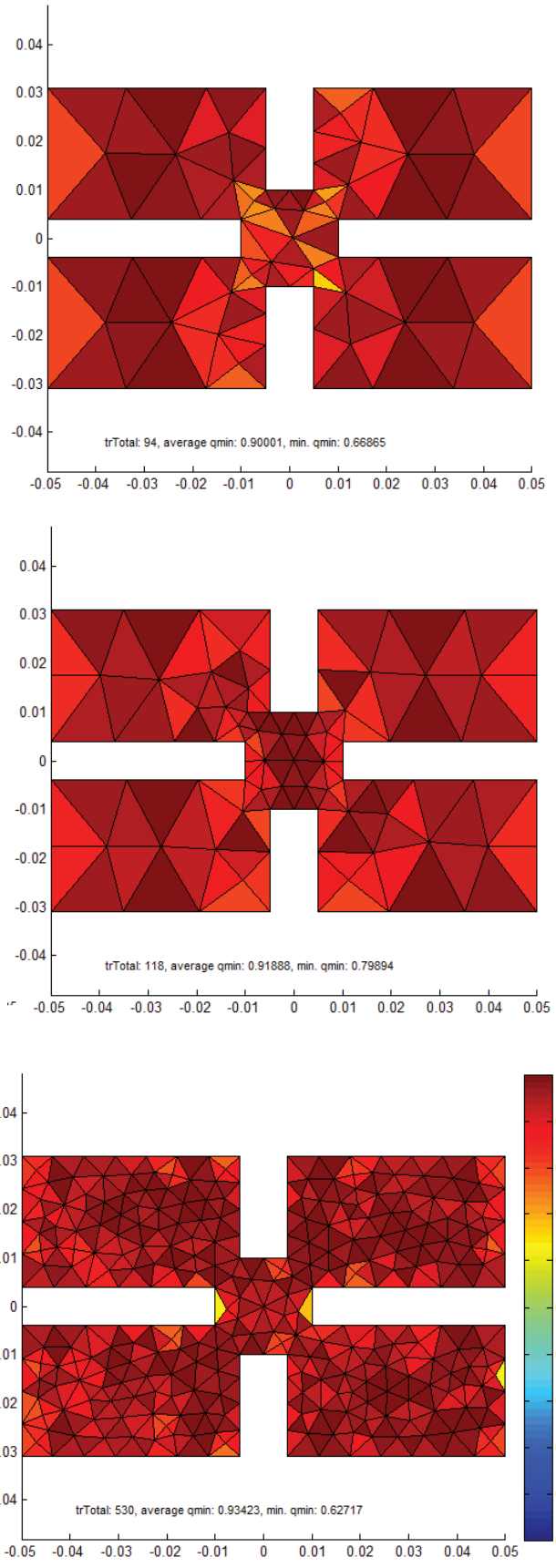

Figure 11. Fractal mesh generation (from coarse to fine, top to bottom). The quality of the triangles was computed according to Equation (10).

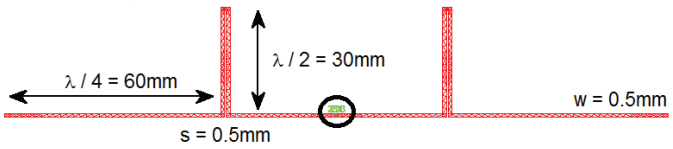

Figure 12. The Franklin antenna.

structures, fractals, and T-junctions, and control the details of the meshing process.

In terms of matrix inversion (direct MoM) as well as matrix decomposition (Theory of Characteristic Modes), it is necessary to control the quality of triangles, which can be defined as

$$\zeta_n = \frac{4\sqrt{3}A_n}{\left|\mathbf{P}_{n1}-\mathbf{P}_{n2}\right|^2+\left|\mathbf{P}_{n1}-\mathbf{P}_{n3}\right|^2+\left|\mathbf{P}_{n2}-\mathbf{P}_{n3}\right|^2}. \quad (10)$$

The quality of some fractal motifs is depicted in Figure 11. Also, the number of triangles, N, is important, because the time complexity of inversion and decomposition is $\mathcal{O}\left[\mathrm{inv}(\mathbf{Z})\right] \propto \mathcal{O}\left(N^2\right)$ and $\mathcal{O}\left[\mathrm{eig}(\mathbf{X},\mathbf{R})\right] \propto \mathcal{O}\left(N^3\right)$, respectively. Interestingly, for the preparation of larger meshes, the user-defined `repmat` function (utilizing the built-in routine `bsx`) is faster than the original function `repmat` in Matlab. (`repmat` is exhaustively used to prepare the impedance matrix. To accelerate the calculations, the authors used vector operations everywhere possible.)

4.3 Eigenvalues

Eigenvalues are obtained directly from the decomposition of the impedance matrix and, with the exception of the tracking, they do not require any post processing. These values are continuous throughout the frequency range, they are equal to zero at resonance, and lie within the range of $(-\infty,+\infty)$. Eigenvalues define the character (capacitive/inductive) of the selected mode at a given frequency.

However, better representation of eigenvalues are the so-called eigenangles [26], defined as

$$\delta_n = 180 - \arctan(\lambda_u). \quad (11)$$

Each eigenangle is in the range of $(90°, 270°)$, and the mode resonates for $\delta_n = 180°$. The eigenangles of the Minkowski fractal of the first iteration are depicted in Figure 13, and the adaptive frequency solver was used.

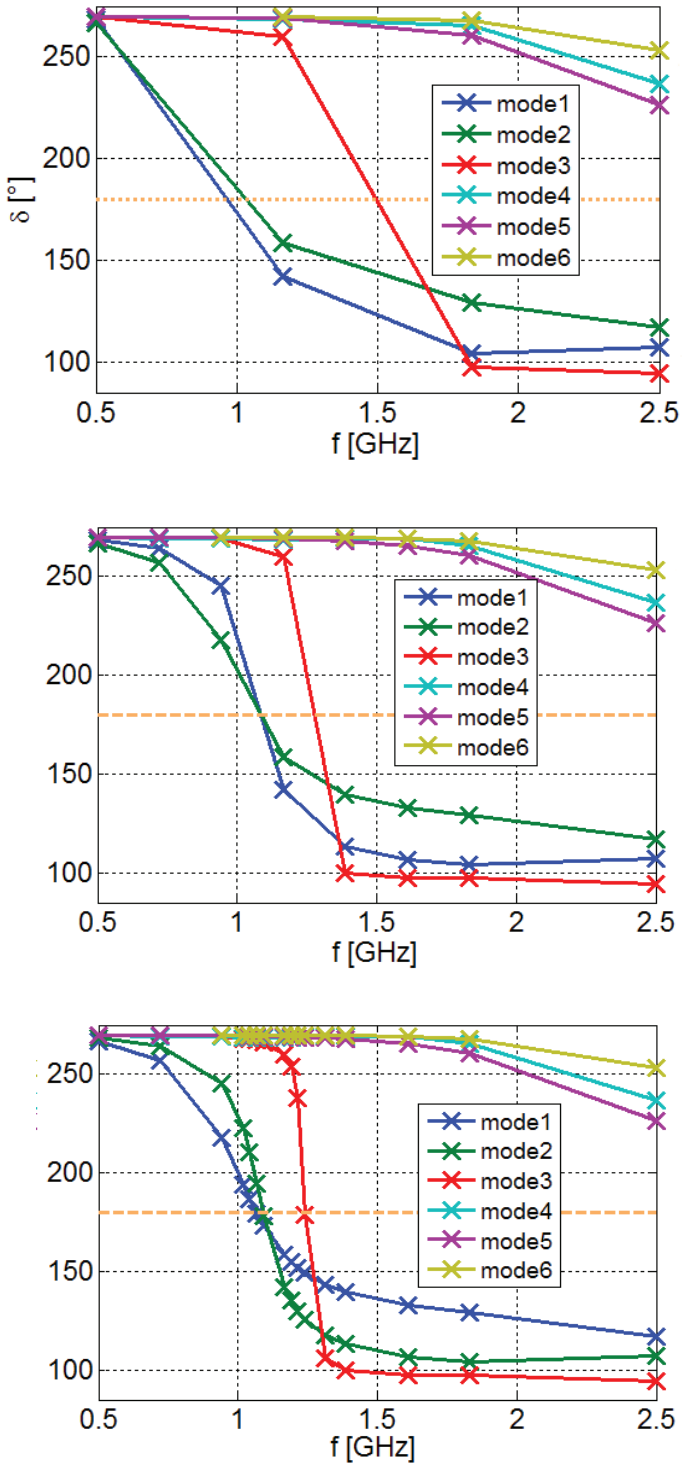

Figure 13. The adaptive frequency sampler: (top to bottom) first, second, and fourth iterations.

4.4 Surface Currents

The eigenvectors are not yet the actual currents flowing on the antenna's surface. The computation of the components of the surface-current density, $\left[J_x, J_y, J_z\right]$, over all triangles is performed by the function `resCurDistrib`. It uses the eigenvectors as MoM expansion coefficients, multiplied by the basis functions [2]: for examples, see Figure 14. Our software contains many post-processing routines, such as the calculation of the radiation pattern, the modal (and total) radiation Q factor, the modal (and total) radiation efficiency, and so on.

4.5 Far-Field Computation

The modal currents are the sources of modal radiated fields and the corresponding modal radiation patterns. Two methods were implemented to compute these radiated fields: a direct method, and the dipole method [27]. The direct method is a numerical integration of analytical expressions for the radiation vector $\mathbf{F}(\theta,\phi)$ [5]. The input is a surface-current density over all triangles, which first has to be computed by the `resEichCur` function. Since the triangulated surface made of the PEC is infinitesimally thin and the current density is assumed to be constant on the triangle, the volume integration is reduced to a surface summation. The contribution to the radiation vector from one triangle is

$$\mathbf{F}_{\theta i}(\theta,\phi) = \left[\cos(\phi)\cos(\theta)J_{xi} + \sin(\phi)\cos(\theta)J_{yi} - \sin(\theta)\right]J_{zi}e^{jk\mathbf{r}\bullet\mathbf{r}'}A_i \qquad (12)$$

and

$$\mathbf{F}_{\phi i}(\theta,\phi) = \left[-\sin(\phi)J_{xi} + \cos(\phi)J_{yi}\right]e^{jk\mathbf{r}\bullet\mathbf{r}'}A_i\,, \qquad (13)$$

where A_i is the area of the ith triangle; J_{xi}, J_{yi}, and J_{zi} are the components of the current density $\mathbf{J}_i$ on the triangle; and

$$\mathbf{r}\bullet\mathbf{r}' = \left[x_i\cos(\phi) + y_i\sin(\phi)\right]\sin(\theta) + z_i\cos(\theta)\,. \qquad (14)$$

The center of the ith triangle is specified by the Cartesian coordinates x_i, y_i, and z_i. The total radiation vector is next computed as a sum of contributions from all triangles:

$$\mathbf{F}_\theta(\theta,\phi) = \sum_i \mathbf{F}_{\theta i}(\theta,\phi)\,, \qquad (15)$$

$$\mathbf{F}_\phi(\theta,\phi) = \sum_i \mathbf{F}_{\phi i}(\theta,\phi)\,. \qquad (16)$$

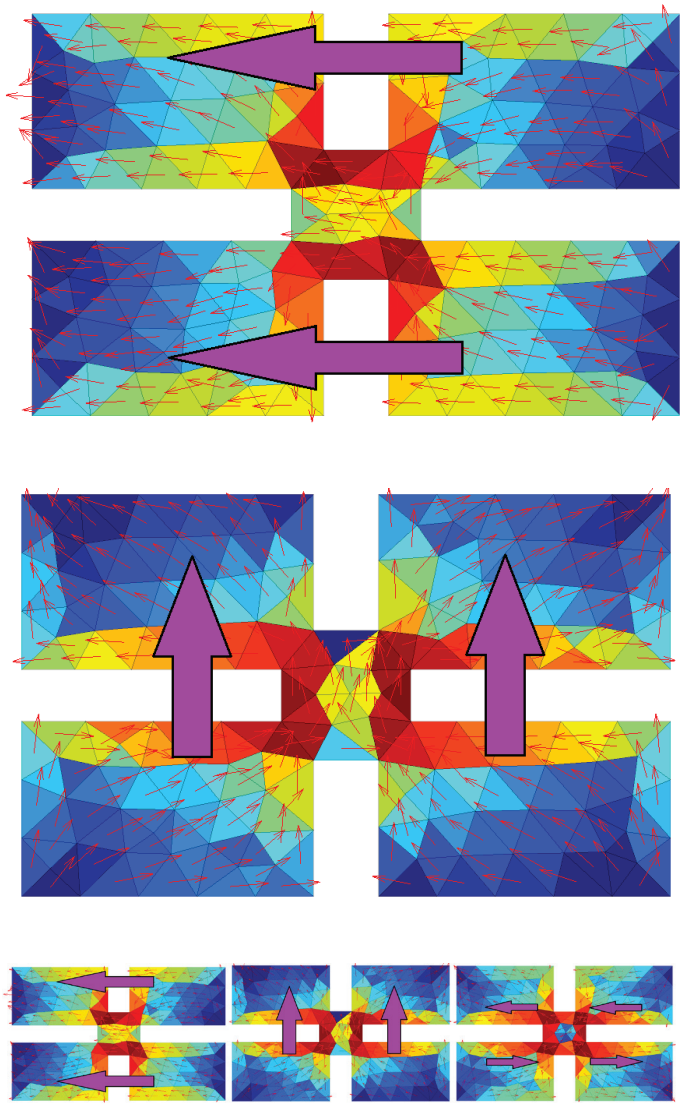

Figure 14. The modal currents (top to bottom: the first, second, and third modes at the resonance frequency).

Table 3. Far-field computations for the Minkowski fractal with different angle steps.

Angle Step	Angle Points	Max. Directivity	Time	Rad. Power
45°	45	2.6521	0.0082	0.9088
20°	190	2.3089	0.0121	0.9836
12°	496	2.2604	0.0194	0.9946
7.2°	1326	2.2433	0.0406	0.9986
4.5°	3321	2.2374	0.0915	1.0000
3°	7381	2.2354	0.1931	1.0004
1.5°	29161	2.2341	0.7478	1.0006
1°	65341	2.2339	1.6610	1.0008
0.5°	260281	2.2338	6.5763	1.0008

From the values of the radiation vector, the electric field in the far-field region, as well as the radiation intensity, **U**, can be computed. To estimate the modal directivity pattern, the radiated power has to be known. It is obtained by numerically integrating **U** over a sphere. As all the modal currents are normalized and the structure is supposed to be lossless, the integration should give a unit radiated power. The algorithm is very fast, even with high angular resolution (see Table 3).

The second approach is the dipole method. This method regards the current flowing along a mesh edge as an infinitesimal dipole. This current is a direct result of the MoM, and in the Theory of Characteristic Modes, these currents can be associated with characteristic vectors. The advantage of the dipole method is that analytical expressions for radiated fields **E** and **H** exist. These expressions were derived without any far-field approximation: they are therefore valid for an arbitrary distance larger than approximately the length of the dipole (edge) [27]. These expressions are thus also suitable for the near-field calculations. The total fields at an arbitrary observation point are computed easily as the sum of contributions to **E** and **H** from all edges (i.e., dipoles).

The dipole method is more general, because it computes **E** and **H** fields at an arbitrary distance. On the other hand, the evaluation is approximately 15-20 times slower than the direct far-field computation.

Let us next consider a visualization of the computed fields. The modal radiation patterns are plotted by a *MATLAB* surface plot. Note that spherical coordinates should be mapped to appropriate Cartesian coordinates before the visualization.

The comparisons of computation times and computed values for different angle steps are in Table 3. Similar convergence was observed for different modes and different structures. It could be seen that both the maximum directivity and the radiated power converged with a smaller angle step. A 3° step was a reasonable compromise between accuracy and computation time. Examples of three-dimensional directivity plots and cuts are in Figures 15 and 16.

4.6 Near Field

As was mentioned in the previous section, the dipole method is valid for arbitrary distances (greater than the edge length). Near-field plots can therefore be created by computing fields at certain points lying on the surface of virtually any shape: for example, see the magnitude of the electric field on a plane in Figure 17.

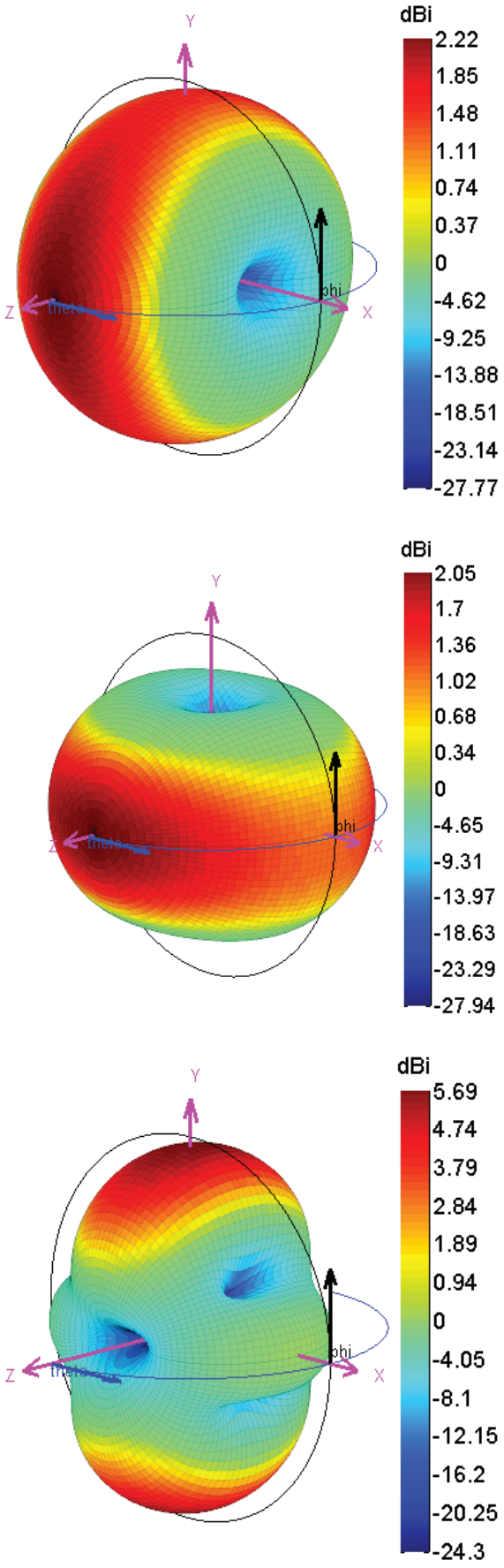

Figure 15. Radiation patterns for the first three modes for the Minkowski fractal motif in free space.

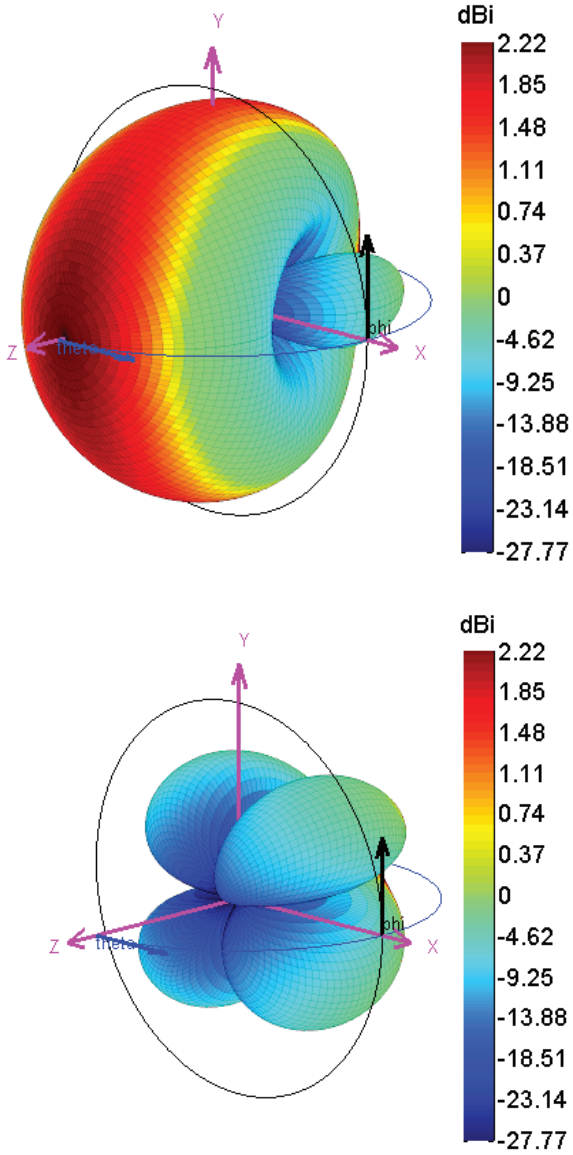

Figure 16. The radiation patterns for the first mode of the Minkowski fractal motif in free space: (top) the Ludwig3 horizontal component, (bottom) the Ludwig3 vertical component.

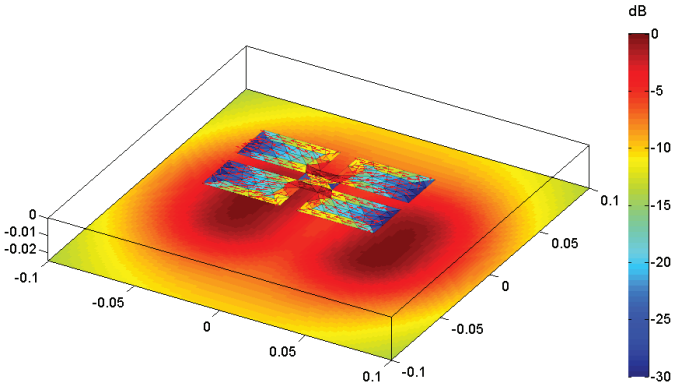

Figure 17. The normalized magnitude of the electric field for mode 1 on a plane $z = -25$ mm of the Minkowski fractal, shown on a logarithmic scale.

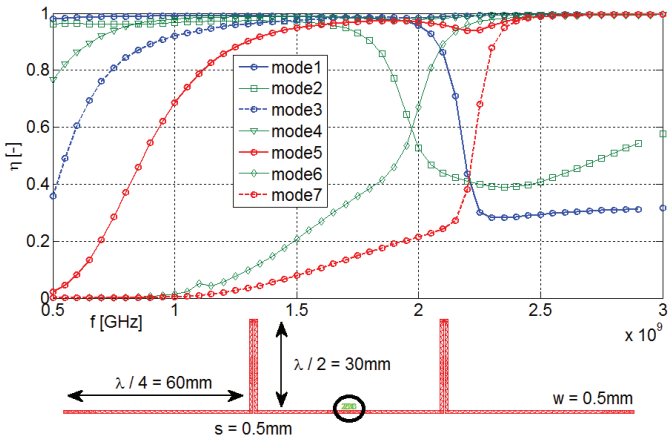

Figure 18. The modal radiation efficiency for the Franklin antenna: $\sigma = 5.85\times10^{7}$ Sm^{-1}, $t = 50$ µm.

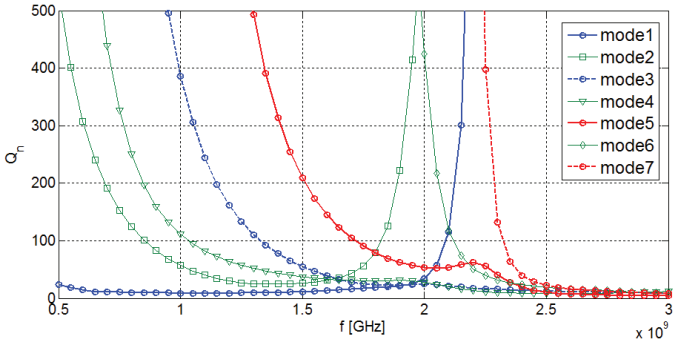

Figure 19. The modal radiation Q factor for the Franklin antenna.

4.7 Radiation Efficiency

While we consider the PEC for the Theory of Characteristic Modes decomposition, the modal radiation efficiency [5] can be estimated for good conductors (such as copper, aluminum, etc.). We demonstrated the results for the case of the Franklin antenna in the frequency range 0.5 GHz to 3 GHz (see Figure 18). Modal efficiencies were computed for the conductivity of copper, $\sigma = 5.85\times10^{7}$ Sm^{-1}, and a metallization thickness of $t = 50$ µm.

4.8 Radiation Q Factor

Based on [28] and [29], the modal radiation Q factors can also be rigorously calculated [18]. The results for the first seven modes are depicted in Figure 19. The Franklin antenna from the previous section was used.

5. Closing Comments

The presented software can be used for educational purposes, as well as for effective antenna design. Nowadays, the major disadvantage is that the modal decomposition is time consuming. This issue can be treated by using a large number of high-speed processors. For this reason, the authors predict a growing interest in modal methods.

To demonstrate the usefulness of the Theory of Characteristic Modes, we concluded with two complex structures that were designed and manufactured with the help of the `TCMapp` software. Both structures were fractal shapes, depicted in Figure 20. While both of them were simulated in professional CST *MWS* software [30], our software gave the first (and very important) insight into their physical behavior. Antenna design is more effective based on this modal information. For details, we refer the reader to [31] and [21].

Together with the authors' other activities (in the fields of optimization, Delaunay triangularization, and electrically

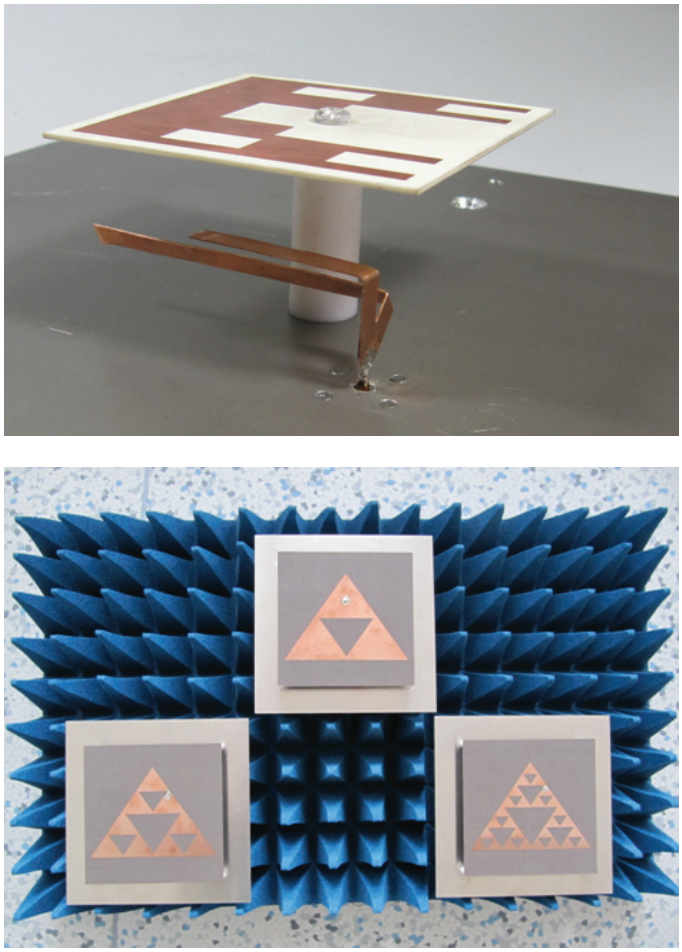

Figure 20. The manufactured fractal antennas that were analyzed with the Theory of Characteristic Modes software.

small antenna design), the *MATLAB* toolbox elements consisting of the new RWG MoM, the Theory of Characteristic Modes simulator with comprehensive post processing, the particle-swarm optimizer, the modal radiation Q factor, and the radiation-efficiency packages, are all scheduled towards the end of 2013. The MoM and the Theory of Characteristic Modes can be further generalized towards multilayered or dielectric structures, which can be the next challenge to interested readers and scientists in the field.

6. Acknowledgement

This work was supported by a project of the Czech Science Foundation, grant No. P102/12/2223, and by the Grant Agency of the Czech Technical University in Prague, grant No. SGS12/142/OHK3/2T/13. The authors also would like to thank N. Bell for his comments.

7. References

1. R. F. Harrington, *Field Computation by Moment Methods*, New York, Wiley-IEEE Press, 1993.

2. S. M. Rao, D. R. Wilton, and A. W. Glisson, "Electromagnetic Scattering by Surfaces of Arbitrary Shape," *IEEE Transactions on Antennas and Propagation*, **AP-30**, 3, May 1982, pp. 409-418.

3. R. F. Harrington and J. R. Mautz, "Theory of Characteristic Modes for Conducting Bodies," *IEEE Transactions on Antennas and Propagation*, **AP-19**, 5, September 1971, pp. 622-628.

4. M. de Berg, O. Cheong, M. van Kreveld, and M. Overmars, *Computational Geometry, Third Edition*, Berlin, Springer, 2008.

5. C. A. Balanis, *Advanced Engineering Electromagnetics*, New York, Wiley, 1989.

6. W. C. Gibson, *The Method of Moments in Electromagnetics*, Boca Raton, FL, Chapman and Hall/CRC, 2007.

7. P. Hazdra and P. Hamouz, "On the Modal Superposition Lying under the MoM Matrix Equations," *Radioengineering*, **17**, 3, September 2008, pp. 42-46.

8. M. Capek, P. Hazdra, and J. Eichler, "Complex Power-Ratio Functional for Radiating Structures with Applications to the Characteristic Mode Theory," submitted to *IEEE Transactions on Antennas and Propagation*.

9. The *MATLAB*, available at http://www.mathworks.com.

10. The MathWorks, *Object-Oriented Programming*, The MathWorks, Inc., 2012.

11. The Jacket, available at http://www.accelereyes.com/.

12. E. Anderson, et al., *LAPACK Users' Guide*, Philadelphia, PA, Society for Industrial and Applied Mathematics (SIAM), 1999.

13. *MATLAB* TCM application, available at www.old.elmag.org/doku.php/wiki:user:capek:tcmapp.

14. S. N. Makarov, *Antenna and EM Modeling with MATLAB*, New York, John Wiley, 2002.

15. M. Capek, P. Hazdra, P. Hamouz, and J. Eichler, "A Method for Tracking Characteristic Numbers and Vectors," *Progress In Electromagnetics Research B*, **33**, 2011, pp. 115-134.

16. B. D. Raines and R. G. Rojas, "Wideband Characteristic Mode Tracking," *IEEE Transactions on Antennas and Propagation*, **AP-60**, 7, July 2012, pp. 3537-3541.

17. The MathWorks, *MATLAB Distributed Computing Server*, The MathWorks, Inc., 2011.

18. M. Capek, P. Hazdra, and J. Eichler, "A Method for the Evaluation of Radiation Q Based on Modal Approach," *IEEE Transactions on Antennas and Propagation*, **AP-60**, 10, October 2012, pp. 4556-4567.

19. J. L. Gustafson, "Reevaluating Amdahl's Law," *Communications of the ACM*, May 1988, pp. 532-533.

20. K. Falconer, *Fractal Geometry: Mathematical Foundations and Applications*, New York, John Wiley, 2003.

21. M. Capek, P. Hazdra, P. Hamouz, and M. Mazanek, "Software Tools for Efficient Generation, Modeling and Optimisation of Fractal Radiating Structures," *IET Microwaves, Antennas and Propagation*, **5**, 8, June 2011, pp. 1002-1007.

22. P. Hamouz, P. Hazdra, M. Polivka, M. Capek, and M. Mazanek, "Radiation Efficiency and Q Factor Study of Franklin Antenna Using the Theory of Characteristic Modes," Proceedings of the EuCAP 2011, Rome, Italy.

23. The MathWorks, *Partial Differential Equation Toolbox*, The MathWorks, Inc., 2012.

24. The Comsol Multiphysics, available: http:// www.comsol.com/.

25. P.-O. Persson, *Mesh Generation for Implicit Geometries*, PhD Thesis, Cambridge, MA, MIT, 2005.

26. E. H. Newman, "Small Antenna Location Synthesis Using Characteristic Modes," *IEEE Transactions on Antennas and Propagation*, **AP-27**, 4, July 1979, pp. 530-531.

27. S. Makarov, "MoM Antenna Simulations with *MATLAB*: RWG Basis Functions," *IEEE Antennas and Propagation Magazine*, **43**, 5, October 2001, pp. 100-107.

28. G. A. E. Vandenbosch, "Reactive Energies, Impedance, and Q Factor of Radiating Structures," *IEEE Transactions on Antennas and Propagation*, **AP-58**, 4, April 2010, pp. 1112-1127.

29. P. Hazdra, M. Capek, and J. Eichler, "Radiation *Q*-Factors of Thin-Wire Dipole Arrangements," *IEEE Antennas Wireless Propagation Letters*, **10**, May 2011, pp. 556-560.

30. Computer Simulation Technology, available at http:// www.cst.com/.

31. J. Eichler, P. Hazdra, M. Capek, T. Korinek, and P. Hamouz, "Design of a Dual-Band Orthogonally Polarized L-Probe-Fed Fractal Patch Antenna Using Modal Methods," *IEEE Antennas and Wireless Propagation Letters*, **10**, May 2011, pp. 1389-1392.

Acceleration Techniques in Matlab for EM Community

Miloslav Capek*, Pavel Hazdra*, Jan Eichler*, Pavel Hamouz*, Milos Mazanek*,

*Department of electromagnetic field, Czech Technical University in Prague
Technicka 2, 166 27, Prague, Czech Republic
Email: miloslav.capek@fel.cvut.cz

***Index Terms*—Computational electromagnetics; Antennas; Scientific computing**

I. Introduction

There is probably no doubt that we can see boom of computational capabilities in recent years. This brough us a new posibilities in computational electromagnetics (CEM), especially for electrically large structures, inverse problems, optimization and so on.

This paper describes an in-house antenna tool [1] implemented in Matlab [2]. Here, we strongly focus on acceleration of computational routines via High Performance Computing (HPC). In terms of Matlab software, it includes parallel and distributive computing on CPU(s) and GPU computing [3].

Up-to-date CPUs have typically 4-8 cores (doubled by hyperthreading technology, which will be also discussed), they have virtually infinite amount of RAM and complex instruction set. On the other hand, modern GPU cards (e.g. with CUDA compute capability 2.0+) have a hundreds of cores, typically 1-6GB RAM and very fast internal bus interface. They are superfast in single precision mode, but significantly slower in double precision. In addition, they are extremely limited in size of memory and simplicity of each fundamental core. Hereafter, in case of GPU implementation, we consider nVidia CUDA technology [4]. Then, overall performance in double precision is mainly given by ratio between total number of stream processors (SP) and number of special function units (SFU).

Almost any CEM problem can be significantly sped up. For example, time-consuming eigen-decomposition (solution of generalized eigenvalue problem in Theory of Characteristic Modes [5]) should be treated via parallel/distributive computing using many CPU cores. On the other hand, most of the post processing routines (all kinds of integration, differentiation etc.) deserve to be solved via general-purpose GPU (GPGPU).

It means that large, complex and basically inseparable tasks that need large amount of memory are potential adepts for parallel/distributive computing on CPU(s). But many same operations with small demands on memory are perfect candidates for paralelization on GPU(s). Whence it follows that our code – if it should be effective – has to respect a mixed approach to the HPC in Matlab. We demonstrate it on two independent examples. The first one is a decomposition to characteristic modes [5], the second one is an calculation of total radiated power [6]. Note that, the relations for total stored electric and magnetic energies have the same form and are used for calculation of modal and total radiation Q factor [7].

For comparison purposes, we specify our testing machine: CPU Intel X980 (6×3.33GHz,12MB); 24GB DDR3; nVidia GTX580 (3GB); SSD Vertex 3.0 (software) + HDD VelociRaptor (data). All GPU routines are developed with ArrayFire (formerly known as Jacket) package [8], parallel and distributive computing on CPUs is utilized in Matlab toolboxes [9] and [10], respectively. All examples were tested in Matlab 2011b with Jacket 2.2 (including DLA and SLA libraries).

A. HPC in Matlab: Theoretical Concepts

Speed-up is usually defined by the Amdahl law [11]:

$$S(p,\tau_s) \leq \frac{1}{\tau_s + \frac{1-\tau_s}{p}}, \tag{1}$$

where p is number of processors and τ_s is computing time of a sequentially performed part of code. According to the Amdahl law it's necessary to maximize the part of code that is running concurrently (is parallelized). In other words, the non-parallelized part of code dominates the maximum speed-up, see Fig. 1. If we are interested in available speed-up, we use rather the Gustafson-Barsis's law. However in this paper we use another formulation of (1):

$$S(p,\tau_s) = \frac{t(1)}{t(p)}, \tag{2}$$

where $t(p)$ is total computing time with p used processors. Before we start with acceleration it is necessary to localize all parallelizable parts (called *kernels*) of our code. Kernel is a part of code that is unceasingly computed in parallel mode (e.g. on GPU). Possible kernels can be located by Matlab `profile` utility.

There are also many other possibilities to accelerate a given code – vectorization, *for*-parts modification (loop interchange, loop fusion, loop reversal, loop unrolling etc.), usage of low-level function like `repmat` or `bsxfun`, JIT modification etc., see documentation [2].

We will discuss all evolutionary grades to fully parallelized code during the EuCAP presentation. Due to lack of space only the final version which is depicted at Fig. 2 is presented.

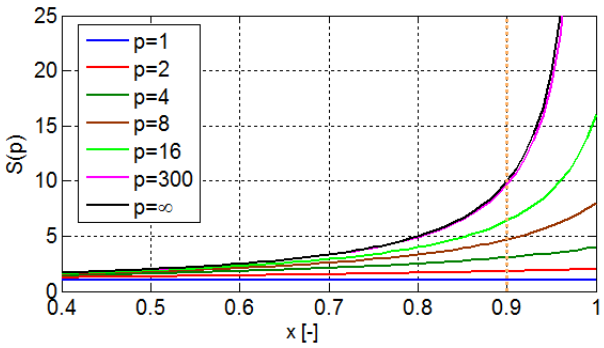

Fig. 1. The speed-up $S(p)$ according the Amdahl law, depending on number of processors (p) and ratio of parallelized code (x-axis)

```
function [Wep Wmp Wr Pr] = test2_GPU_regularFcn1(J,q,Rc,RA,k0)
% no for-loops (full vectorization thanks to the bsxfun function), GPU

% Euclidean distance
Rx  = bsxfun(@minus, Rc(:,1), Rc(:,1)');
Ry  = bsxfun(@minus, Rc(:,2), Rc(:,2)');
Rz  = bsxfun(@minus, Rc(:,3), Rc(:,3)');
r21 = sqrt(Rx.^2 + Ry.^2 + Rz.^2);
% dS segments in double integration
dS  = bsxfun(@times, RA, RA');
clear Rx Ry Rz RA Rc;
% final products of currents
Jx  = bsxfun(@times, J(:,1), conj(J(:,1))');
Jy  = bsxfun(@times, J(:,2), conj(J(:,2))');
Jz  = bsxfun(@times, J(:,3), conj(J(:,3))');
J12 = Jx + Jy + Jz;
% final products of charges
q12 = bsxfun(@times, q, conj(q)');
clear Jx Jy Jz q J;
% goniometrical arguments
CkRoR = cos(k0*r21)./r21;
SkR   = sin(k0*r21);
SkRoR = SkR./r21;
% singularity treatment
CkRoR(isinf(CkRoR)) = 1; %% (for correct treatment see [1])
SkR(isnan(SkR))     = 0;
SkRoR(isnan(SkRoR)) = k0;
% integration
Wep = sum(sum(q12.*CkRoR.*dS));
Wmp = k0^2*sum(sum(J12.*CkRoR.*dS));
Wr  = k0/2*sum(sum((k0^2*J12 - q12).*SkR.*dS));
Pr  = sum(sum((k0^2*J12 - q12).*SkRoR.*dS));
clear CkRoR SkR SkRoR k0 dS J12 q12 r21;
```

Fig. 2. Optimized GPU code for calculation of radiated power and net stored energy.

B. In-house Antenna Tool

Matlab window of the in-house antenna tool is depicted at Fig. 3. It is based on the Method of Moments (MoM, [12]) with the RWG basis functions [13]. The input of the methods is any 3D PEC triangularized surface that can be imported from Comsol Multiphysics [14], Matlab PDE toolbox or from our in-house generator based on distmesh [15] utility. After impedance matrix calculation for selected frequencies, characteristic mode (CM, [5]) decomposition is performed via `eig` function. Advanced tracking procedures [16] are included into the package. Available results are: characteristic numbers, angles and vectors, modal currents, charge densities, radiation patterns, near-fields, modal energies and radiation Q factors. It is possible to include the effect of finite metal thickness

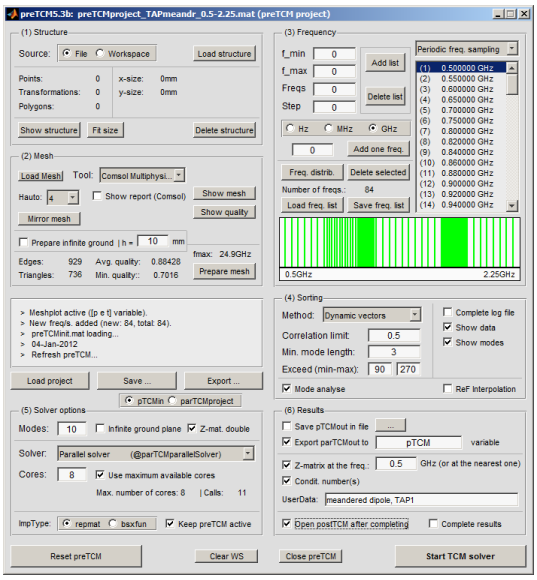

Fig. 3. Screenshot of preTCM tool in Matlab

and conductivity in post processing. After feeding definition (voltage gaps or plane wave) the modal solutions can be summed-up. Note that in this paper, the physical background of presented methods is skipped – for futher details see [1] and citations inside the paper. The problems of time-consuming inversion (MoM) and decomposition (TCM) of the impedance matrix were treated by the CPU acceleration and all postprocessing routines are treated on GPU.

C. CPU Acceleration – parallel mode

Because both the inversion (`inv` or – better – `mrdivide`) and the decomposition (`eig`) are numerically extensive iterative methods, they can be sped-up only with the aid of more CPU cores. In parallel mode only up to 8 cores (they are called *labs* in parallel toolbox) can be used simultaneously on a single machine. An example of typical speed up of mid-sized task (in terms of mesh and number of frequency samples) is depicted at Fig. 4 and speed-up of large task is depicted at Fig. 5. The gray part of all bars is equal to total time of opening and closing of Matlab pool and is more or less constant and takes usually about 10 seconds. It means that `parfor` usage for small tasks is effective only with permanently opened Matlab pool. All variables inside `parfor` loops have to be properly sliced to pass the loop correctly. In fact, Matlab opens new Matlab threads for each lab in pool and that is the reason why is it not possible to easily display any progress bar inside `parfor` loops.

D. CPU Acceleration – distributive mode

Distributive Computing Server allows to use more than 8 threads simultaneously. However, one have to start scheduler (the simplest one is job manager), than prepare job that contains individual tasks (e.g. decomposition for selected frequency sample). All jobs are collected in scheduler and sequentially computed. Executive code as well as necessary

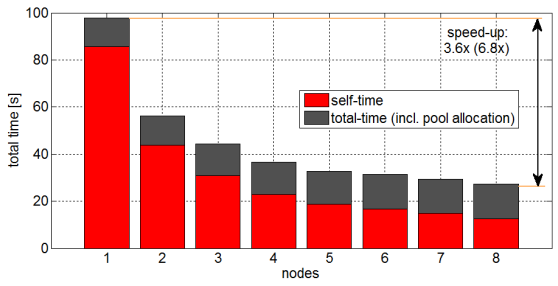

Fig. 4. Overall computational time for middle-sized task depending on number of nodes (359 unknowns, 100 samples)

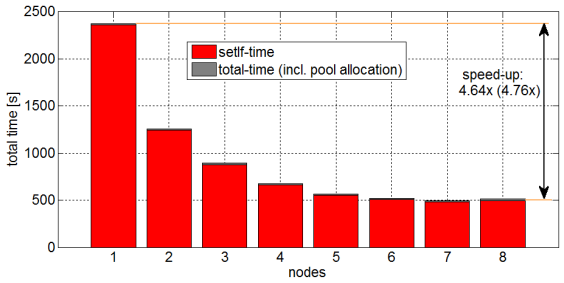

Fig. 5. Overall computational time for large-sized task depending on number of nodes (1012 unknowns, 17 samples)

data have to be saved separately to allow send them to the cluster's nodes (per `FileDependencies`). Distributive mode supports callbacks when task (or job) is computed. The results in distributive mode are send back right after calculation, so there is no order at all. Each job should be deleted (destroyed) after completing.

Table I shows typical speed-ups for small cluster of 8 or 16 single processor machines. Especially for large task it is possible to bring available speed-up near the theoretical limit (in case of decomposition the τ_p part tend to 1). Because of dense LAN traffic, the speed-up for small tasks is inconsiderable.

E. GPU Acceleration

ArrayFire allows comfortable transition from m-code computed on CPU to the GPU (this can be done with Matlab PCT as well). Thus, one can concentrate on implementation of GPU kernels. Table II clearly shows that many fundamental (*build-in*) functions are significantly faster evaluated on GPU compared to CPU. It holds for `plus` and `times` functions in particular (repeat here, that these functions are essential in

	8 nodes		16 nodes	
samples	500 × 500	2000 × 2000	500 × 500	2000 × 2000
1	0.3	0.7	0.2	0.3
16	2.6	4.8	1.5	4.2
64	4.4	7.0	3.2	9.7
512	5.2	7.7	5.7	12.8

TABLE I
SPEED-UP FOR DISTRIBUTED DECOMPOSITION ACROSS CLUSTER (8 OR 16 NODES) DEPENDING ON SIZE OF TASK (500 OR 2000 UNKNOWNS)

Matlab	Matrix		Vector	
function	Single	Double	Single	Double
`chol`	35.51	**1.48**	–	–
`cos`	30.78	12.94	30.10	12.80
`det`	**1.62**	**2.13**	–	–
`inv`	–	3.23	–	–
`lu`	**1.98**	**2.70**	**0.41**	**0.47**
`mldivide`	3.58	3.30	–	–
`plus`	14.77	14.74	14.74	14.79
`rand`	242.29	165.55	248.84	162.93
`times`	14.84	14.84	14.87	14.99

TABLE II
ARRAYFIRE SPEED-UP OF SELECTED FUNCTIONS IN MATLAB (NVIDIA GTX 580 × INTEL I7 980X), MATRIX SIZE: 2000 × 2000, VECTOR SIZE: $4 \cdot 10^6 \times 1$

numerical integration as well as differentiation). As mentioned above, extensive algebraic operations like `det`, `inv` and `lu` are accelerated neither in single precision nor in double precision, see Fig. 6. Unfortunately, ArrayFire does not support generalized eigen-value problem up to now.

Now, let look at the second example performed on CPU (in three different versions) and on GPU. Following expression

$$P_v = \frac{1}{8\pi\omega\epsilon} \iiint_{\Omega'} \iiint_{\Omega''} \Big(k^2 \mathbf{J}(\mathbf{r}') \cdot \mathbf{J}^*(\mathbf{r}'') - \nabla' \cdot \mathbf{J}(\mathbf{r}') \nabla'' \cdot \mathbf{J}^*(\mathbf{r}'') \Big) \frac{\sin(kR)}{R} \, \mathrm{d}\mathbf{r}' \, \mathrm{d}\mathbf{r}'' \tag{3}$$

has to be evaluated to obtain radiated power. The relations for stored energies are of similar form [6]. Implementation is depicted at Fig. 2. This code can be executed on CPU also. Target device is selected based on type of input data which can be `double` (CPU) or `gdouble` (GPU). Thanks to a lot of elementery operation (calculation of Euclidean distance, current amplitudes etc.) the `bsxfun` is extensively used. Note here, that the Euclidean distance calculation is faster based on elementary functions than the usage of `norm` function.

F. Benchmarking

There are many principles that have to be kept during benchmarking. It is necessary to make warm-up of Matlab as well as ArrayFire before each testing. Most suitable functions for measuring of total computing time are `tic – toc` functions. ArrayFire requieres synchronization (`gsync`) and thanks to the lazy calculation it is necessary to enforce the calculation per `geval()` command right after kernel.

The first version (CPU1 at Table III) is based on double `for` loop. In second version (CPU2) one `for` loop was eliminated. And finally, the third version (CPU3) does not need any loop. However this version is very memory-consuming. GPU version is similar to the CPU3 version, typecasting to `gdouble` is performed. The GPU1 code is depicted at Fig. 2.

If we look at the Table III we can see that the maximum speed-up is ≈ 15 for structure with 5000 triangles. Note here, that the third version of our code (CPU3 or GPU1) needs

N	100	250	750	2000	5000	7500	12500
CPU1	0.002	0.013	0.106	0.740	4.555	10.282	29.248
CPU2	0.005	0.013	0.082	0.516	1.748	3.830	9.009
CPU3	0.002	0.005	0.042	0.287	1.736	4.000	10.602
GPU1	0.005	0.006	0.013	0.056	0.297	1.019	6.224
SP	0.50	1.86	7.95	13.26	**15.33**	10.09	4.70

TABLE III
THE COMPUTING TIMES DEPENDING ON NUMBER OF TRIANGLES, SPEED-UP IS IN THE LAST LINE

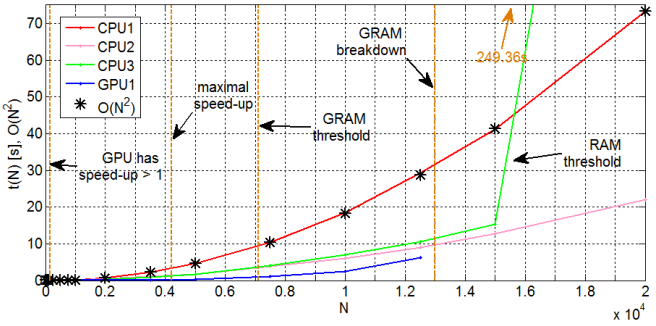

Fig. 6. Computation time for different version depending on number of triangles

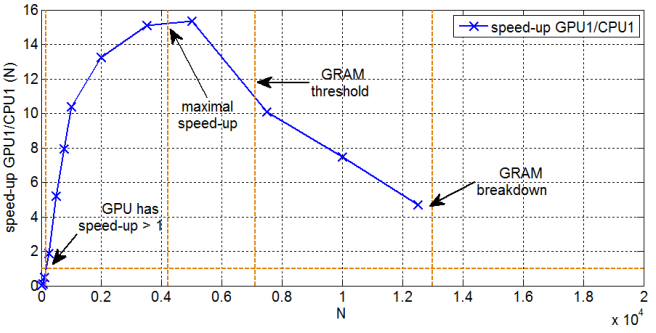

Fig. 7. GPU speed-up for GPU1 version compared to CPU1 version

rougly

$$M_1 = 7DN^2 + 5D \quad [\text{B}], \tag{4}$$

where $D = 8$B for double precision, of free memory. For large structures is usually better to utilize a code with one loop, which reduce the memory requirements to

$$M_2 = 15DN + 11D \quad [\text{B}]. \tag{5}$$

Some interesting phenomenas are depicted at two last figures – see Fig. 6 and Fig. 7.

II. Conclusion

Complex in-house tool for calculation of characteristic modes has been shortly introduced. Then some bottlenecks were identified and modified into parallel and distributive computing mode. One example has been completely adapted to GPU device. Preliminary tests show that practical parallel programing in Matlab is easy and very effective. Further development will be aimed to utilization more than one GPU card in time and to solution of generalized eigen-value problem on GPU.

Acknowledgment

This work was supported by the project of the Czech Science Foundation, grant No. P102/12/2223 (Analysis and Multicriteria Optimization of Compact Radiating Structures based on Modal Decomposition) and by the COST IC1102 (VISTA). The authors would like to thank Neil Bell.

References

[1] M. Capek, P. Hazdra, J. Eichler, "Implementation of the Theory of Characteristic Modes in MATLAB," submitted to *IEEE AP Magazine.*
[2] The Matlab. [Online]. Available: `http://www.mathworks.com/`
[3] J. D. Owens, *et al.*, "GPU Computing," *Proceedings of the IEEE*, vol. 96, no. 5, pp. 879-899, May, 2008.
[4] nVidia Corporation, *CUDA Zone The resource for CUDA developers*. [Online]. Available: `http://www.nvidia.com/cuda/`
[5] R. F. Harrington and J. R. Mautz, "Theory of Characteristic Modes for Conducting Bodies," *IEEE Trans. Antennas Propag.*, vol. 19, no. 5, pp. 622-628, Sept., 1971.
[6] G. A. E. Vandenbosch, "Reactive Energies, Impedance, and Q Factor of Radiating Structures," *IEEE Trans. Antennas Propag.*, vol. 58, no. 4, pp. 1112-1127, Apr., 2010.
[7] M. Capek, P. Hazdra, J. Eichler, "A Method for the Evaluation of Radiation Q Based on Modal Approach," *IEEE Trans. Antennas Propag.*, Vol. 60, No. 10, pp. 4556-4567, 2012.
[8] The ArrayFire Software Library. [Online]. Available: `http://www.accelereyes.com/`
[9] The MathWorks, *Parallel Computing Toolbox*, The MathWorks, Inc., 2011.
[10] The MathWorks, *Matlab Distributed Computing Server*, The MathWorks, Inc., 2011.
[11] J. L. Gustafson, "Reevaluating Amdahl's Law," *Comm. ACM*, pp. 532-533, May, 1988.
[12] W. C. Gibson, *The Method of Moments in Electromagnetics*, Chapman and Hall/CRC, 2007.
[13] S. M. Rao, D. R. Wilton and A. W. Glisson, "Electromagnetic Scattering by Surfaces of Arbitrary Shape," *IEEE Trans. Antennas Propag.*, vol. 30, no. 3, pp. 409-418, May, 1982.
[14] Comsol Multiphysics. [Online]. Available: `http://www.comsol.com/`
[15] DistMesh generator. [Online]. Available: `http://persson.berkeley.edu/distmesh/`
[16] M. Capek, P. Hazdra, P. Hamouz, J. Eichler, J., "A Method for Tracking Characteristic Numbers and Vectors," *PIER-B*, vol. 33, pp. 115-134, 2011.

The Measurable Q Factor and Observable Energies of Radiating Structures

Miloslav Capek, *Student Member, IEEE*, Lukas Jelinek, Pavel Hazdra, *Member, IEEE*, and Jan Eichler, *Student Member, IEEE*

***Abstract*—New expressions are derived to calculate the Q factor of a radiating device. The resulting relations link Q based on the frequency change of the input impedance at the input port (Q_X, Q_Z) with expressions based solely on the current distribution on an radiating device. The question of which energies of a radiating system are observable is reviewed, and then the proposed Q factor as defined in this paper is physical. The derivation is based on potential theory rather than fields. This approach hence automatically eliminates all divergent integrals associated with electromagnetic energies in infinite space. The new formulas allow us to study the radiation Q factor for antennas without feeding (through e.g., characteristic modes) as well as fed by an arbitrary number of ports. The new technique can easily be implemented in any numerical software dealing with current densities. To present the merits of proposed technique, three canonical antennas are studied. Numerical examples show excellent agreement between the measurable Q_Z derived from input impedance and the new expressions.**

***Index Terms*—Antenna theory, electromagnetic theory, Poynting theorem, Q factor.**

I. Introduction

THE radiation Q factor is recognized as one of the most significant parameters of the radiating system and its evaluation for antennas has long been discussed in the literature, see e.g., [1] and references therein. The most recent approaches by Vandenbosch [2] and Gustafsson [3] use the actual distribution of the sources of radiation (currents) from which the electromagnetic energies and radiated power are evaluated. It has recently been shown [4] that Q as defined in [2] (i.e., with the "radiated energy" included) may deliver nonphysical negative values. Hence, the question of which energies should be included as stored in the Q factor is still unsolved.

Rhodes [5] poses exactly this question and develops formulas for the observable energies, i.e., energies which are measurable and thus physical. He defines the observable energy as that part of the total energy that has a measurable effect upon the input impedance and hence upon the frequency bandwidth. His results are interesting from the theoretical point of view, but since electric and magnetic fields in all the space are involved, they are not practical for numerical calculations.

It is known that the total energy of a radiating system in the frequency domain is infinite. This is true for the total energy evaluated from electromagnetic fields (which are stored in an infinite volume) [5], [6]. Rhodes [7] showed that for observable energies the infinities in the integrals cancel in a special way, leaving a finite residue. Vandenbosch [2] was able to analytically subtract the far-field energy from the total energy, isolating the residue and developing expressions for modified vacuum energies based on the currents at the radiating device, and he used them for evaluating Q.

This paper is inspired by [2], [3], [5] and [6], but the line of reasoning is different. It is recognized here for the first time that the only useful and reasonable Q factors of a radiator are the measurable ones, based on frequency changes of the input reactance Q_X, or more generally input impedance Q_Z, see [8]. The proposed development connects sources of radiation (surface currents flowing on an antenna) and the "external world", represented by the frequency behavior of the input impedance at the input port through the complex Poynting theorem. The necessary frequency derivatives on the source side are performed analytically at the level of electromagnetic potentials [9], which are advantageously utilized instead of field quantities [10], [11]. Consequently, there are no infinite integrals present in the derivations. Similarly to previous works, we assume electric currents flowing in free space.

The main result is the expression for Q_Z in terms of different electromagnetic quantities, linked to the current and charge on the antenna through three energy functionals arising from the complex Poynting theorem and its frequency differentation. In this way, a generalized impedance theorem for antennas is established, assuming not only frequency changes of Green's function, as in [2] or [3], but also frequency changes of the current itself. As we show later in the paper, this gives a new additional term: the energy associated to reconfiguration of the current.

A huge advantage over Q_Z as defined by Yaghjian and Best [8] is the possibility of using new expressions for modal currents (i.e., currents computed for a structure without any feeding, see also [12], [13]). It is also possible to examine only a part of the structure of interest and to determine how much this part of the antenna affects the overall Q. In contrast with the quality factors derived in [2] and [3], the Q_Z proposed here is a measurable quantity and hence of interest for the design of arbitrary antennas with respect to their bandwidth.

The paper is organized as follows. In Section II, the measurable Q is derived in terms of the electric currents flowing on the

Manuscript received May 09, 2013; revised October 04, 2013; accepted October 15, 2013. Date of publication October 28, 2013; date of current version December 31, 2013. This work was supported in part by the Grant Agency of the Czech Technical University in Prague under Grant SGS12/142/OHK3/2T/13 and in part by the Grant Agency of the Czech Republic under project 13-09086S.

The authors are with the Department of Electromagnetic Field, Faculty of Electrical Engineering, Czech Technical University in Prague, Technicka 2, 16627, Prague, Czech Republic (e-mail: miloslav.capek@fel.cvut.cz).

Color versions of one or more of the figures in this paper are available online at http://ieeexplore.ieee.org.

Digital Object Identifier 10.1109/TAP.2013.2287519

antenna. Section III discusses differences between previous attempts to calculate radiation Q and the newly derived formulas. Section IV presents numerical examples to verify the proposed theory on three representative antennas: a dipole, a loop and, a small double U-notched loop antenna. The consequences and applications are discussed, and selected results are compared with FEKO [14] and CST [15] software.

II. Measurable Q-Factor in Terms of Field Sources

The purpose of the following derivations is to connect the measurable quality factor with the sources of the field. We will not *a priori* rely on the classic expression $Q = \omega W/P$ as the defining relation with W being the total reactive energy and P the radiated power. Rather, we start with quality factor Q_Z, which originates from the behavior of the RLC circuit [16] and which has been shown to be useful also for estimating antenna performance regarding its impedance bandwidth [8]:

$$Q_Z = \frac{\omega}{2R_{\mathrm{in}}}\left|\frac{\partial Z_{\mathrm{in}}}{\partial \omega}\right| = |Q_R + \jmath Q_X| \tag{1}$$

where

$$Q_R + \jmath Q_X = \frac{\omega}{2R_{\mathrm{in}}}\frac{\partial(R_{\mathrm{in}} + \jmath X_{\mathrm{in}})}{\partial \omega} \tag{2}$$

$\jmath = \sqrt{-1}$ and $Z_{\mathrm{in}} = R_{\mathrm{in}} + \jmath X_{\mathrm{in}}$ is the input impedance of the antenna. In (2) and in the rest of the paper, time harmonic fields [17] with angular frequency ω and the convention $\boldsymbol{\mathcal{F}}(t) = \sqrt{2}\Re\{\mathbf{F}(\omega)\mathrm{e}^{\jmath\omega t}\}$ are assumed.

In order to link (2) with the field sources and their energies, the power definition of the impedance is used

$$P_{\mathrm{in}} = (R_{\mathrm{in}} + \jmath X_{\mathrm{in}})|I_0|^2 \tag{3}$$

where P_{in} is the complex power [9], and I_0 is the input current on the antenna's port. For the same situation, Poynting's theorem [9] allows us to write

$$P_{\mathrm{in}} = -\int_{\Omega} \mathbf{E}\cdot\mathbf{J}^*\,\mathrm{d}\mathbf{r} = \jmath\omega\int_{\Omega}(\mathbf{A}\cdot\mathbf{J}^* - \varphi\rho^*)\,\mathrm{d}\mathbf{r} \tag{4}$$

where $\mathbf{E}$ is the electric field intensity, $\mathbf{J}$ is the current density, and ρ is the charge density inside Ω region, respectively, $\mathbf{A}$ and φ are the vector and scalar potential, respectively, and $*$ denotes complex conjugation. In the last step, the electromagnetic potentials [9] have been used, see the Appendix A. Furthermore, using radiation integrals for $\mathbf{A}$, φ in the Lorentz gauge and charge conservation, (4) can be rewritten as [9]

$$P_{\mathrm{in}} = (P_{\mathrm{m}} - P_{\mathrm{e}}) + \jmath\omega(W_{\mathrm{m}} - W_{\mathrm{e}}) \tag{5}$$

where

$$W_{\mathrm{m}} - \jmath\frac{P_{\mathrm{m}}}{\omega} = k^2\mathcal{L}(\mathbf{J},\mathbf{J}), \tag{6a}$$

$$W_{\mathrm{e}} - \jmath\frac{P_{\mathrm{e}}}{\omega} = \mathcal{L}(\nabla\cdot\mathbf{J}\nabla\cdot\mathbf{J}) \tag{6b}$$

and where, in order to ease the notation, the following energy functional

$$\mathcal{L}(\mathbf{U},\mathbf{V}) = \frac{1}{4\pi\epsilon\omega^2}\int_{\Omega'}\int_{\Omega}\mathbf{U}(\mathbf{r})\cdot\mathbf{V}^*(\mathbf{r}')\frac{\mathrm{e}^{-\jmath kR}}{R}\,\mathrm{d}\mathbf{r}\,\mathrm{d}\mathbf{r}' \tag{7}$$

has been defined. In (7), $R = \|\mathbf{r}-\mathbf{r}'\|$ is the Euclidean distance, $k = \omega/c_0$ is the wavenumber and c_0 is the speed of light. The integration in principle runs over the entire space, but assuming sources of finite extent, the integrals are always finite. Within the chosen naming convention in (5), (6a), (6b), the quantity W_{m} is usually related to magnetic energy, while W_{e} is usually related to electric energy. This association is not unique, however, under the assumption of a linear, passive and lossless antenna, $P_{\mathrm{m}} - P_{\mathrm{e}}$ is the power radiated by the antenna and $\omega(W_{\mathrm{m}} - W_{\mathrm{e}})$ is the net reactive power. Assuming now input current $I_0 = 1\,\mathrm{A}$, substituting (3), (5) into (2), and comparing with (6a) and (6b), it is straightforward to arrive at[1] (8) in which[2]

$$W_{\mathrm{rad}} - \jmath\frac{P_{\mathrm{rad}}}{\omega} = -\jmath k(k^2\mathcal{L}_{\mathrm{rad}}(\mathbf{J},\mathbf{J}) - \mathcal{L}_{\mathrm{rad}}(\nabla\cdot\mathbf{J},\nabla\cdot\mathbf{J})) \tag{9a}$$

$$W_{\omega} - \jmath\frac{P_{\omega}}{\omega} = k^2\mathcal{L}_{\omega}(\mathbf{J},\mathbf{J}) - \mathcal{L}_{\omega}(\nabla\cdot\mathbf{J},\nabla\cdot\mathbf{J}) \tag{9b}$$

and where two more energy functionals are defined as

$$\mathcal{L}_{\mathrm{rad}}(\mathbf{U},\mathbf{V}) = \frac{1}{4\pi\epsilon\omega^2}\int_{\Omega'}\int_{\Omega}\mathbf{U}(\mathbf{r})\cdot\mathbf{V}^*(\mathbf{r}')\,\mathrm{e}^{-\jmath kR}\,\mathrm{d}\mathbf{r}\,\mathrm{d}\mathbf{r}' \tag{10a}$$

$$\mathcal{L}_{\omega}(\mathbf{U},\mathbf{V}) = \frac{1}{4\pi\epsilon\omega^2}\int_{\Omega'}\int_{\Omega}\omega\frac{\partial\mathbf{U}(\mathbf{r})\cdot\mathbf{V}^*(\mathbf{r}')}{\partial\omega}\frac{\mathrm{e}^{-\jmath kR}}{R}\,\mathrm{d}\mathbf{r}\,\mathrm{d}\mathbf{r}' \tag{10b}$$

for details see the Appendix B. In (8) (shown at the bottom of the page), (9a), and (9b) the quantity $W_{\mathrm{rad}} - \jmath P_{\mathrm{rad}}/\omega$ can be attributed to the energy associated with radiation [2], [5],

[1]The upper index (n) in the following expressions denotes the number of included P-terms and W-terms.

[2]Please note that the term denoted as P_{rad}, is not radiated power.

$$\begin{aligned} Q_R^{(4)} + \jmath Q_X^{(4)} &= \frac{\omega}{2(P_{\mathrm{m}} - P_{\mathrm{e}})}\frac{\partial((P_{\mathrm{m}} - P_{\mathrm{e}}) + \jmath\omega\,(W_{\mathrm{m}} - W_{\mathrm{e}}))}{\partial\omega} \\ &= \frac{(P_{\mathrm{m}} + P_{\mathrm{e}} + P_{\mathrm{rad}} + P_{\omega}) + \jmath\omega(W_{\mathrm{m}} + W_{\mathrm{e}} + W_{\mathrm{rad}} + W_{\omega})}{2(P_{\mathrm{m}} - P_{\mathrm{e}})} \end{aligned} \tag{8}$$

while the term $W_\omega - \jmath P_\omega/\omega$ should be interpreted as the energy needed for the current (charge) reconfiguration during a frequency change.

Neglecting the W_ω and P_ω terms in (8) results in

$$Q_R^{(3)} + \jmath Q_X^{(3)} = \frac{(P_\mathrm{m} + P_\mathrm{e} + P_\mathrm{rad}) + \jmath\omega(W_\mathrm{m} + W_\mathrm{e} + W_\mathrm{rad})}{2(P_\mathrm{m} - P_\mathrm{e})} \quad (11)$$

which is just the radiation quality factor derived in [2], [3].

By omitting also the terms associated with radiation (which are usually small in comparison with the reactive power), one obtains

$$Q_R^{(2)} + \jmath Q_X^{(2)} = \frac{(P_\mathrm{m} + P_\mathrm{e}) + \jmath\omega(W_\mathrm{m} + W_\mathrm{e})}{2(P_\mathrm{m} - P_\mathrm{e})}. \quad (12)$$

Note that $Q_X^{(2)}$ is the classical definition of the radiation quality factor [18].

III. Discussion

This section presents some important remarks:

- The derivation of the general result (8) required only measurable quantities as radiated power $(P_\mathrm{m} - P_\mathrm{e})$ and net reactive power $\omega(W_\mathrm{m} - W_\mathrm{e})$. This is in contrast to the approach in [2], [3], which required the ambiguous separation of the net reactive power into an electric part and a magnetic part.
- The structure of the developed quality factor is compatible with the primary definition $Q = \omega W/P$, indirectly validating (1) in [8]. It is now clearly seen how the change of input impedance is transferred into different forms of energy terms arising from various ω derivatives of (3).
- The $Q_Z^{(4)}$ expressed in (8) holds for any angular frequency ω and represents an untuned Q factor that has the strict physical meaning only in the self-resonances of the antenna Ω. One can, however, compensate the nonzero reactive energy $W_\mathrm{m} - W_\mathrm{e}$ of the antenna at each frequency by an additional energy W_add that is mostly concentrated in a adjacent tuning region[3] Ω_add, containing currents $\mathbf{J}_\mathrm{add}$, so that the antenna system $\Omega_0 = \Omega \cup \Omega_\mathrm{add}$ is tuned to the resonance at ω_0. Considering now that the tuning region is lossless and nonradiative, there is $Q_R^{(4)}(\mathrm{tuned}) = Q_R^{(4)}$. Furthermore, it is possible to calculate the $Q_X^{(4)}(\mathrm{tuned})$ according to (8)

$$Q_X^{(4)}(\mathrm{tuned}) = \frac{\omega_0(W_\mathrm{m} + W_\mathrm{e} + W_\mathrm{rad} + W_\omega + W_\mathrm{add})}{2(P_\mathrm{m} - P_\mathrm{e})} \quad (13)$$

  substituting $\mathbf{J}_0 = \mathbf{J} + \mathbf{J}_\mathrm{add}$ into the related functionals (7), (10a) and (10b). At this point it is important to note, that W_add is a function not only of $\mathbf{J}_\mathrm{add}$ but of $\mathbf{J}$ as well. This results from the fact that W-terms are bilinear forms and thus W_add consists of self-terms $(\mathbf{J}_\mathrm{add}, \mathbf{J}_\mathrm{add})$ as well as cross-terms $(\mathbf{J}, \mathbf{J}_\mathrm{add})$ and its permutation.
- In order to get an additional insight, imagine that the compensation is made by a serial lumped reactance $X_\mathrm{add} = -X_\mathrm{in}$. Using the circuit concept one obtains $Q_X(\mathrm{tuned}) \propto \partial(X_\mathrm{add} + X_\mathrm{in})/\partial\omega_0$. On the contrary, the field concept leads to $Q_X(\mathrm{tuned}) \propto \partial\,\omega_0(W_\mathrm{m}(\mathbf{J}_0) - W_\mathrm{e}(\mathbf{J}_0))/\partial\omega_0$.
  Generally, these two $Q_X(\mathrm{tuned})$ will differ, since the circuit concept neglects all the cross-terms mentioned in the previous point. In other words, $X_0 \neq X_\mathrm{in} + X_\mathrm{add}$, where X_0 is the measured input reactance of the antenna system (including the tuning region). However, considering the compensation made by ideal lumped elements, the energy cross-terms will become negligible in comparison to the self-terms due to the field localization at the lumped circuits. In such cases we can approximately write $W_\mathrm{add} \approx L_\mathrm{add} \Leftrightarrow W_\mathrm{m} < W_\mathrm{e}$ in the case of added serial inductor, and $W_\mathrm{add} \approx 1/\omega_0^2 C_\mathrm{add} \Leftrightarrow W_\mathrm{m} > W_\mathrm{e}$ in the case of added serial capacitor.
- On the basis of the previous discussion, the classical concept of tuned Q can be adopted into the proposed definition. Considering that the energies W_m and W_e are positively semi-definite, we obtain from (13)

$$Q_X^{(4)}(\mathrm{tuned}) = \frac{2\omega_0 \max\{W_\mathrm{m}, W_\mathrm{e}\} + \omega_0(W_\mathrm{rad} + W_\omega)}{2(P_\mathrm{m} - P_\mathrm{e})} \quad (14)$$

  or neglecting the W_rad and W_ω

$$Q_X^{(2)}(\mathrm{tuned}) = \frac{\omega_0 \max\{W_\mathrm{m}, W_\mathrm{e}\}}{(P_\mathrm{m} - P_\mathrm{e})} \quad (15)$$

  which is the classical definition of tuned Q, [18], [2].
- The only difference between (8) and the quality factor derived in [2], [3] is the presence of W_ω, P_ω terms. However, in practice, they are not observable in Q_Z, at least for the particular antennas studied in the next section. Furthermore, the terms $W_\omega, P_\omega, W_\mathrm{rad}, P_\mathrm{rad}$ cannot be strictly separated from each other, as their (internal) energy exchange cannot be detected at the port.
- Only W_ω, P_ω terms require current normalization (i.e., specification of the input current I_0). Dropping them (which fortunately has a very small effect on the measurable Q_Z factor) thus allows the calculation of the Q_Z factor of the arbitrary current distribution (for example modal currents) without referring to a particular feeding network.
- By analogy with [2] and [13], the derived expressions for the quality factor are easy to implement in any method of moment (MoM) [19] code as a post processing routine. The only complication is the existence of $\cos(kR)/R$ terms in the energy functionals (7), (10a), (10b). These singularities are, however, removable and integrable analytically [20], [13].

IV. Numerical Results

In this section we will show numerical results for three canonical antennas, discuss the most important features of the Q factor defined by (8), and compare it with other available definitions. To this point, the expressions given in Section II were implemented in our in-house MoM solver [21] based on RWG basis

[3]The same consideration as in [8], Fig. 2 is made for the field concept.

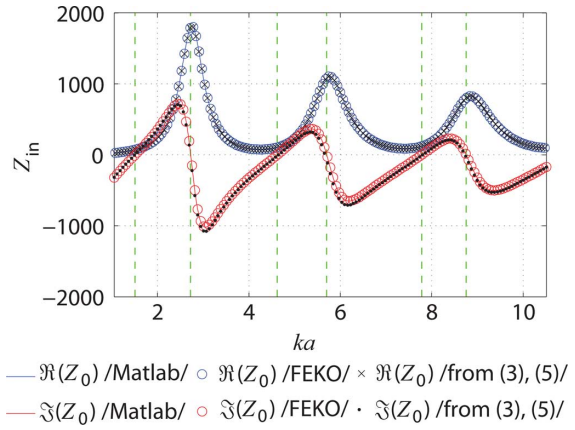

Fig. 1. Real and imaginary parts of the input impedance of a thin-strip dipole simulated in Matlab RWG-MoM and in FEKO software. The "Matlab" and "FEKO" parts are directly calculated as a ratio of voltage and current at the feeding port, while the part denoted as "from (3) and (5)" comes from the direct integration of current distribution on the antenna. The green dashed lines mark resonances and antiresonances.

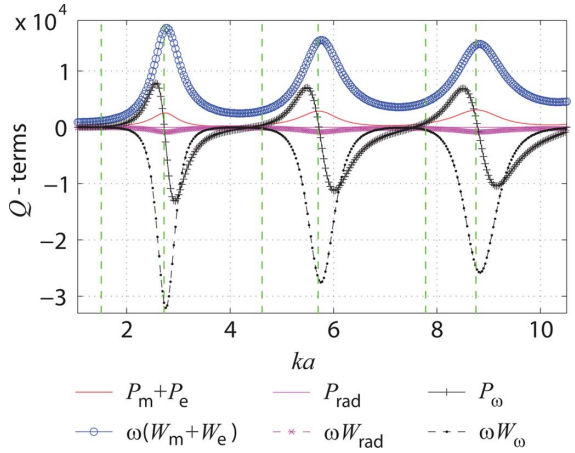

Fig. 2. Frequency dependence of terms composing the nominator of (8) for the thin-strip dipole of Fig. 1.

functions [22] in Matlab [23]. Thanks to implementation on a GPU card [24], all the calculations are extremely fast (about 0.01 s for one frequency sample and 200 RWG functions). Note that in order to keep the discussion as general as possible, a dimensionless quantity ka is used instead of frequency, with a being the smallest radius of a sphere circumscribing all the sources.

A. A Thin-Strip Dipole

The first example deals with a dipole radiating in free space. The dipole is made of an infinitesimally thin perfectly conducting strip with length $2L$ and width $w = 2L/250$. The dipole is discretized into 201 triangles and is fed by a delta gap [?] in its center (the voltage corresponds to the input current $I_0 = 1$ A). The real and imaginary parts of the input impedance are shown in Fig. 1. For comparison, the dipole was also simulated in FEKO software. Note, that almost exact correspondence in Fig. 1 validates the correct implementation of the MoM and the integration routines, and furthermore, it demonstrates the equality between (3) and (5). Good correspondence between the results justifies the use of our Matlab RWG-MoM code in the rest of the paper.

We now turn to a brief discussion of the terms composing the nominator of (8). The most relevant terms are depicted in Fig. 2. The first observation is that P_{rad} can be safely neglected. Its small value is caused by almost exact cancellation of the real parts of otherwise important terms $k^2\mathcal{L}_{\mathrm{rad}}(\mathbf{J},\mathbf{J}), \mathcal{L}_{\mathrm{rad}}(\nabla\cdot\mathbf{J},\nabla\cdot\mathbf{J})$, see (9a). The same is approximately valid also for the W_{rad} term, though there the cancellation is not as perfect. There should thus be no important difference between the quality factor defined by (11) and by (12). The second observation relates to $W_\omega - \jmath P_\omega/\omega$. The absolute value of this quantity evidently reaches its maximum at antiresonances and its minimum in the vicinity of resonances. This is coherent with the interpretation as reconfiguration energy, mentioned in Section II: stable eigenmodes exist in the vicinity of resonances, while the change from one eigenmode to another peaks at antiresonances.

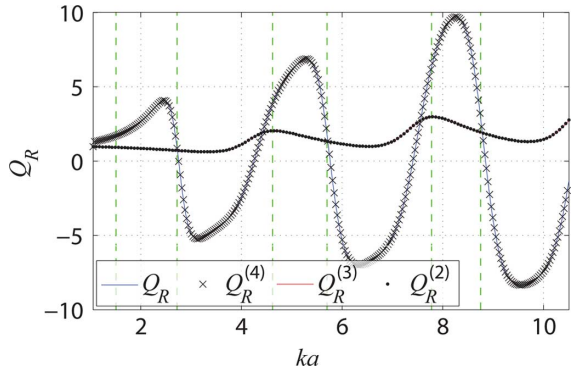

Fig. 3. Comparison of the radiation Q_R factors of the thin-strip dipole of Fig. 1. The green dashed lines mark resonances and antiresonances, see Fig. 1.

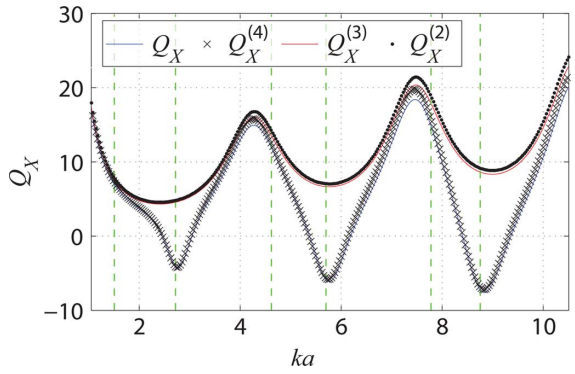

Fig. 4. Comparison of the radiation Q_X factors of the thin-strip dipole of Fig. 1. The green dashed lines mark resonances and antiresonances, see Fig. 1.

In order to check the discussion above, the radiation quality factors given by (2), (8), (11) and (12) are depicted in Figs. 3–5. A central difference has been used to calculate (2). Note that the correspondence between (2) and (8) verifies the numerical implementation, since the expressions are analytically equal. As expected, the quality factors given by (11) and (12) are mostly alike at all frequencies. By contrast, the biggest difference between the $Q_R^{(4)}, Q_X^{(4)}$ factors given by (8) and $Q_R^{(3)}, Q_X^{(3)}$ and

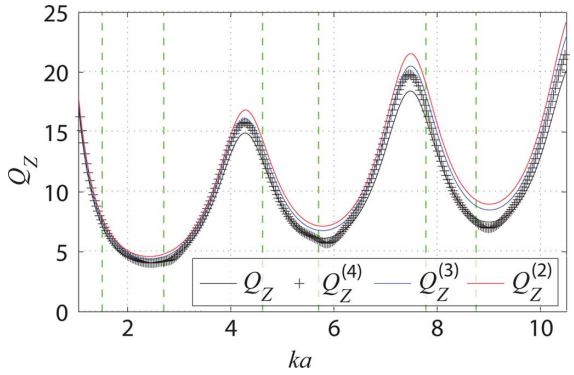

Fig. 5. Comparison of the radiation Q_Z factors of the thin-strip dipole of Fig. 1. The green dashed lines mark resonances and antiresonances, see Fig. 1.

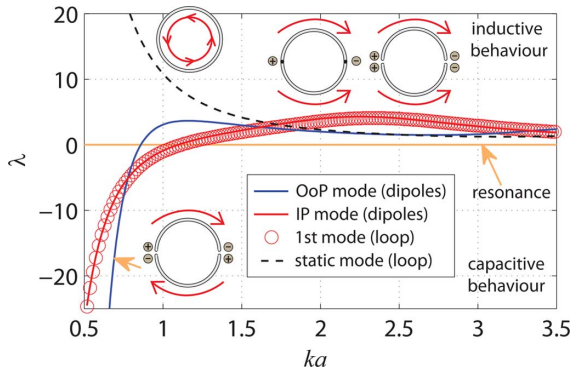

Fig. 6. Eigennumbers of two dipoles and the loop, IP stands for in-phase mode, OoP stands for out-of-phase mode.

$Q_R^{(2)}, Q_X^{(2)}$ appears at antiresonances, which is due to the presence of W_ω, P_ω terms. On the other hand, in the case of resonances the reconfiguration energy is small and all the depicted quality factors are very similar. Observing the differences in the Q_R, Q_X factors, it is however quite remarkable that in the case of Q_Z the W_ω, P_ω terms play almost no role.

B. Modal Solution of a Loop, and an Analogy With Two Dipoles

The second example reveals other benefits of the new technique: the utilization of modal methods. The former Q_Z definition cannot be used in these cases. From the previous example we know that the W_ω term is important for calculating Q_R and Q_X but it can be omitted in calculating Q_Z. Thus, current normalization is not necessary, and no port needs to be specified.

In this example, two basic radiators, a loop and two closely spaced semicircular dipoles that occupy the same volume as the loop does, were decomposed to the characteristic modes, [12], [13]. The radius of the loop is R, and the length of the dipoles is πR. An infinitesimally thin perfectly conducting strip of width $R/12$ is considered both for the loop and the dipoles. The dipoles are separated by a gap of width $R/16$.

The two dipole scenario consists of two possible modes around the first resonant frequency: the in-phase mode (IP) and the out-of-phase mode (OoP), see Fig. 6. The solution of the loop at the same frequency consists of the static (inductive)

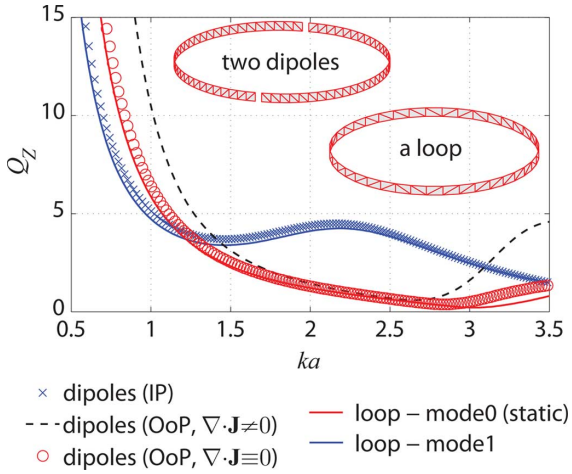

Fig. 7. Equivalence of two topologically different structures—the loop and two closely spaced circular dipoles, IP stands for the in-phase mode, OoP stands for the out-of-phase mode.

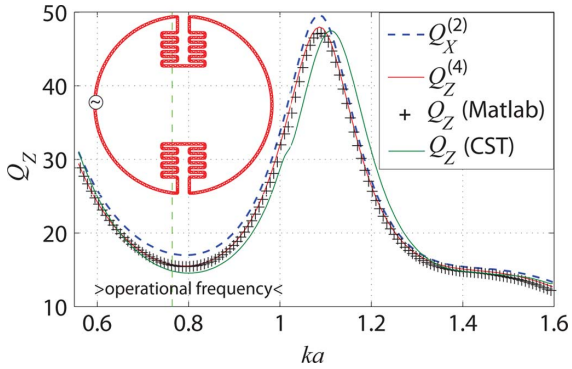

Fig. 8. Comparison of the Q_Z factors from Matlab RWG-MoM (both definition (1) and definition (8) definitions are shown) and CST-MWS [definition (1)]. The antenna operates around the vertical dashed green line.

mode and the first mode, as depicted in Fig. 6. The eigennumbers λ determine the modal behavior, mode is capacitive for $\lambda < 0$, inductive for $\lambda > 0$, and is in resonance for $\lambda = 0$. The eigennumbers for the loop and the dipoles are shown in Fig. 6. The Q_Z factors defined by (8) were calculated from the modal currents. Thanks to the freedom in the current definition, we also calculated the case of OoP dipoles with the charge completely eliminated (setting $\nabla \cdot \mathbf{J} \equiv 0$). As depicted in Fig. 7, the Q_Z of the static mode of the loop looks like the Q_Z of the out-of-phase mode of semicircular dipoles with all charge terms eliminated, see the red line and the red circular marks in Fig. 7. Similarly, the first mode of the loop has the same Q_Z factor as the in-phase mode of the dipoles (no modification is needed in this case because the charge distribution is the same for both cases). Note that the static mode is always excited (irrespective of feed position). Thus, the static mode increases the total Q at all frequencies [13].

C. Small U-Notched Loop Antenna

The electrically small U-notched loop antenna was designed in CST-MWS [15]. The radius of the antenna is R, the width of the infinitesimally thin strip is $R/36$, and PEC is considered, see Fig. 8. To make the antenna electrically smaller, the parts

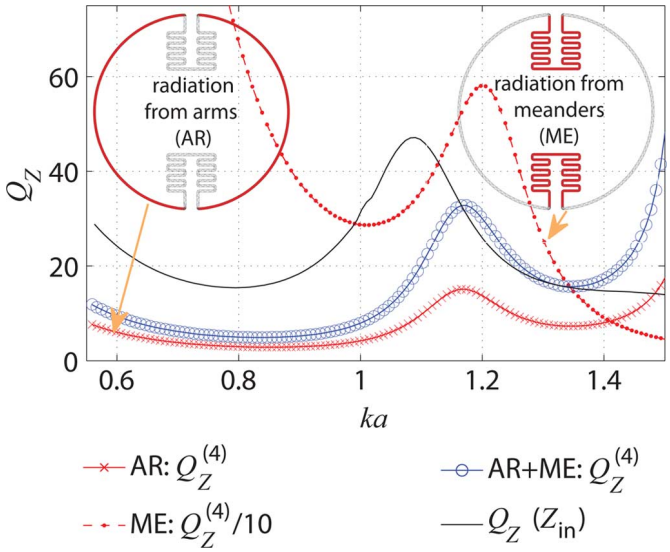

Fig. 9. Study of the particular Q that corresponds to the selected radiating parts of the U-notched loop antenna. AR stands for radiating from the arms, ME stands for radiating from the meanders. The overall Q_Z (solid black line) is added as a reference.

with negligible current density are meandered. The same structure was simulated in Matlab RWG-MoM and decomposed into characteristic modes.

We can estimate the overall Q_Z factor of the fabricated antenna approximately from the -3 dB fractional bandwidth $(\mathrm{FBW}_{-3\,\mathrm{dB}})$ as [8]

$$Q_Z \approx \frac{\sqrt{2}}{2}\frac{1}{\mathrm{FBW}_{-3\,\mathrm{dB}}}. \tag{16}$$

Relation (16) holds for $Q \gg 1$. In the case of the manufactured U-notched antenna, the Q factor (16) is equal to 14.8. For the same procedure in CST-MWS we obtained $Q = 15.5$. From differentiation of Z_{in} in CST-MWS we obtained $Q_Z = 14.8$, and from integrating the current distribution in Matlab we obtained $Q_Z^{(4)} = 15.6$, see Fig. 8. The moderate difference between CST and Matlab in Fig. 8 can be attributed to numerical issues.

The last discussed feature of the proposed definition is calculating the radiation Q_Z factor for a selected part of a radiating device only. While the arms of the antenna radiate well, the meanders accumulate a great deal of net reactive power because of the out-of-phase currents. Thus, we try to calculate the Q_Z of these two parts separately. To do so, the total current distribution $\mathbf{J}$ is separated as

$$\mathbf{J}_1(\mathbf{r}) = \mathbf{J}(\mathbf{r})\delta_1(\mathbf{r}) \tag{17a}$$
$$\mathbf{J}_2(\mathbf{r}) = \mathbf{J}(\mathbf{r})\delta_2(\mathbf{r}) \tag{17b}$$

where $\delta_1(\mathbf{r}) = 1$ for all $\mathbf{r}$ where $|\mathbf{r}| > 35R/36$ and $\delta_1(\mathbf{r}) = 0$ otherwise, $\delta_2 = 1 - \delta_1$. The results are depicted in Fig. 9. While the particular Q that corresponds to the arms of the antenna is very low, the Q factor corresponding to the meanders is extremely high (note that the corresponding values of Q_Z are divided by 10 in Fig. 9).

If we sum up the energetic terms corresponding to the separated arms $(\mathbf{J}_1)$ and meanders $(\mathbf{J}_2)$ and calculate Q_Z, we do not get the overall Q_Z of whole structure $(\mathbf{J})$, Fig. 9. This was expected, and the reason lies in the fact that the operators (7), (10a) and (10b) are not linear for $\mathbf{J} = \mathbf{J}_1 + \mathbf{J}_2$ and thus all possible interactions of the separated parts are omitted. However, these interactions can be calculated by substituting $\mathcal{L}(\mathbf{J}_1, \mathbf{J}_2)$, $\mathcal{L}(\nabla \cdot \mathbf{J}_1, \nabla \cdot \mathbf{J}_2)$ and similarly for (10a), (10b) into the Q_Z calculation.

V. Conclusion

A new formulation of the radiation Q factor is derived in terms of field sources instead of fields. The utilization of the complex Poynting theorem and potential theory had two main effects: a) interpretation and justification of the questionable concept of separating electric and magnetic energy in nonstationary fields is not required, b) integrations over the entire space are not present.

It is well known as the reactance theorem that the total energy of a passive electromagnetic system is proportional to the change of input impedance with frequency. The same derivation is analytically performed on the source side of the complex Poynting theorem, resulting in energetic expressions of a different nature, compactly expressed as functionals of the current. They form the observable quantities which can be measured through the input impedance—and this is the only concept that can be physically tested and thus is of practical interest. Moreover it is shown that the formulas are also valid for modal currents, where no feeding is present.

A novel energy term, related to the current reshaping, is shown to be the cause of negative values of measured Q_X in the antiresonances. Interestingly, this reconfiguration energy is almost not transferred into Q_Z.

The examples, presented here have verified the new expressions and have illustrated some benefits of the method. The proposed concept is easy to implement and offers new challenges in small antenna and MIMO antenna design, especially in conjunction with modal decomposition and optimization.

Appendix A
Complex Power in Terms of Potentials

The purpose of this Appendix is to derive the relation

$$-\int_\Omega \mathbf{E}\cdot\mathbf{J}^*\,\mathrm{d}\mathbf{r} = \jmath\omega\int_\Omega (\mathbf{A}\cdot\mathbf{J}^* - \varphi\rho^*)\,\mathrm{d}\mathbf{r} \tag{18}$$

which has been used in (4). The equality (18) is most easily derived by direct substitution of the defining relation of electromagnetic potentials [9]

$$\mathbf{E} = -\nabla\varphi - \jmath\omega\mathbf{A} \tag{19}$$

into the LHS of (18). This leads to

$$-\int_\Omega \mathbf{E}\cdot\mathbf{J}^*\,\mathrm{d}\mathbf{r} = \jmath\omega\int_\Omega \mathbf{A}\cdot\mathbf{J}^*\,\mathrm{d}\mathbf{r} + \int_\Omega \nabla\varphi\cdot\mathbf{J}^*\,\mathrm{d}\mathbf{r}. \tag{20}$$

The relation (20) can be further rewritten with the use of vector identity

$$\nabla\varphi\cdot\mathbf{J}^* = \nabla\cdot(\mathbf{J}^*\varphi) - \varphi\nabla\cdot\mathbf{J}^* \tag{21}$$

continuity equation

$$\nabla \cdot \mathbf{J} = -\jmath\omega\rho \tag{22}$$

and Gauss theorem into

$$-\int_{\Omega} \mathbf{E}\cdot\mathbf{J}^*\mathrm{d}\mathbf{r} = \jmath\omega\int_{\Omega}(\mathbf{A}\cdot\mathbf{J}^* - \varphi\rho^*)\mathrm{d}\mathbf{r} + \int_{\partial\Omega}\varphi\mathbf{J}^*\cdot\mathrm{d}\mathbf{S}. \tag{23}$$

Now, using the fact that the current component normal to the surface $\partial\Omega$ is zero, the last term in (23) identically vanishes and we arrive at (18).

Appendix B
Derivation of Relation (8)

The first step of the derivation is the use of the radiation integrals for vector and scalar potentials in homogenous, isotropic and open region [9]

$$\mathbf{A}(\mathbf{r}) = \frac{\mu}{4\pi}\int_{\Omega'}\mathbf{J}(\mathbf{r}')\frac{\mathrm{e}^{-\jmath kR}}{R}\,\mathrm{d}\mathbf{r}' \tag{24}$$

and

$$\varphi(\mathbf{r}) = \frac{1}{4\pi\epsilon}\int_{\Omega'}\rho(\mathbf{r}')\frac{\mathrm{e}^{-\jmath kR}}{R}\,\mathrm{d}\mathbf{r}' \tag{25}$$

together with (22) and (7) to obtain

$$\int_{\Omega}(\mathbf{A}\cdot\mathbf{J}^* - \varphi\rho^*)\,\mathrm{d}\mathbf{r} = k^2\mathcal{L}(\mathbf{J},\mathbf{J}) - \mathcal{L}(\nabla\cdot\mathbf{J},\nabla\cdot\mathbf{J}). \tag{26}$$

The next step consists of substituing (4) into (3) and afterwards to (2) and evaluating various ω derivatives. In particular, there is

$$\begin{aligned}\frac{\partial k^2\mathcal{L}(\mathbf{J},\mathbf{J})}{\partial\omega} &= \frac{\partial\dfrac{\mu}{4\pi}\displaystyle\int_{\Omega'}\int_{\Omega}\mathbf{J}(\mathbf{r})\cdot\mathbf{J}^*(\mathbf{r}')\frac{\mathrm{e}^{-\jmath kR}}{R}\,\mathrm{d}\mathbf{r}\,\mathrm{d}\mathbf{r}'}{\partial\omega}\\ &= \frac{k^2}{\omega}(\mathcal{L}_\omega(\mathbf{J},\mathbf{J}) - \jmath k\mathcal{L}_{\mathrm{rad}}(\mathbf{J},\mathbf{J}))\end{aligned} \tag{27}$$

and

$$\begin{aligned}\frac{\partial\mathcal{L}(\nabla\cdot\mathbf{J},\nabla\cdot\mathbf{J})}{\partial\omega} &= \frac{\partial\dfrac{1}{4\pi\epsilon\omega^2}\displaystyle\int_{\Omega'}\int_{\Omega}\nabla\cdot\mathbf{J}(\mathbf{r})\nabla\cdot\mathbf{J}^*(\mathbf{r}')\frac{\mathrm{e}^{-\jmath kR}}{R}\,\mathrm{d}\mathbf{r}\,\mathrm{d}\mathbf{r}'}{\partial\omega}\\ &= -\frac{1}{\omega}(2\mathcal{L}(\nabla\cdot\mathbf{J},\nabla\cdot\mathbf{J}) - \mathcal{L}_\omega(\nabla\cdot\mathbf{J},\nabla\cdot\mathbf{J})\\ &\quad + \jmath k\mathcal{L}_{\mathrm{rad}}(\nabla\cdot\mathbf{J},\nabla\cdot\mathbf{J})).\end{aligned} \tag{28}$$

It is important to remember that although the input current is normalized ($I_0 = 1$ A), the current density $\mathbf{J}$ is still a function of angular frequency.

Putting all together and using the abbreviations (6a), (6b), (9a), and (9b) we immediately arrive at (8).

Acknowledgment

The authors would like to thank Prof. Guy A. E. Vandenbosch for fruitful discussions, as well as the three anonymous reviewers whose remarks improved the clarity of the paper.

References

[1] J. L. Volakis, C.-C. Chen, and K. Fujimoto, *Survey of Small Antenna Theory*, ser. Small Antennas: Miniaturization Techniques & Applications, 1st ed. New York, NY, USA: McGraw-Hill, 2010.

[2] G. A. E. Vandenbosch, "Reactive energies, impedance, and Q factor of radiating structures," *IEEE Trans. Antennas Propag.*, vol. 58, no. 4, pp. 1112–1127, Apr. 2010.

[3] M. Gustafsson and B. L. G. Jonsson, Stored Electromagnetic Energy and Antenna Q [Online]. Available: http://adsabs.harvard.edu/abs/2012arXiv1211.5521G, eprint arXiv: 1211.5521.

[4] M. Gustafsson, M. Cismasu, and B. L. G. Jonsson, "Physical bounds and optimal currents on antennas," *IEEE Trans. Antennas Propag.*, vol. 60, no. 6, pp. 2672–2681, Jun. 2012.

[5] D. R. Rhodes, "Observable stored energies of electromagnetic systems," *J. Franklin Inst.*, vol. 302, no. 3, pp. 225–237, 1976.

[6] D. R. Rhodes, "A reactance theorem," in *Proc. Roy. Soc. Lond. A*, Feb. 1977, vol. 353, pp. 1–10.

[7] D. R. Rhodes, "On the stored energy of planar apertures," *IEEE Trans. Antennas Propag.*, vol. 14, no. 6, pp. 676–684, Nov. 1966.

[8] A. D. Yaghjian and S. R. Best, "Impedance, bandwidth and Q of antennas," *IEEE Trans. Antennas Propag.*, vol. 53, no. 4, pp. 1298–1324, Apr. 2005.

[9] J. D. Jackson, *Classical Electrodynamics*, 3rd ed. Hoboken, NJ, USA: Wiley, 1998.

[10] C. J. Carpenter, "Electromagnetic energy and power in terms of charges and potentials instead of fields," *Proc. IEE A*, vol. 136, no. 2, pp. 55–65, Mar. 1989.

[11] P. Hazdra, M. Capek, and J. Eichler, "Comments to "reactive energies, impedance, and Q factor of radiating structures" by G. Vandenbosch," *IEEE Trans. Antennas Propag.,* to be published.

[12] R. F. Harrington and J. R. Mautz, "Theory of characteristic modes for conducting bodies," *IEEE Trans. Antennas Propag.*, vol. AP-19, no. 5, pp. 622–628, Sep. 1971.

[13] M. Capek, P. Hazdra, and J. Eichler, "A method for the evaluation of radiation Q based on modal approach," *IEEE Trans. Antennas Propag.*, vol. 60, no. 10, pp. 4556–4567, Oct. 2012.

[14] FEKO, EM Software & Systems-S.A [Online]. Available: http://www.feko.info [Online]. Available:

[15] CST Computer Simulation Technology [Online]. Available: http://www.cst.com [Online]. Available:

[16] M. Gustafsson and S. Nordebo, "Bandwidth, Q factor and resonance models of antennas," *PIER*, vol. 62, pp. 1–20, 2006.

[17] R. F. Harrington, *Time-Harmonic Electromagnetic Fields*, 2nd ed. : John Wiley—IEEE Press, 2001.

[18] R. E. Collin and S. Rotchild, "Evaluation of antenna Q," *IEEE Trans. Antennas Propag.*, vol. AP-12, no. 1, pp. 23–27, Jan. 1964.

[19] R. F. Harrington, *Field Computation by Moment Methods*. : John Wiley—IEEE Press, 1993.

[20] P. Arcioni, M. Bressan, and L. Perregrini, "On the evaluation of the double surface integrals arising in the application of the boundary integral method to 3-D problems," *IEEE Trans. Microw. Theory Tech.*, vol. 44, no. 3, pp. 436–438, Mar. 1997.

[21] M. Capek, P. Hamouz, P. Hazdra, and J. Eichler, "Implementation of the theory of characteristic modes in Matlab," *IEEE Antennas Propag. Mag.*, vol. 55, no. 2, pp. 176–189, Apr. 2013.

[22] S. M. Rao, D. R. Wilton, and A. W. Glisson, "Electromagnetic scattering by surfaces of arbitrary shape," *IEEE Trans. Antennas Propag.*, vol. AP-30, no. 3, pp. 409–418, May 1982.

[23] The MathWorks, The Matlab [Online]. Available: http://www.mathworks.com [Online]. Available:

[24] M. Capek, P. Hazdra, J. Eichler, P. Hamouz, and M. Mazanek, "Acceleration techniques in Matlab for EM community," presented at the 7th Eur. Conf. Antennas and Propagation (EUCAP), Gothenburg, Sweden, Apr. 2013.

Miloslav Capek (S'09) received the M.Sc. degree in electrical engineering from the Czech Technical University, Prague, Czech Republic, in 2009, where he is currently pursuing Ph.D. degree in electromagnetic fields.

His research interests are in the area of electromagnetic theory, electrically small antennas, numerical techniques, fractal geometry and optimization.

Lukas Jelinek received the Ph.D. degree from the Czech Technical University (CTU), Prague, Czech Republic, in 2006.

Currently, he is a researcher with the Department of Electromagnetic Fields, Faculty of Electrical Engineering, CTU. His main fields of interest include wave propagation in complex media, general field theory, and numerical techniques. His recent research interest is focused on metamaterials, specifically on resonant ring systems.

Pavel Hazdra (M'03) received the M.S. and Ph.D. degrees in electrical engineering from the Faculty of Electrical Engineering (FEE), Czech Technical University (CTU), Prague, Czech Republic, in 2003 and 2009, respectively.

He is a research and teaching assistant with the Department of Electromagnetic Field, FEE, CTU. His research interests are in the area of electromagnetic theory, computational electromagnetics, fractal geometry, planar antennas, and special prime-feed antennas.

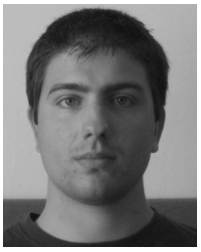

Jan Eichler (S'10) received the B.Sc. and M.Sc. degrees in electrical engineering from the Czech Technical University, Prague, Czech Republic, in 2008 and 2010, respectively, where he is currently pursuing the Ph.D. degree.

His research interests include modal methods for antenna design and connecting them with full-wave methods. He is also interested in developing and simulating active antennas.

A Method for Evaluating Radiation Efficiency Based on a Modal Approach

Miloslav Capek[1], Jan Eichler[1], Pavel Hazdra[1], Milos Mazanek[1]
[1]Department of Electromagnetic Field, Faculty of Electrical Engineering, Czech Technical University in Prague, Prague, Czech Republic, miloslav.capek@fel.cvut.cz

***Abstract*—Radiation efficiency is an important parameter, especially for electrically small antennas. It can be computed directly from the method-of-moments impedance matrix, and also more generally by employing modal decomposition through characteristic modes. This advantageously enables us to study separately the effect of the radiating shape and the feeding. The proposed method does not require any modification of the Electric Field Integral Equation implementation. A perfectly conducting antenna is considered as the only input to the modal decomposition. The conductive losses are taken into account once the surface currents are calculated. Good agreement is observed for the proposed treatment of the skin effect. Verification of the method is numerically performed on an fractal antenna, a thin-strip Sierpinski curve of various iterations. A full-wave software FEKO with implemented IBC is used for comparison purposes.**

***Index Terms*—Antenna theory, eigenvalues and eigenfunctions, electromagnetic theory.**

I. Introduction

Radiation efficiency [1], together with the Q factor (or available bandwidth) [2] and antenna directivity [1], significantly affects the operation of an antenna device, especially if the dimensions are electrically small [3]. In this paper we will explain how modal methods [4] can easily be used for antenna synthesis, especially to maximize the radiation efficiency.

A common approach to computing the radiation efficiency of the antenna considers the lossy material in the numerical simulation. This impedance boundary condition (IBC) technique [5], [6] is general and accurate, but it is time consuming and it does not provide much physical insight into the operation of a lossy antenna. By contrast, our proposed method supposes the current density evaluated on a perfect electric conductor (PEC) to be approximately the same in shape as for a lossy metal of finite thickness. This assumption has been widely used for an estimation of a power loss in the walls of a waveguide [7].

In order to gain a better physical picture of the operation of a lossy antenna, the theory of characteristic modes (TCM) [8], [9], is adopted for evaluating individual modal efficiencies. TCM generalizes the traditional definition, since it is possible to study the radiation structures without any feeding. The constantly growing interest in TCM can be documented by the latest implementation of TCM in the commercial simulator FEKO [10], where, however, there is no estimation of the modal radiation efficiency.

Recently, other methods such as structural decomposition of the radiation body [11], convex optimization [12], and some variational approaches [13] have been derived and used for antenna synthesis. The future possibility of combining all these methods enables us to prepare radiating devices that exactly satisfy both the spatial (structural) and the performance (physical) requirements. Note that the simple calculation of the (modal) radiation efficiency has already been treated [14]. However, in [14] the skin effect was not taken into account and no summation of the modal losses was presented. Thus, generally, we observed a difference between the IE3D MoM software [15] and the modal approach. In contrast, the method described in this paper considers the modal superposition, respects the orthogonal relations correctly, and uses the equivalent volume current, directly calculated from the surface current.

This paper is organized as follows. The fast calculation of the radiation efficiency is presented in Section II and is extended to the modal efficiencies and their superposition in Section III. Section IV presents numerical results verifying the proposed theory on the example of the Sierpinski curve. The utilization of optimization and other possibilities are discussed in Section V. The paper is concluded in Section VI.

II. Description of the Method

Radiation efficiency is defined as [1]

$$\eta_{\mathrm{r}} = \frac{P_{\mathrm{r}}}{P_{\mathrm{r}} + P_{\mathrm{L}}}, \tag{1}$$

in which P_{r} is the radiated power and P_{L} is the power loss due to the finite conductivity of conductors, converted to heat. To obtain a fair estimate of the radiation losses, the following method is used. First, the Electric Field Integral Equation (EFIE) [16] and the method-of-moments (MoM) [17], together with proper discretization of an antenna body Ω, are utilized to transform the antenna to the impedance matrix $\mathbf{Z}$, see Fig. 1a,b. Then, the matrix inversion or any matrix decomposition can be used to obtain surface currents flowing on the Ω shape. Finally, these currents are incorporated into the equivalent circuit in Fig. 1d, where the losses are present. In other words, the proposed method assumes the same currents for the lossless case and for the lossy case. This presumption is limited by certain conditions (frequency, conductivity and metallization thickness), but it will be demonstrated that the error is very small for typical scenarios (e.g. good conductors and small skin depth relative to the metallization thickness). The only

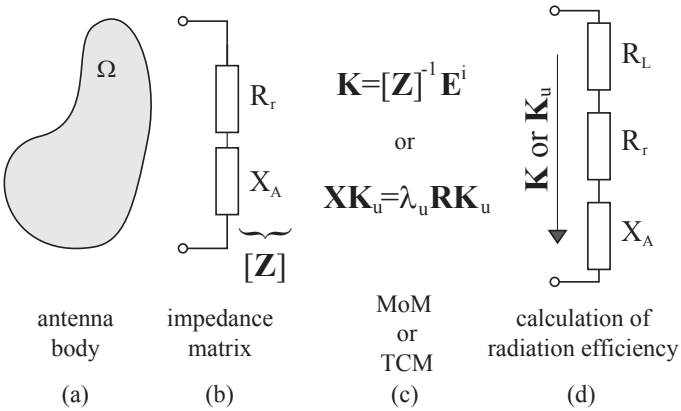

Fig. 1. Description of the fast algorithm for calculating radiation efficiency: (a) original problem, (b) discretized problem (impedance matrix), (c) calculation of source currents (by MoM or by modal decomposition), (d) calculation of the power loss.

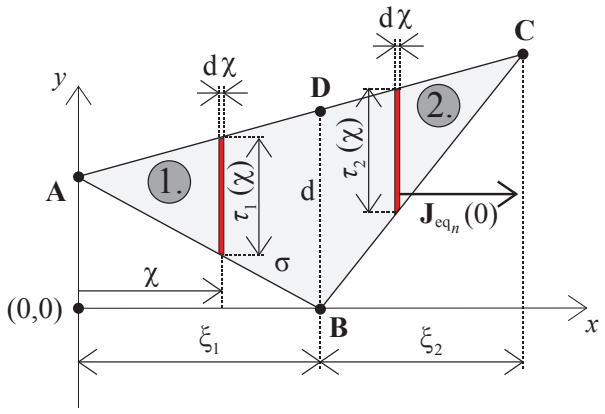

Fig. 2. Conductive losses on the selected triangle n (after affine transformations aligning it to the x-y plane).

task to be done in the post-processing step is to calculate the power loss P_{L} in (1) or, equivalently, the R_{L} in Fig. 1d.

The first step is to evaluate

$$\left| \int_0^t \mathbf{J}_{\mathrm{eq}}(z)\,\mathrm{d}z \right| = \left|\mathbf{K}\right|, \tag{2}$$

in which $\mathbf{J}_{\mathrm{eq}}$ is the equivalent volume current density, $\mathbf{K}$ is the surface current density obtained as results from MoM (or from TCM), and t is the metalization thickness. Next, the skin effect [1] is taken into account as

$$\mathbf{J}_{\mathrm{eq}}(z) = \mathbf{J}_{\mathrm{eq}}\,(0)\ \mathrm{e}^{-(1+\jmath)\gamma z}, \tag{3}$$

in which $\jmath = \sqrt{-1}$, z is the distance from the metal surface, and the attenuation constant for a highly conductive material is [18]

$$\gamma = \sqrt{\frac{\omega\mu\sigma}{2}}, \tag{4}$$

where ω is angular frequency, μ is permeability, and σ is conductivity. By substituting (3) into the key approximation (2), we arrive at

$$|\mathbf{J}_{\mathrm{eq}}\,(0)| = \frac{\sqrt{2}\gamma\,|\mathbf{K}|}{\left|1-\mathrm{e}^{-(1+\jmath)\gamma t}\right|}. \tag{5}$$

Now, the input power dissipated to heat is [18]

$$\begin{aligned} P_{\mathrm{L}} &= \int_V \mathbf{E}\cdot\mathbf{J}_{\mathrm{c}}^{*}\,\mathrm{d}\mathbf{r} = \frac{1}{\sigma}\int_V \mathbf{J}_{\mathrm{c}}\cdot\mathbf{J}_{\mathrm{c}}^{*}\,\mathrm{d}\mathbf{r} \\ &\approx \sum_{n=1}^{N}\frac{1}{\sigma}\int_x\int_y\int_0^t |\mathbf{J}_{\mathrm{eq}_n}\,(z)\,|^2\,\mathrm{d}z\,\mathrm{d}y\,\mathrm{d}x = \sum_{n=1}^{N} P_{\mathrm{L}_n}, \end{aligned} \tag{6}$$

where the discretization into N subdomains is considered, $\mathbf{J}_{\mathrm{c}}$ is the true conductive current flowing inside homogenous volume V and $*$ denotes complex conjugation. Let us assume that the RWG functions are used [19], and thus the antenna shape Ω is discretized into small perfectly conducting triangular surfaces so that $\Omega = \bigcup_n A_n$, in which A_n is the area of the nth triangle. Without loss of generality, we suppose that the nth triangle is aligned with the x-y plane so that the resulting current $\mathbf{J}_{\mathrm{eq_n}}(0)$ flows parallel to the x-axis (note that this kind of affine transformation can be done for any triangle, since heat losses are not dependent on the orientation of the current). The integration in the second line of (6) can be performed separately for the z direction, where utilization of the skin effect (3) is necessary, and for the x, y coordinates. For x, y integration purposes in (6), the nth triangle is divided into two regions $\mathbf{ABD}$ and $\mathbf{BCD}$ with $d = \|\mathbf{D}-\mathbf{B}\|$ perpendicular to the x axis, see Fig. 2, and is parametrized as $\tau_1(\chi) = \chi d/\xi_1$ for $\chi \in (0, \xi_1)$ and $\tau_2(\chi) = d\,(1-(\chi-\xi_1)/\xi_2)$ for $\chi \in (\xi_1, \xi_1+\xi_2)$, which yields

$$\int_0^{\xi_1} \tau_1(\chi)\ \mathrm{d}\chi + \int_{\xi_1}^{\xi_1+\xi_2} \tau_2(\chi)\ \mathrm{d}\chi = \frac{d}{2}\,(\xi_1+\xi_2) = A_n. \tag{7}$$

It is assumed in (7) that the infinite number of resistive sheets $\tau(\chi)\,\mathrm{d}\chi$ is connected in series, forming the surface resistance of the triangle. Then, substituting (7) into (6), and (5) into (3), one obtains

$$P_{\mathrm{L}_n} = \frac{A_n}{\sigma}\int_0^t \frac{2\gamma^2\,|\mathbf{K}_n|^2}{\left|1-\mathrm{e}^{-(1+\jmath)\gamma t}\right|^2}\mathrm{e}^{-(1+\jmath)\gamma z}\left(\mathrm{e}^{-(1+\jmath)\gamma z}\right)^{*}\,\mathrm{d}z, \tag{8}$$

in which $\mathbf{K}_n$ is the surface current flowing on the nth triangle. The result for the power loss is

$$P_{\mathrm{L}} = F(\omega,\sigma,t)\sum_n A_n|\mathbf{K}_n|^2, \tag{9}$$

where

$$F(\omega,\sigma,t) = \frac{\gamma}{\sigma}\frac{\left(1-\mathrm{e}^{-2\gamma t}\right)}{|1-\mathrm{e}^{-(1+\jmath)\gamma t}|^2}. \tag{10}$$

Finally, to obtain the overall radiation efficiency from MoM, (1) together with (9) and (10) can be used.

III. Radiation efficiency for modal currents

Interestingly, radiation efficiency can also be defined for modal currents, without any feeding connected to the antenna body. In this section, TCM will be briefly introduced, then the modal efficiency and the superposition of modal quantities will be derived.

By definition [8], the characteristic modes can be obtained from the generalized eigenvalue problem [20]

$$\mathbf{X}\mathbf{K}_u = \lambda_u \mathbf{R}\mathbf{K}_u, \tag{11}$$

$$\begin{aligned} \langle \mathbf{K}_u, \mathbf{R}\mathbf{K}_v \rangle &= \delta_{uv} = P_{\mathrm{r}}^{uv}, && (12)\\ \langle \mathbf{K}_u, \mathbf{X}\mathbf{K}_v \rangle &= \lambda_u \delta_{uv}, && (13)\\ \langle \mathbf{K}_u, \mathbf{Z}\mathbf{K}_v \rangle &= (1 + \jmath\lambda_u)\, \delta_{uv}, && (14) \end{aligned}$$

in which δ_{uv} is the Kronecker delta, $\langle \mathbf{a}, \mathbf{b} \rangle = \sum_u \sum_v a_{uv} b_{uv}$ is the symmetric product [17], and P_{r}^{uv} is the normalized modal radiated power. From (11) and (12), it is obvious that the modal efficiency of the standalone mode u reads

$$\eta_{\mathrm{r}}^{uu} = \frac{1}{1 + P_{\mathrm{L}}^{uu}}, \tag{15}$$

in which the modal loss power P_{L}^{uu} is calculated by substituting $\mathbf{K}_u$ in (9).

In order to obtain the summation formula for modal radiated efficiencies (15), the total current on the antenna surface

$$\mathbf{K} = \sum_u = \alpha_u \mathbf{K}_u \tag{16}$$

is needed. In (16), the expanding coefficients α_u are [8]

$$\alpha_u = \frac{\langle \mathbf{K}_u, \mathbf{E}^{\mathrm{i}} \rangle}{1 + \jmath\lambda_u}, \tag{17}$$

in which $\mathbf{E}^{\mathrm{i}}$ is an impressed electric field representing the excitation. Considering now (16), the squared absolute value is

$$|\mathbf{K}|^2 = \sum_u \alpha_u \mathbf{K}_u \cdot \left(\sum_v \alpha_v \mathbf{K}_v \right)^* = \sum_u \sum_v \beta_{uv} \mathbf{K}_u \cdot \mathbf{K}_v, \tag{18}$$

where the assumption of real modal currents [8] was used, and the terms of the coupling matrix $\boldsymbol{\beta}$ are defined as

$$\beta_{uv} = \Re\{\alpha_u \alpha_v^*\} = \frac{\langle \mathbf{K}_u, \mathbf{E}^{\mathrm{i}} \rangle \langle \mathbf{K}_v, \mathbf{E}^{\mathrm{i}} \rangle\, (1 + \lambda_u \lambda_v)}{(1 + \lambda_u^2)\,(1 + \lambda_v^2)}. \tag{19}$$

The same matrix $\boldsymbol{\beta} = [\beta_{uv}]$ was obtained for summation of the modal Q factors [21]. Using the same discretization as in the previous section, it is seen from (18) and (9) that the modal power loss is

$$P_{\mathrm{L}}^{uv} = F\,(\omega, \sigma, t) \sum_n A_n \mathbf{K}_{n,u} \cdot \mathbf{K}_{n,v}. \tag{20}$$

This means that, unlike the modal radiated power (12), the modal power loss is generally non-zero for $u \neq v$. Finally, the total power loss may be expressed as

$$P_{\mathrm{L}} = \sum_u \sum_v \beta_{uv} P_{\mathrm{L}}^{uv} = \langle \boldsymbol{\beta}, \mathbf{P}_{\mathrm{L}} \rangle, \tag{21}$$

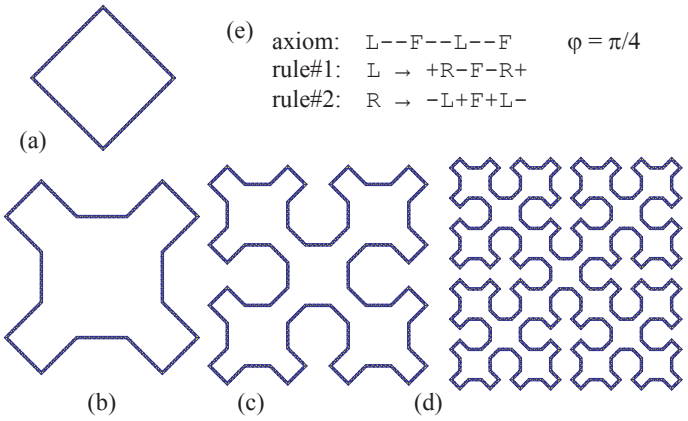

Fig. 3. The Sierpinski cross fractal curve: (a) 0th iter., (b) 1st iter., (c) 2nd iter., (d) 3rd iter., (e) the L-system grammar for generating them [24].

in which $\mathbf{P}_{\mathrm{L}} = [P_{\mathrm{L}}^{uv}]$ is the matrix of modal power losses defined in (20). Employing now the orthonormal property (12) and using (21), definition (1) is finally written as

$$\eta_{\mathrm{r}} = \frac{\mathrm{Tr}\,(\boldsymbol{\beta})}{\mathrm{Tr}\,(\boldsymbol{\beta}) + \langle \boldsymbol{\beta}, \mathbf{P}_{\mathrm{L}} \rangle}. \tag{22}$$

IV. Numerical Examples – Sierpinski curve

In order to verify the method proposed above, the example of a thin-strip antenna made of a Sierpinski fractal curve of iterations $i \in \{0, 1, 2, 3\}$ was chosen, since fractals are known to have high losses as the iteration increases [22]. The Sierpinski curve is a kind of so-called space filling curve [23], which for $i \to \infty$ fills all the space (its topology dimension is $\mathcal{D}_{\mathrm{t}} = 1$, but its Hausdorff dimension is $\mathcal{D}_{\mathrm{h}} = 2$). It is obvious from Fig. 3 that the curve forms a loop, with the dominant mode at frequency f_1^i, where the electrical length l_i is approximately equal to one wavelength.

The limiting square area of $x \times y = \langle -1, 1 \rangle \times \langle -1, 1 \rangle\,\mathrm{m}^2$ was used as a generating region, see Fig. 3. The width of the infinitesimally thin-strip antenna is $w = 0.02\,\mathrm{m}$. This type of study is also interesting from the miniaturization point of view, since the resonant frequency decreases as the iteration increases. All curves are generated by L-system language [24] with the grammar depicted in Fig. 3e, where F stands for "draw a line", and +/- stands for "turn left/right at angle $\varphi = \pi/4$". In order to keep the discussion as general as possible, a dimensionless quantity ka_i is used instead of the frequency, with a_i being the smallest radius of a sphere circumscribing the whole antenna of the ith iteration.

We start with verification of the method against the FEKO software, where the IBC technique is utilized [10]. The antennas are fed by a delta gap [25], connected to the edge which intersects the point $x = -y$. The calculation of (9) and (22) was implemented in Matlab [26], and the important results are presented in Table I. From here, it is seen that the overall length of loop l_i at the given iteration i is doubled at the following iteration $i + 1$. In Table I, a_i is the smallest radius

i	l_i [m]	a_i [m]	ka_i^1 (t.) [-]	ka_i^1 (s.) [-]	$\eta_r\left(ka_1^i\right)$ [-]
0	3.3137	0.6000	1.1376	1.2518	0.9984
1	6.6274	0.9493	0.9001	1.0339	0.9967
2	13.2548	1.1797	0.5591	0.7215	0.9871
3	26.5097	1.3007	0.3084	0.5353	0.9525

TABLE I
COMPARISON OF SOME IMPORTANT PARAMETERS RELATED TO THE SIERPINSKI CURVE OF VARIOUS ITERATIONS.

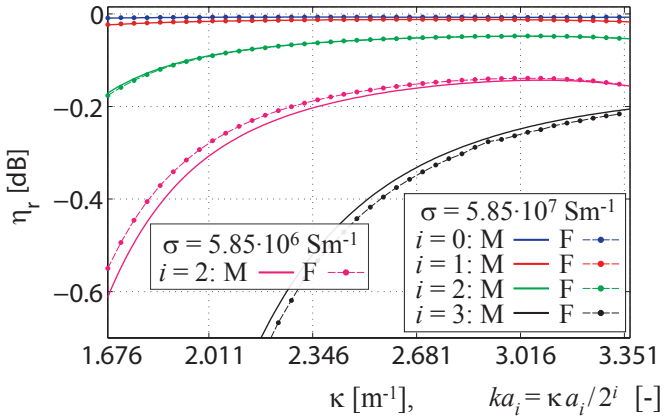

Fig. 4. The total radiation efficiency of the Sierpinski curve of various iterations excited by one delta gap, M – Matlab, F – FEKO.

of a sphere circumscribing the whole antenna (i.e. $a_\infty = \sqrt{2}$), ka_i^1 (t.) is the theoretical resonance of the dominant mode, calculated as $2\pi a_i/l_i$, ka_i^1 (s.) is the resonance of the dominant mode found by simulation, and $\eta_r\left(ka_i^1\right)$ is the relative radiation efficiency evaluated at resonance ka_1^i (s.).

A comparison between radiation efficiency calculated in Matlab (proposed method) and in FEKO (IBC) is depicted in Fig. 4. All data are displayed in dB, and the metallization thickness is $t = 50\,\mu$m. Generally, it can be seen that the overall efficiency slowly decreases as the iteration increases. Note very good agreement, especially if the conductivity is high. The biggest error (in the case of the 3rd iteration and of the 2nd iteration with decreased conductivity) is less than 1%.

Now, we can briefly discuss the modal efficiencies. The Sierpinski antenna of 2nd iteration was decomposed into the characteristic modes. The eigenvalues in terms of eigenangles [27]

$$\delta_u = 180^\circ - \arctan\left(\lambda_u\right) \tag{23}$$

are depicted in Fig. 5. The eigenangles properly scale the eigenvalues, which are typically of large extent. The mode u is at resonance if $\delta_u = 180^\circ$. Note here that the eigenangles of modes $1, 5, 9$ are equal to the eigenangles of modes $2, 6, 10$, respectively. In fact, these modes are degenerate. That is the reason why only some modal efficiencies η_r^{uu} are depicted in Fig. 6. The modal results can be advantageously used in antenna design. For example, by suppressing the 3rd mode at $ka_2 \approx 1.2$ in Fig. 6, the overall radiation efficiency can be improved.

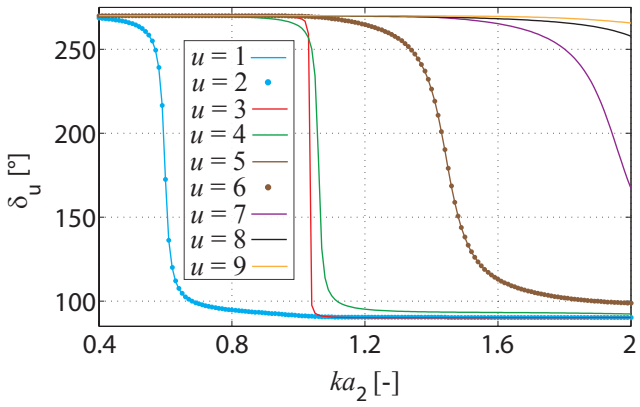

Fig. 5. Eigenangles of Sierpinski curve of 2nd iteration.

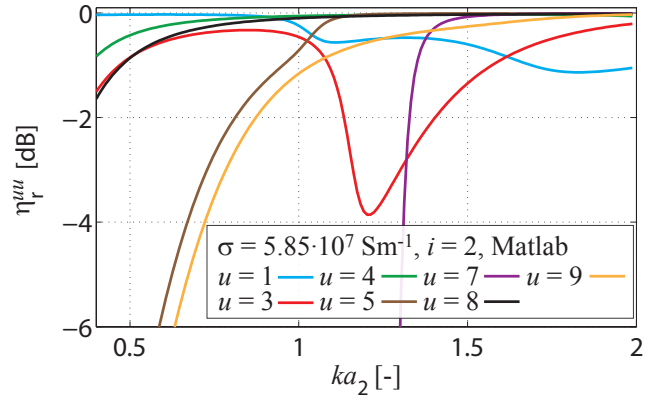

Fig. 6. Modal radiation efficiencies of selected modes of the Sierpinski curve of 2nd iteration.

V. DISCUSSION

This section presents some important remarks:

- The agreement between the proposed method and IBC is extremely good for scenarios in which the skin depth is sufficiently small. In practice, at a given working frequency, very good conductors together with sufficient metallization are used, so that the limiting condition is usually fulfilled. At the same time, the proposed method is very fast and can be used in post-processing without any need to modify the impedance matrix.
- The skin depth should be also negligible in comparison with the curvature of the discretized space.
- Note the similarity of (22) with the superposition of modal Q factors [21]. This unified concept, in which only the $\boldsymbol{\beta}$ matrix of unknown coefficients occurs, opens new possibilities in complex optimization of the feeding networks.
- It is known that fractal curves have small radiation resistance and a small input impedance [28]. This issue can, however, be compensated by off-centre feeding, which can be advantageously found by an optimization routine [29]. In the case of (22), only the unknown coefficients of

The Source Definition of The Quality Factor Q_Z

Miloslav Capek, Lukas Jelinek, Pavel Hazdra, and Jan Eichler
Department of Electromagnetic Field
Czech Technical University in Prague
Prague, 16627, Czech Republic
miloslav.capek@fel.cvut.cz

***Abstract*—New expressions for calculating of the quality factor Q_Z are presented. The resulting relations link Q_Z, based on the frequency change of the input impedance at the input port, with expressions based solely on the current distribution on a radiator. The derivation is based on electromagnetic potentials, automatically eliminating all divergent integrals associated with electromagnetic energies in infinite space.**

I. Introduction

The radiation Q factor is an intrinsic quantity of interest for any electrically small antenna (ESA) since it is, at its higher values, proportional to the fractional bandwidth (FBW) [1]. The calculation of Q is, however, encumbered with difficulties, mainly with the evaluation of the stored energy [2]. The need for the non-measurable stored energy of the radiating device was reconsidered in [3], where the authors proposed an estimation of the Q factor, denoted as Q_Z, which provides the link to the available bandwidth and which is based on a measurable quantity, the input impedance. Even though Q_Z cannot generally be interchanged with Q, it makes an excellent approximation of it for ESA. For this reason, Q_Z is widely used in antenna design practice and its validity and usefulness have been confirmed in many studies, see e.g. [4].

The proposed method starts from the original definition of Q_Z, but uses the complex power expressed by the potentials to replace the input impedance and then performs the frequency derivative over it. As a result, no infinite integrals occur and no separation technique [2], [5] is needed. This definition opens new possibilities of using modal currents (no feeding), or of examining only a part of the whole radiator at hand.

II. Definition of Q_Z in terms of sources

We start with the definition of Q_Z [3]

$$Q_Z = \frac{\omega}{2R_{\mathrm{in}}}\left|\frac{\partial Z_{\mathrm{in}}}{\partial\omega}\right| = \left|Q_R + \mathrm{j}Q_X\right|, \tag{1}$$

where $\mathrm{j}=\sqrt{-1}$ and $Z_{\mathrm{in}} = R_{\mathrm{in}} + \mathrm{j}X_{\mathrm{in}}$ is the input impedance of the antenna. In the rest of the paper, time harmonic fields [6] with angular frequency ω and the convention $\boldsymbol{\mathcal{F}}(t) = \sqrt{2}\Re\left\{\mathbf{F}(\omega)\,\mathrm{e}^{\mathrm{j}\omega t}\right\}$ are assumed. In order to connect the definition (1) with field sources, the power definition of the impedance is used together with the potential definition of the complex power [6]

$$Z_{\mathrm{in}}\left|I_0\right|^2 = -\int_\Omega \mathbf{E}\cdot\mathbf{J}^*\,\mathrm{d}\mathbf{r} = \mathrm{j}\omega\int_\Omega\left(\mathbf{A}\cdot\mathbf{J}^* - \varphi\rho^*\right)\mathrm{d}\mathbf{r}, \tag{2}$$

with $\mathbf{E}$ being the electric field intensity, $\mathbf{J}$ being the current density, and ρ being the charge density inside the Ω region, respectively, $\mathbf{A}$ and φ being the vector and scalar potential, respectively, and $*$ denotes complex conjugation.

Substituting now the RHS of (2) into (1), assuming constant input current (i.e. $I_0 = 1\,\mathrm{A}$) and using radiation integrals for $\mathbf{A}$, φ in the Lorentz gauge [6] and charge conservation, the differentiation with respect to ω leads us to

$$\begin{aligned} Q_R + \mathrm{j}Q_X &= \frac{\omega}{2\left(P_{\mathrm{m}} - P_{\mathrm{e}}\right)}\left|\frac{\partial\left(\mathrm{j}\omega\int_\Omega\left(\mathbf{A}\cdot\mathbf{J}^* - \varphi\rho^*\right)\mathrm{d}\mathbf{r}\right)}{\partial\omega}\right| \\ &= \frac{\left(P_{\mathrm{m}} + P_{\mathrm{e}} + P_{\mathrm{rad}} + P_\omega\right) + \mathrm{j}\omega\left(W_{\mathrm{m}} + W_{\mathrm{e}} + W_{\mathrm{rad}} + W_\omega\right)}{2\left(P_{\mathrm{m}} - P_{\mathrm{e}}\right)}, \end{aligned} \tag{3}$$

where the particular terms are expressed as

$$W_{\mathrm{m}} - \mathrm{j}\frac{P_{\mathrm{m}}}{\omega} = k^2\mathcal{L}\left(\mathbf{J},\mathbf{J}\right), \tag{4a}$$

$$W_{\mathrm{e}} - \mathrm{j}\frac{P_{\mathrm{e}}}{\omega} = \mathcal{L}\left(\nabla\cdot\mathbf{J},\nabla\cdot\mathbf{J}\right), \tag{4b}$$

$$W_{\mathrm{rad}} - \mathrm{j}\frac{P_{\mathrm{rad}}}{\omega} = -\mathrm{j}k\left(k^2\mathcal{L}_{\mathrm{rad}}\left(\mathbf{J},\mathbf{J}\right) - \mathcal{L}_{\mathrm{rad}}\left(\nabla\cdot\mathbf{J},\nabla\cdot\mathbf{J}\right)\right), \tag{4c}$$

$$W_\omega - \mathrm{j}\frac{P_\omega}{\omega} = k^2\mathcal{L}_\omega\left(\mathbf{J},\mathbf{J}\right) - \mathcal{L}_\omega\left(\nabla\cdot\mathbf{J},\nabla\cdot\mathbf{J}\right), \tag{4d}$$

with the following energy functionals

$$\mathcal{L}\left(\mathbf{U},\mathbf{V}\right) = \frac{1}{4\pi\epsilon\omega^2}\int_{\Omega'}\int_\Omega \mathbf{U}\left(\mathbf{r}\right)\cdot\mathbf{V}^*\left(\mathbf{r}'\right)\frac{\mathrm{e}^{-\mathrm{j}kR}}{R}\,\mathrm{d}\mathbf{r}\,\mathrm{d}\mathbf{r}', \tag{5a}$$

$$\mathcal{L}_{\mathrm{rad}}\left(\mathbf{U},\mathbf{V}\right) = \frac{1}{4\pi\epsilon\omega^2}\int_{\Omega'}\int_\Omega \mathbf{U}\left(\mathbf{r}\right)\cdot\mathbf{V}^*\left(\mathbf{r}'\right)\mathrm{e}^{-\mathrm{j}kR}\,\mathrm{d}\mathbf{r}\,\mathrm{d}\mathbf{r}', \tag{5b}$$

$$\mathcal{L}_\omega\left(\mathbf{U},\mathbf{V}\right) = \frac{1}{4\pi\epsilon\omega}\int_{\Omega'}\int_\Omega \frac{\partial\left(\mathbf{U}\left(\mathbf{r}\right)\cdot\mathbf{V}^*\left(\mathbf{r}'\right)\right)}{\partial\omega}\frac{\mathrm{e}^{-\mathrm{j}kR}}{R}\,\mathrm{d}\mathbf{r}\,\mathrm{d}\mathbf{r}', \tag{5c}$$

in which $R = \left\|\mathbf{r}-\mathbf{r}'\right\|$ is the Euclidean distance, $k = \omega/c_0$ is the wavenumber, c_0 is the speed of light and ϵ is the vacuum permittivity. The quantity W_{m} is usually related to the magnetic energy, while W_{e} is related to the electric energy, and the expression $P_{\mathrm{m}} - P_{\mathrm{e}}$ forms the radiated power. The

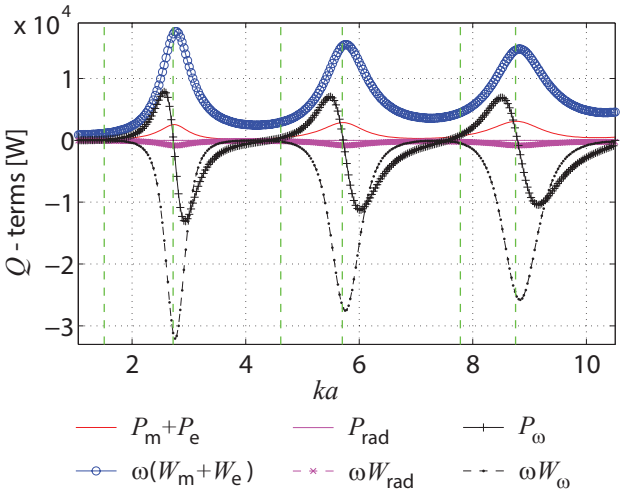

Fig. 1. The components that compose the nominator of (3) for the centre-fed thin-strip dipole. The resonances and antiresonances are marked by green dashed lines.

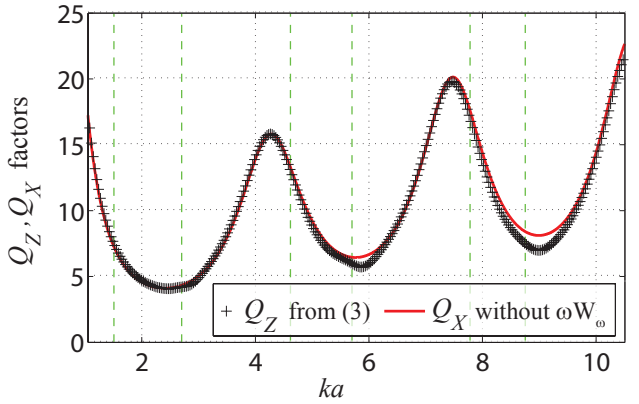

Fig. 2. Comparison of the Q_Z from (3) and Q_X without the ωW_ω term for the centre-fed thin-strip dipole. The resonances and antiresonances are marked by green dashed lines.

expression $W_{\rm rad} - {\rm j}P_{\rm rad}/\omega$ in the LHS of (4c) can be attributed to the energy associated with the radiation [5], while the term $W_\omega - \jmath P_\omega/\omega$ in the LHS of (4d) can be interpreted as the energy needed for the current (charge) reconfiguration during a frequency change. Note also that omitting the ωW_ω, the Q_X of (3) is just the quality factor published in [5].

As defined by (3), Q_Z is generally a quality factor of an untuned antenna. We can, however, consider an ideal lossless element connected in series with $Z_{\rm in}$, which will (at $\omega = \omega_0$) tune the antenna to the resonance. The corresponding tuned Q_X and tuned Q_Z are

$$Q_X^{\rm tuned} = \omega_0 \frac{2\max\{W_{\rm m}, W_{\rm e}\} + W_{\rm rad} + W_\omega}{2\left(P_{\rm m} - P_{\rm e}\right)}, \tag{6a}$$

$$Q_Z^{\rm tuned} = \left|Q_R + {\rm j}Q_X^{\rm tuned}\right|. \tag{6b}$$

Unlike in [5], where separation of the net reactive power into electric and magnetic energy is necessary, the derivation of (3) requires only the potential formulation in the RHS of (2).

III. Numerical Example – Thin-strip Dipole

The numerical example deals with a dipole made of a perfectly conducting and infinitesimally thin strip of length $2L$ and width $w = 2L/250$. The dipole is fed in its centre. The only complication is the existence of $\cos(kR)/R$ terms in the energy functionals (5a)–(5c). These singularities are however removable and integrable analytically [7].

The relevant terms of (3) are depicted in Fig. 1. While the $P_{\rm rad}$ term can be safely neglected, which usually also holds for $\omega W_{\rm rad}$, the newly derived terms P_ω and ωW_ω are surprisingly high, especially in the vicinity of the antiresonances. This is coherent with the interpretation as reconfiguration energy.

Finally, the numerical comparison between Q_Z and Q_X without the ωW_ω term are depicted in Fig. 2. Note the excellent agreement between the two courses, especially for low values of ka and for natural resonances of the dipole. Furthermore, expression (3) has been successfully verified for many other structures of different structural complexity.

IV. Conclusion

Utilizing of the complex power balance and the potential theory makes it possible to express the measurable Q_Z factor in terms of the current sources instead of the fields or the input impedance. All terms are expressed as bilinear functionals of the currents, which can be easily obtained from modern EM solvers. The results have been presented on the example of a centre-fed thin-strip dipole, verifying the derivation of the method and compared to the other definition of Q, reaching excellent agreement. The source definition of the Q_Z factor can be useful in antenna design, in determining lower bounds of Q_Z or in modal analysis.

Acknowledgement

This work was supported by the COST LD 12055 AMTAS (Advanced Modeling and Technologies for Antennas and Sensors) action.

References

[1] J. L. Volakis, C.-C. Chen, and K. Fujimoto, *Survey of Small Antenna Theory*, 1st ed., ser. Small Antennas: Miniaturization Techniques & Applications. McGraw-Hill, 2010.

[2] D. R. Rhodes, "Observable stored energies of electromagnetic systems," *J. Franklin Inst.*, vol. 302, no. 3, pp. 225–237, 1976.

[3] A. D. Yaghjian and S. R. Best, "Impedance, bandwidth and Q of antennas," *IEEE Trans. Antennas Propag.*, vol. 53, no. 4, pp. 1298–1324, April 2005.

[4] S. R. Best and D. L. Hanna, "A performance comparison of fundamental small-antenna designs," *IEEE Antennas Propag. Magazine*, vol. 52, no. 1, pp. 47–70, Feb. 2010.

[5] G. A. E. Vandenbosch, "Reactive energies, impedance, and Q factor of radiating structures," *IEEE Trans. Antennas Propag.*, vol. 58, no. 4, pp. 1112–1127, Apr. 2010.

[6] R. F. Harrington, *Time-Harmonic Electromagnetic Fields*, 2nd ed. John Wiley - IEEE Press, 2001.

[7] M. Capek, P. Hazdra, and J. Eichler, "A method for the evaluation of radiation Q based on modal approach," *IEEE Trans. Antennas Propag.*, vol. 60, no. 10, pp. 4556–4567, Oct. 2012.

Evaluation of Radiation Efficiency from Characteristic Currents

Miloslav Capek, Jan Eichler, and Pavel Hazdra,

***Abstract*—This paper describes an effective technique for modal radiation efficiency calculation based on the decomposition into the characteristic modes. The key consideration is based on the assumption that the current distribution on the perfect electric conductor is almost the same as in the case of a very good conductor, e.g. metals like copper, aluminium and silver. This fact is verified against the conventional technique, the impedance boundary condition, and it makes the calculation extremely fast. The proposed approach does not require any modification of the method of moments formulation for perfectly conducting surfaces which is assumed for the modal decomposition. The modal efficiencies provide additional insight useful especially for small antenna design. Considering the feeding, they can be summed up to obtain the total efficiency. The technique works perfectly for common metals, is fully comparable with the impedance boundary condition and can easily be incorporated into any existent in-house solver. To present the merits of the method, the numerical analysis of three examples, namely the coupled dipoles, the electrically small meandered dipole and the PIFA are presented. The results are in a perfect agreement with the reference commercial package.**

Keywords. Characteristic modes, radiation efficiency, losses, skin effect.

I. Introduction

The radiation efficiency [1] is a very important parameter that significantly affects the operation of an antenna, especially if the electrical dimensions are small [2].

The common approach of computing the radiation efficiency of an antenna is considering lossy material in the numerical simulation. This approach is general and accurate, however it is not fast and it does not provide much physical insight into the lossy antenna operation.

In our approach we suppose the current density evaluated on a perfect electric conductor (PEC) to be approximately the same as for lossy metal of finite thickness. It will be shown that this assumption works perfectly for common metals like copper and aluminum. Moreover the radiation efficiency could be evaluated very quickly in a post processing step, once the currents on PEC are evaluated by the method of moments (MoM) solver.

The more precise evaluation is based on the surface impedance boundary condition (IBC) [3], [4]. However, time-consuming recalculation of MoM matrix is needed whenever the conductivity σ or the thickness t of metal is changed.

This work was supported by the project of Czech Science Foundation, grant No. P102/12/2223 and by the project COST IC1102 VISTA

The authors are with the Department of Electromagnetic Field, Faculty of Electrical Engineering, Czech Technical University in Prague, Technicka 2, 16627, Prague, Czech Republic (e-mail: miloslav.capek@fel.cvut.cz).

In order to gain better physical picture of a lossy antenna operation, the theory of characteristic modes (TCM) [5], [6], [7] is adopted for calculation of individual modal efficiencies. This theory enables to calculate a set of so called characteristic currents by decomposition of the MoM impedance matrix. These currents are orthogonal (with respect to radiated power) and may be summed to form the total current flowing on an antenna if the feeding is connected. Thus the TCM allows to study the antenna geometry without specific feeding and to understand its operation through modal superposition of different quantities based on the surface current density [8], [9].

In this paper a fast and physically illustrative procedure of approximating radiation losses is developed for characteristic modes particularly on RWG [10] meshes, but the technique is not limited to arbitrary discretization scheme.

II. Calculation of Radiation Efficiency from Surface Currents

The expressions for calculation of the radiation efficiency will be derived in this section. The input of the procedure is an antenna consisting of an infinitesimally thin perfect electric conductor (PEC). Next suppose the antenna is discretized using the RWG basis functions and the current density is computed by the method of moments [11].

We begin with the radiation efficiency definition [1]

$$\eta = \frac{P^{\mathrm{R}}}{P^{\mathrm{R}} + P^{\mathrm{L}}}, \tag{1}$$

where P^{R} is the radiated power and P^{L} is the loss power. If no losses are present (i.e. a PEC antenna in a lossless dielectric) the P^{R} is equal to the power accepted by the antenna. Therefore we need to compute P^{L} if there were losses in the metal. The procedure is as follows.

Suppose a PEC surface on which the surface current density $\boldsymbol{J}^{\mathrm{surf}}$ is computed by the MoM. Next the skin-effect will be taken into account by introducing equivalent volume current density

$$\boldsymbol{J}^{\mathrm{eq}}(z) = \boldsymbol{J}_0^{\mathrm{eq}} e^{-(1+j)\gamma z}, \tag{2}$$

where z is the distance from metal surface, and the attenuation constant [12] for a highly conductive material is

$$\gamma = \sqrt{\frac{\omega\mu\sigma}{2}}, \tag{3}$$

where μ is the permeability and ω is the angular frequency. The relation between the surface current density and $\boldsymbol{J}^{\text{eq}}$ is

$$\left| \int_0^t \boldsymbol{J}^{\text{eq}}(z)\ \mathrm{d}z \right| = \left| \boldsymbol{J}^{\text{surf}} \right|, \tag{4}$$

which is the key approximation. From (2) and (4) we have

$$\left| \boldsymbol{J}_0^{\text{eq}} \right| = \frac{\sqrt{2}\gamma \left| \boldsymbol{J}^{\text{surf}} \right|}{\left| 1 - e^{-(1+j)\gamma t} \right|}. \tag{5}$$

Considering now a triangulated surface and constant current $\boldsymbol{J}_n^{\text{surf}}$ on each triangle n, the loss power can be expressed as [12]

$$\begin{aligned} P^{\text{L}} &= \int_\Omega \boldsymbol{E} \cdot \boldsymbol{J}^* \ \mathrm{d}V \approx \sum_n \int_\Omega \frac{\left| \boldsymbol{J}_n^{\text{eq}} \right|^2}{\sigma} \ \mathrm{d}V = \\ &= F(\omega, \sigma, t) \sum_n A_n \left| \boldsymbol{J}_n^{\text{surf}} \right|^2, \end{aligned} \tag{6}$$

where * denotes complex conjugation, A_n is the area of triangle n, $\Omega = \bigcup_n A_n$ is the PEC surface and

$$F(\omega, \sigma, t) = \frac{\gamma}{\sigma} \frac{(1 - e^{-2\gamma t})}{\left| 1 - e^{-(1+j)\gamma t} \right|^2}. \tag{7}$$

III. Modal Radiation Efficiency

The radiation efficiency of a certain characteristic current will be defined in this section. Then a summation formula for those modal radiation efficiencies is obtained. It allows to explore the physical background of how particular modes contribute to the overall radiation efficiency. Since it is enough to include only first few modes for electrically small antenna, this knowledge can help designer to modify the antenna geometry in order to suppress certain modes and increase the overall radiation efficiency of the antenna. The second goal is to derive a fast formula for radiation efficiency computation and optimization. We recall that for certain structure at a given frequency, the impedance matrix need not to be recalculated and the total radiation efficiency is controlled only through position of the feeding port which effects the expanding coefficients.

A. Theory of Characteristic Modes

Basics of the TCM which are important for modal radiation efficiency definition are briefly repeated here. Detailed description of the TCM and its derivation can be found in [5] and the recent revision in [7].

The theory is based on eigen-decomposition of the EFIE operator [13] $\mathcal{Z}(\boldsymbol{J}) = \mathcal{R}(\boldsymbol{J}) + \mathrm{j}\mathcal{X}(\boldsymbol{J})$ on a PEC surface according to the generalized eigenvalue problem

$$\mathcal{X}\boldsymbol{J}_u = \lambda_u \mathcal{R}\boldsymbol{J}_u, \tag{8}$$

where λ_u is the u-th characteristic number and $\boldsymbol{J}_u$ is the characteristic vector or current. All modal current densities are supposed to be normalized at every frequency to radiate a power $P_u^{\text{R}} = 1\text{W}$

$$\langle \boldsymbol{J}_u, \mathcal{R}\boldsymbol{J}_u \rangle = 1 = P_u^{\text{R}}, \tag{9}$$

where the symmetrical product[1] was used. Thus the modes satisfy the orthogonality relations

$$\langle \boldsymbol{J}_u, \mathcal{R}\boldsymbol{J}_v \rangle = \delta_{uv}, \tag{10}$$

$$\langle \boldsymbol{J}_u, \mathcal{X}\boldsymbol{J}_v \rangle = \lambda_u \delta_{uv}, \tag{11}$$

$$\langle \boldsymbol{J}_u, \mathcal{Z}\boldsymbol{J}_v \rangle = (1 + \lambda_u)\delta_{uv}, \tag{12}$$

where δ_{uv} is the Kronecker delta function[2]. The total current on antenna surface can be found by summation as [5]

$$\boldsymbol{J} = \sum_u \alpha_u \boldsymbol{J}_u. \tag{13}$$

For an impressed field $\boldsymbol{E}^{\text{i}}$, representing the excitation, the expanding coefficients α_u are [5]

$$\alpha_u = \frac{\langle \boldsymbol{J}_u, \boldsymbol{E}^{\text{i}} \rangle}{1 + \mathrm{j}\lambda_u}. \tag{14}$$

B. Derivation of Modal Radiation Efficiency

Consider surface current density $\boldsymbol{J}^{\text{surf}}$ expressed as a superposition of characteristic modes according to (13). For $\left| \boldsymbol{J}_n^{\text{surf}} \right|^2$ we then have:

$$\begin{aligned} \left| \boldsymbol{J}_n^{\text{surf}} \right|^2 &= \sum_u \alpha_u \boldsymbol{J}_{nu}^{\text{surf}} \cdot \sum_v \alpha^* (\boldsymbol{J}_{nv}^{\text{surf}})^* \\ &= \sum_u \sum_v \beta_{uv} \boldsymbol{J}_{nu}^{\text{surf}} \cdot (\boldsymbol{J}_{nv}^{\text{surf}})^*. \end{aligned} \tag{15}$$

The coupling $\boldsymbol{\beta} = [\beta_{uv}]$ matrix is defined in [8] as

$$\begin{aligned} \beta_{uv} &= \Re \{ \alpha_u \alpha_v^* \} = \\ &= \frac{\langle \boldsymbol{J}_u, \boldsymbol{E}^i \rangle \langle \boldsymbol{J}_v, \boldsymbol{E}^i \rangle (1 + \lambda_u \lambda_v)}{(1 + \lambda_u^2)(1 + \lambda_v^2)}. \end{aligned} \tag{16}$$

The modal power loss is

$$P_{uv}^{\text{L}} = F(\omega, \sigma, t) \sum_n A_n \boldsymbol{J}_{nu}^{\text{surf}} \cdot \boldsymbol{J}_{nv}^{\text{surf}} \tag{17}$$

Note that the characteristic currents are real by definition [5], so the complex conjugation rising from (15) can be omitted. Since modal radiated power is normalized to 1W, we define the modal radiation efficiency of mode u as

$$\eta_u = \frac{1}{1 + P_{uu}^{\text{L}}}. \tag{18}$$

The total power loss may now be expressed as a superposition of modal radiation losses

$$P^{\text{L}} = \sum_u \sum_v \beta_{uv} P_{uv}^{\text{L}} = \langle \boldsymbol{\beta}, \boldsymbol{P}^{\text{L}} \rangle. \tag{19}$$

Using the orthogonal property of characteristic modes (9) and (1) the radiation efficiency is finally written as

$$\eta = \frac{\sum_u \beta_{uu}}{\sum_u \beta_{uu} + \sum_u \sum_v \beta_{uv} P_{uv}^{\text{L}}} = \frac{\mathrm{Tr}(\boldsymbol{\beta})}{\mathrm{Tr}(\boldsymbol{\beta}) + \langle \boldsymbol{\beta}, \boldsymbol{P}^{\text{L}} \rangle}. \tag{20}$$

[1] Symmetrical product of $\boldsymbol{a}, \boldsymbol{b}$ is defined as $\langle \boldsymbol{a}, \boldsymbol{b} \rangle = \int_\Omega \boldsymbol{a} \cdot \boldsymbol{b}\ \mathrm{d}\Omega$ and the dot product is defined in a usual way as $\boldsymbol{a} \cdot \boldsymbol{b} = \sum a_i b_i$.

[2] $\delta_{uv} = 0$ for $u \neq v$ and $\delta_{uv} = 1$ for $u = v$.

TABLE I
DIMENSIONS OF PIFA

Name	Dimmensions	Color in Fig. 3
Ground plane	100 × 100 mm	grey
Height over ground plane	1 mm	yellow, green
Patch width	15 mm	pink
Patch height	20 mm	pink
Feed width	2 mm	green
Feed x axis position	4 mm	green

IV. NUMERICAL RESULTS

In order to verify that our derivation is valid and the approximations made are reasonable, three test structures were chosen. It is a meandered strip dipole (Fig, 1), coupled active and parasitic dipole (Fig. 2) and a PIFA antenna [14] over a finite ground plane (Fig. 3, Table I). Note that these cases were computed in a wide frequency range and are of different type (electrically small, planar, strips, highly resonant structures, with and without a finite ground plane).

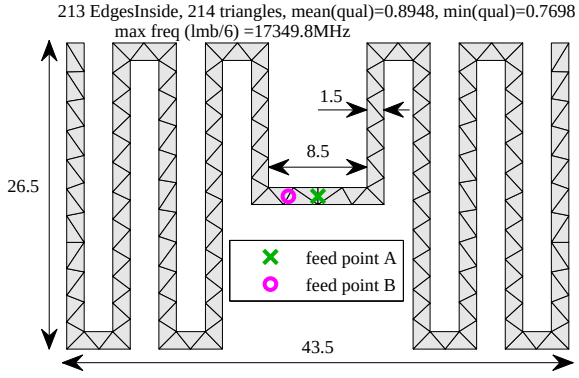

Fig. 1. Triangular mesh of the meandered dipole with different feeding points. Dimmensions in [mm]

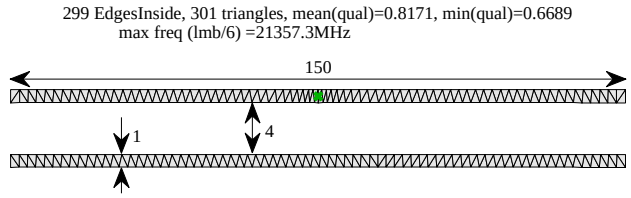

Fig. 2. Triangular mesh of the coupled dipoles, feeding point is at the top dipole, marked by the green cross. Dimmensions in [mm]

A. Effect of Changes in Current Distribution Between Lossy and Lossless Case

In section II we made an assumption that current distribution on an antenna made of thin metal (with $\sigma > 10^5$ S/m) and on antenna made of PEC is approximately the same. Validity of this important assumption will be numerically verified in this section.

The center fed meandered dipole, Fig. 1, feed point A, was modeled in the FEKO [15] and the current density as well as the area of the triangle elements was exported in ASCII format. The data for $\sigma = \{5.85 \cdot 10^7, 5.85 \cdot 10^6, 5.85 \cdot 10^5\}$ S/m and for the PEC were imported into our MATLAB [16] routine and the total radiation efficiency was computed according to (6) and (1), see Fig. 4 for comparison.

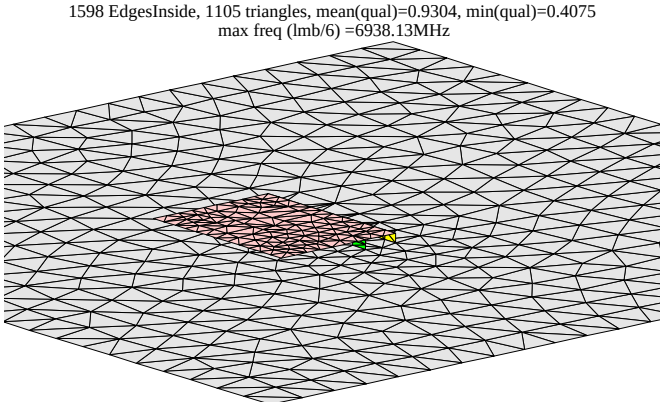

Fig. 3. Detailed view of the triangular mesh of the PIFA. Dimmensions are in Table I

The difference between the radiation efficiency computed from currents on a PEC antenna and on a lossy antenna are generally very small. The same procedure was repeated for each of the test structures and all combination of $\sigma = \{5.85 \cdot 10^7, 5.85 \cdot 10^6, 5.85 \cdot 10^5\}$ S/m and $t = \{18, 50\}$ μm, i. e. 18 different cases. The results were qualitatively similar to Fig. 4. It should be mentioned that radiation efficiency computed from PEC currents is slightly shifted upwards in frequency (25 MHz shift at 8 GHz for meandered dipole, $\sigma = 5.85 \cdot 10^5$ S/m, $t = 50$ μm), Fig. 4. However this 0.3% frequency shift for a low conductive metals can be neglected for practical purposes. Thus we conclude that our initial assumption holds very well for all tested combinations.

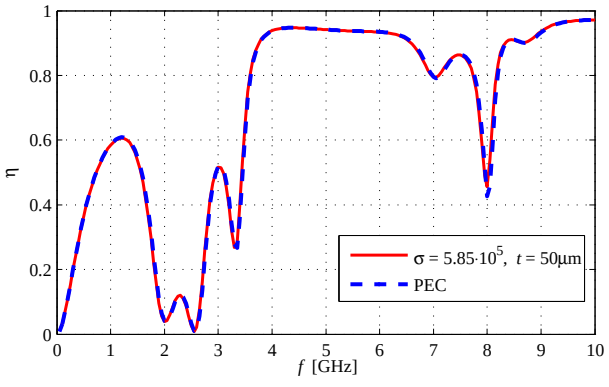

Fig. 4. Computation of radiation efficiency from currents on PEC and lossy surface

B. MoM Solution Using In-house Software Tool

In this section, the results from commercial software package will be compared with our in-house MoM tool [9]. The tool is based on [17] and considers only perfectly conducting metal bodies. The loss power is computed according to (6).

In the FEKO, structure is modeled as infinitesimally thin, however t and σ are defined for a material model based on the IBC [18] used in the simulation. It can be seen in Figs. 5,6,7, that both approaches gives very similar results. The biggest difference for PIFA and low σ is plotted in Fig. 7. Thus we conclude that FEKO (MoM + IBC) and MATLAB code (MoM on PEC + (6)) gives very comparable results.

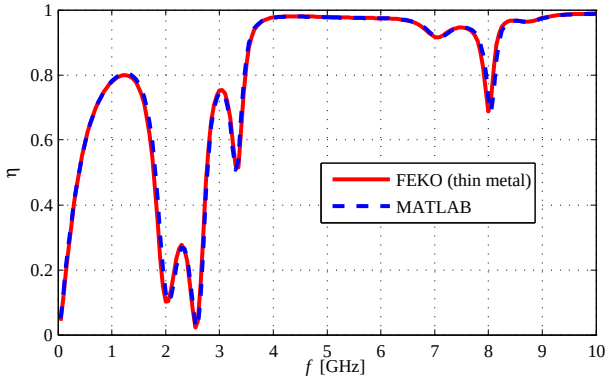

Fig. 5. Radiation efficiency computed by FEKO and MATLAB routine. Meandered dipole, $\sigma = 5.85 \cdot 10^6$ S/m, $t = 50$ μm

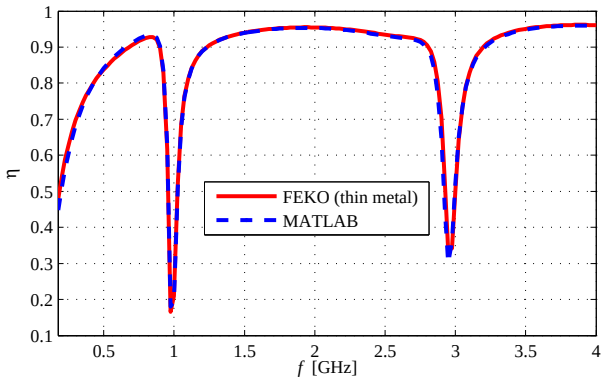

Fig. 6. Radiation efficiency computed by FEKO and MATLAB routine. Coupled dipoles, $\sigma = 5.85 \cdot 10^6$ S/m, $t = 18$ μm

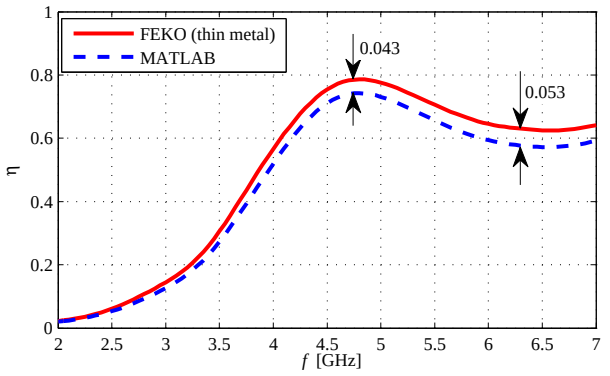

Fig. 7. Radiation efficiency computed by FEKO and MATLAB routine. PIFA, $\sigma = 5.85 \cdot 10^5$ S/m, $t = 50$ μm

C. Modal Radiation Efficiency

Features of modal radiation efficiency will be demonstrated using the example of meandered dipole discussed in the previous section. The impedance matrix obtained by the in-house MoM tool is decomposed into characteristic modes [9]. From this set of modes the beta matrix (16) and the modal loss power matrix (17) are computed. Using these inputs, the total radiation efficiency η is computed using (20) and compared to MoM solution. The structure was approximated by 213 basis functions and all 213 numerically computed modes were used in the superposition. The two results are almost equivalent, see Fig. 8, which is in correspondence with the theoretical development of Section III-B. Small difference can be addressed to numerical errors arising from computationally difficult decomposition.

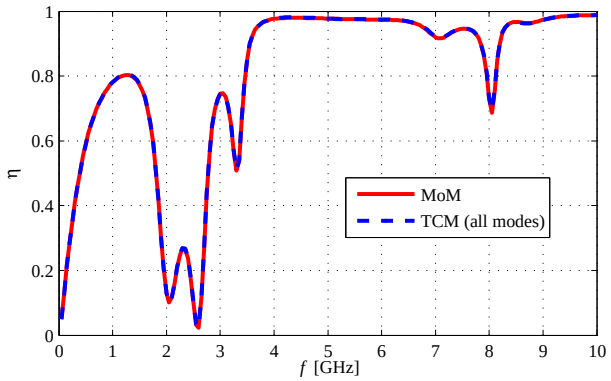

Fig. 8. Radiation efficiency computed from MoM result and through modal superposition. Meandered dipole, $\sigma = 5.85 \cdot 10^6$ S/m, $t = 50$ μm

Next lets examine how modes contribute to the radiation efficiency. If the real feeding is connected, the excitation of meandered dipole will never be ideally symmetrical. Lets investigate the effect of the asymmetrical feeding by exciting feed point B in Fig. 1. One can clearly see that a new minimum of radiation efficiency is present at 1.6 GHz, as shown in Fig. 9.

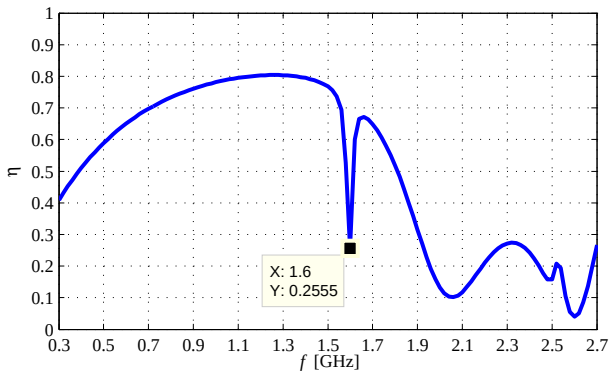

Fig. 9. Radiation efficiency of asymmetrically fed (feed point B) meandered dipole, $\sigma = 5.85 \cdot 10^6$ S/m, $t = 50$ μm

The structure was decomposed into characteristic modes, see β_{uu} and P^{L}_{uu} Table II for the first 7 modes. Even though the cross terms i.e. the $\beta_{uv}, P^{\mathrm{L}}_{uv}; u \neq v$ are necessary in

TABLE II
DIAGONAL TERMS OF COUPLING MATRIX, MODAL LOSS POWER MATRIX AND MODAL RADIATION EFFICIENCY AT 1.6 GHZ

u	β_{uu}	P^{L}_{uu}	η_{uu}	$\beta_{uu}P^{\mathrm{L}}_{uu}$
1	8.62e-05	0.084	**0.92**	7.25e-06
2	2.03e-04	2.25	**0.31**	4.56e-04
3	2.36e-07	0.05	0.95	1.19e-08
4	1.71e-06	1.16	0.46	1.98e-06
5	1.65e-07	1.83	0.35	3.00e-07
6	8.75e-11	5.85	0.15	5.12e-10
7	1.60e-08	61.96	0.016	9.91e-07

TABLE III
DIAGONAL THERMS OF COUPLING MATRIX, MODAL LOSS POWER MATRIX AND MODAL RADIATION EFFICIENCY OF THE MODIFIED MEANDER AT 1.88 GHZ

u	β_{uu}	P^{L}_{uu}	η_{uu}	$\beta_{uu}P^{\mathrm{L}}_{uu}$
1	1.25e-4	0.068	**0.94**	8.57e-06
2	1.06e-3	0.51	**0.66**	5.44e-4
3	1.22e-09	793	0.0013	9.64e-07
4	4.20e-06	0.073	0.93	3.08e-07
5	2.63e-06	0.84	0.54	2.22e-06
6	3.12e-09	0.85	0.54	2.67e-09
7	1.66e-06	2.85	0.26	4.75e-06

(20), the main information about the significance in the sum of radiation efficiencies is readable from the diagonal terms only. Investigating Table II, it is evident that the dominantly excited modes are mode 2 and 1. While the mode 1 is desired and radiates well, mode 2 has low modal radiation efficiency ($\eta_{22} = 31\%$) and thus it contributes strongly to loss power.

Next we would like to eliminate the efficiency drop at 1.6 GHz. This is a difficult task from design point of view, since it is not clear how to achieve this goal from MoM solution. However the TCM gives us a guidance that mode 2 should be suppressed or shifted in frequency. Thus the meander should be modified in order to affect the mode 2 while not effecting the mode 1, see Fig. 10. The good position for modification is the area where currents of mode 2 are maximal i.e. approx. at the center of the meander arm, the modes on a modified structure are in Fig. 11.

The positive effect of the modification on η is visible in Fig. 12. The current path for mode 2 is shortened which shifts its resonant frequency from 1.6 GHz to 1.88 GHz. The resonance of mode 1 is also slightly shifted from 0.96 to 1.02 GHz (computed by the TCM). Since the current of mode 2 on the modified structure flows less in the opposing directions, η_{22} raises from 31 % to 66 %, see Table III. This is reflected in the η in Fig. 12, where the efficiency drop is not as deep as for the original meander.

Another interesting fact is that $\eta = 49.2\%$ at 1.88 GHz while the modal $\eta_2 = 66.12\%$. We would achieve $\eta = \eta_2$ if only the mode 2 was excited. But a nonzero contributions to the P^{L} from all modes can be seen in Table III. Thus in practice the η at the resonant frequency of a certain mode u is always lower than corresponding η_u.

V. CONCLUSION

The theory for evaluating the radiation efficiency from characteristic currents was presented. It was shown that the conduction loss (and thus radiation efficiency) can be understood as a weighted sum of losses associated with characteristic modes. The assumptions made in the derivation holds very well for testing structures, namely the meandered dipole, coupled dipoles and PIFA over finite ground plane and several different metalization thicknesses and conductivities.

The main advantage of the proposed technique is the gained physical interpretation of the sources of conduction loss which contribute to the overall radiation efficiency. This was demonstrated on a simple example of asymmetrically fed

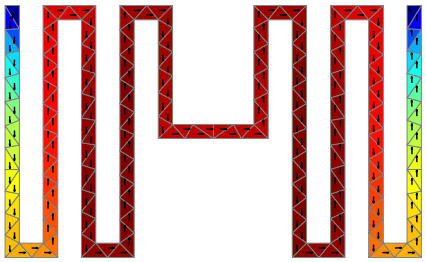

(a) Mode 1

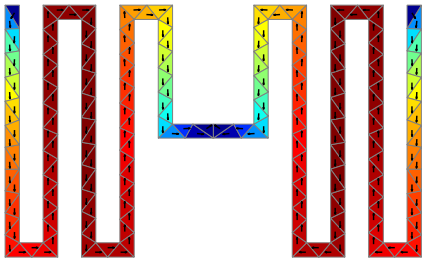

(b) Mode 2

Fig. 10. Characteristic current at 1.6 GHz

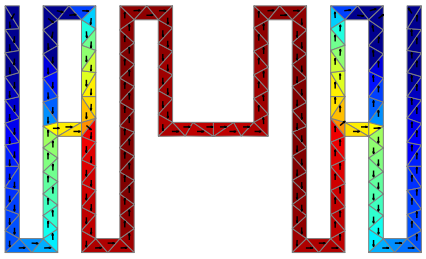

(a) Mode 1

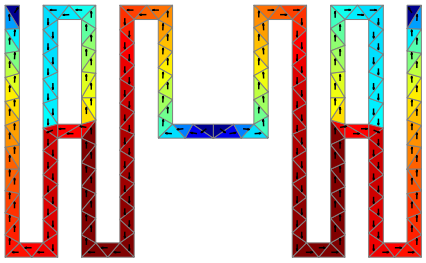

(b) Mode 2

Fig. 11. Modified meandered dipole, characteristic current, 1.88 GHz

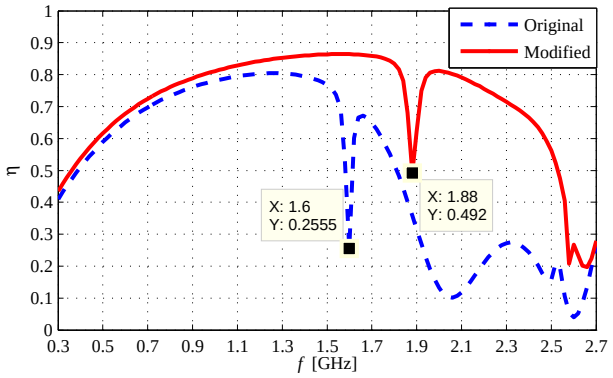

Fig. 12. Comparison of radiation efficiency of the modified and original meandered dipole, feed point B, $\sigma = 5.85 \cdot 10^6$ S/m, $t = 50$ μm

meandered dipole which was modified in order to improve radiation efficiency. Other benefit of the technique is an easy implementation to arbitrary MoM code. The radiation efficiency computation can be performed as a post processing step which is particularly useful for the TCM. It is possible to use this method in a very fast optimization loop as well.

ACKNOWLEDGEMENT

The authors would like to thank M. Polivka, for initial tests in the IE3D software, prof. J. Vrba, N. Bell and P. Hamouz for their comments.

REFERENCES

[1] C. A. Balanis, *Antenna Theory Analysis and Design*, 3rd ed. John Wiley, 2005.
[2] H. A. V. M. Polivka, M. and M. Svanda, "Impedance properties and radiation efficiency of electrically small double and triple split-ring antennas for uhf rfid applications," *IEEE Antennas and Wireless Propag. Letters*, vol. 12, pp. 221–24, 2013.
[3] C. W. C. Qian, Z. G. and R. Suaya, "Generalized impedance boundary condition for conductor modeling in surface integral equation," *IEEE Transactions on Microwave Theory and Techniques*, vol. 55, no. 11, pp. 2354–2364, November 2007.
[4] A. Karlsson, "Approximate boundary conditions for thin structures," *IEEE Trans. Antennas Propag.*, vol. 57, no. 1, pp. 144–148, January 2009.
[5] R. F. Harrington and J. R. Mautz, "Theory of characteristic modes for conducting bodies," *IEEE Trans. Antennas Propag.*, vol. 19, no. 5, pp. 622–628, Sept. 1971.
[6] M. Cabedo-Fabres, "Systematic design of antennas using the theory of characteristic modes," Ph.D. dissertation, UPV, Feb. 2007.
[7] M. Cabedo-Fabres, E. Antonino-Daviu, A. Valero-Nogueira, and M. F. Bataller, "The theory of characteristic modes revisited: A contribution to the design of antennas for modern applications," *IEEE Antennas Propag. Magazine*, vol. 49, no. 5, pp. 52–68, Oct. 2007.
[8] M. Capek, P. Hazdra, and J. Eichler, "A method for the evaluation of radiation Q based on modal approach," *IEEE Trans. Antennas Propag.*, vol. 60, no. 10, pp. 4556–4567, Oct. 2012.
[9] M. Capek, P. Hamouz, P. Hazdra, and J. Eichler, "Implementation of the Theory of Characteristic Modes in Matlab," *IEEE Antennas Propag. Magazine*, vol. 55, no. 2, pp. 176–189, April 2013.
[10] S. M. Rao, D. R. Wilton, and A. W. Glisson, "Electromagnetic scattering by surfaces of arbitrary shape," *IEEE Trans. Antennas Propag.*, vol. 30, no. 3, pp. 409–418, May 1982.
[11] W. C. Gibson, *The Method of Moments in Electromagnetics*, 1st ed. Chapman and Hall/CRC, 2007.
[12] R. F. Harrington, *Time-Harmonic Electromagnetic Fields*, 2nd ed. John Wiley - IEEE Press, 2001.
[13] ——, *Field Computation by Moment Methods*. John Wiley - IEEE Press, 1993.
[14] C. Rowell and E. Y. Lam, "Mobile-phone antenna design," *IEEE Antennas Propag. Magazine*, vol. 54, no. 4, pp. 14–34, August 2012.
[15] EM Software & Systems-S.A. FEKO. [Online]. Available: www.feko.info
[16] The MathWorks. The Matlab. [Online]. Available: www.mathworks.com
[17] S. N. Makarov, *Antenna and EM Modeling with Matlab*. John Wiley, 2002.
[18] Feko, user's manual, suite 6.2.2. EM Software & Systems-S.A. (Pty) Ltd. 32 Techno Avenue, Technopark, Stellenbosch, 7600, South Africa. [Online]. Available: www.feko.info

An Analytical Evaluation and The Lower Bounds of The Measurable Quality Factor Q_Z

Miloslav Capek, *Student Member, IEEE,* Lukas Jelinek, Pavel Hazdra, *Member, IEEE,* and Jan Eichler

***Abstract*—This paper describes an analytical evaluation of the measurable quality factor Q_Z in a separable system in which the vector potential is known. The proposed method uses a potential definition of active and reactive power, implicitly avoiding infinite entire space integration and extraction of radiation energy. Furthermore, the proposed method uses solely measurable quantities and is thus not influenced by commonly used, but ambiguous, separation into electric and magnetic energies. As a result, all the used quantities are finite, and the calculated Q_Z is always non-negative function of frequency. The theory is presented on the canonical example of the currents flowing on a spherical shell. The lower bounds of Q_Z for dominant spherical TM and TE mode are found in closed forms, including both internal and external energies. The proposed analytical method and its results are verified by numerical calculations, including utilization of the theory of characteristic modes and compared to previously published Q factor limits.**

***Index Terms*—Antenna theory, electromagnetic theory, electrically small antennas, spherical antennas, Q factor.**

I. Introduction

THE quality factor is recognized as one of the most significant parameters of the radiating system, especially if the electrical dimensions are small, see e.g. [1] and references therein. However, there are many as yet unresolved issues associated with Q factor of a radiator and available bandwidth. One of them is the upper bound of the available bandwidth of electrically small antenna (ESA), which is commonly obtained from the lower bound of Q factor.

The classical work of Chu [2] considers a sphere of radius a that encloses an ESA. The normalized radial wave impedance for the dominant spherical TM mode is expressed as a continued fraction equivalent to a ladder network with particular R, L, C elements. In this way, the lower bound of Q can be found. However, the Chu's method is restricted to the spherical modes only and does not include the internal energy of the sphere, making the limit overly optimistic. Later, Wheeler [3] reduced the basic radiators, dipole and loop, to the circuit elements and derived practically oriented limits. Expansion to the spherical harmonics was also used by Harrington [4] to evaluate the electric and magnetic energy for each mode. The method, however, operates with separated – and thus ambiguous – energies and the problematic entire space integration. The same approach was presented by Collin and Rothschild [5] for spherical and cylindrical modes. McLean [6] verified the Chu's formula. He obtained the same results, but his approach is based on the field radiated by the Herzian dipole. Thiele, Detweiler and Penno [7] used the "far-field method", based on the separation of the far-field pattern into its visible and invisible parts [8]. Thal [9], [10], [11] used the ladder network to extend the Chu's limit by including the energies inside the enclosing sphere. Hansen and Collin [12] also included internal energies, but they used $\mathbf{E}$- and $\mathbf{H}$-fields together with the subtraction of the radial power-flow. Hansen, Kim and Breinbjerg [13] generalized the results of Hansen and Collin for any spherical TM and TE mode and for a sphere filled with an isotropic medium. The limitations of the dual mode case were studied by Fante [14] and recently by Kim [15].

The most recent approaches to the Q factor calculation utilized the source current distribution. There are obvious benefits: the resultant functionals are of bilinear forms, the calculation is very effective and it is possible to use any current distribution that is available thanks to modern EM simulators or that could even be user-defined. This opens new possibilities in optimization [16] and modal decomposition [17]. The excellent work by Vandenbosch [18] is inspired by the pioneering research of Geiy [19], and directly uses Maxwell equations and the source currents. The same theory has been generalized in the time domain [20]. However, some non-observable terms [21] are neglected, and the technique suffers from the fact that the separation of the electric and magnetic energies is non-unique. Another approach by Gustafsson, Sohl and Kristensson [22] utilized static polarizability. Gustaffson and Jonsson [23] also postulated the uncertainty in Vandenbosch's definition of Q. Unfortunately, their contribution opens a new question about the coordinate dependent term which is strictly non-physical.

Some attempts have also been made to obtain the lower bound of Q by utilizing the sources. This limit was investigated by Vandenbosch and Volski [24], but the method is encumbered with the difficulties mentioned above, and thus the results are provided only for a small radiator. Very interesting work has been done by Seshadri [25], closely related with [26], where the complex power of the spherical modes is already known analytically.

Together with the theoretical achievements, many scientists have sought for an antenna prototype that achieves the given limits, see e.g. [27], [28]. The folded multi-arm spherical helix antenna designed by Best [29] achieved roughly 1.5 times the Chu's limit and almost exactly the limit predicted by Hansen and Collin. An attempt to reach the Chu's limit was undertaken

Manuscript received September 10, 2013; revised November 20, 2013. This work was supported by the Czech Science Foundation, grant No. P102/12/2223, and by the Grant Agency of the Czech Republic under project 13-09086S.

The authors are with the Department of Electromagnetic Field, Faculty of Electrical Engineering, Czech Technical University in Prague, Technicka 2, 16627, Prague, Czech Republic (e-mail: miloslav.capek@fel.cvut.cz).

by Kim and Breinbjerg [30], using a magnetic-coated PEC core.

In connection with realistic ESA, the question arises, whether the classical Q limits, based on knowledge of unmeasurable field energies, should not be replaced by limits imposed on a "measurable" Q factor. In fact, such measurable Q factor (based on the antenna's input impedance) has been proposed by Yaghjian and Best [31], is denoted Q_Z and was revisited by ourselves [32].

This paper attempts to define the lower bounds of Q in the context of the measurable Q_Z factor [31]. The method is based on the differentiation of the complex power, expressed by electromagnetic potentials rather than fields [32]. In this way, the issues with divergent integrals [18] are automatically eliminated, since the subtraction of the far-field energy is inherently present. The complex power differentiation is free of any ambiguous electric and magnetic energy separations which give rise to non-physical quantities like coordinate dependent terms [23] or non-unique or negative energies.

The proposed theory is presented on an example of spherical modes, which have been in the spotlight in recent decades for their ability to establish a general lower bound of Q factor. It is important to stress that thanks to the proposed theory, the whole process is completely analytical, without any approximations or numerical calculations. The final expressions, presented in the closed form, are easy to work with and are compatible with all previous observations. Furthermore, our methodology can establish the Q_Z limits not only for the spherical coordinate system, but for any system in which the vector wave equation is separable [33] and thus the vector potential is analytically known. This gives a possibility of practical Q_Z limits tailored for a particular antenna design.

The paper is organized as follows. The definition of the Q_Z factor is briefly recapitulated in Section II. The complex power and all necessary power and energy terms of the dominant spherical TM and TE modes are presented in Section III and Section IV. Section V presents the measurable and thus practically available fundamental limits of ESA that are represented by the dominant spherical modes, further denoted as TM_{10} and TE_{10}, and compares them with the classical Q limits. Section VI depicts an asymptotic behaviour of the Q_Z factor, and also the values where important quantities reach the minimum.

II. Definition of Q_Z

The exact derivation of the measurable Q_Z factor [31] in terms of sources is provided in [32], including the related discussion and numerical verification, and reads

$$\begin{aligned} Q_Z &= |Q_R + \jmath Q_X| \\ &= \frac{ka}{2\left(P_\mathrm{m} - P_\mathrm{e}\right)} \left| \frac{\partial\Big(\left(P_\mathrm{m} - P_\mathrm{e}\right) + \jmath\omega \left(W_\mathrm{m} - W_\mathrm{e}\right)\Big)}{\partial ka} \right|, \end{aligned} \tag{1}$$

where subscripts Z, R and X represent impedance, resistance and reactance respectively, and where $\jmath = \sqrt{-1}$, ω is the angular frequency of the time harmonic field [34] under the convention $\boldsymbol{\mathcal{F}}\left(t\right) = \sqrt{2}\Re\left\{\mathbf{F}\left(\omega\right)\mathrm{e}^{\jmath\omega t}\right\}$, where $\boldsymbol{\mathcal{F}}$ is any time-harmonic quantity, $k = \omega/c_0$ is the wavenumber, c_0 is the speed of light, a is the smallest radius of a sphere circumscribing all the sources, $P_\mathrm{m} - P_\mathrm{e}$ is the total radiated power [35], $\omega\left(W_\mathrm{m} - W_\mathrm{e}\right)$ is the total reactive power [35], and the total input current at the antenna's port is normalized to $I_0 = 1\mathrm{A}$. Considering an arbitrary source current distribution $\mathbf{J}$ and charge density ρ inside Ω source region, and $\mathbf{A}$ and φ as the vector and scalar potential [35], the separated Q_R and Q_X terms in (1) can be written as

$$Q_R = \frac{P_\mathrm{m} + P_\mathrm{e} + P_\mathrm{rad} + P_\omega}{2\left(P_\mathrm{m} - P_\mathrm{e}\right)}, \tag{2}$$

and

$$Q_X = \frac{\omega\left(W_\mathrm{m} + W_\mathrm{e} + W_\mathrm{rad} + W_\omega\right)}{2\left(P_\mathrm{m} - P_\mathrm{e}\right)}, \tag{3}$$

where the particular terms are expressed as

$$W_\mathrm{m} - \jmath\frac{P_\mathrm{m}}{\omega} = \int\limits_\Omega \mathbf{A}\cdot\mathbf{J}^*\,\mathrm{d}\mathbf{r}, \tag{4a}$$

$$W_\mathrm{e} - \jmath\frac{P_\mathrm{e}}{\omega} = \int\limits_\Omega \varphi\rho^*\,\mathrm{d}\mathbf{r}, \tag{4b}$$

$$W_\mathrm{rad} - \jmath\frac{P_\mathrm{rad}}{\omega} = -\jmath k\left(k^2\mathcal{L}_\mathrm{rad}\left(\mathbf{J},\mathbf{J}\right) - \mathcal{L}_\mathrm{rad}\left(\nabla\cdot\mathbf{J},\nabla\cdot\mathbf{J}\right)\right), \tag{4c}$$

$$W_\omega - \jmath\frac{P_\omega}{\omega} = k^2\mathcal{L}_\omega\left(\mathbf{J},\mathbf{J}\right) - \mathcal{L}_\omega\left(\nabla\cdot\mathbf{J},\nabla\cdot\mathbf{J}\right), \tag{4d}$$

with

$$\mathcal{L}_\mathrm{rad}\left(\mathbf{U},\mathbf{V}\right) = \frac{1}{4\pi\epsilon\omega^2}\int\limits_{\Omega'}\int\limits_{\Omega} \mathbf{U}\left(\mathbf{r}\right)\cdot\mathbf{V}^*\left(\mathbf{r}'\right)\mathrm{e}^{-\jmath kR}\,\mathrm{d}\mathbf{r}\,\mathrm{d}\mathbf{r}', \tag{5a}$$

$$\mathcal{L}_\omega\left(\mathbf{U},\mathbf{V}\right) = \frac{1}{4\pi\epsilon\omega}\int\limits_{\Omega'}\int\limits_{\Omega} \frac{\partial\left(\mathbf{U}\left(\mathbf{r}\right)\cdot\mathbf{V}^*\left(\mathbf{r}'\right)\right)}{\partial\omega}\frac{\mathrm{e}^{-\jmath kR}}{R}\,\mathrm{d}\mathbf{r}\,\mathrm{d}\mathbf{r}', \tag{5b}$$

in which $R = \|\mathbf{r} - \mathbf{r}'\|$ is the Euclidean distance, ϵ is the vacuum permittivity, and $*$ denotes complex conjugation. The detailed derivation of the above relations is described in [32].

The Q_X in (3) and Q_Z in (1) are Q factors of an untuned antenna [1] and thus they will be denoted as Q_X^untuned and Q_Z^untuned in the rest of the paper. One can, however, tune the antenna to its resonance at angular frequency ω_0 by a reactive lumped element. Then, the Q factors of tuned antenna will be denoted as Q_X^tuned and Q_Z^tuned, and they can be evaluated as [32]

$$Q_X^\mathrm{tuned} = \omega_0\frac{2\max\left\{W_\mathrm{m},W_\mathrm{e}\right\} + W_\mathrm{rad} + W_\omega}{2\left(P_\mathrm{m} - P_\mathrm{e}\right)}, \tag{6a}$$

$$Q_Z^\mathrm{tuned} = \left|Q_R + \jmath Q_X^\mathrm{tuned}\right|. \tag{6b}$$

Note that tuning by purely reactive elements leaves the Q_R factor unchanged.

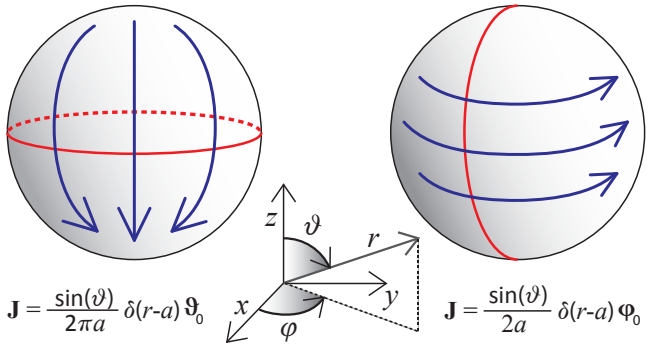

Fig. 1. Sketch of modal currents on a sphere of radius a: dipole mode (TM_{10}) on the left and loop mode (TE_{10}) on the right. The input current is normalized with respect to the red contours. The coordinate system considered throughout the paper is depicted in the middle of the figure.

III. Complex power and the Q_Z of the TM_{10} mode

Let us consider the TM_{10} mode, which is described by the current density

$$\mathbf{J} = \frac{\sin(\vartheta)}{2\pi a}\delta(r-a)\,\boldsymbol{\vartheta}_0 \tag{7}$$

flowing on a spherical shell of radius a situated in a vacuum, where δ is the Dirac delta and $\boldsymbol{\vartheta}_0$ is the unit vector co-directional with ϑ, see Fig. 1. The current density (7) is normalized so that the current flowing through the x-y plane is $I_0 = 1\mathrm{A}$. The corresponding charge density is

$$\rho = \jmath\frac{\cos(\vartheta)}{\omega\pi a^2}\delta(r-a). \tag{8}$$

The vector and scalar potentials of the TM_{10} mode are (see appendix A)

$$A_\vartheta = -\frac{\jmath\mu}{2\pi ka}\sin(\vartheta)\left(2\mathrm{h}_1^{(2)}(ka)\,\mathrm{j}_1(ka) + \left(\mathrm{h}_1^{(2)}(ka) - ka\,\mathrm{h}_0^{(2)}(ka)\right)\left(\mathrm{j}_1(ka) - ka\,\mathrm{j}_0(ka)\right)\right) \tag{9}$$

and

$$\varphi = \frac{\omega\mu}{\pi k}\mathrm{h}_1^{(2)}(ka)\,\mathrm{j}_1(ka)\cos(\vartheta), \tag{10}$$

where j_n and $\mathrm{h}_n^{(2)} = \mathrm{j}_n - \jmath\mathrm{y}_n$ are the spherical Bessel and Hankel functions of the nth order [36]. Substituting the potentials into (4a) and (4b) leads to

$$P_\mathrm{m} = \frac{4}{6\pi}Z_0\left(2\mathrm{j}_1^2(ka) + \left(\mathrm{j}_1(ka) - ka\,\mathrm{j}_0(ka)\right)^2\right), \tag{11a}$$

$$P_\mathrm{e} = \frac{4}{3\pi}Z_0\mathrm{j}_1^2(ka), \tag{11b}$$

$$\omega W_\mathrm{m} = -\frac{4}{6\pi}Z_0\Big(2\mathrm{y}_1(ka)\,\mathrm{j}_1(ka) + \left(\mathrm{y}_1(ka) - ka\,\mathrm{y}_0(ka)\right)\left(\mathrm{j}_1(ka) - ka\,\mathrm{j}_0(ka)\right)\Big), \tag{11c}$$

$$\omega W_\mathrm{e} = -\frac{4}{3\pi}Z_0\mathrm{y}_1(ka)\,\mathrm{j}_1(ka), \tag{11d}$$

where $Z_0 = \sqrt{\mu/\epsilon}$ is the free space impedance. Note here that the distribution (7) does not vary with the frequency, $\partial\mathbf{J}(\vartheta)/\partial\omega = 0$, and thus from (4d) we have

$$P_\omega = \omega W_\omega = 0. \tag{12}$$

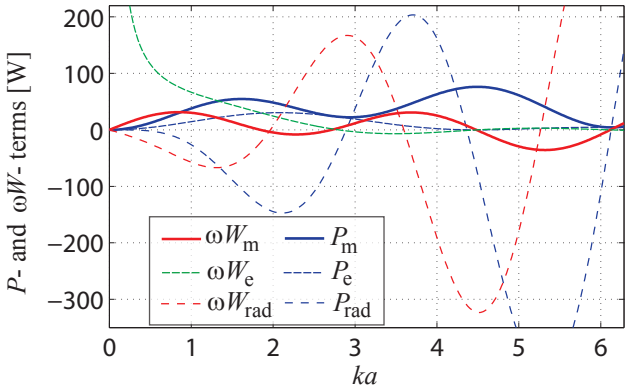

Fig. 2. The radiated power terms P_m and P_e, the reactive power terms ωW_m and ωW_e, and the power terms associated with radiation P_rad and ωW_rad for the TM_{10} mode.

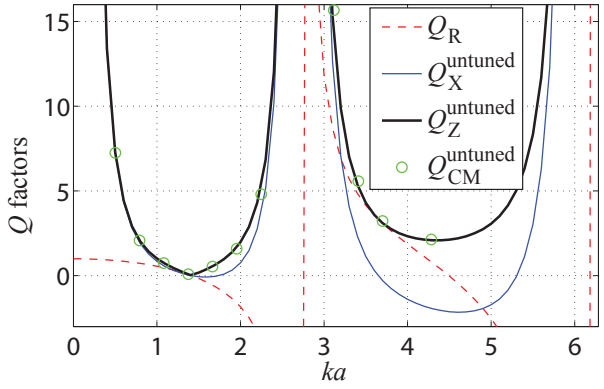

Fig. 3. Comparison of the Q_Z^untuned, its parts Q_R and Q_X^untuned, and verification against characteristic modes for the TM_{10} mode. Both Q_R and Q_X^untuned can be negative. They can be interpreted only according to (1).

Finally, by comparing (1) with (2) and (3), and using (12), we can deduce that

$$P_\mathrm{rad} = ka\frac{\partial(P_\mathrm{m} - P_\mathrm{e})}{\partial ka} - (P_\mathrm{m} + P_\mathrm{e}), \tag{13a}$$

$$\omega W_\mathrm{rad} = ka\frac{\partial\omega(W_\mathrm{m} - W_\mathrm{e})}{\partial ka} - \omega(W_\mathrm{m} + W_\mathrm{e}). \tag{13b}$$

The above expressions have been simplified in Mathematica [37] and evaluated in Matlab [38], and the results are depicted in Fig. 2.

We now turn to a brief discussion of the Q_R, Q_X^untuned and Q_Z^untuned of the TM_{10} mode which are depicted in Fig. 3. First of all, both Q_R and Q_X^untuned can be negative. This means that the standalone Q_X^untuned cannot be generally regarded as an estimation of the Q factor. The overall Q_Z^untuned is always non-negative thanks to the absolute value in (1). It reaches zero at $ka = \sqrt{2}$, and the first maximum is located at $ka \approx 2.7437$, where $W_\mathrm{m} - W_\mathrm{e} = 0$. Interestingly, the results in Fig. 3 can be verified by implementing the characteristic modes [39]. The characteristic current distribution of the TM_{10} mode is the same as (7), except for a constant which ensures the unitary radiated power [40]. The inherence of the frequency dependent constant is eliminated by setting $P_\omega = \omega W_\omega = 0$

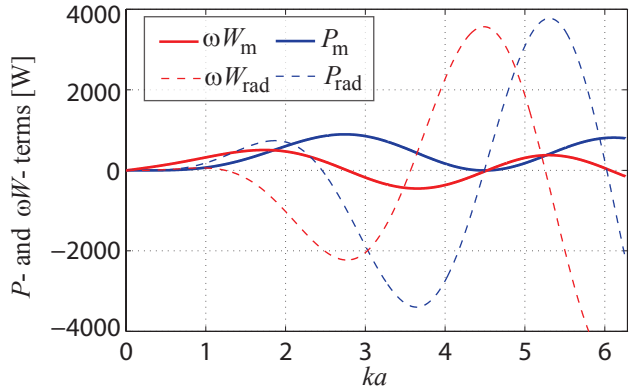

Fig. 4. The radiated power term P_{m}, the reactive power term ωW_{m}, and the power terms associated with radiation P_{rad} and ωW_{rad} for the TE_{10} mode.

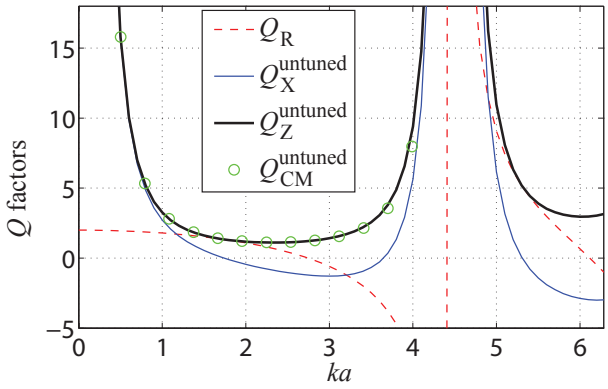

Fig. 5. Comparison of the Q_Z^{untuned}, its parts Q_R and Q_X^{untuned}, and verification against characteristic modes for the TE_{10} mode. Both Q_R and Q_X^{untuned} can be negative. They can be interpreted only according (1).

in postprocessing. Thus, after discretization of the sphere [41], preparation of the impedance matrix and solution of generalized eigenvalue problem in Matlab [42], we arrive at the modal current which was used for calculating (4a)–(4c). The Q_Z of the corresponding characteristic mode, $Q_{\mathrm{CM}}^{\mathrm{untuned}}$, is compared with Q_Z^{untuned} in Fig. 3. Checking the green circular markers, one can observe that the results are in excellent agreement with the analytical calculation.

IV. Complex power and the Q_Z of the TE_{10} mode

The procedure from the previous section can be used for the TE_{10} mode as well. In that case, the current density is

$$\mathbf{J} = \frac{\sin(\vartheta)}{2a}\delta(r-a)\,\boldsymbol{\varphi}_0, \tag{14}$$

where $\boldsymbol{\varphi}_0$ is the unit vector co-directional with φ, see Fig. 1. The current density is normalized so that the current flowing through the z-$(x>0)$ half-plane is $I_0 = 1\mathrm{A}$. The corresponding charge density vanishes, $\rho = 0$, and so

$$\varphi = 0, \tag{15a}$$
$$P_{\mathrm{e}} = 0, \tag{15b}$$
$$\omega W_{\mathrm{e}} = 0. \tag{15c}$$

Furthermore, as the current is frequency independent, (12)–(13b) are still valid. The vector potential is again found by the method described in appendix A, and is equal to

$$A_\varphi = -\frac{\jmath\mu}{2}\sin(\vartheta)\,ka\,\mathrm{j}_1(ka)\,\mathrm{h}_1^{(2)}(ka), \tag{16}$$

which leads to

$$P_{\mathrm{m}} = \frac{2\pi}{3}Z_0(ka)^2\,\mathrm{j}_1^2(ka), \tag{17a}$$
$$\omega W_{\mathrm{m}} = -\frac{2\pi}{3}Z_0(ka)^2\,\mathrm{j}_1(ka)\,\mathrm{y}_1(ka). \tag{17b}$$

All non-zero terms related to the TE_{10} mode are depicted in Fig. 4. Their behaviour is very similar to the TM_{10} case. An interesting point is located near $ka \approx 4.5$, where $P_{\mathrm{m}} = \omega W_{\mathrm{m}} = P_{\mathrm{rad}} = 0$ and thus only ωW_{rad} has a non-zero value.

The Q_Z^{untuned} and its parts Q_R and Q_X^{untuned} of the TE_{10} mode are depicted in Fig. 5. In spite of the fact that both Q_R and Q_X^{untuned} can be negative, the Q_Z^{untuned} is (thanks to the absolute value) always positive. Notwithstanding the absolute value, the Q_Z^{untuned} has continuous derivative in every point, except of the isolated singularities. As in the case of the TM_{10} mode, the results were verified by integrating the characteristic current and evaluating $Q_{\mathrm{CM}}^{\mathrm{untuned}}$, see the green circular markers in Fig. 5.

V. The limitations for ESA and asymptotic behaviour of the Q_Z factor for the TM_{10} and the TE_{10} mode

In this section, we will discuss the Q and the Q_Z factors for the spherical TM_{10} and TE_{10} modes that are tuned to its resonance at given ka by the external reactive lumped element. Particularly, the Q_Z^{tuned} obtained from (6b) is compared with the classical Chu's limit [2] Q_{Chu} (formula (8) in [5]), with the limit found by Hansen and Collin [12] Q_{HC} (formulas (9) and (12) of [12]) and with the recent limits found by Vandenbosh [18]. Note that within the context of this paper (with $P_\omega = \omega W_\omega = 0$) the quality factor used by Vandenbosh [18] is just the Q_X^{tuned}.

The results for the TM_{10} mode are depicted in Fig. 6, while the results for the TE_{10} mode are depicted in Fig. 7, with the ESA region highlighted. When making a comparison between the depicted results, it is important to remember that various Q definitions should only be compared in the region of high Q (approx. $Q > 3$), where the quality factor has its regular meaning – it is inversely proportional to FBW. Out of this region, the results are shown mostly for the sake of completeness (yielding the minimum $Q_Z^{\mathrm{tuned}} = 0.4851$ at $ka \approx 1.4756$ for the TM_{10} mode, and similarly the minimum $Q_Z = 0.9494$ at $ka \approx 2.2923$ for TE_{10} mode).

Having this restriction in mind, the agreement between Q_Z^{tuned}, Q_X^{tuned} and Q_{HC} can be denoted as excellent. On the other hand, the Chu's limit is clearly too optimistic and cannot be practically achieved due to the fact that Chu excluded the reactive power inside the bounding sphere. This

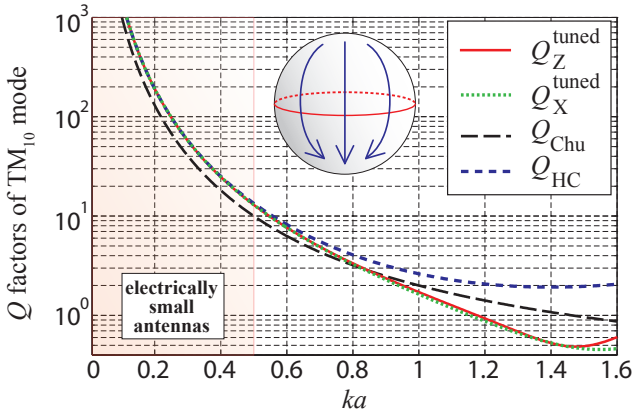

Fig. 6. Comparison of the Q and the Q_Z factors for the spherical TM_{10} mode: the Q_Z^{tuned} of this paper, the Q_{Chu} from [5], the Q_{HC} from [12] and Q_X^{tuned} of this paper which is equivalent to that of [18]. The electrically small antenna regime is highlighted.

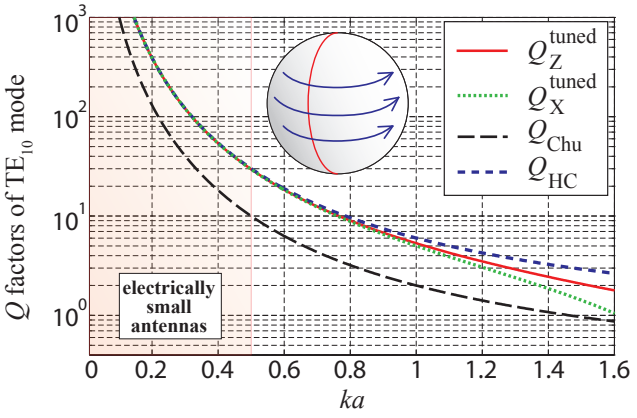

Fig. 7. Comparison of the Q and the Q_Z factors for the spherical TE_{10} mode: the Q_Z^{tuned} of this paper, the Q_{Chu} from [5], the Q_{HC} from [12] and Q_X^{tuned} of this paper which is equivalent to that of [18]. The electrically small antenna regime is highlighted.

is particularly significant in the case of the TE_{10} mode, which stores approximately one third of the total stored energy inside the sphere. It should be also noted that the TM_{10} mode for $ka \to 0$ behaves like the Hertzian dipole with $\omega W_{\mathrm{e}} \to \infty$ [43]. Conversely, the TE_{10} mode for $ka \to 0$ behaves like a small loop with $W_{\mathrm{m}} = L_{\mathrm{TE}}$, where L_{TE} is the self-inductance of the mode [44]. It is often of practical interest to define a power series expansion of the exact formulas, which simplifies the final expressions. Furthermore, the power series expansions are usually excellent approximations in the region of practical interest, i.e. the ESA region. As for the Q_R, Q_X^{tuned} and Q_Z^{tuned} factors derived in this paper, the power series read

$$Q_R = 1 - \frac{2}{5}(ka)^2 + \mathcal{O}(ka)^4, \tag{18a}$$

$$Q_X^{\mathrm{tuned}} = \frac{3}{2(ka)^3} + \frac{3}{5(ka)} - \frac{813ka}{1400} + \mathcal{O}(ka)^3, \tag{18b}$$

$$Q_Z^{\mathrm{tuned}} = Q_X^{\mathrm{tuned}} + \mathcal{O}(ka)^3, \tag{18c}$$

for the TM_{10} mode and

$$Q_R = 2 - \frac{(ka)^2}{5} + \mathcal{O}(ka)^4, \tag{19a}$$

$$Q_X^{\mathrm{tuned}} = \frac{3}{(ka)^3} + \frac{3}{ka} - \frac{174ka}{175} + \mathcal{O}(ka)^3, \tag{19b}$$

$$Q_Z^{\mathrm{tuned}} = Q_X^{\mathrm{tuned}} + \mathcal{O}(ka)^3, \tag{19c}$$

for the TE_{10} mode. For both modes, the Q_Z^{tuned} is almost identical to Q_X^{tuned} for $ka \to 0$), since $Q_X^{\mathrm{tuned}} \gg Q_R$, see Fig. 3 and Fig. 5. For comparison we also present power series of the classical Chu's limit [2] in the version of [5] which reads

$$Q_{\mathrm{Chu}} = \frac{1}{(ka)^3} + \frac{1}{ka}, \tag{20}$$

(note that this expansion is an exact formula) and the power series of Q_{HC} of the TM_{10} mode [12] which reads

$$Q_{\mathrm{HC}} \approx \frac{3}{2(ka)^3} + \frac{1}{\sqrt{2}ka}. \tag{21}$$

Lastly, the Q_{HC} of the TE_{10} mode [12] reads

$$Q_{\mathrm{HC}} \approx 3Q_{\mathrm{Chu}}. \tag{22}$$

Comparing the above expressions, a good correspondence between (21), (18c) and (22), (19c) is now evident.

VI. On the Total Stored Energy of the TM_{10} and the TE_{10} Mode

We have enough information to go back and recall the classical definition of the radiation Q factor, which is inspired by [5] and try to apply it to the Q_Z as

$$Q_Z^{\mathrm{untuned}} \equiv \frac{\omega\widetilde{W}}{P_{\mathrm{m}} - P_{\mathrm{e}}}, \tag{23}$$

in which $\widetilde{W}$ can be thought as an analogy to the classical time-averaged stored energy. Seeking for the proper meaning of (20), we compare definitions (1) and (20) and directly obtain

$$\widetilde{W} = \frac{\left|P_{\mathrm{m}} + P_{\mathrm{e}} + P_{\mathrm{rad}} + P_{\omega} + \jmath\omega\left(W_{\mathrm{m}} + W_{\mathrm{e}} + W_{\mathrm{rad}} + W_{\omega}\right)\right|}{2\omega}. \tag{24}$$

To verify (24), we investigate the behaviour of the numerator and the denominator of (20) for the TM_{10} and the TE_{10} modes, see Fig. 8 and Fig. 9. The interesting observation is that the $\widetilde{W}$ is constant for $ka \gg 1$. The product of $\omega\widetilde{W}$ correlates with the physical nature of the TM_{10} and the TE_{10} modes: while ωW_{m} for the TM_{10} mode starts from positive infinity (and reaches zero at $ka = \sqrt{2}$), the ωW_{m} for the TE_{10} mode starts from zero.

The asymptotic behaviour for $ka \gg 1$ can be characterized by $\widetilde{W} = 40a/c_0$ for the TM_{10} mode and by $\widetilde{W} = 40\pi^2 a/c_0$ for the TE_{10} mode, see Fig. 8 and Fig. 9. Considering the excellent agreement between all presented results (e.g. the positions of internal/external resonances, the value of the Q_Z for small arguments of ka), it is evident what P- and W-terms are essential for the proper Q_Z definition and how the $\widetilde{W}$ is established. The interesting extrema are depicted in Table I.

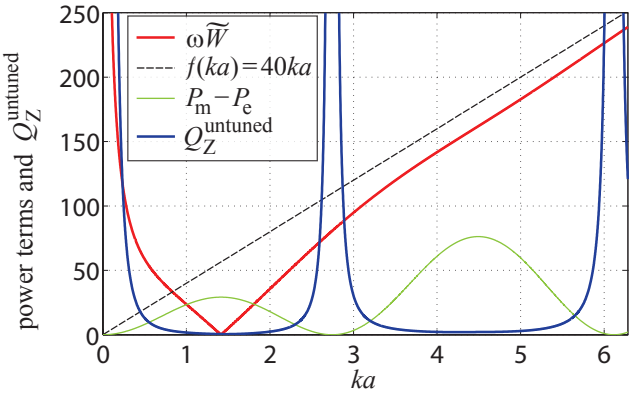

Fig. 8. Study of the asymptotic behaviour of the product $\omega\widetilde{W}$ of the TM_{10} mode that forms the numerator of Q_Z^{untuned}.

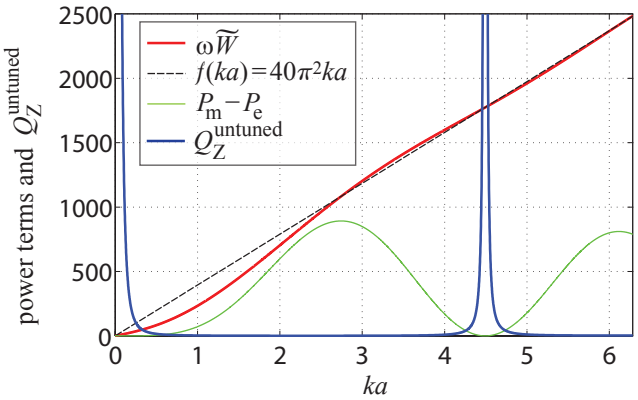

Fig. 9. Study of the asymptotic behaviour of the product $\omega\widetilde{W}$ of the TE_{10} mode that forms the numerator of Q_Z^{untuned}.

Notice also $ka > 0$ where the $Q_Z \to \infty$, which are the internal resonances of a PEC spherical cavity [34].

The presented results indirectly verify the hypothesis that the radiated energy travels in the radial direction at the speed of light from the antenna sphere to the far-field region, since they are in good accordance with the separation methods [5], [6], in which the speed of light is assumed for outgoing energy. Thus, the alternative concepts [45] seem not to be valid.

VII. Conclusion

The potential theory has been employed to obtain the measurable quality factor Q_Z of important spherical current distributions, particularly of the fundamental TM and TE modes. It has been shown that the presented approach is effective, leading to unique and finite energy terms with the far-field extraction implicitly included. For the presented cases of the spherical coordinate system, the Q_Z was obtained in closed form for any ka. The fundamental lower limit of the Q_Z of electrically small antennas was then obtained by series expansion of these expressions for small ka. Excellent agreement with the previous work of Thal and Hansen has been observed.

Although the proposed approach has been presented on spherical modes, it is not restricted to them, and can also easily be extended to other separable coordinate systems. In this respect, the elliptic coordinates may be of considerable interest, as they can closely match the shape of many realistic antennas. The lower bounds of the Q_Z obtained in this way would then represent practically oriented limits for antenna designers. Another challenge is to investigate the the Q_Z of the dual mode case.

	TM_{10}		TE_{10}	
	value	ka	value	ka
$W_{\text{m}} - W_{\text{e}}$	0	2.7437	0	2.7983
$P_{\text{m}} - P_{\text{e}}$	0	2.7437	0	4.4934
$\min\limits_{ka}\{Q_Z^{\text{untuned}}\}$	0	$\sqrt{2}$	1.1098	2.3323
$\min\limits_{ka}\{Q_Z^{\text{tuned}}\}$	0.4851	1.4756	0.9494	2.2923
$\min\limits_{ka}\{\omega\widetilde{W}\}$	0	$\sqrt{2}$	0	0

TABLE I
Comparison of some important parameters related to the limits of the measurable Q_Z factor. The values were found from the analytical equations processed in Mathematica.

Appendix A
Vector and Scalar Potentials of the TM_{10} and TE_{10} Mode

The vector and scalar potentials are found by the expansion method of appendix B. For the particular case of the TM_{10} and the TE_{10} modes, we obtain the corresponding vector and scalar potentials regular for $r = [0, \infty)$ by using (36a)–(36c) with $\mathbf{a} = \mathbf{z}_0$, $\psi_{00} = \text{z}_0(kr)$ for $\mathbf{M}$-, $\mathbf{N}$-terms and with $\psi_{10} = \text{z}_1(kr)\cos(\vartheta)$ for $\mathbf{L}$-terms, where $\text{z}_n(x)$ is a spherical Bessel function of order n and where we will use $\text{z}_n(x) = \text{j}_n(x)$ for $r < a$ and $\text{z}_n = \text{h}_n^{(2)}$ for $r > a$. The resulting vector wave functions read

$$\mathbf{M}_{10} = \boldsymbol{\varphi}_0 k\,\text{z}_1(kr)\sin(\vartheta)\,, \tag{25a}$$

$$\mathbf{N}_{10} = \mathbf{r}_0\frac{2}{r}\text{z}_1(kr)\cos(\vartheta) + \boldsymbol{\vartheta}_0\frac{1}{r}\left(\text{z}_1(kr) - kr\,\text{z}_0(kr)\right)\sin(\vartheta)\,, \tag{25b}$$

$$\mathbf{L}_{10} = \mathbf{r}_0\frac{1}{r}\left(\text{z}_1(kr) - kr\,\text{z}_2(kr)\right)\cos(\vartheta) - \boldsymbol{\vartheta}_0\frac{1}{r}\text{z}_1(kr)\sin(\vartheta)\,. \tag{25c}$$

The vector potential of the TM_{10} mode will be expressed as a linear combination of (25b) and (25c) because of the non-vanishing charge density and the need for the $\mathbf{L}_{10}$-term. The vector potential of the TE_{10} mode will be expressed in terms of (25a) only, since there is no charge density and thus no scalar potential.

According to the above, in order to find the vector and the scalar potential of the TM_{10} mode, we choose

$$\left.\begin{aligned}\mathbf{A} &= C_1\mathbf{N}_{10} + D_1\mathbf{L}_{10},\\ \varphi &= -\jmath\omega D_1\psi_{10}\end{aligned}\right\} r < a \tag{26a}$$

$$\left.\begin{aligned}\mathbf{A} &= C_2\mathbf{N}_{10} + D_2\mathbf{L}_{10},\\ \varphi &= -\jmath\omega D_2\psi_{10}\end{aligned}\right\} r > a, \tag{26b}$$

where C, D are constants to be determined. The $C_{1,2}$ can be determined from the boundary conditions on the current shell at $r = a$, i.e. by continuity of the tangential electric field $\mathbf{n}_0 \times (\mathbf{E}_1 - \mathbf{E}_2) = 0$ and discontinuity of the tangential magnetic field $\mathbf{n}_0 \times (\mathbf{H}_1 - \mathbf{H}_2) = \mathbf{K}$, where $\mathbf{K}$ is the surface current density and where the normal $\mathbf{n}_0$ points to the region 1, [35]. The boundary conditions lead to

$$C_1 = -\frac{\jmath\mu}{2\pi k}\left(\mathrm{h}_1^{(2)}(ka) - ka\,\mathrm{h}_0^{(2)}(ka)\right), \tag{27a}$$

$$C_2 = -\frac{\jmath\mu}{2\pi k}\left(\mathrm{j}_1(ka) - ka\,\mathrm{j}_0(ka)\right). \tag{27b}$$

For the unknown constants $D_{1,2}$ in (26a) and (26b), the only condition that needs to be satisfied is the wave equation for the scalar potential in the Lorentz gauge

$$\nabla^2\varphi + k^2\varphi = -\frac{\rho}{\epsilon}. \tag{28}$$

Choosing then the scalar potential being continuous at $r = a$, (28) dictates

$$\frac{\partial\varphi}{\partial r}\Big|_{r=a^+} - \frac{\partial\varphi}{\partial r}\Big|_{r=a^-} = -\jmath\frac{\cos(\vartheta)}{\omega\epsilon\pi a^2}, \tag{29}$$

which leads to

$$D_1 = \frac{\jmath\mu}{k\pi}\mathrm{h}_1^{(2)}(ka), \tag{30a}$$

$$D_2 = \frac{\jmath\mu}{k\pi}\mathrm{j}_1(ka). \tag{30b}$$

Putting all together we have for $r < a$

$$A_\vartheta = -\frac{\jmath\mu}{2\pi kr}\sin(\vartheta)\left(2\mathrm{h}_1^{(2)}(ka)\,\mathrm{j}_1(kr)\right. \tag{31a}$$

$$\left. + \left(\mathrm{h}_1^{(2)}(ka) - ka\,\mathrm{h}_0^{(2)}(ka)\right)\left(\mathrm{j}_1(kr) - kr\,\mathrm{j}_0(kr)\right)\right)$$

$$\varphi = \frac{\omega\mu}{\pi k}\mathrm{h}_1^{(2)}(ka)\,\mathrm{j}_1(kr)\cos(\vartheta), \tag{31b}$$

and for $r > a$

$$A_\vartheta = -\frac{\jmath\mu}{2\pi kr}\sin(\vartheta)\left(2\mathrm{h}_1^{(2)}(kr)\,\mathrm{j}_1(ka)\right. \tag{32a}$$

$$\left. + \left(\mathrm{h}_1^{(2)}(kr) - kr\,\mathrm{h}_0^{(2)}(kr)\right)\left(\mathrm{j}_1(ka) - ka\,\mathrm{j}_0(ka)\right)\right)$$

$$\varphi = \frac{\omega\mu}{\pi k}\mathrm{h}_1^{(2)}(kr)\,\mathrm{j}_1(ka)\cos(\vartheta), \tag{32b}$$

where the first terms in the vector potential come from $\mathbf{L}_{10}$ and the second terms come from $\mathbf{N}_{10}$.

The derivation of the scalar and vector potential of the TE_{10} mode is analogous to the above, and results in

$$A_\varphi = -\frac{\jmath\mu}{2}\sin(\vartheta)\,ka\,\mathrm{j}_1(kr)\,\mathrm{h}_1^{(2)}(ka) \tag{33a}$$

$$\varphi = 0, \tag{33b}$$

for $r < a$, and

$$A_\varphi = -\frac{\jmath\mu}{2}\sin(\vartheta)\,ka\,\mathrm{j}_1(ka)\,\mathrm{h}_1^{(2)}(kr) \tag{34a}$$

$$\varphi = 0, \tag{34b}$$

for $r < a$.

APPENDIX B
EXPANSION OF THE VECTOR WAVE EQUATION IN SEPARABLE SYSTEMS

In this appendix, we recall the expansion of the vector wave equation and point out some aspects important for a consistent definition of Q. This approach leads to the analytical calculation of the Q factor for the separable systems.

According to [46], the general solution of $\nabla^2\mathbf{A} + k^2\mathbf{A} = 0$ can be written as

$$\mathbf{A} = \sum_n \left(\alpha_n\mathbf{M}_n + \beta_n\mathbf{N}_n + \gamma_n\mathbf{L}_n\right), \tag{35}$$

where

$$\mathbf{M}_n = \nabla\times(\mathbf{a}\psi_n), \tag{36a}$$

$$\mathbf{N}_n = \frac{1}{k}\nabla\times\mathbf{M}_n, \tag{36b}$$

$$\mathbf{L}_n = \nabla\psi_n, \tag{36c}$$

$\mathbf{a}$ is a constant vector, and scalar function ψ_n satisfies

$$\nabla^2\psi_n + k^2\psi_n = 0. \tag{37}$$

The conventional notation from [47] is used for clarity of the paper.

Taking now the vector field $\mathbf{A}$ as a magnetic vector potential in the Lorentz gauge, one can verify that the scalar potential is

$$\varphi = -\frac{1}{\jmath\omega\epsilon\mu}\nabla\cdot\mathbf{A} = -\jmath\omega\sum_n\gamma_n\psi_n, \tag{38}$$

where μ is the permeability of the vacuum, and that the field quantities read

$$\mathbf{E} = -\frac{\jmath\omega}{k^2}\left(\nabla\nabla\cdot\mathbf{A} + k^2\mathbf{A}\right) = -\jmath\omega\sum_n\left(\alpha_n\mathbf{M}_n + \beta_n\mathbf{N}_n\right), \tag{39a}$$

$$\mathbf{H} = \frac{1}{\mu}\nabla\times\mathbf{A} = \frac{k}{\mu}\sum_n\left(\alpha_n\mathbf{N}_n + \beta_n\mathbf{M}_n\right), \tag{39b}$$

where we used the fact that $\nabla\times\mathbf{N}_m = k\mathbf{M}_n$.

It is worth noting that any measurable quantity is independent of $\mathbf{L}_n$-terms (which is equivalent to gauge invariance). Particularly, if a volume is chosen so that it contains all the sources and if the vector potential (35) is divided as $\mathbf{A} = \mathbf{A}^{M,N} + \mathbf{A}^L$, with $\mathbf{A}^{M,N}$ belonging to $\mathbf{M}_n$-, $\mathbf{N}_n$-terms and $\mathbf{A}^L$ belonging to $\mathbf{L}_n$-terms, then, one can easily realize that

$$\int_\Omega\left(\mathbf{A}^L\cdot\mathbf{J}^* - \varphi\rho^*\right)\mathrm{d}\mathbf{r} = 0, \tag{40}$$

and thus that only the $\mathbf{M}_n$-, $\mathbf{N}_n$-terms participate in the definition of the complex power [35]

$$\jmath\omega\int_\Omega\left(\mathbf{A}\cdot\mathbf{J}^* - \varphi\rho^*\right)\mathrm{d}\mathbf{r} = \jmath\omega\int_\Omega\left(\mathbf{A}^{M,N}\cdot\mathbf{J}^*\right)\mathrm{d}\mathbf{r}. \tag{41}$$

ACKNOWLEDGEMENT

The authors would like to thank Dr. Zdenek Hradecky for his encouragement and unremitting support.

REFERENCES

[1] J. L. Volakis, C.-C. Chen, and K. Fujimoto, *Survey of Small Antenna Theory*, 1st ed., ser. Small Antennas: Miniaturization Techniques & Applications. McGraw-Hill, 2010.

[2] L. J. Chu, "Physical limitations of omni-directional antennas," *J. Appl. Phys.*, vol. 19, pp. 1163–1175, 1948.

[3] H. A. Wheeler, "The radiansphere around a small antenna," *Proc. of IRE*, vol. 47, no. 8, pp. 1325–1331, 1959.

[4] R. F. Harrington, "Effects of antenna size on gain, bandwidth, and efficiency," *J. Nat. Bur. Stand.*, vol. 64-D, pp. 1–12, 1960.

[5] R. E. Collin and S. Rothschild, "Evaluation of antenna Q," *IEEE Trans. Antennas Propag.*, vol. 12, pp. 23–27, 1964.

[6] J. S. McLean, "A re-examination of the fundamental limits on the radiation Q of electrically small antennas," *IEEE Trans. Antennas Propag.*, vol. 44, no. 5, pp. 672–675, May 1996.

[7] G. A. Thiele, P. T. Detweiler, and R. P. Penno, "On the lower bound of the radiation Q for electrically small antennas," *IEEE Trans. Antennas Propag.*, vol. 51, no. 6, pp. 1263–1269, June 2003.

[8] D. R. Rhodes, "On the stored energy of planar apertures," *IEEE Trans. Antennas Propag.*, vol. 14, no. 6, pp. 676–684, Nov. 1966.

[9] H. L. Thal, "New radiation Q limits for spherical wire antennas," *IEEE Trans. Antennas Propag.*, vol. 54, no. 10, pp. 2757–2763, Oct. 2006.

[10] ——, "Comments on A New Chu Formula for Q"," *IEEE Antennas Propag. Magazine*, vol. 52, no. 1, pp. 214–215, Feb. 2010.

[11] ——, "Q bounds for arbitrary small antennas: A circuit approach," *IEEE Trans. Antennas Propag.*, vol. 60, no. 7, pp. 3120–3128, July 2012.

[12] R. C. Hansen and R. E. Collin, "A new Chu formula for Q," *IEEE Antennas Propag. Magazine*, vol. 51, no. 5, pp. 38–41, Oct. 2009,

[13] T. V. Hansen, O. S. Kim, and O. Breinbjerg, "Stored energy and quality factor of spherical wave functions – in relation to spherical antennas with material cores," *IEEE Trans. Antennas Propag.*, vol. 60, no. 3, pp. 1281–1290, March 2012.

[14] R. L. Fante, "Quality factor of general ideal antennas," *IEEE Trans. Antennas Propag.*, vol. 17, no. 2, pp. 151–157, 1969.

[15] O. S. Kim, "Minimum Q electrically small antennas," *IEEE Trans. Antennas Propag.*, vol. 60, no. 8, pp. 3551–3558, Aug. 2012.

[16] M. Gustafsson and S. Nordebo, "Optimal antenna currents for Q, superdirectivity, and radiation patterns using convex optimization," *IEEE Trans. Antennas Propag.*, vol. 61, no. 3, pp. 1109–1118, March 2013.

[17] M. Capek, P. Hazdra, and J. Eichler, "A method for the evaluation of radiation Q based on modal approach," *IEEE Trans. Antennas Propag.*, vol. 60, no. 10, pp. 4556–4567, Oct. 2012.

[18] G. A. E. Vandenbosch, "Reactive energies, impedance, and Q factor of radiating structures," *IEEE Trans. Antennas Propag.*, vol. 58, no. 4, pp. 1112–1127, Apr. 2010.

[19] Y. Geyi, "A method for the evaluation of small antenna Q," *IEEE Trans. Antennas Propag.*, vol. 51, no. 8, pp. 2124–2129, Aug. 2003.

[20] G. A. E. Vandenbosch, "Radiators in time domain, part I: Electric, magnetic, and radiated energies," *IEEE Trans. Antennas Propag.*, vol. 61, no. 8, pp. 3995–4003, Aug. 2013.

[21] D. R. Rhodes, "Observable stored energies of electromagnetic systems," *J. Franklin Inst.*, vol. 302, no. 3, pp. 225–237, 1976.

[22] M. Gustafsson, C. Sohl, and G. Kristensson, "Physical limitations on antennas of arbitrary shape," *Proc. of Royal Soc. A: Math., Phys. and Engineering Sciences*, vol. 463, pp. 2589–2607, 2007.

[23] M. Gustafsson and B. L. G. Jonsson. Stored electromagnetic energy and antenna Q. eprint arXiv: 1211.5521. [Online]. Available: http://adsabs.harvard.edu/abs/2012arXiv1211.5521G

[24] G. A. E. Vandenbosch and V. Volski, "Lower bounds for radiation Q of very small antennas of arbitrary topology," in *Proceedings of the 4th European Conference on Antennas and Propagation (EUCAP)*, Barcelona, Spain, April 2010, pp. 1–4.

[25] S. R. Seshadri, "Resonances of a spherical antenna," in *Radio Science Meeting (USNC-URSI NRSM)*, 2013.

[26] ——, "Constituents of power of an electric dipole of finite size," *J. Opt. Soc. Am. A*, vol. 25, no. 3, pp. 805–810, March 2008.

[27] Sievenpiper, D. F., et al., "Exprerimental validation of performance limits and design guidelines for small antennas," *IEEE Trans. Antennas Propag.*, vol. 60, no. 1, pp. 8–19, Jan. 2012.

[28] S. R. Best and D. L. Hanna, "A performance comparison of fundamental small-antenna designs," *IEEE Antennas Propag. Magazine*, vol. 52, no. 1, pp. 47–70, Feb. 2010.

[29] S. R. Best, "The radiation properties of electrically small folded spherical helix antennas," *IEEE Trans. Antennas Propag.*, vol. 52, no. 4, pp. 953–960, April 2004.

[30] O. S. Kim and O. Breinbjerg, "Reaching the chu lower bound on Q with magnetic dipole antennas using a magnetic-coated PEC core," *IEEE Trans. Antennas Propag.*, vol. 59, no. 8, pp. 2799–2805, Aug. 2011.

[31] A. D. Yaghjian and S. R. Best, "Impedance, bandwidth and Q of antennas," *IEEE Trans. Antennas Propag.*, vol. 53, no. 4, pp. 1298–1324, April 2005.

[32] M. Capek, L. Jelinek, P. Hazdra, and J. Eichler, "The measurable Q factor and observable energies of radiating structures," *IEEE Trans. Antennas Propag.*, vol. 62, no. 1, pp. 311–318, Jan. 2014.

[33] P. M. Morse and H. Feshbach, *Methods of Theoretical Physics*. McGraw-Hill, 1953.

[34] R. F. Harrington, *Time-Harmonic Electromagnetic Fields*, 2nd ed. John Wiley - IEEE Press, 2001.

[35] J. D. Jackson, *Classical Electrodynamics*, 3rd ed. John Wiley, 1998.

[36] A. Jeffrey and H.-H. Dai, *Handbook of Mathematical Formulas and Integrals*, 4th ed. Academic Press, 2008.

[37] Wolfram. Mathematica. [Online]. Available: http://www.wolfram.com/mathematica/

[38] The MathWorks. The Matlab. [Online]. Available: www.mathworks.com

[39] R. F. Harrington and J. R. Mautz, "Computation of characteristic modes for conducting bodies," *IEEE Trans. Antennas Propag.*, vol. 19, no. 5, pp. 629–639, Sept. 1971.

[40] R. J. Garbacz, "A generalized expansion for radiated and scattered fields," Ph.D. dissertation, The Ohio State Univ., 1968.

[41] S. M. Rao, D. R. Wilton, and A. W. Glisson, "Electromagnetic scattering by surfaces of arbitrary shape," *IEEE Trans. Antennas Propag.*, vol. 30, no. 3, pp. 409–418, May 1982.

[42] M. Capek, P. Hamouz, P. Hazdra, and J. Eichler, "Implementation of the Theory of Characteristic Modes in Matlab," *IEEE Antennas Propag. Magazine*, vol. 55, no. 2, pp. 176–189, April 2013.

[43] S. A. Schelkunoff and H. T. Friis, *Antennas: Theory and Practice*. John Wiley, 1952.

[44] C. R. Paul, *Inductance: Loop and Partial*. John Wiley, 2010.

[45] W. A. Davis, T. Yang, E. D. Caswell, and W. L. Stutzman, "Fundamental limits on antenna size: A new limit," *IET Microw. Antennas Propag.*, vol. 5, no. 11, pp. 1297–1302, Aug. 2011.

[46] W. W. Hansen, "A new type of expansion in radiation problems," *Phys. Rev.*, vol. 47, no. 2, pp. 139–143, Jan. 1935.

[47] J. A. Stratton, *Electromagnetic Theory*. John Wiley - IEEE Press, 2007.

Miloslav Capek (S'09) received the M.Sc. degree in electrical engineering from the Czech Technical University, Prague, Czech Republic, in 2009, and is currently working towards a Ph.D. degree in electromagnetic fields at the same University.

His research interests are in the area of electromagnetic theory, electrically small antennas, numerical techniques, fractal geometry and optimization.

Lukas Jelinek received the Ph.D. degree from the Czech Technical University in Prague, Prague, Czech Republic, in 2006.

Currently, he is a researcher with the Department of Electromagnetic Field, CTU-FEE. His main fields of interest include wave propagation in complex media, general field theory, and numerical techniques. His recent research interest is in metamaterials, specifically resonant ring systems.

Pavel Hazdra (M'03) received the M.Sc. and Ph.D. degrees in electrical engineering from the Czech Technical University in Prague, Faculty of Electrical Engineering in 2003 and 2009, respectively.

He is a research and teaching assistant with the Department of Electromagnetic Field, CTU-FEE. His research interests are in the area of electromagnetic theory, computational electromagnetics, fractal geometry, planar antennas and special prime-feed antennas.

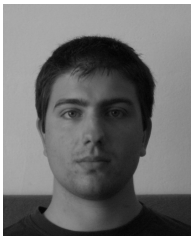

Jan Eichler received the M.Sc. degrees in electrical engineering from the Czech Technical University in Prague in 2010. He is currently working towards a Ph.D. degree at the same University.

His research interests include modal methods for antenna design and connecting them with full-wave methods. He is also interested in developing and simulating active antennas.

A Scheme for Stored Energy Evaluation and a Comparison with Contemporary Techniques

Miloslav Capek, *Member, IEEE,* Lukas Jelinek, Guy A. E. Vandenbosch, *Fellow, IEEE,* and Pavel Hazdra, *Member, IEEE*

***Abstract*—This paper treats the old problem of defining and understanding stored electromagnetic energy. Three different concepts for evaluating the stored energy and the radiation Q factor of an antenna are introduced. The first two use time harmonic quantities and are based on the work of Vandenbosch and Yaghjian. The third concept is a time-domain method which aims to deliver the true stored energy. The concepts are discussed and compared on the basis of examples of varying complexity, including evaluation of Q factors for non-radiating lumped RLC circuits and a canonical dipole radiator. It is shown that all three concepts unite for special cases of parallel and series RLC circuits. For other (even very simple) circuits, the approaches yield significantly different results.**

***Index Terms*—Antenna theory, electromagnetic theory, electrically small antennas, Q factor.**

I. Introduction

In physics, an oscillating system is commonly characterized [1] by its oscillation frequency and quality factor Q, which is a quantity giving a measure of the lifetime of its free oscillations. In antenna design, the need to determine a radiation Q factor comes from a belief that the Q factor is inversely proportional to the intrinsic antenna bandwidth, seen at the input port [2]. The Q factor is traditionally defined as the ratio between the stored energy and the lost energy per cycle. For antennas, the lost energy does not pose any problem and may be evaluated as the sum of the radiated energy and the energy dissipated due to material losses [3]. Unfortunately, in a non-stationary electromagnetic field associated with radiators, the definition of stored (non-propagating) electric and magnetic energies, and consequently a proper determination of the radiation Q factor, presents a problem that has not yet been fully solved [4]. The issue of the stored energy has, in fact, deep roots, see e.g. [5], and can be traced back to the formulation of Poynting's theorem both in the time domain [6] and the frequency domain [7].

Both the operational bandwidth and the radiated power of an antenna system [8] are indeed always finite. A physically meaningful stored energy must thus also be finite. Many authors have addressed the problem of the definition of stored energies, either directly or indirectly, through the antenna bandwidth. Most attempts have been performed in the domain of time harmonic fields. Collin and Rothschild [9] proposed to subtract the energy density associated with the radial energy flowing from an antenna (propagating energy) from the total energy density. It is well known that such subtraction leads to good results for a few canonical systems, [9]–[11]. Starting from this point of view, Vandenbosch recently [12] generalized the expressions of Geyi for very small structures [13] and derived expressions that implement the concept of radiated energy density subtraction for an arbitrary antenna shape. The resulting energy is then finite, since the expressions only involve a finite volume of the radiator. In [14] it was shown that far-field energy density subtraction is naturally present in the complex Poynting's theorem. However, it is already known [15] that these expressions fail under certain conditions (giving negative values for certain current distributions) and this approach therefore also remains incomplete [16].

The problem of stored energy has seldom been addressed directly in the time domain. Nevertheless, there are some interesting works dealing with time-dependent energies. Shlivinski [17], [18] expanded the fields into spherical waves, a technique also often used in the frequency domain [9], [19]. Collarday [20] proposed a brute force technique utilizing FDTD. In [21], Vandenbosch derived expressions for electric and magnetic energies in the time domain and proved [22] that these relations are equivalent to his expressions derived in the frequency domain [12].

A different approach to the determination of Q utilizes circuit theory and Fosters reactance theorem [3]. The antenna is reduced to a lossy series or parallel resonant circuit, and Q is based on the frequency derivative of the input reactance [23] or the total input impedance [24]. The total input impedance is in fact an a priori postulated definition of radiation Q, which yields an extremely good approximation for available fractional bandwidth. Thanks to this property, the resultant measurable Q factor is widely used in practical applications [25], [26]. Recently, the concept of complex power has been utilized to transform this definition of Q into a function of potentials and currents, or even into a function of currents flowing on an antenna only [27].

In this paper, three definitions of the radiation Q factor are compared and the issue of the related stored energies is closely investigated. The first definition is based on the time harmonic expressions of Vandenbosch [12]. The second definition uses

Manuscript received September 10, 2013; revised November 20, 2013. This work was supported by the COST LD 12055 AMTAS (Advanced Modeling and Technologies for Antennas and Sensors) action, by the COST IC1102 (VISTA) and by the Grant Agency of the Czech Republic under project 13-09086S.

M. Capek, L. Jelinek and P. Hazdra are with the Department of Electromagnetic Field, Faculty of Electrical Engineering, Czech Technical University in Prague, Technicka 2, 16627, Prague, Czech Republic (e-mail: miloslav.capek@fel.cvut.cz).

G. A. E. Vandenbosch is with the Department of Electrical Engineering, Division ESAT-TELEMIC (Telecommunications and Microwaves), Katholieke Universiteit Leuven, B-3001, Leuven, Belgium (e-mail: guy.vandenbosch@esat.kuleuven.be).

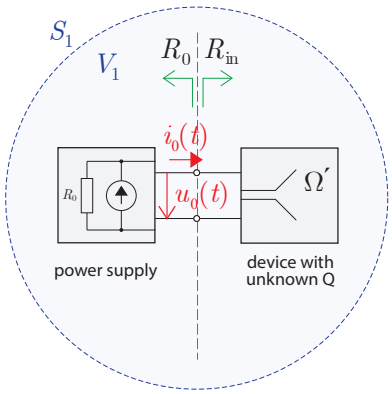

Fig. 1. A device with unknown Q that is fed by a shielded power supply with internal resistance R_0. Without loss of generality, the device is assumed to be tuned to its resonance.

the input impedance approximation, as introduced by Yaghjian in [24]. The third definition is based on a novel line of reasoning in the time domain, which will be developed further in this paper. The working out of all the three concepts starts solely from the currents flowing on an antenna, which are usually given as a result in modern EM simulators. This opens challenging possibilities of modal analysis [28] and optimization [29]. The concepts are discussed and compared on the basis of examples of varying complexity, which are numerically solved.

The paper is organized as follows. Section II introduces the two different concepts of Q that are based on electromagnetic energies, both in the frequency and in the time domain. Then, in section III the Q factor derived from the input impedance is formulated in terms of currents on an antenna. The following two sections present numerical examples. Section IV treats non-radiating circuits, and section V deals with the half-wavelength dipole, one of the most basic radiating devices. The paper is concluded in section VI.

II. Energy Concept of Q

In the context of energy, the quality factor is most commonly defined as

$$Q = \langle \mathcal{Q}(t) \rangle = 2\pi \frac{\langle \mathcal{W}_{\text{sto}}(t) \rangle}{W_{\text{lost}}} = 2\pi \frac{W_{\text{sto}}}{W_{\text{lost}}}, \tag{1}$$

where a time-harmonic steady state with angular frequency ω_0 is assumed, with $\mathcal{W}_{\text{sto}}(t)$ as the electromagnetic stored energy, $\langle \mathcal{W}_{\text{sto}}(t) \rangle = W_{\text{sto}}$ as the cycle mean of $\mathcal{W}_{\text{sto}}(t)$ and W_{lost} as the lost electromagnetic energy during one cycle [7]. Following the font convention introduced above, calligraphic font will from now on be used for quantities defined in the time domain, while normal font will be used for frequency domain quantities.

A typical Q-measurement scenario is depicted in Fig. 1, which shows an antenna fed by the shielded power source. The antenna input impedance in the time-harmonic steady state at frequency ω_0 seen by the source is R_{in} (the antenna is tuned to its resonance). Assuming that the antenna is made of conductors with ideal non-dispersive conductivity σ and lossless non-dispersive dielectrics, we can state that the lost energy during one cycle, needed for (1), can be evaluated as

$$W_{\text{lost}} = \int_{\alpha}^{\alpha+T} i_0(t)\, u_0(t)\, \mathrm{d}t = \frac{\pi}{\omega_0} R_{\text{in}} I_0^2 = W_{\text{r}} + W_{\sigma}, \tag{2}$$

in which R_{in} is the input resistance of the tuned antenna, I_0 is the amplitude of $i_0(t)$, see Fig. 1, W_{r} is the radiation loss and W_{σ} is the energy lost in one cycle via conduction. The part W_{σ} of (2) can be calculated as

$$W_{\sigma} = \frac{\pi}{\omega_0} \int_{\Omega'} \sigma \|\mathbf{E}(\mathbf{r}', \omega_0)\|^2 \, \mathrm{d}\mathbf{r}', \tag{3}$$

with $\mathbf{r}' \in \Omega'$, Ω' being the shape of the antenna and $\mathbf{E}$ being the time-harmonic electric field intensity under the convention $\boldsymbol{\mathcal{E}}(t) = \Re\{\mathbf{E}(\omega)\, \mathrm{e}^{\jmath\omega t}\}$. At the same time, the near-field of the antenna [30] contains stored energy $\mathcal{W}_{\text{sto}}(t)$, which is bound to the sources and does not escape from the antenna towards infinity. In the following subsections, the stored energy will be evaluated via the power balance [3].

A. Stored energy in the time domain

Imagine a spherical volume V_1, see Fig. 1, centered around the system, the radius of which is large enough to lie in a far-field region [30]. The total electromagnetic energy content of the sphere (it also contains heat W_{σ}) is

$$\mathcal{W}(V_1, t) = \mathcal{W}_{\text{sto}}(t) + \mathcal{W}_{\text{r}}(V_1, t), \tag{4}$$

in which $\mathcal{W}_{\text{r}}(V_1, t)$ is the energy contained in the radiation fields that have already escaped from the sources. Imagine now that the power source was switched on at $t = -\infty$, bringing the system into a steady state and then switched off at $t = t_{\text{off}}$. For $t \in [t_{\text{off}}, \infty)$ the system will be in a transient state, during which all the energy $\mathcal{W}(V_1, t_{\text{off}})$ will either be changed into heat at resistor R_0 and the antenna's conductors or radiated through the bounding envelope S_1. Explicitly, Poynting's theorem [3] states that

$$\begin{aligned} \mathcal{W}(V_1, t_{\text{off}}) = {} & R_0 \int_{t_{\text{off}}}^{\infty} i_{\text{R}_0}^2(t)\, \mathrm{d}t \\ & + \int_{t_{\text{off}}}^{\infty} \int_{\Omega'} \boldsymbol{\mathcal{E}}(\mathbf{r}', t) \cdot \boldsymbol{\mathcal{J}}(\mathbf{r}', t)\, \mathrm{d}\mathbf{r}'\, \mathrm{d}t \\ & + \int_{t_{\text{off}}}^{\infty} \oint_{S_1} \boldsymbol{\mathcal{E}}_{\text{far}}(\mathbf{r}, t) \times \boldsymbol{\mathcal{H}}_{\text{far}}(\mathbf{r}, t) \cdot \mathrm{d}\mathbf{S}_1\, \mathrm{d}t, \end{aligned} \tag{5}$$

in which $\mathbf{r}' \in \Omega'$ points into the source region and $\mathbf{r} \in S_1$ points into the far-field region.

As a special, but important, example let us assume a radiating device made exclusively of perfect electric conductors

(PEC). In such case, the far-field can be written as [7]

$$\boldsymbol{\mathcal{H}}_{\mathrm{far}}\left(\mathbf{r},t\right)=-\frac{1}{4\pi c_0}\int\limits_{\Omega'}\frac{\mathbf{n}_0\times\dot{\boldsymbol{\mathcal{J}}}\left(\mathbf{r}',t'\right)}{R}\,\mathrm{d}\mathbf{r}', \tag{6a}$$

$$\boldsymbol{\mathcal{E}}_{\mathrm{far}}\left(\mathbf{r},t\right)=-\frac{\mu}{4\pi}\int\limits_{\Omega'}\frac{\dot{\boldsymbol{\mathcal{J}}}\left(\mathbf{r}',t'\right)-\left(\mathbf{n}_0\cdot\dot{\boldsymbol{\mathcal{J}}}\left(\mathbf{r}',t'\right)\right)\mathbf{n}_0}{R}\,\mathrm{d}\mathbf{r}' \tag{6b}$$

and

$$\boldsymbol{\mathcal{H}}_{\mathrm{far}}\left(\mathbf{r},t\right)=\frac{\mathbf{n}_0\times\boldsymbol{\mathcal{E}}_{\mathrm{far}}\left(\mathbf{r},t\right)}{Z_0}, \tag{7}$$

in which c_0 is the speed of light, Z_0 is the free space impedance, $\mathbf{r}'\in\Omega'$, $R=\|\mathbf{r}-\mathbf{r}'\|$, $\mathbf{n}_0=\left(\mathbf{r}-\mathbf{r}'\right)/R$, $t'=t-R/c_0$ is the retarded time, and where a dot represents a derivative with respect to time argument, i.e.

$$\dot{\boldsymbol{\mathcal{J}}}\left(\mathbf{r}',t'\right)=\left.\frac{\partial\boldsymbol{\mathcal{J}}\left(\mathbf{r}',\tau\right)}{\partial\tau}\right|_{\tau=t'}. \tag{8}$$

Since we are in the far-field, we can further write [8] $R\approx r$ for amplitudes, $R\approx r-\mathbf{r}_0\cdot\mathbf{r}'$ for time delays (phase) and then $\mathbf{n}_0\approx\mathbf{R}/R=\mathbf{r}_0$, where $r=\|\mathbf{r}\|$. Using (6a)–(7) and the above-mentioned approximations, the last term in (5) can be written as

$$\begin{aligned}&\int\limits_{t_{\mathrm{off}}}^{\infty}\oint\limits_{S_1}\boldsymbol{\mathcal{E}}_{\mathrm{far}}\left(\mathbf{r},t\right)\times\boldsymbol{\mathcal{H}}_{\mathrm{far}}\left(\mathbf{r},t\right)\cdot\mathbf{r}_0\,\mathrm{d}S_1\,\mathrm{d}t\\&=\frac{1}{Z_0}\int\limits_{t_{\mathrm{off}}}^{\infty}\oint\limits_{S_1}\left\|\boldsymbol{\mathcal{E}}_{\mathrm{far}}\left(\mathbf{r},t\right)\right\|^2\mathrm{d}S_1\,\mathrm{d}t\\&=\frac{\mu^2}{Z_0\left(4\pi\right)^2}\int\limits_{t_{\mathrm{off}}}^{\infty}\int\limits_0^{\pi}\int\limits_0^{2\pi}\left\|\int\limits_{\Omega'}\left(\dot{\boldsymbol{\mathcal{J}}}\left(\mathbf{r}',t'\right)\right.\right.\\&\quad\left.\left.-\left(\mathbf{r}_0\cdot\dot{\boldsymbol{\mathcal{J}}}\left(\mathbf{r}',t'\right)\right)\mathbf{r}_0\right)\mathrm{d}\mathbf{r}'\right\|^2\sin\theta\,\mathrm{d}\varphi\,\mathrm{d}\theta\,\mathrm{d}t,\end{aligned} \tag{9}$$

where $t'=t-r/c_0+\mathbf{r}_0\cdot\mathbf{r}'/c_0$. Using (5) and (9) we are thus able to find the total electromagnetic energy inside S_1.

Note here that the electromagnetic energy content of the sphere could also be found as

$$\mathcal{W}\left(V_1,t_{\mathrm{off}}\right)=\frac{1}{2}\int\limits_{V_1}\left(\mu\left\|\boldsymbol{\mathcal{H}}\left(\mathbf{r},t_{\mathrm{off}}\right)\right\|^2+\epsilon\left\|\boldsymbol{\mathcal{E}}\left(\mathbf{r},t_{\mathrm{off}}\right)\right\|^2\right)\mathrm{d}\mathbf{r} \tag{10}$$

which could seem to be simpler than the above-mentioned scheme. The simplicity is, however, only formal. The main disadvantage of (10) is that the integration volume includes also the near-field region, where the fields are rather complex (and commonly singular). Also, the radius of the sphere plays an important role in (10) unlike in (9), where it appears only via a static time shift r/c_0. In fact, it will be shown later that this dependence can be completely eliminated in the calculation of stored energy.

In order to obtain the stored energy $\mathcal{W}_{\mathrm{sto}}\left(t_{\mathrm{off}}\right)$ inside S_1 we, however, need to know the radiation content of the sphere at $t=t_{\mathrm{off}}$. Expression (9) suggests a simple way to get it. To

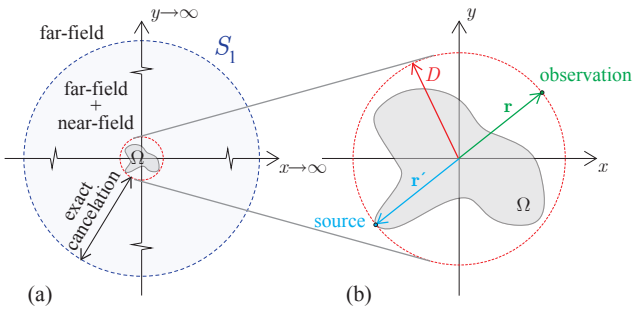

Fig. 2. Sketch of the far-field cancelation.

that point, imagine that during the calculation of $\mathcal{W}\left(V_1,t_{\mathrm{off}}\right)$ we were capturing the time course of the current at every point $\boldsymbol{\mathcal{J}}\left(\mathbf{r}',t\right)$ and we are afterwards able to use it as a source (impressed sources in a vacuum with no actual radiator Ω'). This allows us to exactly mimic the radiation of an actual radiator and even more. Imagine, having $\boldsymbol{\mathcal{J}}\left(\mathbf{r}',t\right)$ as impressed sources that we can change at our will, that for $t>t_{\mathrm{off}}$ we will set $\boldsymbol{\mathcal{J}}\left(\mathbf{r}',t\right)=\boldsymbol{\mathcal{J}}\left(\mathbf{r}',t_{\mathrm{off}}\right)$. Expression (9) then claims that for $t<t_{\mathrm{off}}$ the current was radiating as in the original problem, but for $t>t_{\mathrm{off}}$ the radiation was instantly stopped (without producing any transient observable in the far-field). So, if we now evaluate (9) over the new currents, it will give exactly the radiation energy $\mathcal{W}_{\mathrm{r}}\left(V_1,t_{\mathrm{off}}\right)$. Subtracting it from $\mathcal{W}\left(V_1,t_{\mathrm{off}}\right)$ we obtain the stored electromagnetic energy $\mathcal{W}_{\mathrm{sto}}\left(t_{\mathrm{off}}\right)$ and averaging over one period we obtain the cycle mean stored energy

$$\left\langle\mathcal{W}_{\mathrm{sto}}\left(t_{\mathrm{off}}\right)\right\rangle=\frac{1}{T}\int\limits_{\alpha}^{\alpha+T}\mathcal{W}_{\mathrm{sto}}\left(t_{\mathrm{off}}\right)\,\mathrm{d}t_{\mathrm{off}}. \tag{11}$$

With respect to the freezing of the current, it is important to realize that this could mean an indefinite accumulation of charge at a given point. However, this operation has to be seen as performed on the impressed sources, which can be chosen freely.

When subtracting the radiated energy from the total energy, it is important to realize that for $t<t_{\mathrm{off}}$ the currents in both situations were the same. Thus defining $D=\max\{\|\mathbf{r}'\|\}$, we can state that for $t<t_{\mathrm{off}}+\left(r-D\right)/c_0$ the integrals (9) will exactly cancel during the subtraction, see Fig. 2. Relation (9) can thus be safely evaluated only for $t'=t-2D/c_0+\mathbf{r}_0\cdot\mathbf{r}'/c_0$ (worst case scenario depicted in Fig. 2b), which means that the currents need to be saved only for $t>t_{\mathrm{off}}-2D/c_0$. It is very important to realize that this is equivalent to saying that, after all, the bounding sphere S_1 does not need to be situated in the far field. It is enough (and computationally advantageous) if it just encloses the radiator, the rest of the far-field is anyhow cancelled, see Fig. 2a.

B. Stored Energy in Frequency Domain

By analogy with the previous section, the complex Poynting's theorem will now be used to evaluate the stored energy in the frequency domain. Particularly, the theorem states [7]

that

$$-\frac{1}{2}\int\limits_{\Omega'}\mathbf{E}\cdot\mathbf{J}^{*}\,\mathrm{d}\mathbf{r}'=P_{\mathrm{m}}-P_{\mathrm{e}}+\jmath\omega\left(W_{\mathrm{m}}-W_{\mathrm{e}}\right)=P_{\mathrm{in}},\quad(12)$$

in which P_{in} is the complex power, the terms P_{m} and P_{e} form the radiated power, $P_{\mathrm{r}}=P_{\mathrm{m}}-P_{\mathrm{e}}$, and $\omega\left(W_{\mathrm{m}}-W_{\mathrm{e}}\right)$ is the reactive net power. In can be shown [27] that

$$P_{\mathrm{in}}=\frac{\jmath\omega}{2}\int\limits_{\Omega'}\left(\mathbf{A}\cdot\mathbf{J}^{*}-\varphi\rho^{*}\right)\mathrm{d}\mathbf{r}',\quad(13)$$

in which $\mathbf{A}$ is the vector and φ is the scalar potential, and ρ is the charge density. Consequently, one may presume that based on (12) and (13) and using the radiation integrals for vector and scalar potentials [30], the magnetic and electric energies can be defined as [27]

$$W_{\mathrm{m}}-\jmath\frac{P_{\mathrm{m}}}{\omega}=k^{2}\mathcal{L}\left(\mathbf{J},\mathbf{J}\right)\quad(14)$$

and

$$W_{\mathrm{e}}-\jmath\frac{P_{\mathrm{e}}}{\omega}=\mathcal{L}\left(\nabla\cdot\mathbf{J},\nabla\cdot\mathbf{J}\right),\quad(15)$$

where the bilinear functional

$$\mathcal{L}\left(\mathbf{U},\mathbf{V}\right)=\frac{1}{8\pi\epsilon\omega^{2}}\int\limits_{\Omega'}\int\limits_{\Omega'}\mathbf{U}\left(\mathbf{r}_{1}'\right)\cdot\mathbf{V}^{*}\left(\mathbf{r_{2}}'\right)\frac{\mathrm{e}^{-\jmath kR}}{R}\,\mathrm{d}\mathbf{r}_{1}'\,\mathrm{d}\mathbf{r}_{2}',\quad(16)$$

has been defined, in which $k=\omega/c_{0}$ is the wavenumber, $\mathbf{r}_{1,2}'\in\Omega'$, $R=\|\mathbf{r}_{1}'-\mathbf{r}_{2}'\|$, and where only the electric currents $\mathbf{J}$ flowing in a vacuum are assumed. Unfortunately, the above-mentioned separation of magnetic and electric energy has a physical meaning only in the case when the displacement current vanishes [31], and is thus valid only for quasistatic fields [32].

Some attempts have been undertaken to define the separated energies even for non-stationary cases [33]. One such contribution suffered from extensive criticism [34], [35], mainly due to the variance of the separated energies under the gauge transformations. This issue was recently attacked in [12] by using analytical and coordinate independent subtraction of the radiation field. The presumably correct magnetic and electric energies read [12]

$$\widetilde{W}_{\mathrm{m}}=W_{\mathrm{m}}+\frac{W_{\mathrm{rad}}}{2},\quad(17a)$$

$$\widetilde{W}_{\mathrm{e}}=W_{\mathrm{e}}+\frac{W_{\mathrm{rad}}}{2},\quad(17b)$$

where the particular term

$$W_{\mathrm{rad}}=-\Im\left\{k\left(k^{2}\mathcal{L}_{\mathrm{rad}}\left(\mathbf{J},\mathbf{J}\right)-\mathcal{L}_{\mathrm{rad}}\left(\nabla\cdot\mathbf{J},\nabla\cdot\mathbf{J}\right)\right)\right\}\quad(18)$$

is associated with the radiation field, and where

$$\mathcal{L}_{\mathrm{rad}}\left(\mathbf{U},\mathbf{V}\right)=\frac{1}{8\pi\epsilon\omega^{2}}\int\limits_{\Omega'}\int\limits_{\Omega'}\mathbf{U}\left(\mathbf{r}_{1}'\right)\cdot\mathbf{V}^{*}\left(\mathbf{r}_{2}'\right)\mathrm{e}^{-\jmath kR}\,\mathrm{d}\mathbf{r}_{1}'\,\mathrm{d}\mathbf{r}_{2}'\quad(19)$$

and it is claimed [12] that $\widetilde{W}_{\mathrm{sto}}=\widetilde{W}_{\mathrm{m}}+\widetilde{W}_{\mathrm{e}}$ is the stored energy W_{sto}. This, however, cannot be completely correct, since it was shown [15] that $\widetilde{W}_{\mathrm{sto}}$ can be negative. We thus have to conclude that the stored energy defined by the frequency domain concept [12], $\widetilde{W}_{\mathrm{sto}}$, can only be approximately equal to the true stored energy W_{sto}, i.e.

$$\widetilde{W}_{\mathrm{sto}}\approx W_{\mathrm{sto}},\quad(20)$$

and then by analogy with (1)

$$\widetilde{Q}=2\pi\frac{\widetilde{W}_{\mathrm{sto}}}{W_{\mathrm{lost}}}=2\pi\frac{\widetilde{W}_{\mathrm{m}}+\widetilde{W}_{\mathrm{e}}}{W_{\mathrm{lost}}}\approx Q\quad(21)$$

is defined.

III. Fractional bandwidth concept of Q

It well-known that for $Q\gg1$, the Q factor is approximately proportional to the (fractional) bandwidth, FBW:

$$Q_{Z}\approx\frac{\chi}{\mathrm{FBW}},\quad(22)$$

where χ is a given constant and $\mathrm{FBW}=(\omega^{+}-\omega^{-})/\omega_{0}$. The Q factor, which is known to fulfil (22), was found by Yaghjian [24] utilizing an analogy with RLC circuits [36] and using the transition from conductive to VSWR bandwidth. Its explicit definition reads

$$Q_{Z}=\frac{\omega}{2\,\Re\{P_{\mathrm{in}}\}}\left|\frac{\partial P_{\mathrm{in}}}{\partial\omega}\right|=\left|Q_{R}+\jmath Q_{X}\right|,\quad(23)$$

where the total input current at the antenna's port is normalized, e.g. to $I_{0}=1\mathrm{A}$.

The differentiation of the complex power in the form (13) can be used to find the source definition of (23), and leads to [27]

$$Q_{R}=\frac{P_{\mathrm{m}}+P_{\mathrm{e}}+P_{\mathrm{rad}}+P_{\omega}}{2\left(P_{\mathrm{m}}-P_{\mathrm{e}}\right)},\quad(24a)$$

$$Q_{X}=\frac{\omega\left(W_{\mathrm{m}}+W_{\mathrm{e}}+W_{\mathrm{rad}}+W_{\omega}\right)}{2\left(P_{\mathrm{m}}-P_{\mathrm{e}}\right)},\quad(24b)$$

in which

$$P_{\mathrm{rad}}=\Re\left\{\omega k\left(k^{2}\mathcal{L}_{\mathrm{rad}}\left(\mathbf{J},\mathbf{J}\right)-\mathcal{L}_{\mathrm{rad}}\left(\nabla\cdot\mathbf{J},\nabla\cdot\mathbf{J}\right)\right)\right\},\quad(25a)$$

$$W_{\omega}-\jmath\frac{P_{\omega}}{\omega}=k^{2}\mathcal{L}_{\omega}\left(\mathbf{J},\mathbf{J}\right)-\mathcal{L}_{\omega}\left(\nabla\cdot\mathbf{J},\nabla\cdot\mathbf{J}\right)\quad(25b)$$

with $\mathcal{L}_{\mathrm{rad}}$ expressed by (19) and

$$\mathcal{L}_{\omega}\left(\mathbf{U},\mathbf{V}\right)=\frac{1}{8\pi\epsilon\omega}\int\limits_{\Omega'}\int\limits_{\Omega'}\frac{\partial\mathbf{U}\left(\mathbf{r}_{1}'\right)\cdot\mathbf{V}^{*}\left(\mathbf{r}_{2}'\right)}{\partial\omega}\frac{\mathrm{e}^{-\jmath kR}}{R}\,\mathrm{d}\mathbf{r}_{1}'\,\mathrm{d}\mathbf{r}_{2}'.\quad(26)$$

As particular cases of (24a) and (24b), we obtain Rhodes' definition of the Q factor as $|Q_{X}|$, and Vandenbosch's definition (21) as Q_{X} with omission W_{ω} from (24b).

For the purposes of this paper, we can observe from (1), (23), (24a) and (24b) that the stored energy in the case of the FBW concept is equivalent to

$$W_{\mathrm{sto}}^{Z}\equiv\frac{1}{2}\left|\frac{\partial P_{\mathrm{in}}}{\partial\omega}\right|=\frac{\left|P_{\mathrm{m}}+P_{\mathrm{e}}+P_{\mathrm{rad}}+P_{\omega}+\jmath\omega\left(W_{\mathrm{m}}+W_{\mathrm{e}}+W_{\mathrm{rad}}+W_{\omega}\right)\right|}{4},\quad(27)$$

but remark here that (27) was not intended to be stored energy [24].

IV. NON-RADIATING CIRCUITS

Previous sections have defined three generally different concepts of stored energy, namely $W_{\rm sto}$, $\widetilde{W}_{\rm sto}$ and $W^{Z}_{\rm sto}$. Since $W_{\rm lost}$ is uniquely defined, we can advantageously use the corresponding dimensionless quality factors Q, $\widetilde{Q}$ and Q_Z for comparing them, which is done for non-radiating circuits in this section, and for radiating systems in the following section. Particularly, in this section, we assume a passive lossy but non-dispersive and non-radiating one-port, and the three concepts of Q factors are investigated in the following subsections.

A. Time domain stored energy for lumped elements

Following the general procedure of Section II-A, imagine a general RLC circuit that was for $t \in (-\infty, t_{\rm off})$ fed by a time harmonic source (current or voltage) $s(t) = \sin(\omega_0 t)$ and was afterwards switched off for $t \in [t_{\rm off}, \infty)$. Since the circuit is non-radiating, the total energy $\mathcal{W}(V_1, t_{\rm off})$ is directly equal to $\mathcal{W}_{\rm sto}(t_{\rm off})$. Furthermore, choosing properly the voltage (or current) source for a given circuit we can eliminate the internal resistance of the source and we are thus left with

$$W_{\rm sto} = \sum_k \frac{R_k}{T} \int_{\alpha}^{\alpha+T} \int_{t_{\rm off}}^{\infty} i^2_{{\rm R},k}(t)\, {\rm d}t\, {\rm d}t_{\rm off}, \tag{28}$$

where $i_{{\rm R},k}(t)$ is the transient current in the k-th resistor.

The currents $i_{{\rm R},k}$ are advantageously evaluated in the Fourier domain. The Fourier transform of the source reads [37]

$$\begin{aligned} S(\omega) = {} & \frac{\jmath\pi}{2}\left(\delta(\omega+\omega_0) - \delta(\omega-\omega_0)\right) \\ & + \frac{{\rm e}^{-\jmath\omega t_{\rm off}}}{2}\left(\frac{{\rm e}^{\jmath\omega t_{\rm off}}}{\omega-\omega_0} - \frac{{\rm e}^{-\jmath\omega t_{\rm off}}}{\omega+\omega_0}\right). \end{aligned} \tag{29}$$

We can then write $I_{{\rm R},k}(\omega) = T_{{\rm R}_k}(\omega)\, S(\omega)$, where $T_{{\rm R}_k}(\omega)$ is the transfer function. Then

$$\begin{aligned} i_{{\rm R},k}(t) = {} & \frac{1}{2\pi}\int_{-\infty}^{\infty} T_{{\rm R}_k}(\omega)\, S(\omega)\, {\rm e}^{\jmath\omega t}\, {\rm d}\omega \\ = {} & \frac{1}{2}\Im\left\{T_{{\rm R}_k}(\omega_0)\, {\rm e}^{\jmath\omega_0 t}\right\} \\ & + \frac{\omega_0}{4\pi}\int_{-\infty}^{\infty} T_{{\rm R}_k}(\omega)\left(\frac{{\rm e}^{\jmath\omega_0 t_{\rm off}}}{\omega-\omega_0} - \frac{{\rm e}^{-\jmath\omega_0 t_{\rm off}}}{\omega+\omega_0}\right){\rm e}^{\jmath\omega(t-t_{\rm off})}\, {\rm d}\omega. \end{aligned} \tag{30}$$

As the studied circuit is lossy, the $T_{{\rm R}_k}(\omega)$ has no poles on the real ω-axis and the second integral can be evaluated by standard contour integration in the complex plane of ω along a semi-circular contour in the upper ω half-plane omitting points $\omega = \pm\omega_0$. The result of the contour integration for $t > t_{\rm off}$ can be written as

$$\begin{aligned} i_{{\rm R},k}(t) = \frac{\jmath}{2}\sum_m \operatorname*{res}_{\omega\to\omega_{m,k}} \Bigg\{ & T_{{\rm R}_k}(\omega)\Big(\frac{{\rm e}^{\jmath\omega_0 t_{\rm off}}}{\omega-\omega_0} \\ & - \frac{{\rm e}^{-\jmath\omega_0 t_{\rm off}}}{\omega+\omega_0}\Big){\rm e}^{\jmath\omega(t-t_{\rm off})}\Bigg\}, \end{aligned} \tag{31}$$

where $\omega_{m,k}$ are the poles of $T_{{\rm R}_k}(\omega)$ with $\Im\{\omega_{m,k} > 0\}$. Substituting (31) into (28) gives the mean stored energy. It is also important to realize that in this case both integrations in (28) can easily be performed analytically. It can be shown that the result is identical to the cycle mean of the classical definition of stored energy

$$\mathcal{W}_{\rm sto}(t_{\rm off}) = \frac{1}{2}\left(\sum_m L_m i^2_{{\rm L},m}(t_{\rm off}) + \sum_n C_n u^2_{{\rm C},n}(t_{\rm off})\right), \tag{32}$$

which is the lumped circuit form of (10), with $i_{{\rm L},m}(t)$ being the current in the m-th inductor and $u_{{\rm C},n}(t)$ being the voltage on the n-th capacitor.

B. Frequency domain stored energy for lumped elements

Without the radiation ($P_{\rm rad} = 0, \omega W_{\rm rad} = 0$), the cycle mean of (10), which is also equal to cycle mean (32), is identical to the frequency domain expression

$$\begin{aligned} \widetilde{W}_{\rm sto} = W_{\rm m} + W_{\rm e} = {} & \frac{1}{4}\sum_m L_m |I^2_{{\rm L},m}| + \sum_n C_n |U^2_{{\rm C},n}| \\ = {} & \frac{1}{4}\int_{\Omega'} \left(\mu\|\mathbf{H}^2\| + \epsilon\|\mathbf{E}^2\|\right) {\rm d}\mathbf{r}', \end{aligned} \tag{33}$$

where $W_{\rm m}$ and $W_{\rm e}$ are defined by (14) and (15). We thus conclude that for non-radiating circuits $W_{\rm sto} = \widetilde{W}_{\rm sto}$ and $Q = \widetilde{Q}$.

C. Frequency domain stored energy for lumped elements from FBW concept

In order to evaluate (23), the same procedure as in the derivation of Foster's reactance theorem [3] can be employed (keeping in mind the unitary input current and assuming non-zero conductivity), leading to

$$\begin{aligned} & W^{\rm FBW}_{\rm sto} \\ & = \left|\frac{\jmath}{4}\int_{\Omega'} \left(\mu\|\mathbf{H}^2\| + \epsilon\|\mathbf{E}^2\|\right) {\rm d}\mathbf{r}' + \frac{\sigma}{2}\int_{\Omega'} \mathbf{E}^* \cdot \frac{\partial \mathbf{E}}{\partial \omega}\, {\rm d}\mathbf{r}'\right| \\ & = \frac{1}{4}\left|\sum_m L_m |I^2_{{\rm L},m}| + \sum_n C_n |U^2_{{\rm C},n}| - 2\jmath \sum_k R_k I^*_{{\rm R},k}\frac{\partial I_{{\rm R},k}}{\partial \omega}\right|, \end{aligned} \tag{34}$$

in which $I_{{\rm R},k}$ is the amplitude of the current through the k-th resistor. The above formula clearly reveals a fundamental difference between $W_{\rm sto}$ and $W^{Z}_{\rm sto}$, which is the last term on the RHS of (34). This means that $W^{Z}_{\rm sto}$ does not generally represent the time-averaged stored energy.

D. Results

In the previous sections we have shown that for non-radiating circuits there is no difference between the quality factors defined in the time domain (Q) and in the frequency domain ($\widetilde{Q}$). There is, however, a fundamental difference between Q and Q_Z, which will be presented in this section on two representative examples, depicted in Fig. 3. We do not explicitly consider simple series and parallel RLC circuits in

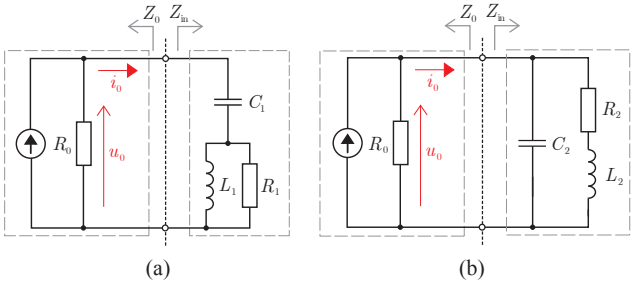

Fig. 3. Studied RLC circuits: (a) C_1 in series with parallel L_1 and R_1, and (b) C_2 in parallel with serial R_2 and L_2

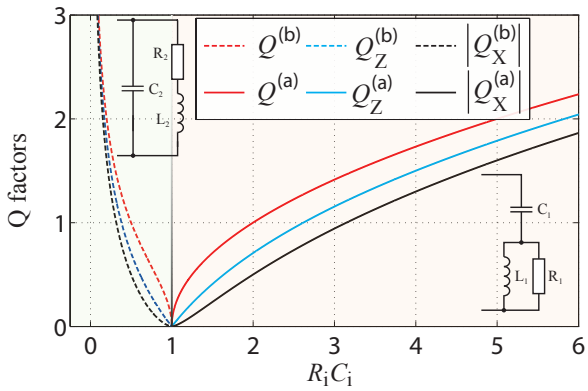

Fig. 4. The Q factors for the two particular lumped RLC circuits of Fig. 3. The curves correspond to $R_i/L_i = 1\,\mathrm{s}^{-1}$, where index i at the x-axis is $i \in \{1, 2\}$.

this paper, since the three definitions for stored energy and Q deliver exactly the same results, i.e. $Q = \omega_0 L/R = \omega_0 RC$. The reason is the frequency independence of the current flowing through the resistor (the series resonance circuit), or of the voltage on the resistor (the parallel resonance circuit) and thus the identically vanishing last term of (34). This fact is the very reason why the FBW approach works perfectly for radiators that can be approximated around resonance by a parallel or a series RLC circuit. However, it also means that for antennas that need to be approximated by other circuits, the approach may not deliver the correct energy and the corresponding quality factor. This is probably why this approach seems to fail for antennas with slightly separated resonances or wideband antennas.

In the case of the circuits depicted in Fig. 3, the input impedances are

$$Z_{\mathrm{in}}^{(a)} = \frac{1}{\jmath\omega C_1} + \frac{1}{\frac{1}{R_1} + \frac{1}{\jmath\omega L_1}}, \quad Z_{\mathrm{in}}^{(b)} = \frac{1}{\frac{1}{R_2+\jmath\omega L_2} + \jmath\omega C_2}, \tag{35}$$

and the corresponding resonance frequencies read

$$\omega_0^{(a)} = \frac{R_1}{L_1}\frac{1}{\sqrt{\frac{C_1 R_1^2}{L_1} - 1}}, \quad \omega_0^{(b)} = \frac{R_2}{L_2}\sqrt{\frac{L_2}{C_2 R_2^2} - 1}. \tag{36}$$

Utilizing the method from Sec. IV-A, it can be shown that the energy Q factors are

$$Q^{(a)} = \widetilde{Q}^{(a)} = \frac{R_1}{\omega_0^{(a)} L_1}, \quad Q^{(b)} = \widetilde{Q}^{(b)} = \frac{\omega_0^{(b)} L_2}{R_2}, \tag{37}$$

while the FBW Q factors are

$$Q_Z^{(a)} = \kappa^{(a)} Q^{(a)}, \quad Q_Z^{(b)} = \kappa^{(b)} Q^{(b)}, \tag{38}$$

where

$$\kappa^{(a)} = \frac{1}{\omega_0^{(a)}\sqrt{L_1 C_1}}, \quad \kappa^{(b)} = \omega_0^{(b)}\sqrt{L_2 C_2}. \tag{39}$$

For completeness' sake the Rhodes Q factors [23] are found to be

$$\left|Q_X^{(a)}\right| = \left(\kappa^{(a)}\right)^2 \mathcal{Q}^{(a)}, \quad \left|Q_X^{(b)}\right| = \left(\kappa^{(b)}\right)^2 \mathcal{Q}^{(b)}. \tag{40}$$

The comparison of the above-mentioned Q factors is depicted in Fig. 4, using parametrization by R_i/L_i and R_iC_i, where $i \in \{1, 2\}$. Circuit (a) in Fig. 3 is resonant for $R_1C_1 > L_1/R_1$, and circuit (b) in the same figure is resonant for $R_1C_1 < L_1/R_1$. It can be observed that the difference between the depicted Q factors decays with growing quality factor, finally vanishing for $Q \to \infty$. On the other hand, there are significant differences for $Q < 2$.

Therefore, we can conclude that for general RLC circuits made of lumped (non-radiating) elements

$$W_{\mathrm{sto}} \equiv \widetilde{W}_{\mathrm{sto}} \neq W_{\mathrm{sto}}^{Z} \Longrightarrow Q \equiv \widetilde{Q} \neq Q_Z. \tag{41}$$

V. Radiating Circuits

Evaluation of the Q factor for radiating circuits is far more involved than for non-radiating circuits. For this reason we present the results only for the canonical structure of a PEC infinitesimally thin-strip half-wave dipole [38] of length L and width $w = L/200$. The dipole radiates in a vacuum, is fed by a voltage source [30] placed in its centre and operates at its resonance. For the purpose of the following calculations, the dipole is centred in the Cartesian coordinate system with its axis coinciding with the z-axis.

The dipole was simulated in CST-MWS [39] with a voltage source (user-defined time signal) placed into a physical gap of length w, and the resulting surface current densities were exported into Matlab [40] for final post-processing, i.e. for (5), (9), (1) for time domain calculation. The dipole was enclosed in open boundaries at a distance of half of the resonance wavelength from the dipole.

To calculate $\widetilde{Q}$ by (14), (15), (18), (20) in the frequency domain, we used our in-house MoM solver [41] based on RWG functions [42] in Matlab. In this case, the dipole was fed by a delta gap in its centre (the input voltage corresponds to the input current $I_0 = 1\,\mathrm{A}$).

Calculation of the FBW Q factor (12), (23) was performed for both EM models described above (both in CST and in the MoM solver written in Matlab). The resultant input impedances of both simulations were compared to verify that the models are comparable. No significant differences were observed ($Z_{\mathrm{in}}^{\mathrm{CST}}(\omega_0) = 70.3\,\Omega$, $Z_{\mathrm{in}}^{\mathrm{Matlab}}(\omega_0) = 71.4\,\Omega$).

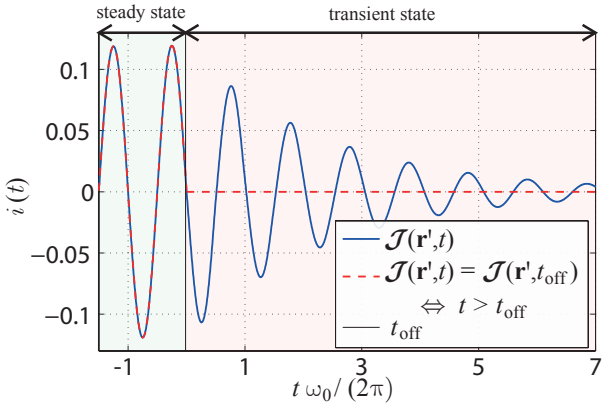

Fig. 5. Current flowing through the voltage gap. The blue line shows the steady state and the transient state for the original currents $\boldsymbol{\mathcal{J}}(\mathbf{r}', t)$, while the red line corresponds to the modified currents $\boldsymbol{\mathcal{J}}(\mathbf{r}', t) = \boldsymbol{\mathcal{J}}(\mathbf{r}', t_{\text{off}}) \iff t > t_{\text{off}}$. The depicted curves correspond to a source with the voltage $u(t) = U_0 \sin(\omega_0 t)$, where the U_0 was chosen so that the mean radiated power equals 0.5 W.

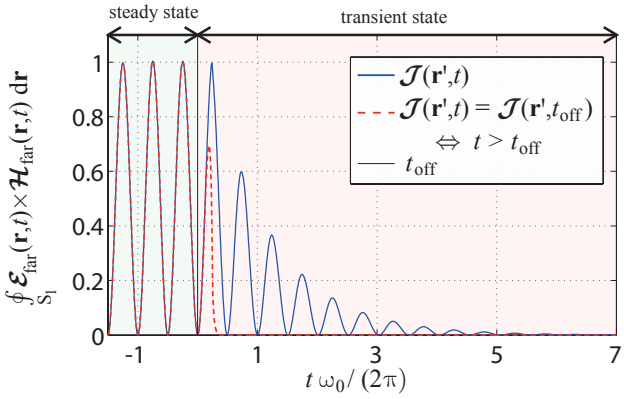

Fig. 6. Radiated power passing through the surface S_1. The blue line shows the steady state and the transient state for the original currents $\boldsymbol{\mathcal{J}}(\mathbf{r}', t)$, while the red line corresponds to the modified currents $\boldsymbol{\mathcal{J}}(\mathbf{r}', t) = \boldsymbol{\mathcal{J}}(\mathbf{r}', t_{\text{off}}) \iff t > t_{\text{off}}$. The depicted curves correspond to a source with the voltage $u(t) = U_0 \sin(\omega_0 t)$, where the U_0 was chosen so that the mean radiated power equals 0.5 W.

A. Radiation Q factor in the time domain

At the operation frequency (first resonance of the dipole), the electrical width of the dipole is exceedingly small ($w \approx \lambda/400$). To a very high degree of precision we can thus substitute $\boldsymbol{\mathcal{J}}(\mathbf{r}', t)\,\mathrm{d}\mathbf{r}'$ by $I(z', t)\,\mathbf{z}_0\,\mathrm{d}z'$ with $I(z', t)$ being the electric current along the dipole. Furthermore, as the dipole is made of PEC and it is fed by an ideal voltage source $u(t) = U_0 \sin(\omega_0 t)$, the two first integrals in (5) vanish and we are left with

$$\begin{aligned}\mathcal{W}(V_1, t_{\text{off}}) &= \int_{t_{\text{off}}}^{\infty} \oint_{S_1} \boldsymbol{\mathcal{E}}_{\text{far}}(\mathbf{r}, t) \times \boldsymbol{\mathcal{H}}_{\text{far}}(\mathbf{r}, t) \cdot \mathbf{r}_0 \,\mathrm{d}S_1 \,\mathrm{d}t \\ &= \frac{\mu^2}{8\pi Z_0} \int_{t_{\text{off}}}^{\infty} \int_{-1}^{1} \mathcal{S}_{\text{far}}(\zeta, t)\,\mathrm{d}\zeta\,\mathrm{d}t,\end{aligned} \tag{42}$$

where

$$\mathcal{S}_{\text{far}}(\zeta, t) = \left| \int_{-\frac{L}{2}}^{\frac{L}{2}} \dot{I}\left(z', t - \frac{L}{2c_0} + \zeta\frac{z'}{c_0}\right) \mathrm{d}z' \right|^2 \left(1 - \zeta^2\right). \tag{43}$$

According to Sec. II-A, this integration will be evaluated for total energy (with transient currents for $t > t_{\text{off}}$) and also for radiated energy (with constant currents for $t > t_{\text{off}}$). For both calculations only the scenario with transient currents needs to be actually simulated. The second scenario (in which the currents are impressed sources) is a result of post-processing. At this point it is very instructive to show explicitly the time course of the current at the centre of the dipole and of the power passing through the surface S_1 in both scenarios. The results are depicted in Figs. 5, 6. Defining a normalized time $t_{\text{n}} = t\omega_0/(2\pi)$, where ω_0 is the angular frequency at resonance, the source has been switched off at $t_{\text{n}} = 0$. During the following transient (blue line in Fig. 5, 6), all the energy content of the sphere is lost by the radiation. Within the second scenario, with all the currents constant for $t > t_{\text{off}}$, the radiation of the dipole is instantaneously stopped at $t_{\text{off}} = 0$. The power radiated for $t_{\text{off}} > 0$ (red line in Fig. 6) then represents a radiation that was at $t = t_{\text{off}}$ within the sphere but needed some time to leave the volume. Subtracting the blue and red curve in Fig. 6 and integrating in time for $t > t_{\text{off}}$ then gives the stored energy at $t = t_{\text{off}}$. Varying t_{off}, we can obtain $\mathcal{Q}(t_{\text{off}})$ and Q, which are depicted in Fig. 7. Since the calculation for a single value of t_{off} is computationally expensive (it requires a single run of CST and two runs of the Matlab routine) the stored energy was evaluated only for six different switch-off times. The resulting $\mathcal{Q}(t_{\text{off}})$ was then fitted by

$$\mathcal{Q}(t_{\text{off}}) = A + B\sin(2\omega_0 t_{\text{off}} + \beta) \tag{44}$$

with $A = 7.3$, $B = -0.99$ and $\beta = -0.18$. The fitting was exact (within the used precision) in all fitted points, which allowed us to consider (44) as an exact expression for all t_{off}.

B. Radiation Q factor in frequency domain

After MoM solution, the surface current and surface charge densities were used to evaluate (21), which gives $\widetilde{Q} = 7.6$, see Fig. 7. Note that since $\widetilde{Q}$ is defined in the frequency domain and calculated at angular frequency ω_0, it is not a function of time in Fig. 7 (for a non-radiating circuit it was a cycle mean value of stored energy).

C. Radiation Q factor from FBW concept

Now, Q_Z can be evaluated by (23) for both above-mentioned models of the dipole. In CST we obtained $Q_Z^{\text{CST}} = 7.1$, and in Matlab we obtained $Q_Z^{\text{Matlab}} = 7.2$. Even though two different software tools with different feeding were used, the Q_Z^{CST} and Q_Z^{Matlab} factors are almost identical. This justifies the comparison of all the Q factors in Fig. 7, where we can observe very good correspondence. All the Q factors are between 7.1 and 7.6, and the newly proposed energy concept yields $Q = 7.3$.

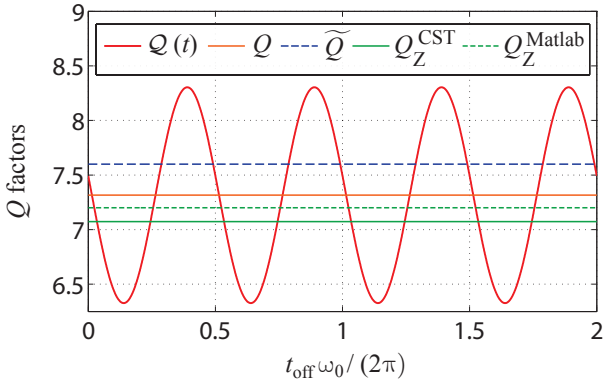

Fig. 7. A comparison of all Q factors for a half-wave dipole. The depicted curves correspond to a source with the voltage $u(t) = U_0 \sin(\omega_0 t)$, where the U_0 was chosen so that the mean radiated power equals 0.5 W.

VI. Conclusion

Three different concepts aiming to evaluate the stored energy and the resulting quality factor of a radiator have been investigated in this paper. The first uses frequency domain quantities and classical radiation energy extraction. The second is based on the frequency derivative of the input impedance of the radiator. The third is a novel time domain scheme. All methods have been thoroughly compared theoretically and their differences are presented on general non-radiating RLC networks and on a canonical dipole radiator.

It has been explicitly shown that the most practical scheme based on the frequency derivative of the input impedance generally fails to give the correct quality factor, but could serve as a very good estimate of it for structures which could well be approximated by series or parallel resonant circuits. The frequency domain concept with far field energy extraction was shown to work correctly for general RLC circuits and a simple radiator. Unlike the time domain scheme, it could however give negative values of stored energy, which is actually known to happen for specific current distributions. In this respect, the novel time domain method proposed in this paper could be denoted as a reference, and a future goal is to use it for solving the puzzle of negative energies.

Acknowledgement

The authors are grateful to Ricardo Marques (Department of Electronics and Electromagnetism, University of Seville) and Raul Berral (Department of Applied Physics, University of Seville) for many valuable discussions that stimulated some of the core ideas of this contribution. The authors are also grateful to Jan Eichler (Department of Electromagnetic Field, Czech Technical University in Prague) for his help with the CST simulations and to Milos Mazanek (Department of Electromagnetic Field, Czech Technical University in Prague) for the opportunity to collaborate on the problem of stored energy and the Q factor.

References

[1] P. M. Morse and H. Feshbach, *Methods of Theoretical Physics*. McGraw-Hill, 1953.

[2] R. E. Collin, *Foundations for Microwave Engineering*, 2nd ed. John Wiley - IEEE Press, 1992.

[3] R. F. Harrington, *Time-Harmonic Electromagnetic Fields*, 2nd ed. John Wiley - IEEE Press, 2001.

[4] J. L. Volakis, C.-C. Chen, and K. Fujimoto, *Survey of Small Antenna Theory*, 1st ed., ser. Small Antennas: Miniaturization Techniques & Applications. McGraw-Hill, 2010.

[5] A. Tonning, "Energy density in continuous electromagnetic media," *IRE Trans. Antennas Propag.*, vol. 8, no. 4, pp. 428–434, July 1960.

[6] D. J. White and P. L. Overfelt, "Poynting's theorems and their relationship to antenna power, Q, and bandwidth," Naval Air Warfare Center Weapons Division, China Lake, CA, Tech. Rep. NAWCWPNS 8419, 1999.

[7] J. D. Jackson, *Classical Electrodynamics*, 3rd ed. John Wiley, 1998.

[8] C. A. Balanis, *Antenna Theory Analysis and Design*, 3rd ed. John Wiley, 2005.

[9] R. E. Collin and S. Rothschild, "Evaluation of antenna Q," *IEEE Trans. Antennas Propag.*, vol. 12, pp. 23–27, 1964.

[10] J. S. McLean, "A re-examination of the fundamental limits on the radiation Q of electrically small antennas," *IEEE Trans. Antennas Propag.*, vol. 44, no. 5, pp. 672–675, May 1996.

[11] M. Manteghi, "Fundamental limits of cylindrical antennas," Virginia Tech, Tech. Rep. 1, 2010.

[12] G. A. E. Vandenbosch, "Reactive energies, impedance, and Q factor of radiating structures," *IEEE Trans. Antennas Propag.*, vol. 58, no. 4, pp. 1112–1127, Apr. 2010.

[13] Y. Geyi, "A method for the evaluation of small antenna Q," *IEEE Trans. Antennas Propag.*, vol. 51, no. 8, pp. 2124–2129, Aug. 2003.

[14] P. Hazdra, M. Capek, and J. Eichler, "Comments to 'Reactive Energies, Impedance, and Q Factor of Radiating Structures' by G. Vandenbosch," *IEEE Trans. Antennas Propag.*, vol. 61, no. 12, pp. 6266–6267, Dec. 2013.

[15] M. Gustafsson, M. Cismasu, and B. L. G. Jonsson, "Physical bounds and optimal currents on antennas," *IEEE Trans. Antennas Propag.*, vol. 60, no. 6, pp. 2672–2681, June 2012.

[16] G. A. E. Vandenbosch, "Reply to "Comments on 'Reactive energies, impedance, and Q factor of radiating structures'"," *IEEE Trans. Antennas Propag.*, vol. 61, no. 12, p. 6268, Dec. 2013.

[17] A. Shlivinski and E. Heyman, "Time-domain near-field analysis of short-pulse antennas - Part I: Spherical wave (multipole) expansion," *IEEE Trans. Antennas Propag.*, vol. 47, no. 2, pp. 271–279, Feb. 1999.

[18] ——, "Time-domain near-field analysis of short-pulse antennas - Part II: Reactive energy and the antenna Q," *IEEE Trans. Antennas Propag.*, vol. 47, no. 2, pp. 280–286, Feb. 1999.

[19] M. Capek, L. Jelinek, P. Hazdra, and J. Eichler, "An analytical evaluation and the lower bounds of the measurable quality factor Q_Z," *IEEE Trans. Antennas Propag.*, pp. 1–9, 2014, submitted (arXiv: 1311.1750v1).

[20] S. Collardey, A. Sharaiha, and K. Mahdjoubi, "Calculation of small antennas quality factor using FDTD method," *IEEE Antennas Wireless Propag. Lett.*, vol. 5, pp. 191–194, 2006.

[21] G. A. E. Vandenbosch, "Radiators in time domain, part I: Electric, magnetic, and radiated energies," *IEEE Trans. Antennas Propag.*, vol. 61, no. 8, pp. 3995–4003, Aug. 2013.

[22] ——, "Radiators in time domain-part II: Finite pulses, sinusoidal regime and Q factor," *IEEE Trans. Antennas Propag.*, vol. 61, no. 8, pp. 4004–4012, Aug. 2013.

[23] D. R. Rhodes, "Observable stored energies of electromagnetic systems," *J. Franklin Inst.*, vol. 302, no. 3, pp. 225–237, 1976.

[24] A. D. Yaghjian and S. R. Best, "Impedance, bandwidth and Q of antennas," *IEEE Trans. Antennas Propag.*, vol. 53, no. 4, pp. 1298–1324, April 2005.

[25] S. R. Best and D. L. Hanna, "A performance comparison of fundamental small-antenna designs," *IEEE Antennas Propag. Magazine*, vol. 52, no. 1, pp. 47–70, Feb. 2010.

[26] Sievenpiper, D. F., et al., "Exprerimental validation of performance limits and design guidelines for small antennas," *IEEE Trans. Antennas Propag.*, vol. 60, no. 1, pp. 8–19, Jan. 2012.

[27] M. Capek, L. Jelinek, P. Hazdra, and J. Eichler, "The measurable Q factor and observable energies of radiating structures," *IEEE Trans. Antennas Propag.*, vol. 62, no. 1, pp. 311–318, Jan. 2014.

[28] M. Capek, P. Hazdra, and J. Eichler, "A method for the evaluation of radiation Q based on modal approach," *IEEE Trans. Antennas Propag.*, vol. 60, no. 10, pp. 4556–4567, Oct. 2012.

[29] M. Gustafsson and S. Nordebo, "Optimal antenna currents for Q, superdirectivity, and radiation patterns using convex optimization," *IEEE Trans. Antennas Propag.*, vol. 61, no. 3, pp. 1109–1118, March 2013.

[30] C. A. Balanis, *Advanced Engineering Electromagnetics*. John Wiley, 1989.
[31] J. C. Maxwell, *A Treatise on Electricity and Magnetism*. Clarendon Press, 1873, vol. 1.
[32] W. Geyi, *Foundations of Applied Electrodynamics*. John Wiley, 2010.
[33] C. J. Carpenter, "Electromagnetic energy and power in terms of charges and potentials instead of fields," *Proc. of IEE A*, vol. 136, no. 2, pp. 55–65, March 1989.
[34] M. Uehara, J. E. Allen, and C. J. Carpenter, "Comments to electromagnetic energy and power in terms of charges and potentials instead of fields," *Proc. of IEE A*, vol. 139, no. 1, pp. 42–44, Jan. 1992.
[35] V. G. Endean, "Comments to electromagnetic energy and power in terms of charges and potentials instead of fields," *Proc. of IEE A*, vol. 139, no. 6, pp. 338–342, Nov. 1992.
[36] M. Gustafsson and S. Nordebo, "Bandwidth, Q factor and resonance models of antennas," *PIER*, vol. 62, pp. 1–20, 2006.
[37] E. J. Rothwell and M. J. Cloud, *Electromagnetics*. CRC Press, 2001.
[38] E. Hallen, *Electromagnetic Theory*. Chapman & Hall, 1962.
[39] CST Computer Simulation Technology. [Online]. Available: www.cst.com
[40] The MathWorks. The Matlab. [Online]. Available: www.mathworks.com
[41] M. Capek, P. Hamouz, P. Hazdra, and J. Eichler, "Implementation of the Theory of Characteristic Modes in Matlab," *IEEE Antennas Propag. Magazine*, vol. 55, no. 2, pp. 176–189, April 2013.
[42] S. M. Rao, D. R. Wilton, and A. W. Glisson, "Electromagnetic scattering by surfaces of arbitrary shape," *IEEE Trans. Antennas Propag.*, vol. 30, no. 3, pp. 409–418, May 1982.

Miloslav Capek (S'09) received the M.Sc. degree in electrical engineering from the Czech Technical University, Prague, Czech Republic, in 2009, and is currently working towards a Ph.D. degree in electromagnetic fields at the same University.

Currently, he is a researcher with the Department of Electromagnetic Field, CTU-FEE. His research interests are in the area of electromagnetic theory, electrically small antennas, numerical techniques, fractal geometry and optimization.

Lukas Jelinek received the Ph.D. degree from the Czech Technical University in Prague, Prague, Czech Republic, in 2006.

Currently, he is a researcher with the Department of Electromagnetic Field, CTU-FEE. His main fields of interest include wave propagation in complex media, general field theory, and numerical techniques. His recent research interest is focused on metamaterials, specifically on resonant ring systems.

Guy Vandenbosch (M'92, SM'08, F'12) received the M.S. and Ph.D. degrees in electrical engineering from the Katholieke Universiteit Leuven, Leuven, Belgium, in 1985 and 1991, respectively, and holds a certificate of the postacademic course in Electro-Magnetic Compatibility at the Technical University of Eindhoven, the Netherlands.

From 1991 to 1993, he held a postdoctoral research position at the Katholieke Universiteit Leuven. Since 1993, he has been a Lecturer, and since 2005, a Full Professor at the same university. He has taught or teaches courses on "Electromagnetic Waves," "Antennas," "Electromagnetic Compatibility," "Electrical Engineering, Electronics, and Electrical Energy," and "Digital Steer and Measuring Techniques in Physics." His research interests are in the area of electromagnetic theory, computational electromagnetics, planar antennas and circuits, nano-electromagnetics, EM radiation, EMC, and bio-electromagnetics. His work has been published in ca. 170 papers in international journals and has been presented in ca. 275 papers at international conferences.

Prof. Vandenbosch has been a member of the "Management Committees" of the consecutive European COST actions on antennas since 1993. Within the ACE Network of Excellence of the EU (2004-2007), he was a member of the Executive Board and coordinated the activity on the creation of a European antenna software platform. At present, he leads the EuRAAP Working Group on Software and represents this group within the EuRAAP Delegate Assembly. From 2001 to 2007, he was the President of SITEL, the Belgian Society of Engineers in Telecommunication and Electronics. Since 2008, he has been a member of the board of FITCE Belgium, the Belgian branch of the Federation of Telecommunications Engineers of the European Union. In the period 1999-2004, he was vice-chairman, and in the period 2005-2009 secretary of the IEEE Benelux Chapter on Antennas and Propagation. Currently he holds the position of chairman of this Chapter. In the period 2002-2004 he was secretary of the IEEE Benelux Chapter on EMC. He is currently secretary of the Belgian National Committee for Radio-electricity (URSI), where he is also in charge of commission E.

Pavel Hazdra (M'03) received the M.S. and Ph.D. degrees in electrical engineering from the Czech Technical University in Prague, Faculty of Electrical Engineering in 2003 and 2009, respectively.

He is a research and teaching assistant with the Department of Electromagnetic Field, CTU-FEE. His research interests are in the area of electromagnetic theory, computational electromagnetics, fractal geometry, planar antennas and special prime-feed antennas.

Complex Power-Ratio Functional for Radiating Structures with Applications to the Characteristic Mode Theory

Miloslav Capek, *Student Member, IEEE,* Pavel Hazdra, *Member, IEEE,* and Jan Eichler, *Student Member, IEEE*

***Abstract*—In this paper a complex power-ratio functional is derived in terms of currents flowing on a radiating device. It is shown that the Characteristic Modes (CM) minimize this quadratic-form ratio, i.e. they maximize radiated power while minimizing the net stored power. Solution of the impedance matrix equations is then not needed a priori and since in many cases the modal current distributions could well be estimated, the proposed functional gives additional insight. Its properties and strengths are demonstrated on important canonical examples including a dipole(s) and a loop with prescribed current distributions.**

Based on these studies the difference between the modal superposition and direct Method of Moments (MoM) solution is addressed and attacked. The issue lies in scaling of the generalized eigenvalue problem. A simple correction formula is proposed, which increase the convergence rate of the modal solution yielding a near-perfect match with the MoM current.

***Index Terms*—Characteristic modes, eigenvalues and eigenfunctions, electromagnetic theory, Poynting theorem, modal superposition.**

I. Introduction

THE Theory of Characteristic Modes (TCM) has become very popular in recent years. The TCM produces a set of modal (characteristic or eigen) currents with associated eigen-numbers, no losses other than radiation are assumed. These modes form an orthogonal basis dependent only on surface shape and frequency and they are independent of any excitation. The theory was formally developed by R. Garbacz [1] and significantly revised by R. Harrington and J. Mautz in [2].

The number of publications dealing with the TCM is growing. However, most of them have an application character only, see e.g. [3], [4] and [5].

This paper starts with a derivation of an analytical functional which represents the ratio between radiated and stored energy. A stationary quadratic form is defined only in terms of current flowing on a radiating device using the Electric Field Integral Equation (EFIE) [6] and complex Poynting theorem [7]. The solution of such a problem is clearly a variational problem. Numerical minimization is treated by Lagrange multipliers constituting a generalized eigenvalue problem. This problem has been stated by Harrington as the TCM.

However, the proposed functional is not restricted to the characteristic basis only and is very similar to the quadratic form of the radiation Q factor, [8]. Hence it is possible to define any current distribution and to compare it with classical characteristic modes. Based on this fundamental result, the radiation properties of canonical shapes are investigated leading to a rationale for non-radiating ("inductive") modes. This observation can only be made with the analytical fuctional which is more general than characteristic modes.

In the last section, the residual current occuring as the difference between the MoM and TCM solutions is studied and eliminated denoting that the cause is an ill-conditioned generalized eigenvalue problem. The elimination process utilized all knowledge of analytic as well as algebraic formulation of the proposed power-ratio.

Manuscript received July 19, 2011; revised January 11, 2011. This work was supported by the project of the Czech Science Foundation, grant No. P102/12/2223 (Analysis and Multicriteria Optimization of Compact Radiating Structures based on Modal Decomposition) and by the COST LD 12055 AMTAS (Advanced Modeling and Technologies for Antennas and Sensors) action.

The authors are with the Department of Electromagnetic Field, Faculty of Electrical Engineering, Czech Technical University in Prague, Technicka 2, 16627, Prague, Czech Republic (e-mail: miloslav.capek@fel.cvut.cz).

II. Analytical Functional

In this section, a particular energetic functional, defined directly for the sources (currents/charges) on the antenna, is derived. This functional is intimately connected with the characteristic modes, as they minimize its value. The presented approach extends the original definition [2] which is based on characteristic fields only, i.e. on fields in all the space. Thanks to "source" formulation, one is able to study the arbitrarily defined current distribution on the defined geometry and to compare its radiating properties with the characteristic modes. We hope that in the future, a closed-form solution for characteristic modes on simple structures might be found.

Let's start from the EFIE formulation

$$\mathbf{n}_0 \times \mathbf{E}^i(\mathbf{r}) = -\mathbf{n}_0 \times \mathbf{E}^s(\mathbf{r}) = \mathbf{n}_0 \times \mathbf{Z}\big(\mathbf{J}(\mathbf{r})\big). \tag{1}$$

The incident electric field is given by

$$\begin{aligned}\mathbf{E}^i(\mathbf{r}) =& \jmath\omega\mu \iiint\limits_{\Omega} \Big(G(\mathbf{r},\mathbf{r}')\mathbf{J}(\mathbf{r}') \\ &- \frac{1}{k^2}\nabla G(\mathbf{r},\mathbf{r}')\nabla'\cdot\mathbf{J}(\mathbf{r}')\Big)\,\mathrm{d}\mathbf{r}',\end{aligned} \tag{2}$$

where $\mathbf{r} \in \Omega$, $\mathbf{r}' \in \Omega'$ and $\Omega = \Omega'$ is a region containing all the sources, $\jmath = \sqrt{-1}$, $\mathbf{J}$ is an as yet unknown electric current density and $G(\mathbf{r},\mathbf{r}')$ is the scalar Green function [9].

The following identity [10] is employed:

$$\iiint_{\Omega} \nabla G(\mathbf{r},\mathbf{r}')\cdot\mathbf{J}(\mathbf{r})\,\mathrm{d}\mathbf{r} = -\iiint_{\Omega} G(\mathbf{r},\mathbf{r}')\nabla\cdot\mathbf{J}(\mathbf{r})\,\mathrm{d}\mathbf{r}. \quad (3)$$

We also make use of the complex Poynting theorem [7]

$$\iiint_{V} \mathbf{E}^i\cdot\mathbf{J}^*\,\mathrm{d}V = \oiint_{S}\mathbf{S}\cdot\mathbf{n}_0\,\mathrm{d}S + 2\jmath\omega\iiint_{V}(w_m-w_e)\,\mathrm{d}V, \quad (4)$$

where V is the volume enclosed by the surface S, $\mathbf{S}=\mathbf{E}\times\mathbf{H}^*$ is the Poynting vector and $\mathbf{n}_0$ is the unit vector that points outwards from S, w_e and w_m are the electric and magnetic energy densities respectively. After some manipulations one obtains for the real and the imaginary part of (4)

$$\Re\left\{\iiint_{\Omega}\mathbf{E}^i\cdot\mathbf{J}^*\,\mathrm{d}\mathbf{r}\right\} = \Re\left\{\oiint_{\partial\Omega}\mathbf{S}\cdot\mathbf{n}_0\,\mathrm{d}\mathbf{r}\right\} \quad (5)$$

and

$$\Im\left\{\iiint_{\Omega}\mathbf{E}^i\cdot\mathbf{J}^*\,\mathrm{d}\mathbf{r}\right\} = \Im\left\{\oiint_{\partial\Omega}\mathbf{S}\cdot\mathbf{n}_0\,\mathrm{d}\mathbf{r}\right\} + 2\omega\iiint_{\Omega}(w_m-w_e)\,\mathrm{d}\mathbf{r}, \quad (6)$$

respectively. Considering an infinitely large sphere V_∞ for the fields in (4), the first integral on the right-hand side of (6) vanishes.

Next take an inner product[1] of (2) with a current $\mathbf{J}\in\Omega$ and applying (3) we get

$$\begin{aligned}\big\langle\mathbf{ZJ}(\mathbf{r}),\mathbf{J}(\mathbf{r})\big\rangle &= \big\langle\mathbf{E}^i(\mathbf{r}),\mathbf{J}(\mathbf{r})\big\rangle \\ &= \jmath\omega\mu\iiint_{\Omega}\iiint_{\Omega'}\Big(\mathbf{J}(\mathbf{r})\cdot\mathbf{J}^*(\mathbf{r}')G(\mathbf{r},\mathbf{r}') \\ &\quad -\frac{1}{k^2}\nabla\cdot\mathbf{J}(\mathbf{r})\cdot\nabla'\cdot\mathbf{J}^*(\mathbf{r}')G(\mathbf{r},\mathbf{r}')\Big)\,\mathrm{d}\mathbf{r}\,\mathrm{d}\mathbf{r}'.\end{aligned} \quad (7)$$

The scalar Green function is separated into its real and imaginary parts for further purposes as

$$G(\mathbf{r},\mathbf{r}') = \frac{\cos(kR)}{4\pi R} - \jmath\frac{\sin(kR)}{4\pi R}, \quad (8)$$

where $R=\|\mathbf{r}-\mathbf{r}'\|$. In order to make the equations more readable, the parts of (8) will be denoted as $G(\mathbf{r},\mathbf{r}') = C(kR)-\jmath S(kR)$ and the single integral sign will be used for all following double and triple integrals. Using (8) and (7) and splitting the real and imaginary parts results in

$$\begin{aligned}\big\langle\mathbf{E}^i(\mathbf{r}),\mathbf{J}(\mathbf{r})\big\rangle &= \frac{\omega\mu}{4\pi}\int_{\Omega}\int_{\Omega'}\mathbf{J}(\mathbf{r})\cdot\mathbf{J}^*(\mathbf{r}')S(kR)\,\mathrm{d}\mathbf{r}\,\mathrm{d}\mathbf{r}' \\ &\quad -\frac{\omega\mu}{4\pi k^2}\int_{\Omega}\int_{\Omega'}\nabla\cdot\mathbf{J}(\mathbf{r})\nabla'\cdot\mathbf{J}^*(\mathbf{r}')S(kR)\,\mathrm{d}\mathbf{r}\,\mathrm{d}\mathbf{r}' \\ &\quad +\jmath\Bigg(\frac{\omega\mu}{4\pi}\int_{\Omega}\int_{\Omega'}\mathbf{J}(\mathbf{r})\cdot\mathbf{J}^*(\mathbf{r}')C(kR)\,\mathrm{d}\mathbf{r}\,\mathrm{d}\mathbf{r}' \\ &\quad -\frac{\omega\mu}{4\pi k^2}\int_{\Omega}\int_{\Omega'}\nabla\cdot\mathbf{J}(\mathbf{r})\nabla'\cdot\mathbf{J}^*(\mathbf{r}')C(kR)\,\mathrm{d}\mathbf{r}\,\mathrm{d}\mathbf{r}'\Bigg).\end{aligned} \quad (9)$$

Now, putting (9) into the context of (5) and (6), the radiated and reactive powers are

$$\begin{aligned}P_r = \frac{1}{4\pi\omega\epsilon}\int_{\Omega}\int_{\Omega'}\Big(&k^2\mathbf{J}(\mathbf{r})\cdot\mathbf{J}(\mathbf{r}') \\ &-\nabla\cdot\mathbf{J}(\mathbf{r})\nabla'\cdot\mathbf{J}(\mathbf{r}')\Big)S(kR)\,\mathrm{d}\mathbf{r}\,\mathrm{d}\mathbf{r}'\end{aligned} \quad (10)$$

and

$$\begin{aligned}2\omega\int_{V_\infty}(w_m-w_e)\,\mathrm{d}\mathbf{V} &= 2\omega(W_m-W_e)\Big|_{V_\infty} \\ &= \frac{1}{4\pi\omega\epsilon}\int_{\Omega}\int_{\Omega'}\Big(k^2\mathbf{J}(\mathbf{r})\cdot\mathbf{J}(\mathbf{r}') \\ &\quad -\nabla\cdot\mathbf{J}(\mathbf{r})\nabla'\cdot\mathbf{J}(\mathbf{r}')\Big)C(kR)\,\mathrm{d}\mathbf{r}\,\mathrm{d}\mathbf{r}'.\end{aligned} \quad (11)$$

On the right side of (11), the symbol $|_{V_\infty}$ reminds us that we are taking fields from all of space into account [13]. According to the Lagrange principle [14] the energetic functional is established as

$$\begin{aligned}\mathcal{F}(\mathbf{J}) &= \frac{2\omega(W_m-W_e)\Big|_{V_\infty}}{P_r} = \kappa \\ &= \frac{\displaystyle\int_{\Omega}\int_{\Omega'}\Big(k^2\mathbf{J}(\mathbf{r})\cdot\mathbf{J}(\mathbf{r}')-\nabla\cdot\mathbf{J}(\mathbf{r})\nabla'\cdot\mathbf{J}(\mathbf{r}')\Big)C(kR)\,\mathrm{d}\mathbf{r}\,\mathrm{d}\mathbf{r}'}{\displaystyle\int_{\Omega}\int_{\Omega'}\Big(k^2\mathbf{J}(\mathbf{r})\cdot\mathbf{J}(\mathbf{r}')-\nabla\cdot\mathbf{J}(\mathbf{r})\nabla'\cdot\mathbf{J}(\mathbf{r}')\Big)S(kR)\,\mathrm{d}\mathbf{r}\,\mathrm{d}\mathbf{r}'},\end{aligned} \quad (12)$$

where κ is the Rayleigh quotient [15]. Formally, the functional (12) can be expressed in the standard Method of Moment notation [16]

$$\mathcal{F}(\mathbf{J}) = \frac{\langle\mathbf{J},\mathcal{X}\mathbf{J}\rangle}{\langle\mathbf{J},\mathcal{R}\mathbf{J}\rangle} = \kappa. \quad (13)$$

where operators $\mathcal{X}$ and $\mathcal{R}$ have to be discretized to obtain an algebraic solution.

III. Theory of Characteristic Modes – Common Background

Based on the EFIE formulation (1), an impedance operator $\mathbf{Z}$ is defined. Continuous (and bounded, see [17]) integro-differential operator $\mathbf{Z}$ can be separated as

$$\mathbf{Z} = \mathbf{R} + \jmath\mathbf{X}, \quad (14)$$

[1]We utilize two different notations to avoid confusion. The reaction [11], which is also called a symmetric product is defined as

$$\langle\mathbf{A},\mathbf{B}\rangle_r = \iiint_{\Omega}\mathbf{A}\cdot\mathbf{B}\,\mathrm{d}\mathbf{r},\quad \mathbf{r}\in\Omega,$$

and the inner product [12] is defined as

$$\langle\mathbf{A},\mathbf{B}\rangle = \iiint_{\Omega}\mathbf{A}\cdot\mathbf{B}^*\,\mathrm{d}\mathbf{r},\quad \mathbf{r}\in\Omega,$$

where $*$ denotes the complex conjugate.

where $\mathbf{R}$ and $\mathbf{X}$ are real and symmetric operators. Thus, $\mathbf{Z}$ is non-hermitian and symmetric.

Now, we try to find a so-called characteristic basis, defined with a proper weighting operator $\mathbf{M}$ and an eigenvalue υ_n as

$$(\mathbf{R} + \jmath\mathbf{X})\mathbf{J}_n = \upsilon_n \mathbf{M}\mathbf{J}_n. \tag{15}$$

Obviously, one of the possible choices is $\mathbf{M} = \mathbf{R}$ and $\upsilon_n = 1 + \jmath\lambda_n$. This is Harrington's approach from [2]. Then (15) becomes

$$\mathbf{X}\mathbf{J}_n = \lambda_n \mathbf{R}\mathbf{J}_n. \tag{16}$$

The above stated Generalized Eigenvalue Problem (GEP, [18]) generates the characteristic basis of eigencurrents $\{\mathbf{J}_n\}$ and associated eigenvalues λ_n and due to the properties of impedance matrix all eigenvalues are real and all eigencurrents are equiphased (also can be selected as real). The formulation (16) is known as the Theory of Characteristic Modes [2] and determines a basis of such modes that maximize radiated power and minimize the total stored energy. Note that the extreme value of radiated power relative to stored energy is considered for the basis as a whole. In spite of the fact that (16) looks quite simple, we show that there are many theoretical as well as numerical issues that have to be considered.

The GEP forms an orthogonal system thus normalization should be performed. The important one is

$$\langle \mathbf{J}_m, \mathbf{R}\mathbf{J}_n \rangle_r = \delta_{mn}, \tag{17}$$

$$\langle \mathbf{J}_m, \mathbf{X}\mathbf{J}_n \rangle_r = \delta_{mn}\lambda_n, \tag{18}$$

$$\langle \mathbf{J}_m, \mathbf{Z}\mathbf{J}_n \rangle_r = (1 + \jmath\lambda_n)\delta_{mn}, \tag{19}$$

where $\mathbf{J}_m$ and $\mathbf{J}_n$ are characteristic modes, $\langle\ ,\ \rangle_r$ is reaction and δ_{mn} is the Kronecker delta function. Relations (14)–(19) form a common background to the TCM.

It is also known that the GEP (16) minimizes an energetic functional

$$\mathcal{F}(\mathbf{J}_n) = \frac{\langle \mathbf{J}_n, \mathbf{X}\mathbf{J}_n \rangle}{\langle \mathbf{J}_n, \mathbf{R}\mathbf{J}_n \rangle} = \lambda_n. \tag{20}$$

For the practical interpretation of the TCM, see e.g. [19] and [20]. Further generalization of the TCM was presented in [21]. These generalized characteristic modes (CM) exhibit orthogonality over any desired region.

Here, the characteristic modes are obtained by Matlab [22] with Lapack [23] subroutines. The impedance matrix $\mathbf{Z}$ is calculated with an in-house Method of Moments code (MoM) [6], [24] and eigenvectors and eigenvalues are tracked, see [25].

Typical results of numerical decomposition (16), like an analysis of a patch, a circle, a bowtie, and others, are discussed in [20]. Recently, the authors published an extensive work [26], dealing with the (superposition of) modal energies, powers and radiation Q factors. Finally, to complete the summary of recent developments, we have to mention [27] and [28] as well.

IV. Interpretation of TCM in terms of analytical power-ratio functional

It is important to stress that (12) is minimized by characteristic currents, i.e. solutions of (16). Such an eigen-basis maximizes the radiated power and minimizes the total stored energy. The crucial step is a calculation of the impedance matrix. Then, the extremum of (12) is given by the characteristic basis $\{\mathbf{J}_n\}$ with associated eigenvalues:

$$\min_{\mathbf{J}} \Big\{ \mathcal{F}\big(\mathbf{J}\big) \Big\} = \mathbf{J}_n \Leftrightarrow \kappa = \lambda_n. \tag{21}$$

For such modes the Hermitian quadratic forms of functions (10) and (11) are used. The notations are $W^{m,n}_{m/e} = f(\mathbf{J}_m, \mathbf{J}_n)$ and $P^{m,n}_{r} = g(\mathbf{J}_m, \mathbf{J}_n)$ for modal net stored energy and modal radiated power, respectively. For $m = n$ we abbreviate to $W^{n}_{m/e}$ and P^{n}_{r}. Note, that the extreme value of radiated power relative to stored energy is considered for the basis as a whole.

Indeed, an exact analytical solution for current is exceedingly complicated, if not impossible even for the simplest geometries. On the other hand the expression (12) allows definition of an arbitrary current distribution $\breve{\mathbf{J}}_n$ without the necessity of numerical computation of the impedance matrix $\mathbf{Z}$ in (16). In addition, if we try to analytically find a basis $\{\breve{\mathbf{J}}_n\}$ that is similar to the true CM basis (at least at one frequency) we can analyse exactly its behaviour and estimate, how close is the selected current distribution to the optimal solution.

For instance if we are interested in loop-like topologies where the modes are well known (see the next section), it's not necessary to recalculate characteristic modes if the geometry is modified.

V. Elementary Radiators – Case Studies

Let's try to demonstrate why the analytical functional (12) is of interest. We inspect three canonical examples:

- a thin-wire dipole,
- two parallel coupled dipoles, separated by distance h with in-phase and out-of-phase modes,
- a loop with the static mode.

These examples offer a direct way to understand and interpret the non-radiating (inductive) mode(s). We will see that these are fulfilling the condition $\nabla \cdot \mathbf{J}(\mathbf{r}) = 0$. Some of the following results are partially known, but it is interesting to put them into the modal context.

A. Thin-wire dipole

Consider a thin-wire dipole of length $L = \pi/2$ and radius $a = L/500$ ($a << L$). It is evident, that there are no inductive modes and that any current under consideration has to fulfill the Dirichlet boundary condition and the equation of continuity for which the EFIE was derived. It is also important that the choice of any mode from the basis predestines the basis as a whole as the modes are orthogonal. To investigate the radiation properties of the dominant mode ($n = 1$) on a dipole, consider the natural current basis

$$\breve{\mathbf{J}}_n(x) = \mathbf{x}_0 I_0 \delta(y)\delta(z) \sin\Big(\frac{\pi n x}{L}\Big). \tag{22}$$

Although characteristic modes vary slightly with frequency, we assume in (22) that they are held constant for simplicity. The corresponding charge is

$$\frac{\mathrm{d}\breve{\mathbf{J}}_n(x)}{\mathrm{d}x} = \delta(y)\delta(z) I_0 \frac{\pi n}{L} \cos\Big(\frac{\pi n x}{L}\Big), \tag{23}$$

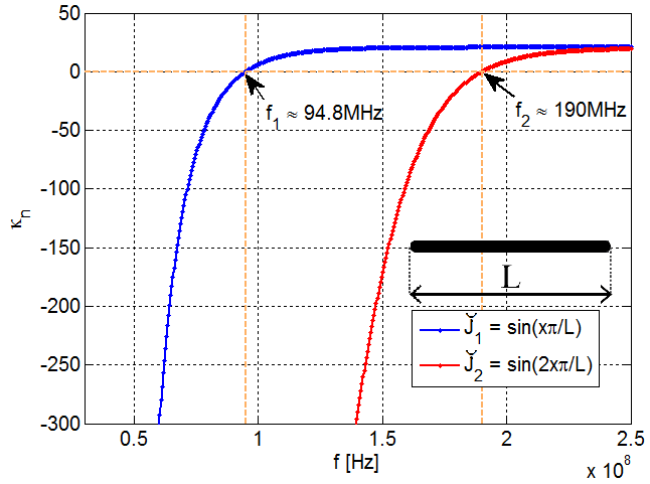

Fig. 1. The radiation quotients κ for the first two modes of a dipole $L = \pi/2$.

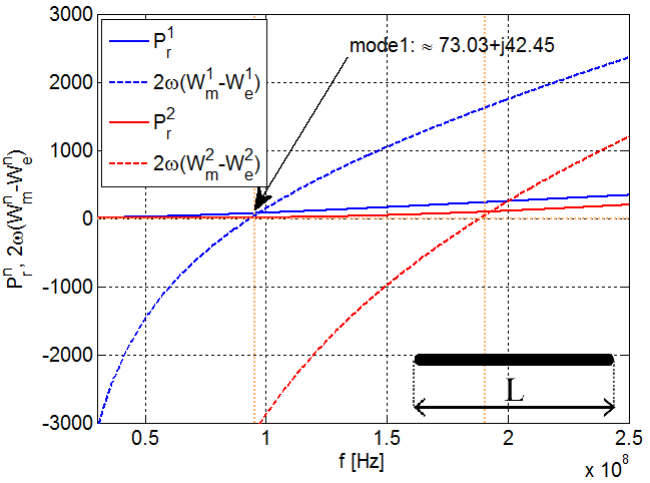

Fig. 2. The stored net power and radiated power for the first two modes of a half-wave dipole.

where $x \in (0, L)$ and $I_0 = 1\text{A}$ is assumed.

By definition, the nth mode is in resonance $f = f_n$ if

$$2\omega(W_m^n - W_e^n) = 0. \tag{24}$$

The nth mode has a capacitive character (i. e. $W_m^n < W_e^n$) for $f < f_n$ and an inductive character (i. e. $W_m^n > W_e^n$) for $f > f_n$.

Because of complexity, the functional (12) was solved numerically in Matlab (the dipole was discretized into $N = 101$ elements for that purpose). The first two modes ($n = 1$ and $n = 2$) are considered and the electrical length of the dipole is $L = \tilde{\lambda}/2$ where $\tilde{\lambda}$ is the free space wavelength.

Fig. 1 shows the κ quotients of selected modes, Fig. 2 shows the radiated powers and stored energies. Resonant frequencies can be observed from both figures; $f_1 \approx 94.8\text{MHz}$ and $f_2 \approx 190\text{MHz}$. Important fact is that $P_r^n \to 0$ for $f < f_n$ (and is still positive).

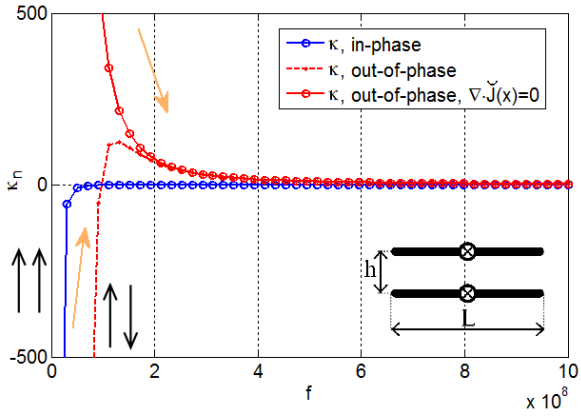

Fig. 3. The radiation quotients κ for in-phase, out-of-phase, and testing mode of two short-distance half-wave dipoles.

B. Two thin-wire dipoles

The next scenario involves two closely spaced collinear half-wave dipoles, both of them fed at the middle. The separation distance $h = L/50$ is considered much smaller than the length $L = \pi/2$, the radius is $a = L/500$. Now, there are two possible fundamental modes (depending on excitation) at the same frequency f_1 as in the previous example.

First, let's discuss the so-called in-phase excitation resulting in an in-phase mode [29]. For a very small h/L ratio the course of an in-phase quotient κ (solid blue line) is similar to that of the dominant mode on a single dipole in Fig. 3. This also applies for the course of radiated power and reactive power in Fig. 4. Consequently it is concluded that the in-phase mode radiates well (in comparison to the out-of-phase mode). The ratio between the radiated power and the reactive power remains more or less the same.

This is not the case for an out-of-phase mode, where the reactive power rapidly increases compared to radiated power, see Fig. 4. Such a mode doesn't radiate well and generates a great deal of reactive power. Consequently, Fig. 3 depicts the steep resonance of an out-of-phase mode. Other properties, especially those regarding the radiated Q factors, have been discussed in [26].

The functional (12) together with the current defined in (22) makes it possible to investigate the hypothetical situation where the currents on the dipoles are out-of-phase but the charge density is eliminated ($\nabla \cdot \mathbf{J} \equiv 0$). It strongly resembles the situation where the ends of the dipoles are connected (forming a loop). We split (11) in to magnetic

$$\widetilde{W}_m^n = W_m^n + \frac{W_r^n}{2} \tag{25}$$

and electric

$$\widetilde{W}_e^n = W_e^n + \frac{W_r^n}{2} \tag{26}$$

energy, respectively. The term $W_r^n/2$

$$\frac{W_r^n}{2} = -\frac{k}{8\pi\epsilon\omega^2} \int_\Omega \int_{\Omega'} \Big(k^2 \mathbf{J}(\mathbf{r}) \cdot \mathbf{J}(\mathbf{r}') - \nabla \cdot \mathbf{J}(\mathbf{r}) \nabla' \cdot \mathbf{J}(\mathbf{r}') \Big) \sin(kR)\, \mathrm{d}\mathbf{r}\, \mathrm{d}\mathbf{r}'. \tag{27}$$

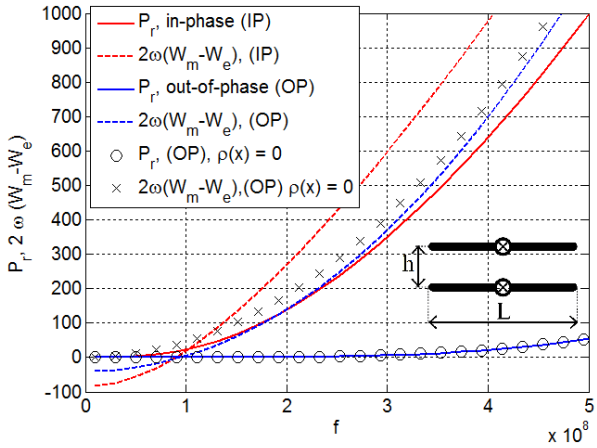

Fig. 4. The stored net power and radiated power for in-phase, out-of-phase, and testing mode ($\nabla \cdot \mathbf{J} \equiv 0$) of two short-distance half-wave dipoles.

is eliminated in (12), for details see [13]. Although the results in Fig. 4 seem similar to the pure out-of-phase mode, they are not the same. Fig. 3 reveals that such a mode doesn't resonate because of its pure inductive character. Interestingly the radiated power and total reactive power are more or less the same as in the out-of-phase case. We show that this behaviour is similar to the static (zero) mode on a loop.

C. A loop

A loop is an elementary radiator whereon the static mode ($\mathbf{J}_0$) does exist[2] and its behaviour is similar to the modified out-of-phase mode analyzed in the previous section. Consider a loop with perimeter 1m and wire radius 0.5mm discretized into N = 500 segments. The static mode on the loop is given in cylindrical coordinates (r,φ,z) as

$$\breve{\mathbf{J}}_0(\varphi) = \boldsymbol{\varphi}_0 I_0 \delta(r)\delta(z), \quad \nabla \cdot \breve{\mathbf{J}}_0(\varphi) = 0, \tag{28}$$

and (12) simplifies to

$$\kappa_0 = \mathcal{F}\big(\breve{\mathbf{J}}_0(\varphi)\big) = \frac{\int_0^{2\pi}\int_0^{2\pi} \cos(\varphi-\varphi') \dfrac{\cos\big(kr|\varphi-\varphi'|\big)}{r|\varphi-\varphi'|}\,\mathrm{d}\varphi\,\mathrm{d}\varphi'}{\int_0^{2\pi}\int_0^{2\pi} \cos(\varphi-\varphi') \dfrac{\sin\big(kr|\varphi-\varphi'|\big)}{r|\varphi-\varphi'|}\,\mathrm{d}\varphi\,\mathrm{d}\varphi'}. \tag{29}$$

The static mode cannot resonate due to the lack of electric energy, see Fig. 5. Symmetry of the loop makes it possible to reduce the N^2 integration steps to N steps only. The denominator and the numerator of (29) were also discussed and further investigated in terms of the minimization of Q in [31]. Such a mode doesn't radiate and accumulates a great deal of stored magnetic energy, see Fig. 6 where both W_m^0 and $\widetilde{W}_m^0$ are compared as a function of ka. Thus the static mode on a loop can be explained through the out-of-phase mode on two dipoles with $\nabla \cdot \mathbf{J} \equiv 0$.

[2]The analytical solution of a homogeneous Helmholtz equation in cylindrical coordinates [30] makes this static mode possible.

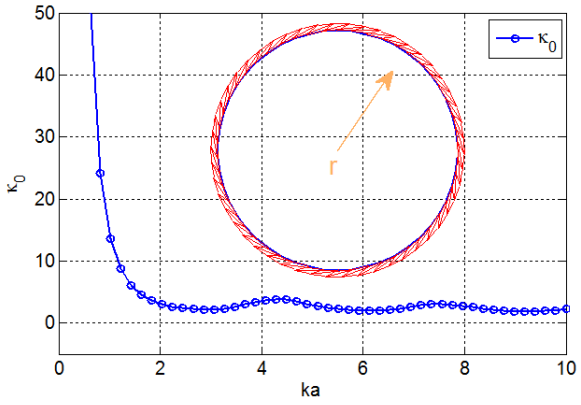

Fig. 5. The radiation quotient κ for static mode of loop.

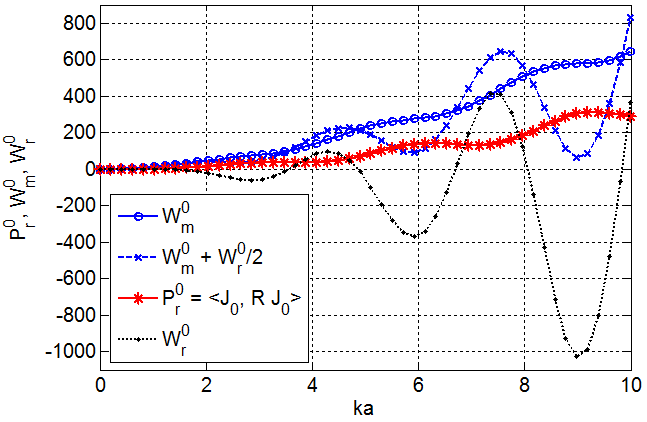

Fig. 6. The stored net power and radiated power for static mode of loop.

VI. Modal Superposition

If the solution of (1) is complete, we should be able to obtain the total current from the basis of modal currents. To do this, we are looking for unknown coefficients γ_n in the summation

$$\mathbf{n}_0 \times \sum_n \gamma_n \mathbf{Z}(\mathbf{J}_n) = \mathbf{n}_0 \times \mathbf{E}^i \tag{30}$$

It can be easily shown (see e.g. [2]) that the total solution has the form

$$\mathbf{J} = \sum_n \gamma_n \mathbf{J}_n, \tag{31}$$

in which

$$\gamma_n = \frac{\langle \mathbf{J}_n, \mathbf{E}^i \rangle_r}{1 + \jmath\lambda_n}. \tag{32}$$

Thanks to the (31), testing similar to (7) is possible for the total current

$$\langle \mathbf{E}^i, \mathbf{J} \rangle = \left\langle \mathbf{E}^i, \sum_n \frac{\langle \mathbf{J}_n, \mathbf{E}^i \rangle_r}{1 + \jmath\lambda_n} \mathbf{J}_n \right\rangle. \tag{33}$$

Due to lack of space, only the compact form $\langle\ ,\ \rangle$ is used. We

rewrite (33) with respect to (31) in terms of reactions

$$\left\langle \mathbf{E}^i, \left(\sum_n \frac{\langle \mathbf{J}_n, \mathbf{E}^i \rangle_r}{1+\jmath\lambda_n} \mathbf{J}_n \right)^* \right\rangle_r = \left\langle \mathbf{E}^i, \sum_n \frac{\langle \mathbf{J}_n, \mathbf{E}^i \rangle_r^*}{(1+\jmath\lambda_n)^*} \mathbf{J}_n \right\rangle_r . \quad (34)$$

Now, if we interchange the summation and the integration and use $AA^* = |A|^2$, we get

$$\sum_n \frac{\langle \mathbf{J}_n, \mathbf{E}^i \rangle_r^* \langle \mathbf{J}_n, \mathbf{E}^i \rangle_r}{(1-\jmath\lambda_n)(1+\jmath\lambda_n)} (1+\jmath\lambda_n) = \sum_n \gamma_n^* \gamma_n (1+\jmath\lambda_n) = \sum_n |\gamma_n|^2 (1+\jmath\lambda_n). \quad (35)$$

Comparing (35) with equation (19), considering feeding and thus operating on total current $\mathbf{J}$, we have

$$P_r = \sum_n |\gamma_n|^2, \quad (36)$$

$$2\omega \iiint_{V_\infty} (w_m - w_e)\, \mathrm{d}V = \sum_n |\gamma_n|^2 \lambda_n, \quad (37)$$

in which $|\gamma_n|^2 = P_r^n$ and $|\gamma_n|^2 \lambda_n = 2\omega(W_m^n - W_e^n)$. Relations (36) and (37) can be used for calculation of (modal) radiation Q as well as for calculation of (modal) radiation efficiency. For these purposes, the $\boldsymbol{\beta}$ matrix has been derived in [26]. Elements of the matrix are given by

$$\beta_{m,n} = \frac{\langle \mathbf{J}_m, \mathbf{E}^i \rangle \langle \mathbf{J}_n, \mathbf{E}^i \rangle (1+\lambda_m\lambda_n)}{(1+\lambda_m^2)(1+\lambda_n^2)} \quad (38)$$

for $m, n \in \{1, \ldots, N\}$. The coupling matrix (38) is real and symmetric. According to [2] and with reference to (17)–(19), it can be shown that P_r^n and $2\omega(W_m^n - W_e^n)$ are orthogonal in far field region with respect to the modal currents. This confirms that the total radiation power in [26] can be computed as $P_r = \sum_n P_r^n = \mathrm{Trace}(\boldsymbol{\beta})$.

VII. The Residual Current

Another interesting problem is the existence of the residual current (also called the "evanescent" mode in [32]). This current represents a residuum after subtraction of the total currents (obtained by the MoM and the TCM)

$$\mathbf{J}_{res} = \mathbf{J}_{MoM} - \mathbf{J}_{TCM} = \mathbf{Z}^{-1}\mathbf{E}^i - \sum_n \gamma_n \mathbf{J}_n. \quad (39)$$

To demonstrate the problem clearly, we implement the simplest thin-wire Galerkin formulation of the MoM according to [6]. This method generates perfectly symmetrical matrices $\mathbf{R}$ and $\mathbf{X}$. Let's discuss an example of a thin-wire dipole of length $L = 0.1$m with radius $a << L$ ($a = 0.1\mu$m), discretized to $N = 101$ elements. An $(N \times N)$ impedance matrix is constructed and a voltage gap [33] of one volt at the middle of the dipole is connected. The resulting residual current between the MoM solution and the TCM summation of 101 characteristic modes is depicted in Fig. 7 (the real part of all currents) and Fig. 8 (the imaginary part, which will later be shown to be dominant).

Some efforts have been made to eliminate (39), see [32] and [34] for example. However, the proposed approach doesn't respect the nature of the problem because it supposes that the operator $\mathbf{Z}$ is unbounded. To handle this difficulty, we start with a numerical characterization.

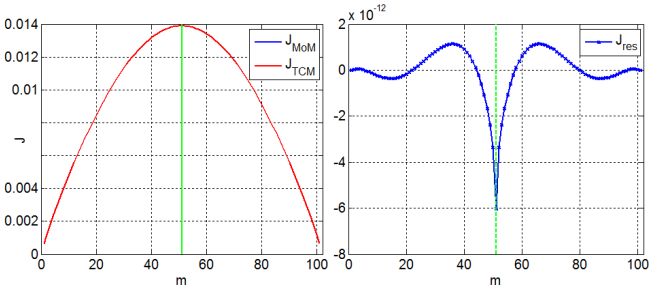

Fig. 7. The real part of $\mathbf{J}_{MoM}$ and $\mathbf{J}_{TCM}$ (left) and the real part of the residual current (right), green line indicates the feeding position.

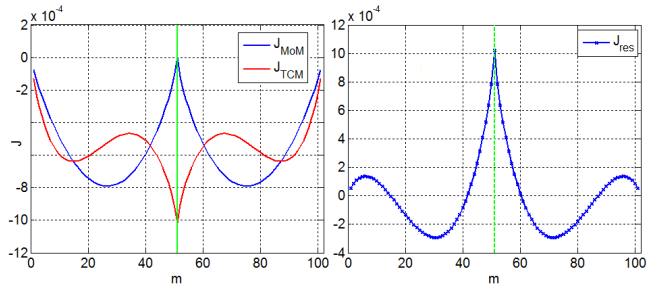

Fig. 8. The imaginary part of $\mathbf{J}_{MoM}$ and $\mathbf{J}_{TCM}$ (left) and the imaginary part of the residual current (right), green line indicates the feeding position.

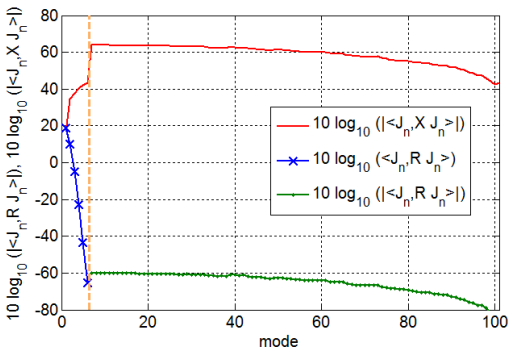

Fig. 9. Numerator and denominator of (20) with highlighted negative values (green line) of $\langle \mathbf{J}_n, \mathbf{R}\mathbf{J}_n \rangle$, half-wave dipole in resonance, fed to the middle. The negative values were multiplied by -1 and separated by dashed line, all values are depicted in [dB].

A. Numerical characterization of TCM

From (17) it is obvious that the modal (as well as the total) radiated power is assumed to be non-negative. Hence $\mathbf{R}$ has to be a semi-definite operator. Now, the key question arises: Does this presumption hold *for all modes* in the discretized basis $\{\mathbf{J}_n\}$? It can be shown that – from the numerical point of view – the *answer is no*.

To give support to this statement, we calculate separately the $\langle \mathbf{J}_n, \mathbf{X}\mathbf{J}_n \rangle$ and $\langle \mathbf{J}_n, \mathbf{R}\mathbf{J}_n \rangle$ parts of (20) for the dipole from the previous section. The results are shown in Fig. 9. Contrary to the analytical case depicted in Fig. 2, one can clearly observe that all modes $n > 6$ radiate a small amount of negative

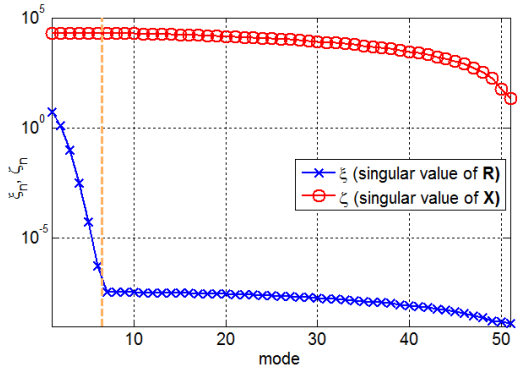

Fig. 10. The singular values of the real and the imaginary parts of the impedance matrix. Same example as in the previous figure.

power (depicted by the green line without cross marks). In other words, the operator $\mathbf{R}$ is in practice indefinite for all modes $n \in \{6, \ldots, 101\}$. This problem was mentioned earlier in [19] but the summation (31) has not changed accordingly.

The residual current issue may also be studied by a Singular Value Decomposition (SVD, [35]) of the real part of the impedance matrix $\mathbf{Z}$

$$\mathbf{R} = \mathbf{U}\xi\mathbf{V}^{\mathrm{T}}. \tag{40}$$

By definition all singular values ξ_n are non-negative. Supposing that $\mathbf{R}$ is real, symmetric and positive semi-definite, the unitary matrices $\mathbf{U}$ and $\mathbf{V}$ are equal and the singular values ξ are exactly the (positive) eigenvalues of $\mathbf{R}$.

To verify this premise, the dipole is divided into 51 elements and then the singular value decomposition of impedance matrix $\mathbf{Z} = \mathbf{R} + \jmath\mathbf{X}$ is performed. The singular values are depicted at Fig. 10 at the resonant frequency of the dominant mode. It is obvious that the imaginary part $\mathbf{X}$ is numerically well-conditioned but the real part $\mathbf{R}$ contains some strongly dominant solutions that radiate well and the rest of them are ill-conditioned. Because $\mathbf{R}$ serves as the weighting operator in the TCM formulation (16), all the mentioned difficulties are transferred to the solution of the GEP. These problems can be addressed to the scaling problems of the matrix pencil $(\mathbf{X} - \lambda\mathbf{R})$, as pointed out in [15].

Because the matrix $\mathbf{R}$ has to fulfill requirements on symmetry, we subtract the matrices as $\mathbf{D} = \mathbf{U} - \mathbf{V}$. The resulting matrix $\mathbf{D}$ is shown in Fig. 11. While the first six columns contain zeros as they should, the rest of $\mathbf{D}$ contains exactly two times the rest of the matrix $\mathbf{U}$ (i. e. $\mathbf{U} = -\mathbf{V}$). This means that the positive semi-definite behaviour does not hold for all modes, the rest of the modes radiate a small amount of negative power (no matter how they are normalized).

B. Compensation of non-positive radiated power

To avoid the implications of a non-positive operator $\mathbf{R}$, the following modification is suggested. The summation (31) is split into two parts. The first part is the original sum up to the mode M, for which $P_r^n > 0$ ($M = 6$ in the case of the dipole above). The second part is modified to obtain a negative

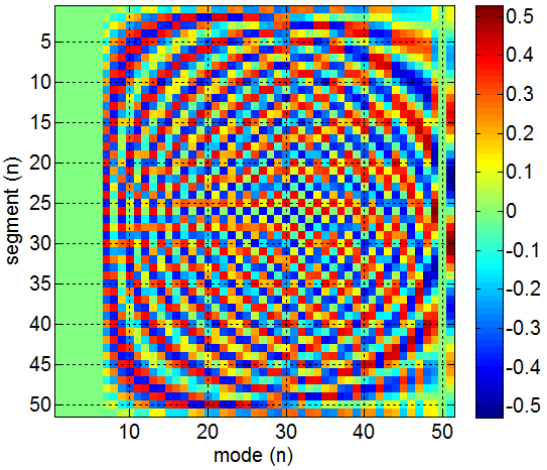

Fig. 11. The difference $\mathbf{D} = \mathbf{U} - \mathbf{V}$, based on (40). The thin-wire half-wave dipole which was discretized to 51 elements is considered at the resonant frequency of the dominant mode.

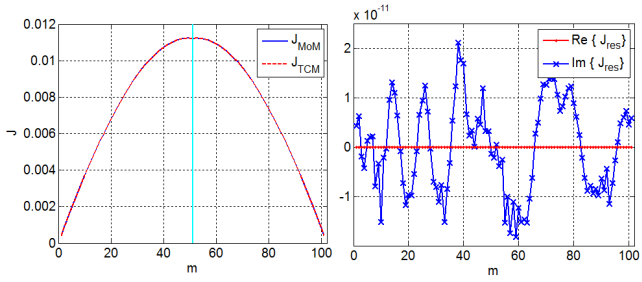

Fig. 12. The absolute value of $\mathbf{J}_{MoM}$ and $\widetilde{\mathbf{J}}_{TCM}$ (left) and the real and imaginary parts of compensated residual current calculated as $\mathbf{J}_{MoM} - \mathbf{J}_{TCM}$ (right), half-wave dipole at 1.5GHz, fed at the middle, blue line indicates the feeding position.

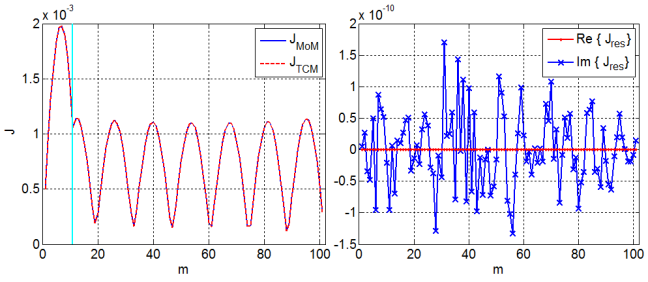

Fig. 13. The absolute value of $\mathbf{J}_{MoM}$ and $\widetilde{\mathbf{J}}_{TCM}$ (left) and the real and imaginary parts of compensated residual current calculated as $\mathbf{J}_{MoM} - \mathbf{J}_{TCM}$ (right), half-wave dipole at 11GHz, fed at one tenth of the dipole length, blue line indicates the feeding position.

eigenvalue λ_n:

$$\widetilde{\mathbf{J}}_{TCM} = \sum_{m=1}^{M} \frac{\langle \mathbf{J}_m, \mathbf{E}^i \rangle_r}{1 + \jmath\lambda_m} \mathbf{J}_m + \sum_{n=M+1}^{N} \frac{\langle \mathbf{J}_n, \mathbf{E}^i \rangle_r}{1 - \jmath|\lambda_n|} \mathbf{J}_n. \tag{41}$$

To verify the newly proposed sum (41), consider the example of the dipole again. For comparison with Fig. 7 and Fig. 8, the dipole at the first resonance was recalculated, see Fig. 12. In addition, a more complicated example of the same dipole of $L = 0.1m$ at $f = 11$GHz and fed at one tenth of its length is

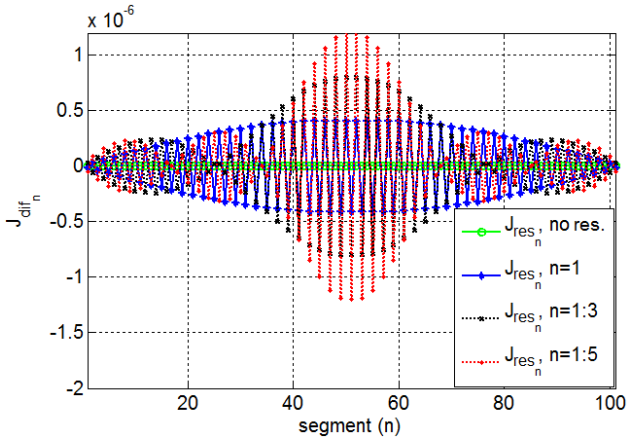

Fig. 14. Increase in the residual mode, $n = M + 1$ (no resid. mode), $n_2 = M + 3$ (small resid. mode, blue solid line), $n_3 = M + 5$ ($n_3 > n_2$, black dotted line)

depicted in Fig. 13. The agreement between $\widetilde{\mathbf{J}}_{TCM}$ and $\mathbf{J}_{MoM}$ is excellent for both cases (the residual current is of about of eight orders below the total current values), thus we conclude that

$$\widetilde{\mathbf{J}}_{TCM} = \mathbf{J}_{MoM} = \mathbf{J}_{TCM} + \mathbf{J}_{res}. \tag{42}$$

Interestingly, the residuum can be isolated. Subtract the original term (31) from the corrected term (41)

$$\mathbf{J}_{res} = \sum_{n=M+1}^{N} \frac{\langle \mathbf{J}_n, \mathbf{E}^i \rangle_r}{1 - \jmath|\lambda_n|} \mathbf{J}_n - \sum_{n=M+1}^{N} \frac{\langle \mathbf{J}_n, \mathbf{E}^i \rangle_r}{1 + \jmath\lambda_n} \mathbf{J}_n. \tag{43}$$

The total residuum

$$\mathbf{J}_{res} = \sum_{n=M+1}^{N} \langle \mathbf{J}_n, \mathbf{E}^i \rangle_r \mathbf{J}_n \left(\frac{1}{1 - \jmath|\lambda_n|} - \frac{1}{1 + \jmath\lambda_n} \right) \tag{44}$$

can be separated into particular modal residual currents, corresponding to the characteristic mode n:

$$\begin{aligned} \mathbf{J}_{res_n} &= \langle \mathbf{J}_n, \mathbf{E}^i \rangle_r \mathbf{J}_n \left(\frac{1}{1 - \jmath|\lambda_n|} - \frac{1}{1 + \jmath\lambda_n} \right) \\ &= \langle \mathbf{J}_n, \mathbf{E}^i \rangle_r \mathbf{J}_n \frac{1 + \jmath\lambda_n - 1 + \jmath|\lambda_n|}{1 + \jmath\lambda_n - \jmath|\lambda_n| - \jmath^2|\lambda_n|\lambda_n}. \end{aligned} \tag{45}$$

Assume that all modes for which this correction is applied originally had positive (instead of negative) eigenvalues. This simplifies the previous equation to the form

$$\mathbf{J}_{res_n} = \jmath \frac{|\lambda_n| + \lambda_n}{1 + \lambda_n^2} \mathbf{J}_n \langle \mathbf{J}_n, \mathbf{E}^i \rangle_r. \tag{46}$$

The expression (46) explains why the residual current in Fig. 7 and Fig. 8 has a purely imaginary character for real feeding.

The rise of the residuum is depicted in Fig. 14 where the dipole is fed at the middle. Here, we try to correct not only all necessary modes where $n > 6$ ($n = M + 1$), but also modes where $n > 8$ ($n = M + 3$), $n > 10$ ($n = M + 5$) and where $n > 12$ ($n = M+7$), respectively. With more and more modes omitted the residual current rapidly grows (see the red line in Fig. 14).

Notice that the residuum (46) vanishes if the associated value λ_n has the correct (negative) eigenvalue. The proposed correction also shows that only the badly radiating modes have to be treated by (41). These modes are the modes far from their own resonances and all the non-radiating[3] (inductive) modes. In the case of a dipole divided into 101 elements, the residual mode spontaneously vanishes at frequencies higher than $51 f_1 = 76.5$GHz (which was tested and confirmed by the calculation).

VIII. Conclusion

The paper is devoted to the source formulation of the theory of characteristic modes as introduced by Harrington and Mautz. A brief revision of the theory is given in section III. The analytical functional formulation of the TCM is developed and the final analytical expression is a spatial function of only the current which is minimized by the characteristic modes. This expression provides a different perspective on the TCM.

The usefulness and "strength" of the functional is shown on three canonical examples: a dipole, two closely spaced dipoles and a loop. It was shown that the functional formulation is more suitable for analytical solution than the original formulation, because there is no impedance matrix involved. Deep investigation into the 1st mode on a dipole revealed the limitations of the approximation of the current distribution by simple sin function. The functional allows us to observe a connection between the zeroth (static) mode on a loop and two closely separated dipoles. Moreover it was possible to explain the behaviour of the radiated power and reactive power in terms of the sources of the fields – characteristic currents.

The second main issue treated in the paper is the modal superposition. In theory, the current obtained as a sum of the complete set of characteristic currents is exactly equal to the total current (as given e.g. by the method of moments). This statement is mathematically correct although the results are usually computed numerically. It was observed by several researchers that there is a substantial residue after subtracting the sum of modal currents from the total current.

The issue is investigated and a solution is proposed in this paper. It was found that the problems can be addressed to a numerical scaling involved in GEP. In order to correct the results a modification of the numerical superposition formula was proposed. Using the new procedure the residual current on a dipole in different frequency bands and for different feed positions was eliminated. Therefore a near-perfect match between $\widetilde{\mathbf{J}}_{TCM}$ and $\mathbf{J}_{MoM}$ can be obtained numerically.

Acknowledgement

The authors would like to thank L. Jelinek and N. Bell for their comments. Also, the authors would like to thank three anonymous reviewers. Their remarks have led to the significant improvement of the manuscript and made the paper more straightforward.

[3]Correction (41) can also be obtained by the analysis of Lagrange multipliers that constitutes (16) if we include several modes which "radiate" a small amount of negative power.

REFERENCES

[1] R. J. Garbacz, "A generalized expansion for radiated and scattered fields," Ph.D. dissertation, The Ohio State Univ., 1968.

[2] R. F. Harrington and J. R. Mautz, "Theory of characteristic modes for conducting bodies," *IEEE Trans. Antennas Propag.*, vol. 19, no. 5, pp. 622–628, Sept. 1971.

[3] E. Antonino-Daviu, M. Cabedo-Fabres, M. Gallo, M. Ferrando-Bataller, and M. Bozzetti, "Design of a multimode mimo antenna using characteristic modes," in *Proceedings of the 3rd European Conference on Antennas and Propagation (EUCAP)*, Berlin, Germany, March 2009, pp. 1840–1844.

[4] K. A. Obeidat, "Design methodology for wideband electrically small antennas based on the theory of characteristic modes," Ph.D. dissertation, Univ. of Illinois, 2010.

[5] J. J. Adams, "Characteristic modes for impedance matching and broadbanding of electrically small antennas," Ph.D. dissertation, Univ. of Illinois, 2011.

[6] R. F. Harrington, *Field Computation by Moment Methods*. John Wiley - IEEE Press, 1993.

[7] W. Geyi, *Foundations of Applied Electrodynamics*. John Wiley, 2010.

[8] M. Gustafsson and S. Nordebo, "Antenna currents for optimal Q, superdirectivity, and radiation patterns using convex optimization," *IEEE Trans. Antennas Propag.*, vol. X, no. X, XXXX, will be published.

[9] W. C. Gibson, *The Method of Moments in Electromagnetics*. Chapman & Hall/CRC, 2008.

[10] S. M. Rao, D. R. Wilton, and A. W. Glisson, "Electromagnetic scattering by surfaces of arbitrary shape," *IEEE Trans. Antennas Propag.*, vol. 30, no. 3, pp. 409–418, May 1982.

[11] V. H. Rumsey, "Reaction concept in electromagnetic theory," *Phys. Rev.*, vol. 94, no. 6, pp. 1483–1491, June 1954.

[12] N. I. Akhiezer and I. M. Glazman, *Theory of Linear Operators in Hilbert Space*. Dover, 1993.

[13] G. A. E. Vandenbosh, "Reactive energies, impedance, and Q factor of radiating structures," *IEEE Trans. Antennas Propag.*, vol. 58, no. 4, pp. 1112–1127, Apr. 2010.

[14] R. Courant and D. Hilbert, *Methods of Mathematical Physics*. John Wiley, 1966, vol. 1.

[15] G. W. Stewart and J. Sun, *Matrix Perturbation Theory*. Academic Press, 1990.

[16] M. Gustafsson and B. L. G. Jonsson. Stored electromagnetic energy and antenna Q. eprint arXiv: 1211.5521. [Online]. Available: http://adsabs.harvard.edu/abs/2012arXiv1211.5521G

[17] P. Hazdra and P. Hamouz, "On the modal superposition lying under the MoM matrix equations," *Radioengineering*, vol. 17, no. 3, pp. 42–46, Sept. 2008.

[18] H. Sagan, *Boundary and Eigenvalue Problems in Mathematical Physics*. Dover, 1989.

[19] R. F. Harrington and J. R. Mautz, "Computation of characteristic modes for conducting bodies," *IEEE Trans. Antennas Propag.*, vol. 19, no. 5, pp. 629–639, Sept. 1971.

[20] M. Cabedo-Fabres, E. Antonino-Daviu, A. Valero-Nogueira, and M. Ferrando-Bataller, "The theory of characteristic modes revisited: A contribution to the design of antennas for modern applications," *IEEE Antennas Propag. Magazine*, vol. 49, no. 5, pp. 52–68, Oct. 2007.

[21] D. Liu, R. J. Garbacz, and D. M. Pozar, "Antenna synthesis and optimization using generalized characteristic modes," *IEEE Trans. Antennas Propag.*, vol. 38, no. 6, pp. 862–868, June 1990.

[22] The Matlab. [Online]. Available: www.mathworks.com/

[23] E. Anderson, et al., *LAPACK Users' Guide*. Society for Industrial and Applied Mathematics (SIAM), 1999.

[24] M. Capek, P. Hazdra, P. Hamouz, and M. Mazanek, "Software tools for efficient generation, modelling and optimisation of fractal radiating structures," *IET Microw. Antennas Propag.*, vol. 5, pp. 1002–1007, 2011.

[25] M. Capek, P. Hazdra, P. Hamouz, and J. Eichler, "A method for tracking characteristic numbers and vectors," *PIER-B*, vol. 33, pp. 115–134, 2011.

[26] M. Capek, P. Hazdra, and J. Eichler, "A method for the evaluation of radiation Q based on modal approach," *IEEE Trans. Antennas Propag.*, vol. 60, no. 10, pp. 4556–4567, Oct. 2012.

[27] J. L. T. Ethier and D. A. McNamara, "Modal significance measure in characteristic mode analysis of radiating structures," *IET Electronics Letters*, vol. 46, no. 2, pp. 107–108, Jan. 2010.

[28] ——, "Through the looking glass: A characteristic mode view of electromagnetic modeling & design," in *ANTEM-AMEREM*, July 2010, pp. 1–4.

[29] P. Hazdra, M. Capek, and J. Eichler, "Radiation Q-factors of thin-wire dipole arrangements," *IEEE Antennas Wireless Propag. Lett.*, vol. 10, pp. 556–560, 2011.

[30] S. J. Farlow, *Partial Differential Equations for Scientists and Engineers*. Dover, 1993.

[31] M. Gustafsson, M. Cismasu, and B. L. G. Jonsson, "Physical bounds and optimal currents on antennas," *IEEE Trans. Antennas Propag.*, vol. 60, no. 6, pp. 2672–2681, June 2012.

[32] M. Cabedo-Fabres, "Systematic design of antennas using the theory of characteristic modes," Ph.D. dissertation, UPV, Feb. 2007.

[33] C. A. Balanis, *Advanced Engineering Electromagnetics*. John Wiley, 1989.

[34] M. Cabedo-Fabres, A. Valero-Nogueira, J. I. Herranz-Herruzo, and M. Ferrando-Bataller, "A discussion on the characteristic mode theory limitations and its improvement for the effective modeling of antennas and arrays," in *Antennas Propag. Society International Symposium*, vol. 1, 2004, pp. 121–124.

[35] J. Kiusalaas, *Numerical Methods in Engineering with Matlab*. Cambridge University Press, 2005.

Miloslav Capek (S'09) received the M.Sc. degree in electrical engineering from the Czech Technical University, Prague, Czech Republic, in 2009, and is currently working towards the Ph.D. degree in electromagnetic fields at the same University.

His research interests are in the area of electromagnetic theory, electrically small antennas, numerical techniques, fractal geometry and optimization.

Pavel Hazdra (M'03) received the M.S. and Ph.D. degrees in electrical engineering from the Czech Technical University in Prague, Faculty of Electrical Engineering in 2003 and 2009, respectively. He is a research and teaching assistant with the Department of Electromagnetic Field, CTU-FEE.

His research interests are in the area of electromagnetic theory, computational electromagnetics, fractal geometry, planar antennas and special prime-feed antennas.

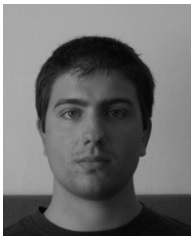

Jan Eichler (S'10) received the B.Sc. and M.Sc. degrees in electrical engineering from the Czech Technical University in Prague in 2008 and 2010, respectively. He is currently working towards the Ph.D. degree at the same University.

His research interests include modal methods for antenna design as well as their connection to the full-wave methods. He is also interested in development and simulation of active antennas.

Chapter 6

Appendix A.2 – AtoM leaflet

The package AtoM (Antenna toolbox in Matlab) developed under one thesis' objective, is a subject of project, which has been submitted to the Technology Agency of Czech Republic (TACR). The leaflet of the AtoM is depicted in this appendix.

AToM Antenna Toolbox for Matlab

BRNO UNIVERSITY OF TECHNOLOGY

MECAS ESI s.r.o.

AToM/Features

EM model

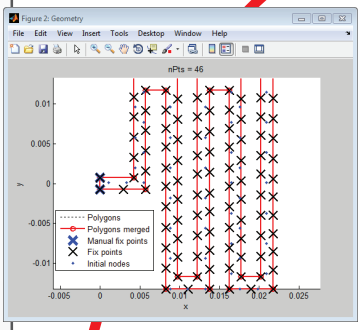

synthetic fractals supported, IFS, L-system generators

import from FEKO/Comsol/Matlab, 3D model editor

fully parametrized model (import from .dwg, and bitmaps possible)

fast gradient/robust heuristic/hybrid optimization algorithms

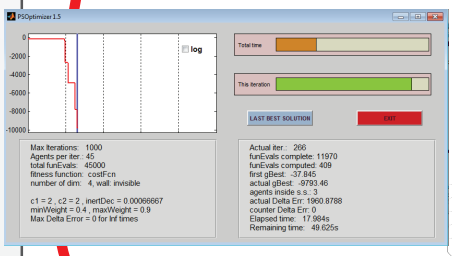

Discretization

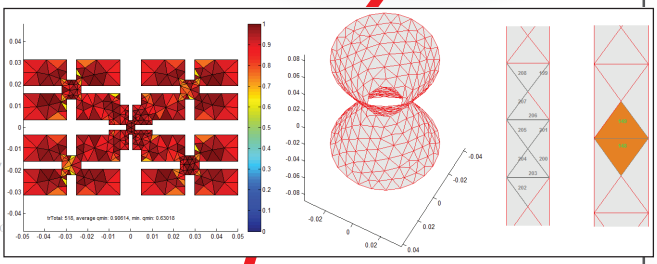

RWG basis functions, local refinement possible

parallel and distributed computing implicitly supported

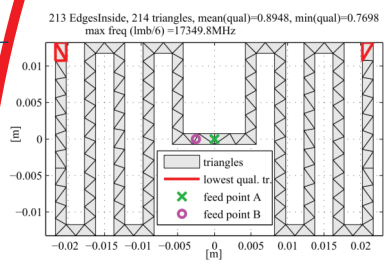

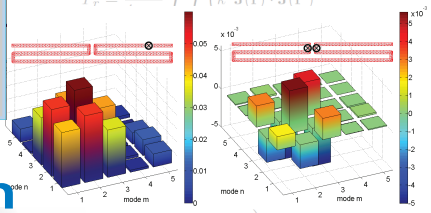

adaptive frequence solver

advanced eigenvalue tracking

Optimization
parametric sweep

all routines are editable, all functions are user defined

job manager is developed, all routines are available from command line

EM solvers
MoM, TCM

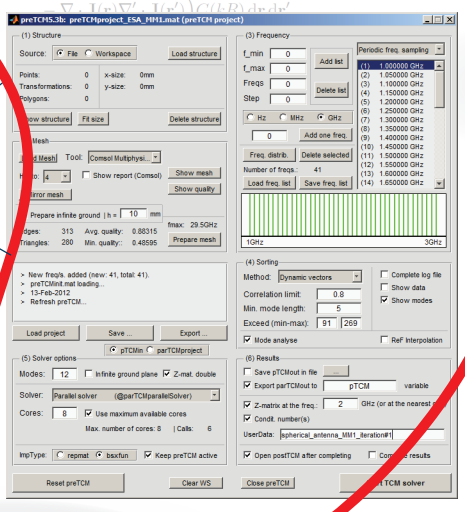

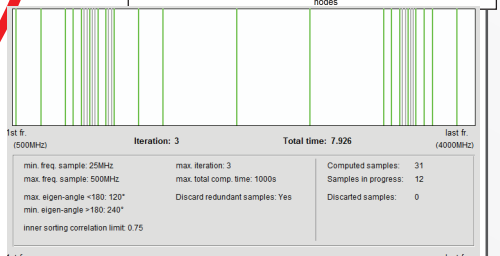

both modal and total quantities available (all near-, far-field and circuit parameters)

Post Processing

measurable Q concept integrated

all data can be exported into IEEE template graphs

both modal (TCM) and structural decomposition is available

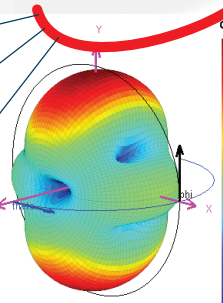

GPU supported

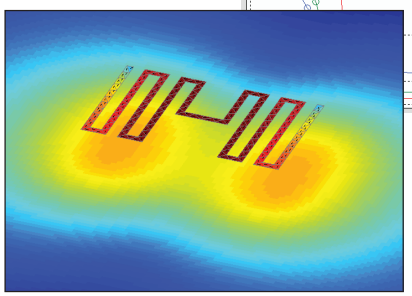

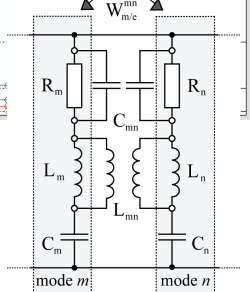

AToM | Antenna Toolbox for Matlab

elmag.org UREL MECAS ESI s.r.o.

AToM/Description

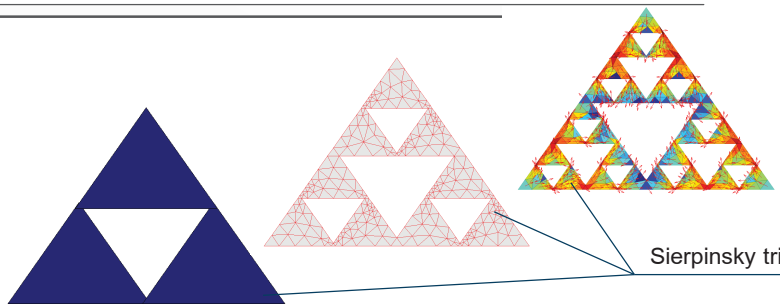

Sierpinsky triangle from 1st to 3rd iteration, from model to modal currents.

Background

AToM/ Thousands of lines in Matlab have been written for research purposes of the antenna group at the CTU-FEE in Prague.

AToM/ These codes utilize current theoretical findings and present a unique electromagnetic software tool based on MoM solver followed by modal decomposition of radiation sources.

AToM/ Since this tool might be of interest of broader scientific community and since most universities and researchers use Matlab platform, we propose to embed our codes into user-friendly pack as a Matlab toolbox named AToM.

AToM/ Still, lot of programming effort is required. We are going to ask The Technological grant agency (TACR) of the Czech Republic for support in transferring this academic research into commercial software. Importantly, the TACR funding will allow to employ four postDocs for 3 years.

AToM/ Cooperation with Brno University of Technology and MECAS-ESI is planned.

Overview of the AToM software

AToM/ So far the codes were used for conducting research on electrically small antennas, fractal, diversity and reconfigurable antennas and related issues (radiation Q factor, radiation efficiency). This effort already led to several papers in recognized international journals [1]-[4].

AToM/ The core is based on MoM and Characteristic modes decomposition, but the uniqueness lies in strong modularity and additional components (PSO/MOSOMA optimizer and fractal generator to name a few).

AToM/ All the components could be used standalone, or in user-defined chain; for example consider optimization of radiation efficiency while maintaining two operating bands.

AToM/ The AToM supports current hardware technology (distributive computing, GPU)

Fractal electrically small antennas designed by AToM.

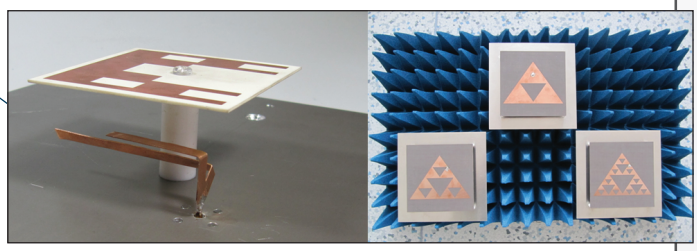

Contact:
Miloslav Capek, Pavel Hazdra
miloslav.capek@fel.cvut.cz, hazdrap@fel.cvut.cz
CTU-FEE in Prague, Technicka 2, 166 27, Prague, Czech Republic

[1] Capek, M., Hazdra, P., Hamouz, P., Mazanek, M.: *Software tools for efficient generation, modeling and optimisation of fractal radiating structures*. IET Microw., Antennas & Propagation, Vol. 5, p.1002-1007, 2011.

[2] Capek, M., Hamouz, P., Hazdra, P., Eichler, J.: *Implementation of the Theory of Characteristic Modes in MATLAB*. IEEE Antennas & Propagation Magazine, Vol. 55, No. 2, p. 176-189, April 2013.

[3] Capek, M., Hazdra, P., Eichler, J.: *A Method For the Evaluation of Modal Radiation Q*. IEEE Transactions on Antennas & Propagation, Vol. 60, No. 10, p.4556-4567, 2012.

[4] Eichler, J., Hazdra, P., Capek, M., Korinek, T., Hamouz, P.: *Design of a Dual Band Orthogonally Polarized L-probe Fed Fractal Patch Antenna using Modal Methods*. IEEE Antennas & Propagation Letters, Vol. 10, p. 1389-1392, 2011.